

# 博士論文

**Studies on Introduction of MnO<sub>2</sub> into Prebleaching Stage and  
Mechanism of MnO<sub>2</sub> Oxidation of Lignin Model Compounds**  
(前漂白過程への MnO<sub>2</sub> の導入およびリグニンモデル化合物の  
MnO<sub>2</sub> 酸化機構に関する研究)

孫 世榮

**Shirong Sun**



# 博士論文

**Studies on Introduction of MnO<sub>2</sub> into Prebleaching Stage and  
Mechanism of MnO<sub>2</sub> Oxidation of Lignin Model Compounds**  
(前漂白過程への MnO<sub>2</sub> の導入およびリグニンモデル化合物の  
MnO<sub>2</sub> 酸化機構に関する研究)

孫 世栄

**Shirong Sun**

**Laboratory of Wood Chemistry  
Department of Biomaterial Sciences  
Graduate School of Agricultural and Life Sciences  
The University of Tokyo**

**2021**



# CONTENTS

## List of Tables

## List of Figures

<b>1 Introduction .....</b>	<b>1</b>
1.1 Preface .....	2
1.2 Oxygen-alkali bleaching .....	3
1.2.1 Reactivity of molecular oxygen .....	3
1.2.2 Degradation of lignin under oxygen-alkali conditions .....	4
1.2.3 Degradation of carbohydrates under oxygen-alkali conditions .....	7
1.3 Primary considerations of MnO <sub>2</sub> oxidation .....	10
1.3.1 Manganese chemistry .....	10
1.3.2 Chemical properties of MnO <sub>2</sub> .....	11
1.3.3 Chemistry of MnO <sub>2</sub> oxidation .....	12
1.4 Objectives in this study .....	20
1.5 References .....	21
<b>2 Utilization of Recyclable MnO<sub>2</sub> in Prebleaching Stage as a Catalyst for Oxygen Delignification or as a Delignifying Agent .....</b>	<b>31</b>
2.1 Introduction .....	32
2.2 Materials and methods .....	34
2.2.1 Materials .....	34
2.2.2 Methods .....	34
2.3 Results and discussion .....	38
2.3.1 Reaction of model compound .....	38
2.3.2 Oxygen delignification in the presence of MnO <sub>2</sub> .....	39
2.3.3 Oxygen delignification in the presence of MnO <sub>2</sub> generated <i>in-situ</i> in pulp fibers .....	42
2.3.4 Successive stages of oxygen delignification and MnO <sub>2</sub> oxidation .....	44
2.3.5 Possibility on the recycle of MnO <sub>2</sub> .....	47
2.4 Conclusions .....	48
2.5 References .....	49
<b>3 Differences in the Mechanisms of MnO<sub>2</sub> Oxidation between C<sub>6</sub>-C<sub>1</sub>-type Monomeric Lignin Model Compounds with the <i>p</i>-Hydroxyphenyl, Guaiacyl, and Syringyl Nuclei ....</b>	<b>51</b>
3.1 Introduction .....	52
3.2 Materials and methods .....	54
3.2.1 Materials .....	54
3.2.2 Methods .....	75
3.3 Results and discussion .....	78
3.3.1 Description of the reaction system .....	78
3.3.2 MnO <sub>2</sub> oxidation of benzene analogues (compounds I) .....	79
3.3.3 MnO <sub>2</sub> oxidation of benzyl alcohol analogues (compounds II) .....	83

3.3.4 MnO <sub>2</sub> oxidation of deuterated benzyl alcohol analogues (compounds III).....	87
3.3.5 Possible reaction modes of C <sub>6</sub> -C <sub>1</sub> -type monomeric lignin model compounds in MnO <sub>2</sub> oxidation.....	90
3.4 Conclusions.....	94
3.5 References.....	95
<b>4 Further Investigation of the Mechanisms of MnO<sub>2</sub> Oxidation using C<sub>6</sub>-C<sub>2</sub>-type Monomeric Lignin Model Compounds with the <i>p</i>-Hydroxyphenyl, Guaiacyl, and Syringyl Nuclei.....</b>	<b>99</b>
4.1 Introduction.....	100
4.2 Materials and methods.....	102
4.2.1 Materials.....	102
4.2.2 Methods.....	112
4.3 Results and discussion.....	114
4.3.1 MnO <sub>2</sub> oxidation of C <sub>6</sub> -C <sub>2</sub> -type monomeric lignin model compounds (compounds IV).....	114
4.3.2 MnO <sub>2</sub> oxidation of deuterated C <sub>6</sub> -C <sub>2</sub> -type monomeric lignin model compounds (compounds V).....	119
4.3.3 Possible reaction modes of C <sub>6</sub> -C <sub>2</sub> -type monomeric lignin model compounds in the MnO <sub>2</sub> oxidation and the comparison with C <sub>6</sub> -C <sub>1</sub> -type compounds.....	122
4.4 Conclusions.....	125
4.5 References.....	126
<b>5 MnO<sub>2</sub> Oxidation of <math>\beta</math>-O-4-type Lignin Model Compounds with Syringyl or Guaiacyl Nucleus Focusing on the Difference in the Reactivities between the <i>erythro</i> and <i>threo</i> Diastereomers .....</b>	<b>127</b>
5.1 Introduction.....	128
5.2 Materials and methods.....	131
5.2.1 Materials.....	131
5.2.2 Methods.....	145
5.3 Results and discussion.....	147
5.3.1 Reaction products derived from the MnO <sub>2</sub> oxidation of $\beta$ -O-4-type lignin model compounds .....	147
5.3.2 Effects of whether the A-ring is syringyl or guaiacyl, whether the side-chain is the <i>erythro</i> or <i>threo</i> , and whether the $\gamma$ -hydroxymethyl group is present or absent on the reaction rates of the MnO <sub>2</sub> oxidation .....	156
5.3.3 Possible mechanisms for the reaction of GG and SG .....	157
5.3.4 Possible mechanisms for the reaction of G'G and S'G.....	159
5.4 Conclusions.....	160
5.5 References.....	161
<b>6 Summary.....</b>	<b>163</b>
<b>Acknowledgement .....</b>	<b>171</b>
<b>List of Publications.....</b>	<b>173</b>

## List of Tables

<b>Table 1-1</b> Reactive species generated in oxygen bleaching.....	4
<b>Table 2-1</b> Kappa number and viscosity of the pulps employed for the preparation of <b>Figure 2-4</b> with the final pH.....	41
<b>Table 2-2</b> Kappa number and viscosity of the pulps obtained by oxygen delignification at pHs lower than 12.5, with the initial and final pH.....	42
<b>Table 2-3</b> Kappa number and viscosity of the pulps employed for the preparation of <b>Figures 2-6</b> with the final pH. ....	46
<b>Table 3-1</b> HPLC analysis methods for MnO <sub>2</sub> oxidation of lignin model compounds and their respective internal standards for quantification. ....	77
<b>Table 3-2</b> Observed pseudo-first-order reaction rate constants ( $k_{\text{obs}}$ ), squares of the correlation coefficients ( $R^2$ ) in the approximations, and ratios of $k_{\text{obs}}$ values between compounds <b>II</b> and <b>III</b> ( $k_{\text{obs}}(\text{II})/k_{\text{obs}}(\text{III})$ ) for estimation of the magnitudes of the kinetic isotope effects. ....	82
<b>Table 4-1</b> HPLC analysis methods for MnO <sub>2</sub> oxidation of C <sub>6</sub> -C <sub>2</sub> -type monomeric lignin model compounds and their respective internal standards for quantification. ....	113
<b>Table 4-2</b> Observed pseudo-first-order reaction rate constants ( $k_{\text{obs}}$ ), squares of the correlation coefficients ( $R^2$ ) in the approximations, and ratios of $k_{\text{obs}}$ values between compounds <b>IV</b> and <b>V</b> ( $k_{\text{obs}}(\text{IV})/k_{\text{obs}}(\text{V})$ ) for estimation of the magnitudes of the kinetic isotope effects. ....	118
<b>Table 4-3</b> Ratios observed pseudo-first-order reaction rate constants ( $k_{\text{obs}}$ values) between compounds <b>II</b> and <b>III</b> ( $k_{\text{obs}}(\text{II})/k_{\text{obs}}(\text{III})$ ), and the ratios between compounds <b>IV</b> and <b>V</b> ( $k_{\text{obs}}(\text{IV})/k_{\text{obs}}(\text{V})$ ) for estimation of the magnitudes of the kinetic isotope effects. Ratios between compound <b>II</b> and <b>IV</b> ( $k_{\text{obs}}(\text{II})/k_{\text{obs}}(\text{IV})$ ), and the ratios between compounds <b>III</b> and <b>V</b> ( $k_{\text{obs}}(\text{III})/k_{\text{obs}}(\text{V})$ ) for estimation of the differences between C <sub>6</sub> -C <sub>2</sub> - and C <sub>6</sub> -C <sub>1</sub> -type monomeric lignin model compounds. ....	123
<b>Table 5-1</b> HPLC and GC analysis methods for MnO <sub>2</sub> oxidation of lignin model compounds and their respective internal standard for quantification. ....	146
<b>Table 5-2</b> Reaction products of $\beta$ -O-4-type lignin model compounds in MnO <sub>2</sub> oxidation. ..	155
<b>Table 5-3</b> Observed pseudo-first-order reaction rate constants ( $k_{\text{obs}}$ ), squares of the correlation coefficients ( $R^2$ ) in the approximations of lignin model compounds. ....	157

## List of Figures

<b>Figure 1-1</b> Four one-electron transfer steps and two-electron transfer steps of stepwise reduction of oxygen.....	4
<b>Figure 1-2</b> Alkaline autoxidation of phenolic units to give hydroperoxide intermediates. <sup>[3]</sup> ....	5
<b>Figure 1-3</b> Intramolecular nucleophilic attack by peroxide anions to give, <i>via</i> dioxetane intermediates, oxirane-, muconic acid- and carbonyl structures. <sup>[3]</sup> .....	6
<b>Figure 1-4</b> The oxidation of non-phenolic lignin units with HO• under alkaline bleaching conditions. ....	7
<b>Figure 1-5</b> Oxidation of secondary alcohol groups of cellulose, $\beta$ -elimination reaction of cellulose and oxidation of ketone alcohol. ....	8
<b>Figure 1-6</b> Peeling and stopping reactions of carbohydrates.....	9
<b>Figure 1-7</b> The Mn cycle of oxidation states found in nature. Mn(II) is thermodynamically stable in the absence of O <sub>2</sub> and at low pH, whereas in the presence of O <sub>2</sub> , Mn(III) and Mn(IV), which occur primarily as insoluble Mn (oxyhydr)oxides, are favored. <sup>[60]</sup> .....	10
<b>Figure 1-8</b> Possible mechanisms of bacterial Mn(II) oxidation. <sup>[60]</sup> .....	11
<b>Figure 1-9</b> Manganese oxides with different chemical composition and crystal structure: (a) $\alpha$ -MnO <sub>2</sub> , (b) $\beta$ -MnO <sub>2</sub> , (c) $\gamma$ -MnO <sub>2</sub> , (d) $\delta$ -MnO <sub>2</sub> , (e) $\lambda$ -MnO <sub>2</sub> . ....	12
<b>Figure 1-10</b> Oxidation reaction of vitamin A to corresponding aldehyde. ....	13
<b>Figure 1-11</b> The mechanisms of oxidation of alcohols with MnO <sub>2</sub> .....	14
<b>Figure 1-12</b> Representative reactions of selective oxidation of unsaturated alcohols by MnO <sub>2</sub> . ....	16
<b>Figure 1-13</b> Representative reactions of unsaturated alcohols with functional group sensitivity to oxidation with MnO <sub>2</sub> .....	17
<b>Figure 1-14</b> Representative reactions of unsaturated alcohols performed <i>in-situ</i> during oxidations with MnO <sub>2</sub> . ....	18
<b>Figure 1-15</b> Representative side reactions of unsaturated alcohols during oxidations with MnO <sub>2</sub> . ....	19
<b>Figure 2-1</b> Possible reaction scheme for a phenolic compound under oxygen delignification conditions. ....	33
<b>Figure 2-2</b> Chemical structures of a phenolic compound of vanillyl alcohol (Valc) as an active	

oxygen species generator and a carbohydrate model compound of methyl  $\beta$ -D-glucopyranoside (MGP). ..... 34

**Figure 2-3** Time course of changes in the residual yields of MGP (white and black circles) and Valc (white and black diamonds) when treated together under conditions simulating oxygen delignification in the presence of MnO<sub>2</sub>. (white marks: 1st trial, black marks: 2nd trial) ..... 39

**Figure 2-4** Correlation between viscosities and kappa numbers of pulps obtained when hardwood unbleached kraft pulp was oxygen-delignified in the absence of MnO<sub>2</sub> (reference, black stars), or in the presence of commercial MnO<sub>2</sub> (white circles) or synthesized MnO<sub>2</sub> (white diamonds) at an oxygen pressure of 0.6 MPa, initial pH of 12.5, pulp consistency of 4.0%, and 95°C for 40, 80, 120, 240, or 360 min. .... 40

**Figure 2-5** Correlation between viscosities and kappa numbers of pulps obtained when hardwood unbleached kraft pulp was oxygen-delignified in the presence of MnO<sub>2</sub> generated *in-situ* in pulp fibers at an oxygen pressure of 0.6 MPa, initial pH of 12.5, pulp consistency of 4.0%, and 95°C for 40, 80, or 120 min (white squares). (Black stars are the reference, and the same as those shown in **Figure 2-4**.) ..... 43

**Figures 2-6** Correlation between viscosities and kappa numbers of pulps obtained in the reference oxygen delignification (black stars), in the successive stages of oxygen delignification for 120 min, and in the synthetic MnO<sub>2</sub> oxidation. (a) The synthetic MnO<sub>2</sub> oxidation stage was conducted at a pH of 2 (black circle) or 1 (black diamond) prepared by H<sub>2</sub>SO<sub>4</sub>. (b) The synthetic MnO<sub>2</sub> oxidation stage was conducted at a pH of 2 prepared by sulfate buffer (white stars). (Black stars are the reference and the same as those shown in **Figure 2-4**.) ..... 45

**Figure 3-1** Non-phenolic lignin model compounds (the **H**-, **G**-, and **S**-types) and *p*-ethylphenyl type compounds (the **E**-types) employed in this study..... 54

**Figure 3-2** Quantified reaction products as well as another possible one without detection (product **B<sub>H</sub>**) in the MnO<sub>2</sub> oxidation. .... 56

**Figure 3-3** <sup>1</sup>H-NMR (top) and <sup>13</sup>C-NMR (bottom) spectra of compound **III<sub>H</sub>**. ..... 63

**Figure 3-4** <sup>1</sup>H-NMR (top) and <sup>13</sup>C-NMR (bottom) spectra of compound **III<sub>G</sub>**. ..... 64

**Figure 3-5** <sup>1</sup>H-NMR (top) and <sup>13</sup>C-NMR (bottom) spectra of compound **III<sub>S</sub>**. ..... 65

**Figure 3-6** <sup>1</sup>H-NMR (top) and <sup>13</sup>C-NMR (bottom) spectra of compound **III<sub>E</sub>**. .... 66

**Figure 3-7** <sup>1</sup>H-NMR (top) and <sup>13</sup>C-NMR (bottom) spectra of product **A'<sub>H</sub>**. ..... 67

**Figure 3-8** <sup>1</sup>H-NMR (top) and <sup>13</sup>C-NMR (bottom) spectra of product **A'<sub>G</sub>**. .... 68

**Figure 3-9** <sup>1</sup>H-NMR (top) and <sup>13</sup>C-NMR (bottom) spectra of product **A'<sub>S</sub>**. ..... 69

<b>Figure 3-10</b> $^1\text{H}$ -NMR (top) and $^{13}\text{C}$ -NMR (bottom) spectra of product <b>A'E</b> . .....	70
<b>Figure 3-11</b> $^1\text{H}$ -NMR (top) and $^{13}\text{C}$ -NMR (bottom) spectra of product <b>B<sub>G</sub></b> . .....	71
<b>Figure 3-12</b> $^1\text{H}$ -NMR (top) and $^{13}\text{C}$ -NMR (bottom) spectra of product <b>B<sub>s</sub></b> . .....	72
<b>Figure 3-13</b> GC/MS spectra of synthesized model compounds and reaction products employed in this chapter. ....	74
<b>Figure 3-14</b> Time course of the changes in the recovery yield of compound <b>I<sub>G</sub></b> and yield of product <b>B<sub>G</sub></b> in the $\text{MnO}_2$ oxidation of compound <b>I<sub>G</sub></b> . ....	81
<b>Figure 3-15</b> Time course of the changes in the recovery yield of compound <b>I<sub>s</sub></b> and yield of product <b>B<sub>s</sub></b> in the $\text{MnO}_2$ oxidation of compound <b>I<sub>s</sub></b> . ....	82
<b>Figure 3-16</b> Time course of the changes in the recovery yield of compound <b>II<sub>H</sub></b> and yield of product <b>A<sub>H</sub></b> in the $\text{MnO}_2$ oxidation of compound <b>II<sub>H</sub></b> . ....	85
<b>Figure 3-17</b> Time course of the changes in the recovery yield of compound <b>II<sub>G</sub></b> and yield of product <b>A<sub>H</sub></b> in the $\text{MnO}_2$ oxidation of compound <b>II<sub>G</sub></b> . ....	86
<b>Figure 3-18</b> Time course of the changes in the recovery yield of compound <b>II<sub>s</sub></b> and yields of products <b>A<sub>s</sub></b> and <b>B<sub>s</sub></b> in the $\text{MnO}_2$ oxidation of compound <b>II<sub>s</sub></b> . ....	86
<b>Figure 3-19</b> Time course of the changes in the recovery yield of compound <b>II<sub>E</sub></b> and yield of product <b>A<sub>E</sub></b> in the $\text{MnO}_2$ oxidation of compound <b>II<sub>E</sub></b> . ....	87
<b>Figure 3-20</b> Time course of the changes in the recovery yield of compound <b>III<sub>H</sub></b> and yield of product <b>A<sub>H</sub>'</b> in the $\text{MnO}_2$ oxidation of compound <b>III<sub>H</sub></b> . ....	88
<b>Figure 3-21</b> Time course of the changes in the recovery yield of compound <b>III<sub>G</sub></b> and yield of product <b>A<sub>G</sub>'</b> in the $\text{MnO}_2$ oxidation of compound <b>III<sub>G</sub></b> . ....	89
<b>Figure 3-22</b> Time course of the changes in the recovery yield of compound <b>III<sub>s</sub></b> and yields of products <b>A<sub>s</sub>'</b> and <b>B<sub>s</sub></b> in the $\text{MnO}_2$ oxidation of compound <b>III<sub>s</sub></b> . ....	89
<b>Figure 3-23</b> Time course of the changes in the recovery yield of compound <b>III<sub>E</sub></b> and yield of product <b>A<sub>E</sub>'</b> in the $\text{MnO}_2$ oxidation of compound <b>III<sub>E</sub></b> . ....	90
<b>Figure 3-24</b> Three possible reaction modes in the $\text{MnO}_2$ oxidations of the benzyl alcohol analogues, compounds <b>II</b> and <b>III</b> . The former is representatively described although the latter also undergoes these modes. ....	91
<b>Figure 4-1</b> Non-phenolic $\text{C}_6\text{-C}_2$ -type monomeric lignin model compounds (the <b>H</b> -, <b>G</b> -, and <b>S</b> -types) and <i>p</i> -ethylphenyl type compounds (the <b>E</b> -types) employed in this chapter. ....	101
<b>Figure 4-2</b> Quantified reaction products and possible two without detection (product <b>B<sub>H</sub></b> and <b>B<sub>G</sub></b> ) in the $\text{MnO}_2$ oxidation. ....	103

<b>Figure 4-3</b> $^1\text{H}$ -NMR (top) and $^{13}\text{C}$ -NMR (bottom) spectra of compound <b>V<sub>H</sub></b> .	107
<b>Figure 4-4</b> $^1\text{H}$ -NMR (top) and $^{13}\text{C}$ -NMR (bottom) spectra of compound <b>V<sub>G</sub></b> .	108
<b>Figure 4-5</b> $^1\text{H}$ -NMR (top) and $^{13}\text{C}$ -NMR (bottom) spectra of compound <b>V<sub>S</sub></b> .	109
<b>Figure 4-6</b> $^1\text{H}$ -NMR (top) and $^{13}\text{C}$ -NMR (bottom) spectra of compound <b>V<sub>E</sub></b> .	110
<b>Figure 4-7</b> GC/MS spectra of synthesized model compounds employed in this chapter.	111
<b>Figure 4-8</b> Time course of the changes in the recovery yield of compound <b>IV<sub>H</sub></b> and yield of product <b>C<sub>H</sub></b> in the $\text{MnO}_2$ oxidation of compound <b>IV<sub>H</sub></b> .	116
<b>Figure 4-9</b> Time course of the changes in the recovery yield of compound <b>IV<sub>G</sub></b> and yield of product <b>C<sub>G</sub></b> in the $\text{MnO}_2$ oxidation of compound <b>IV<sub>G</sub></b> .	117
<b>Figure 4-10</b> Time course of the changes in the recovery yield of compound <b>IV<sub>S</sub></b> and yields of products <b>C<sub>S</sub></b> and <b>B<sub>S</sub></b> in the $\text{MnO}_2$ oxidation of compound <b>IV<sub>S</sub></b> .	117
<b>Figure 4-11</b> Time course of the changes in the recovery yield of compound <b>IV<sub>E</sub></b> and yield of product <b>C<sub>E</sub></b> in the $\text{MnO}_2$ oxidation of compound <b>IV<sub>E</sub></b> .	118
<b>Figure 4-12</b> Time course of the changes in the recovery yield of compound <b>V<sub>H</sub></b> and yield of product <b>C<sub>H</sub></b> in the $\text{MnO}_2$ oxidation of compound <b>V<sub>H</sub></b> .	120
<b>Figure 4-13</b> Time course of the changes in the recovery yield of compound <b>V<sub>G</sub></b> and yield of product <b>C<sub>G</sub></b> in the $\text{MnO}_2$ oxidation of compound <b>V<sub>G</sub></b> .	120
<b>Figure 4-14</b> Time course of the changes in the recovery yield of compound <b>V<sub>S</sub></b> and yields of products <b>C<sub>S</sub></b> and <b>B<sub>S</sub></b> in the $\text{MnO}_2$ oxidation of compound <b>V<sub>S</sub></b> .	121
<b>Figure 4-15</b> Time course of the changes in the recovery yield of compound <b>V<sub>E</sub></b> and yield of product <b>C<sub>E</sub></b> in the $\text{MnO}_2$ oxidation of compound <b>V<sub>E</sub></b> .	121
<b>Figure 4-16</b> Three possible reaction modes in the $\text{MnO}_2$ oxidations of the $\text{C}_6\text{-C}_2$ -type monomeric lignin model compounds <b>IV</b> and <b>V</b> . The former is representatively described although the latter also undergoes these modes.	122
<b>Figure 5-1</b> The <i>erythro</i> and <i>threo</i> stereostructures in the side-chain portion of the $\beta$ -O-4-type substructure of lignin.	129
<b>Figure 5-2</b> Chemical structures of the dimeric non-phenolic $\beta$ -O-4-type lignin model compounds employed in this chapter. <b>GGe</b> and <b>GGt</b> : the <i>erythro</i> and <i>threo</i> isomers, respectively, of 2-(2-methoxyphenoxy)-1-(3,4-dimethoxyphenyl)propane-1,3-diol; <b>SGe</b> and <b>SGt</b> : the <i>erythro</i> and <i>threo</i> isomers, respectively, of 2-(2-methoxyphenoxy)-1-(3,4,5-trimethoxyphenyl)propane-1,3-diol; <b>G'G</b> : 2-(2-methoxyphenoxy)-1-(3,4-dimethoxyphenyl)ethanol; <b>S'G</b> : 2-(2-methoxyphenoxy)-1-(3,4,5-trimethoxyphenyl)ethanol.	130

<b>Figure 5-3</b> Exclusive major reaction products from the A- and B-rings, and of dimer with the $\alpha$ -ketone.....	132
<b>Figure 5-4</b> Synthetic route of <b>SG</b> and <b>S'G</b> . Reagents and conditions were as follows: (1) Br <sub>2</sub> , C <sub>2</sub> H <sub>5</sub> OH, rt, (2) K <sub>2</sub> CO <sub>3</sub> , acetone, 40°C, (3) HCHO, THF, K <sub>2</sub> CO <sub>3</sub> , 35°C, (4) NaBH <sub>4</sub> , C <sub>2</sub> H <sub>5</sub> OH, rt, (5) EtOH solution containing K <sub>2</sub> B <sub>4</sub> O <sub>7</sub> , anion exchange chromatography, (6) NaBH <sub>4</sub> , C <sub>2</sub> H <sub>5</sub> OH, rt. ....	133
<b>Figure 5-5</b> Synthetic route of products <b>B<sub>1</sub></b> and <b>B<sub>2</sub></b> . Reagents and conditions were as follows: (1) NaOH, C <sub>2</sub> H <sub>5</sub> OH, reflux, (2) NaIO <sub>4</sub> , CH <sub>2</sub> Cl <sub>2</sub> , rt, (3) HCHO, THF, 35°C. ....	137
<b>Figure 5-6</b> <sup>1</sup> H-NMR (top) and <sup>13</sup> C-NMR (bottom) spectra of compound <b>SGe</b> .....	139
<b>Figure 5-7</b> <sup>1</sup> H-NMR (top) and <sup>13</sup> C-NMR (bottom) spectra of compound <b>SGt</b> . ....	140
<b>Figure 5-8</b> <sup>1</sup> H-NMR (top) and <sup>13</sup> C-NMR (bottom) spectra of compound <b>S'G</b> . ....	141
<b>Figure 5-9</b> <sup>1</sup> H-NMR (top) and <sup>13</sup> C-NMR (bottom) spectra of product <b>B<sub>1</sub></b> . ....	142
<b>Figure 5-10</b> <sup>1</sup> H-NMR (top) and <sup>13</sup> C-NMR (bottom) spectra of product <b>B<sub>2</sub></b> . ....	143
<b>Figure 5-11</b> GC/MS spectra of <b>B<sub>1</sub></b> and <b>B<sub>2</sub></b> .....	144
<b>Figure 5-12</b> Time course of the changes in the recovery yield of <b>GGe</b> and yields of products from A-ring (top) and B-ring (bottom) in the MnO <sub>2</sub> oxidation of <b>GGe</b> . ....	149
<b>Figure 5-13</b> Time course of the changes in the recovery yield of <b>GGt</b> and yields of products from A-ring (top) and B-ring (bottom) in the MnO <sub>2</sub> oxidation of <b>GGt</b> . ....	150
<b>Figure 5-14</b> Time course of the changes in the recovery yield of <b>G'G</b> and yields of products from A-ring (top) and B-ring (bottom) in the MnO <sub>2</sub> oxidation of <b>G'G</b> .....	151
<b>Figure 5-15</b> Time course of the changes in the recovery yield of <b>SGe</b> and yields of products from A-ring (top) and B-ring (bottom) in the MnO <sub>2</sub> oxidation of <b>SGe</b> . ....	152
<b>Figure 5-16</b> Time course of the changes in the recovery yield of <b>SGt</b> and yields of products from A-ring (top) and B-ring (bottom) in the MnO <sub>2</sub> oxidation of <b>SGt</b> .....	153
<b>Figure 5-17</b> Time course of the changes in the recovery yield of <b>S'G</b> and yields of products from A-ring (top) and B-ring (bottom) in the MnO <sub>2</sub> oxidation of <b>S'G</b> .....	154
<b>Figure 5-18</b> Exclusive major reaction products derived from the A-rings and side-chains of the lignin model compounds. ....	155
<b>Figure 5-19</b> Possible formation mechanisms for identified products <i>via</i> benzyl cation intermediates and aryl cation radicals in MnO <sub>2</sub> oxidation reactions of compounds <b>GG</b> and <b>SG</b> . ....	158
<b>Figure 5-20</b> Possible formation mechanisms for identified products <i>via</i> benzyl cation	

intermediates and aryl cation radicals in MnO <sub>2</sub> oxidation reactions of compounds <b>G'</b> <b>G</b> and <b>S'</b> <b>G</b> . .....	159
---	-----



# **1 Introduction**

## 1.1 Preface

Oxygen delignification has widely been applied as a prebleaching stage due to its environmental and economic benefits. However, severe degradation of the carbohydrates has still been a serious drawback in oxygen delignification. The delignification is therefore terminated when the kappa number reaches about half that of the original unbleached pulp. Although the chemistry of oxygen delignification has been extensively studied to suppress the severe degradation of carbohydrates,<sup>[1-38]</sup> this goal has not yet been achieved.

The degradation of carbohydrates in oxygen delignification is caused by active oxygen species, whose formations accompany the decomposition of peroxides produced by reactions of the phenolic substructure in lignin with  $O_2$ .<sup>[1,16-17,23,27]</sup> The decomposition of peroxides including  $H_2O_2$  thus affects the degradation of carbohydrates in oxygen delignification. It is well known that some metal ions affect the stability of  $H_2O_2$ , and efficiency of radical formation accompanying the decomposition of  $H_2O_2$  and consequently damage carbohydrates in hydrogen peroxide bleaching.<sup>[39-41]</sup>

$MnO_2$  catalyzes the decomposition of  $H_2O_2$  to  $H_2O$  and  $O_2$  without the formation of any active oxygen species (radicals). If  $MnO_2$  catalyzes the decomposition of not only  $H_2O_2$  but also organic peroxides, without radical formation, addition of  $MnO_2$  should suppress the degradation of carbohydrates in oxygen delignification. In fact, the addition of  $Mn^{2+}$ , which was converted *in-situ* to  $MnO_2$  by the  $O_2$  oxidation, to an alkaline aerobic treatment under oxygen delignification conditions suppressed the degradation of a carbohydrate model compound, methyl  $\beta$ -D-glucopyranoside (MGP), when MGP was co-treated with a phenolic compound, 2,4,6-trimethylphenol, and active oxygen species were generated by reactions of the phenolic compound with  $O_2$ .<sup>[22]</sup> The same addition suppressed the progress of oxidation of a dioxane-lignin isolated from an unbleached pulp.<sup>[24]</sup> These results suggest that the *in-situ* generated  $MnO_2$  catalyzes the decomposition of organic peroxides as well as  $H_2O_2$  produced in the system without formation of radicals, and has the potential to suppress the degradation

of carbohydrates in oxygen delignification.

Except for the catalytic property of  $\text{MnO}_2$ , another essential property of  $\text{MnO}_2$  is its high selectivity for the oxidation of allylic and benzylic alcohols over those of other types of alcohol under mildly acidic conditions.  $\text{MnO}_2$  can also be used as an oxidant to oxidize lignin model compounds.<sup>[42]</sup> Therefore, it is anticipated that a  $\text{MnO}_2$  delignification process under mildly acidic conditions where carbohydrates are not severely hydrolyzed can be achieved.

Besides,  $\text{MnO}_2$  is a recyclable chemical mainly due to its insolubility and oxidation-reduction interconversion with soluble  $\text{Mn}^{2+}$ . This property gives it a potential to be an economically and environmentally friendly chemical for pulp bleaching and lignin oxidation. However, the catalytic activity of  $\text{MnO}_2$  in oxygen-alkali bleaching and its potential delignification ability are still confusing.

## 1.2 Oxygen-alkali bleaching

### 1.2.1 Reactivity of molecular oxygen

Molecular oxygen is triplet in its ground state and has the property of biradical. Because the ground state of oxygen is triplet with unpaired electrons and unparallel spins, it has low reactivity with most organic substrates. Active oxygen species generated during oxidation have higher oxidation potentials than molecular oxygen in the ground state. **Figure 1-1** illustrates the process of four one-electron transfer steps and two two-electron transfer steps of molecular oxygen reduced to water.<sup>[43-44]</sup> Reduced oxygen species generated by reduction of molecular oxygen are shown in **Table 1-1**. Superoxide anion radical,  $\text{O}_2^{\cdot-}$ , and its conjugate acid, hydroperoxyl radical,  $\text{HOO}^{\cdot}$ , have reactivity significantly affected by reaction conditions. Under common conditions of oxygen bleaching (alkaline),  $\text{O}_2^{\cdot-}$  is mainly generated.<sup>[15,45]</sup> It has been known that a small amount of  $\text{H}_2\text{O}_2$  is formed in an oxygen-alkali bleaching system. In the presence of some transition metals,  $\text{H}_2\text{O}_2$  can decompose to generate hydroxyl radical,  $\text{HO}^{\cdot}$ .<sup>[15]</sup>  $\text{HO}^{\cdot}$  has strong reactivity generated in oxygen bleaching, which can react not only lignin but also carbohydrates through the processes of hydrogen abstraction,

one-electron oxidation, electrophilic addition, radical coupling reaction, *etc.*<sup>[46]</sup> Under strong alkaline condition, its conjugate base,  $O_2^{\bullet-}$ , is the main form of existence.

**Table 1-1** Reactive species generated in oxygen bleaching.

Reduced oxygen species	Conjugate base
Hydroperoxyl radical ( $HOO\bullet$ )	Superoxide anion radical ( $O_2^{\bullet-}$ )
Hydrogen peroxide ( $H_2O_2$ )	Hydroperoxide anion ( $HOO^-$ )
Hydroxyl radical ( $HO\bullet$ )	Oxyl anion radical ( $O^{\bullet-}$ )

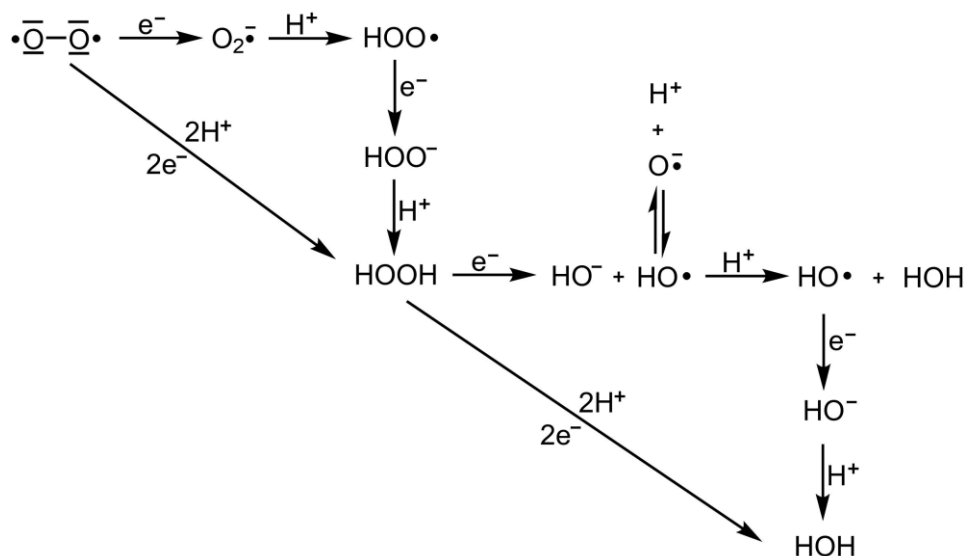


**Figure 1-1** Four one-electron transfer steps and two-electron transfer steps of stepwise reduction of oxygen.

### 1.2.2 Degradation of lignin under oxygen-alkali conditions

The chemistry of oxygen delignification is quite complicated due to the complexity of lignin structure and different oxygen-relating species generated during oxygen bleaching. During alkaline or kraft pulping, new phenolic structures are formed from the cleavage of aryl ether bonds of lignin in wood or non-wood raw materials.<sup>[47]</sup> Phenolic groups in the residual lignin of pulp, the only reaction site in the lignin for molecular oxygen, play an important role in oxygen delignification and are consumed in the oxygen-alkali bleaching process. Reactions between lignin phenolic substructures and oxygen have become the subject of many studies.<sup>[2,48-49]</sup> The detailed degradation pathways and reaction kinetics have been clarified in

oxygen-alkali treatments. The initial reaction steps in the autoxidation of these structures, i.e. conversion into phenoxy radicals and addition of the oxidant to the mesomeric forms of these radicals are shown in **Figure 1-2**.<sup>[3]</sup> However, due to the diradical nature of oxygen, the immediate addition product is a peroxy radical (not shown) which abstracts a further electron from phenolate ions and converts into a peroxide anion. The peroxide anion attacks the carbonyl carbon or a vinylogous carbon in the cyclohexadienone or quinone methide intermediates in an intramolecular nucleophilic reaction giving rise to four-membered cyclic peroxides (dioxetanes) (**Figure 1-3**).<sup>[2-3,49]</sup> These finally rearrange resulting in the formation of oxirane structures (uppermost part), cleavage of the originally aromatic nucleus (middle part) or fragmentation by cleavage of the C $_{\alpha}$ -C $_{\beta}$  bond (lowest part).<sup>[3]</sup>

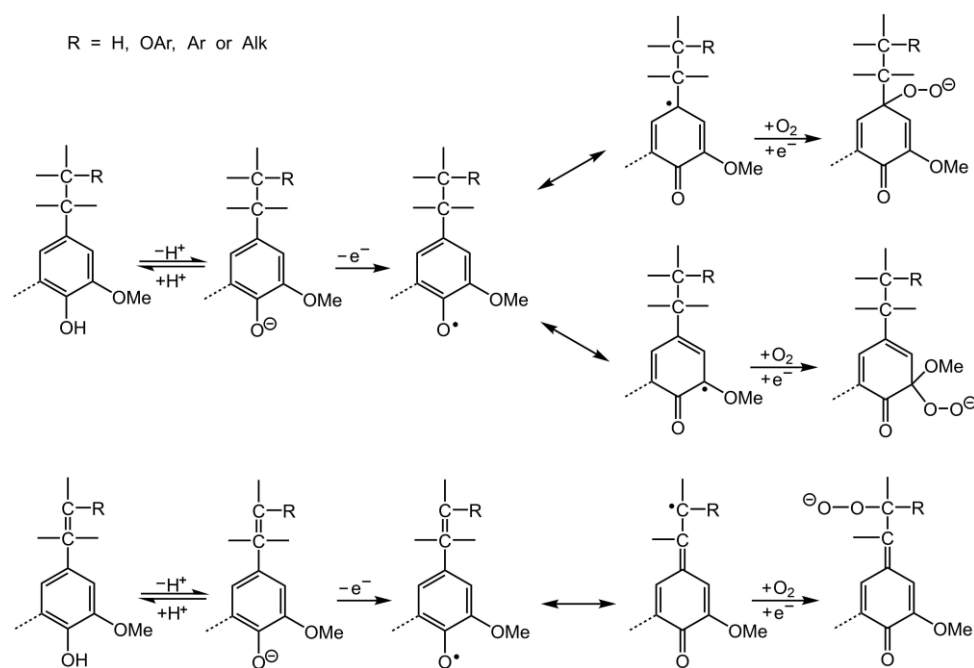


**Figure 1-2** Alkaline autoxidation of phenolic units to give hydroperoxide intermediates.<sup>[3]</sup>

As for the reactions of non-phenolic units under oxygen-alkali bleaching conditions, these units are oxidized through one-electron oxidation by active oxygen species and subsequent oxidation by active oxygen species or molecular oxygen. Hydroxyl radical (HO•), an active oxygen species, has a very strong oxidizing ability produced by the reductive

decomposition of hydroperoxides.  $\text{HO}\cdot$  exhibits electrophilic property and reacts with not only phenolic units but also non-phenolic units.<sup>[12,14,18-19,26]</sup> Under oxygen-alkali bleaching conditions, it not only tends to attack aromatics in lignin but also attacks the side-chain structure of lignin. **Figure 1-4** illustrates representative reaction schemes.  $\text{HO}\cdot$  initially attaches to the  $\pi$ -electron system of the aromatic ring to form a hydroxycyclohexadienyl radical, and then to form a hydroxyl group on the aromatic ring accompanied by further reactions.  $\text{HO}\cdot$  can also initially attach to the  $\pi$ -electron system, followed by a rearrangement effect, and eventually lead to a side-chain reaction of lignin. The side-chain reactions that  $\text{HO}\cdot$  directly reacts with are also listed in **Figure 1-4**. However, under strong alkalinity system ( $\text{pH} > 12$ ), the  $\text{HO}\cdot$  converts into its conjugate base, oxyl anion radical ( $\text{O}\cdot^-$ ), which also has a strong oxidizing ability, but the reactivity of  $\text{O}\cdot^-$  toward aromatic ring is lower than  $\text{HO}\cdot$  due to carrying the negative charge. In addition to  $\text{HO}\cdot$  and  $\text{O}\cdot^-$ , some other active oxygen species can also react with non-phenolic lignin units under oxygen-alkali bleaching conditions.

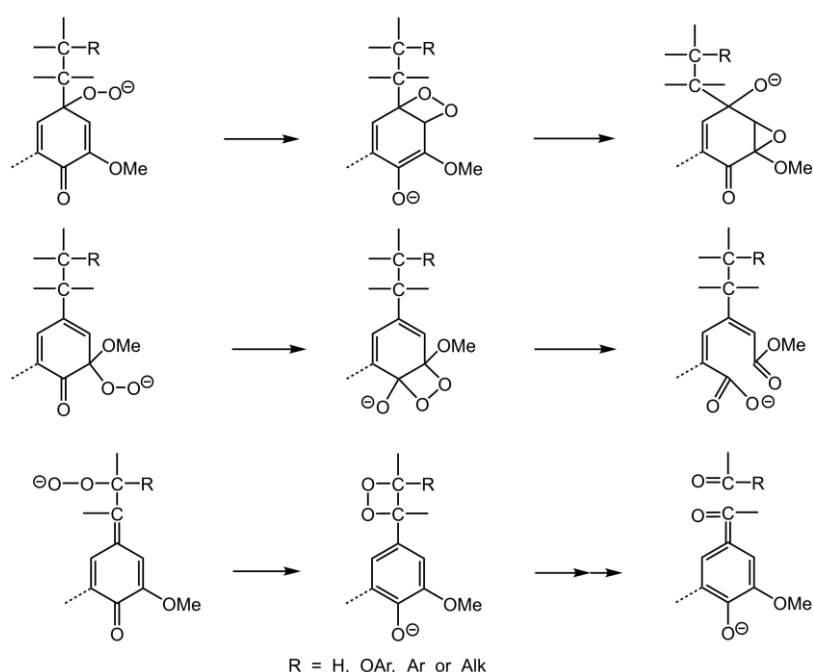
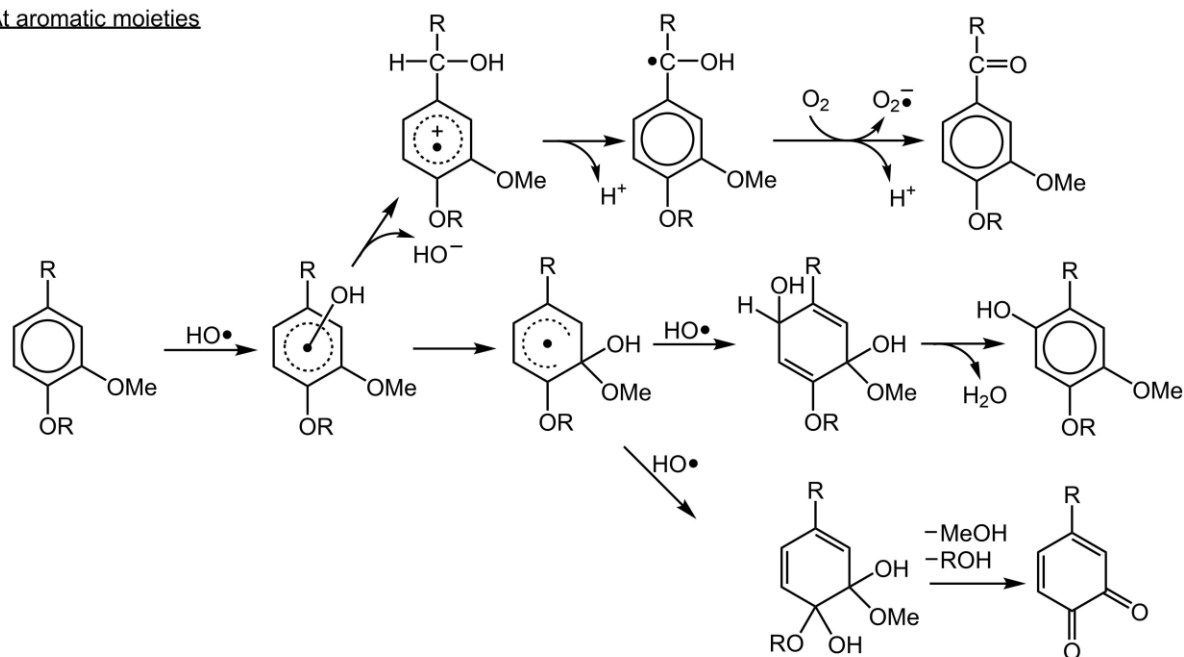


**Figure 1-3** Intramolecular nucleophilic attack by peroxide anions to give, *via* dioxetane intermediates, oxirane-, muconic acid- and carbonyl structures.<sup>[3]</sup>

At aromatic moieties



At side-chain structure

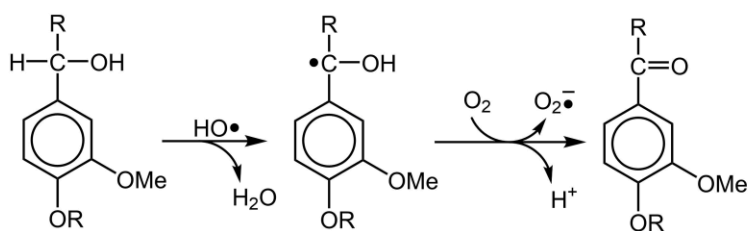


**Figure 1-4** The oxidation of non-phenolic lignin units with  $\text{HO}\cdot$  under alkaline bleaching conditions.

### 1.2.3 Degradation of carbohydrates under oxygen-alkali conditions

There are three main reaction categories in the degradation of carbohydrates under oxygen-alkali bleaching conditions. The first is the oxidative degradation reaction by active oxygen species under alkaline conditions. The second is the alkaline-promoted reactions involving the peeling reaction and alkaline hydrolysis reaction. The third is the oxidation of the reducing end groups by molecular oxygen involving the production of aldonic acid end groups.<sup>[50-52]</sup>

In carbohydrates,  $\text{HO}\cdot$  abstracts hydrogen atom from C-2 or C-3 position of cellulose and hemicellulose under oxygen-alkali conditions followed by the oxygenation of a carbon-centered radical and the liberation of  $\text{O}_2\cdot^-$  to form a carbonyl group, as shown in **Figure 1-5**.

Then, the structure of the carbonyl group and the enol will be exchanged, and then the  $\beta$ -elimination reaction promoted by the alkali will occur, resulting in the cleavage of the glycosidic bond and the viscosity and strength of the pulp will decrease. The peeling reaction of carbohydrates starts from their reducing end groups. **Figure 1-6** shows the reaction paths of the peeling reaction. The reaction stops by forming a stable carboxylic acid group through the stopping reaction. Peeling reaction occurs not only in the absence the oxygen but also in the presence of oxygen. Fortunately, the peeling reaction is suppressed under oxygen-alkali bleaching conditions, because the reducing end groups of carbohydrates are rapidly oxidized to aldonic acid end groups during oxygen-alkali bleaching, and the yield of pulp bleaching is improved by this conversion.

It should be noted that some metals have effects on the degradation of carbohydrates during oxygen-alkali bleaching.<sup>[53-59]</sup> Metals mainly existing in pulp are iron, copper, manganese, and magnesium. However, the effects of these metals on suppression or promotion of cellulose degradation under oxygen-alkali bleaching conditions are still confusing. It seems that the addition of excess amount of magnesium can suppress the degradation of cellulose during oxygen-alkali bleaching, which is the only acceptable result.<sup>[53-54,59]</sup> Manganese is one of the transition metals that commonly exist in pulp. The role of manganese in pulp oxygen-alkali bleaching process is also confusing. Some researchers reported that the addition promotes the degradation of cellulose,<sup>[58]</sup> while some researchers reported that it suppresses the degradation of cellulose.<sup>[57]</sup>

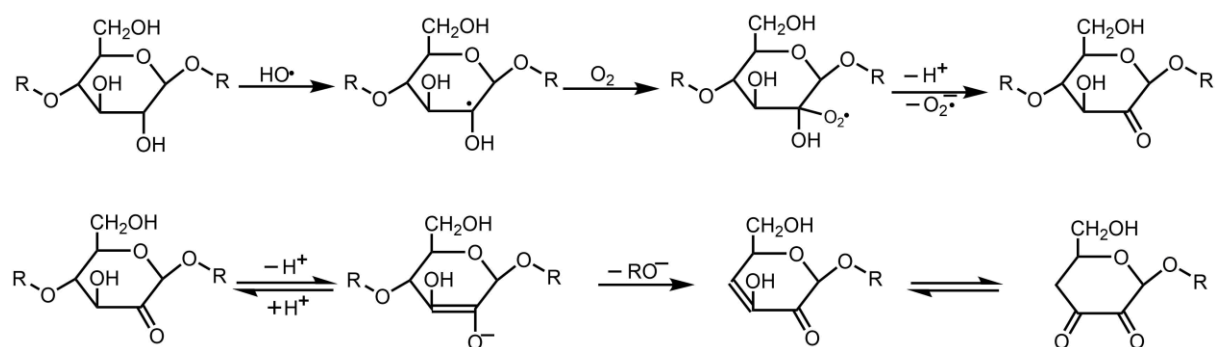


**Figure 1-5** Oxidation of secondary alcohol groups of cellulose,  $\beta$ -elimination reaction of

cellulose and oxidation of ketone alcohol.

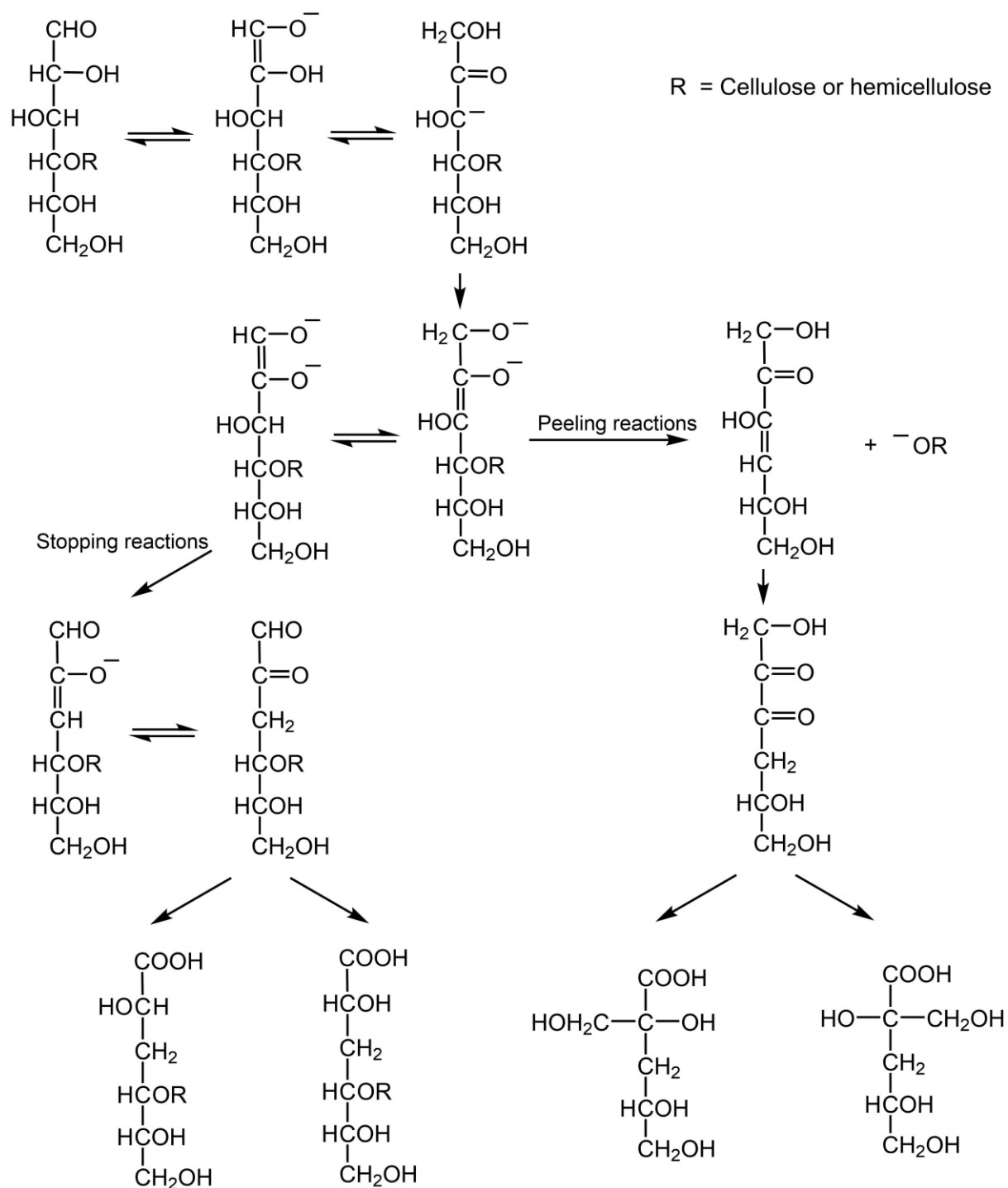


**Figure 1-6** Peeling and stopping reactions of carbohydrates.

## 1.3 Primary considerations of MnO<sub>2</sub> oxidation

### 1.3.1 Manganese chemistry

Manganese is the second most abundant transition metal on Earth next to iron in content and is similar to iron in some aspects of its geochemistry. Like iron, manganese exists in many valence states in nature and is an essential micronutrient for most organisms. Among the various oxidation states of Mn, +II, +III and +IV are the most common in nature (**Figure 1-7**).<sup>[60]</sup>

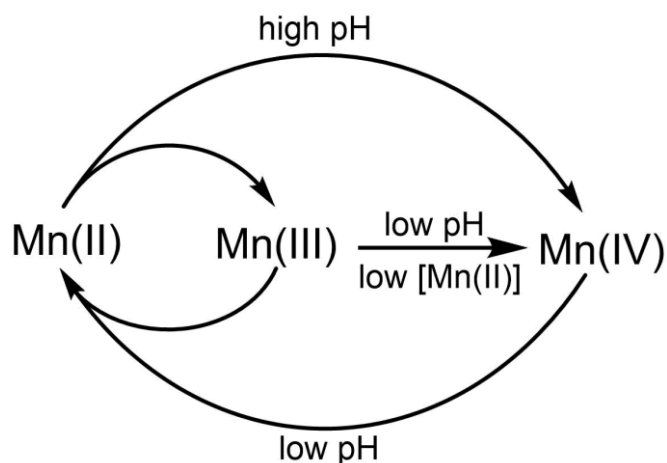
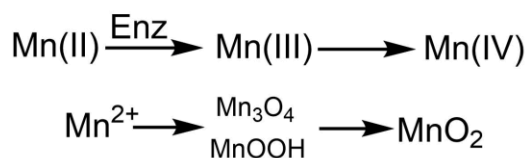


**Figure 1-7** The Mn cycle of oxidation states found in nature. Mn(II) is thermodynamically stable in the absence of O<sub>2</sub> and at low pH, whereas in the presence of O<sub>2</sub>, Mn(III) and Mn(IV), which occur primarily as insoluble Mn (oxyhydr)oxides, are favored.<sup>[60]</sup>

Generally, under anaerobic and low pH conditions, Mn(II) is thermodynamically favored, while Mn(III) and Mn(IV) are thermodynamically favored under aerobic and high pH conditions. Mn(II) usually exists in the form of cations (Mn<sup>2+</sup>) in solution; it can form insoluble phosphate or carbonate; it also exists in other minerals as a minor component. Under aerobic conditions, the concentration of Mn<sup>2+</sup> in natural water may be as high as millimolar. Because of the high activation energy, the oxidation of Mn(II) to Mn(III) and Mn(IV) is largely catalyzed by microorganisms in nature.<sup>[60]</sup> Mn(III) is thermodynamically unstable and disproportionation occurs in aqueous media to form Mn(II) and Mn(IV). Mn(III) only exists in certain organic complexes and certain minerals. Mn(IV) usually exists in the

form of insoluble oxides, oxyhydroxides, and hydroxides, and contains different contents of Mn(III), which are important components of soil and minerals. Mn(III) and Mn(IV) are also commonly found in natural minerals in the form of ferromanganese (oxyhydr) oxide minerals. Mn(III)/Mn(II) and Mn(IV)/Mn(II) couples have particularly high redox potential. Mn(III) and Mn(IV) become strong oxidants in the environment and coexist with many other minerals in reduced states.

#### Solid Phase Intermediate



#### Enzyme-bound Intermediate

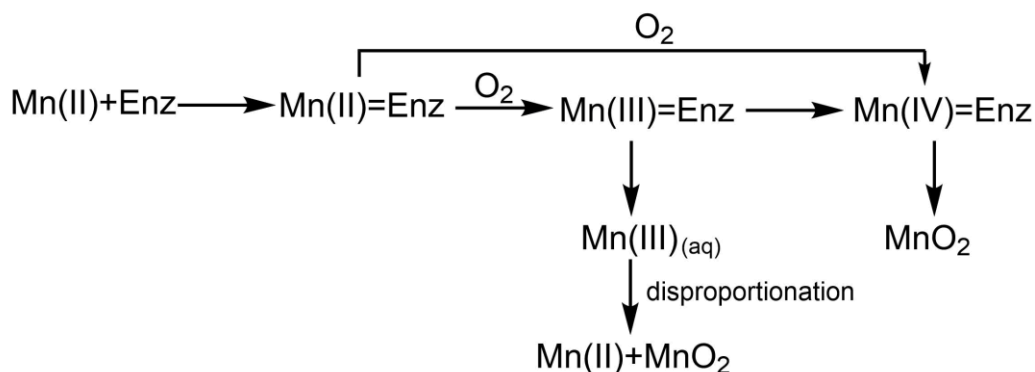


**Figure 1-8** Possible mechanisms of bacterial Mn(II) oxidation.<sup>[60]</sup>

### 1.3.2 Chemical properties of MnO<sub>2</sub>

Manganese dioxide has more than 30 different crystal structures in natural minerals, and it is difficult to determine the structure, and the physical and chemical properties are also different.<sup>[61]</sup> The MnO<sub>2</sub> frame is composed of [MnO<sub>6</sub>] octahedrons sharing corners and edges, and can form a one-dimensional, two-dimensional or three-dimensional (1D, 2D or 3D, respectively) structure.<sup>[62-63]</sup> Existing studies have shown that under different synthesis

conditions, the structures of  $\text{MnO}_2$  are also different (i.e.,  $\alpha$ ,  $\beta$ ,  $\gamma$ ,  $\delta$ ,  $\epsilon$ , and  $\lambda$ )<sup>[64]</sup>. Representative structures of  $\text{MnO}_2$  are shown in **Figure 1-9**.<sup>[65]</sup> Among them,  $\alpha$ -,  $\beta$ - and  $\gamma$ - $\text{MnO}_2$  have a 1D chain structure, while  $\delta$ - $\text{MnO}_2$  and  $\lambda$ - $\text{MnO}_2$  have a 2D layered structure and a 3D structure, respectively. Besides, manganese dioxide under different synthesis conditions will also show different morphologies, such as urchin-, rod-, and flower-like morphologies.<sup>[66]</sup>

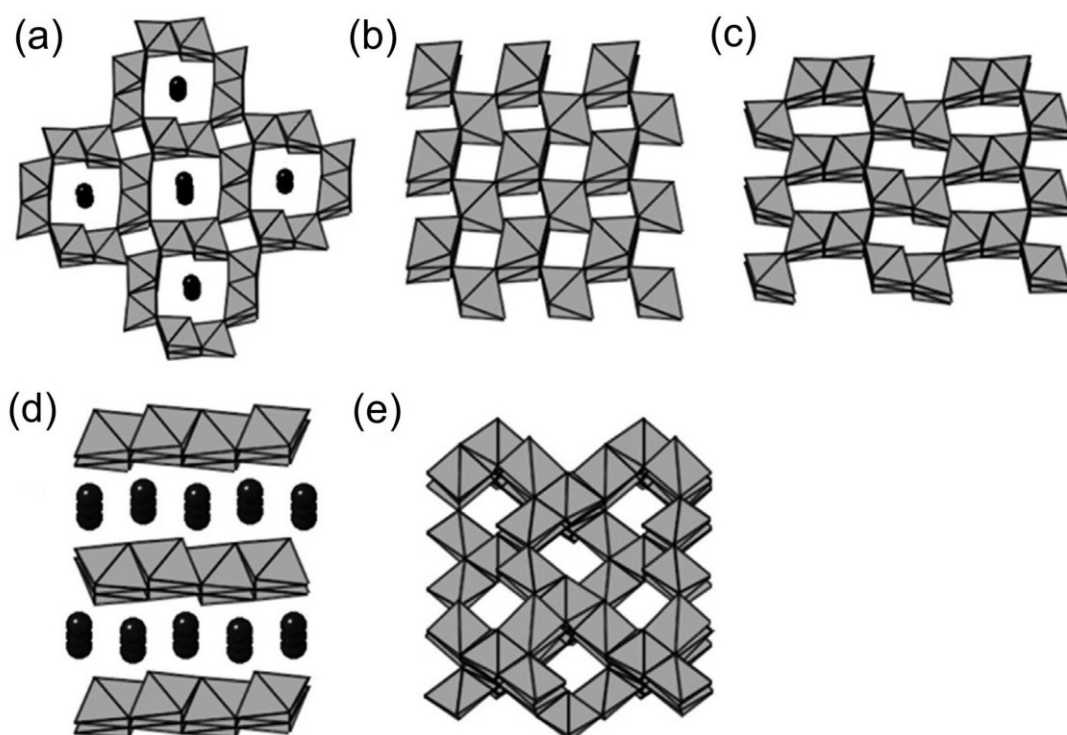


**Figure 1-9** Manganese oxides with different chemical composition and crystal structure: (a)  $\alpha$ - $\text{MnO}_2$ , (b)  $\beta$ - $\text{MnO}_2$ , (c)  $\gamma$ - $\text{MnO}_2$ , (d)  $\delta$ - $\text{MnO}_2$ , (e)  $\lambda$ - $\text{MnO}_2$ .

### 1.3.3 Chemistry of $\text{MnO}_2$ oxidation

#### 1.3.3.1 General<sup>[67-75]</sup>

In the 1940s, Ball *et al.* needed to oxidize vitamin A to the corresponding aldehyde to study the preparation of retinene (**Figure 1-10**).<sup>[67]</sup> When  $\text{KMnO}_4$  was used as an oxidant to prepare aldehydes, it had a relatively low yield.<sup>[67]</sup> Therefore, the researchers began to explore the experimental conditions to get the best yield. Afterward, good results can be obtained

when using a dark precipitate formed by the decomposition of  $\text{KMnO}_4$  in the dark in the aqueous solution. This dark precipitate is  $\text{MnO}_2$ . It was discovered that vitamin A could be oxidized by shaking in light petroleum solution in the presence of excessive suspended  $\text{MnO}_2$ . Different  $\text{MnO}_2$  can exhibit very diverse oxidation effects. Fortunately, they prepared  $\text{MnO}_2$  in a very active form by a mixed aqueous solution of  $\text{MnCl}_2$  and  $\text{KMnO}_4$ .<sup>[68]</sup> Subsequently,  $\text{MnO}_2$  is widely used as standard oxidant for the transformation of allylic and benzylic alcohols into aldehydes and ketones.<sup>[69]</sup> One important property of  $\text{MnO}_2$  is its high selectivity for oxidation of allylic and benzylic alcohols versus saturated alcohols when it is not employed at a high temperature, although  $\text{MnO}_2$  can also oxidize saturated alcohols under prolonged heating.<sup>[70]</sup>

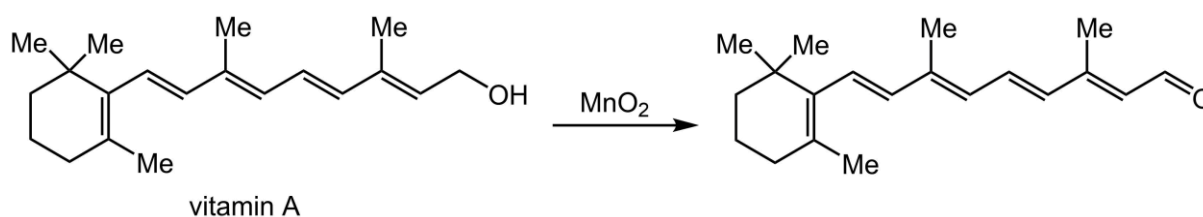


**Figure 1-10** Oxidation reaction of vitamin A to corresponding aldehyde.

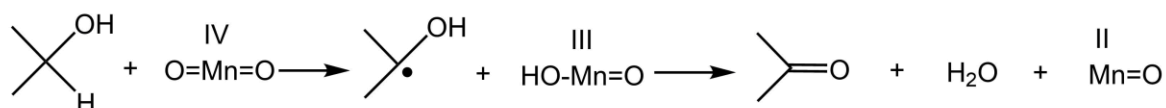
There are many difficulties in studying the  $\text{MnO}_2$  mechanisms of oxidizing alcohols, including: first, the heterogeneity of the reaction, and second, the oxidizing ability of  $\text{MnO}_2$  samples obtained by different synthesis methods is different. In addition, when oxidizing allylic alcohols with excess  $\text{MnO}_2$  at room temperature, there is no absolute certainty about the chemical properties of the real reagent. Excessive  $\text{MnO}_2$  must be used in the reaction process, thereby increasing the possibility of impurities as oxidants participating in the reaction. In addition, when using  $\text{MnO}_2$  with a water content of 4% to 8%,<sup>[69]</sup> a higher reaction rate and yield can be obtained, and  $\text{MnO}_2$  samples containing a large amount of impurities may also have higher activity.<sup>[71]</sup>

The experimental facts of studying the oxidation mechanism of  $\text{MnO}_2$  confirmed that the alcohol complex on the surface of the  $\text{MnO}_2$  particles could be formed followed by oxidation

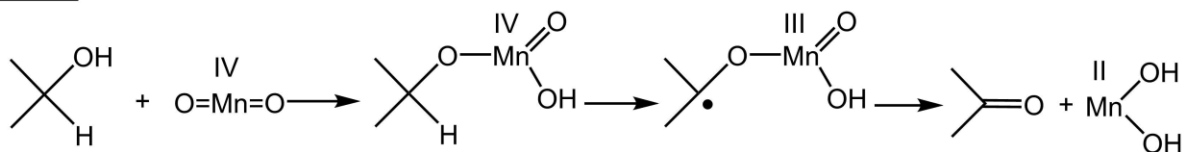
and desorption of carbonyl compounds.<sup>[67,71]</sup> This phenomenon explains that the oxidations of allylic and benzylic alcohols are best to choose apolar solvents without competing with alcohols for adsorption on MnO<sub>2</sub> particles.

The three possible reaction mechanisms of MnO<sub>2</sub> oxidation of alcohol to aldehyde are shown in **Figure 1-11**. They are the reaction mechanism *via* radicals (Mode A),<sup>[72]</sup> the formation of manganese ether intermediates (Mode B), and the hydrogen transfer mechanism by way of a cyclic five-membered transition state (Mode C).<sup>[73-74]</sup>

#### Model A



#### Model B



#### Model C

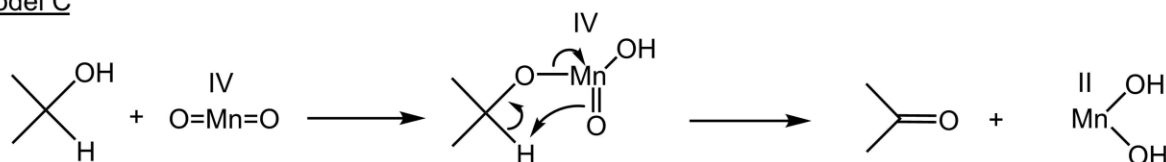


**Figure 1-11** The mechanisms of oxidation of alcohols with MnO<sub>2</sub>.

#### 1.3.3.2 General procedure for selective oxidation of alcohols with MnO<sub>2</sub><sup>[75-78]</sup>

The reaction is usually carried out at room temperature, and alcohol is dissolved in a dry organic solvent. The reaction usually requires adding 6-50 equivalents of active MnO<sub>2</sub> and shaking vigorously until most of the unsaturated alcohol is oxidized. The excess MnO<sub>2</sub> was filtered using filter paper, the reaction mixture was washed with the used organic solvent and concentrated the collected organic phase.

The precise amount of water contained in the reaction solvent can increase the reactivity of active  $\text{MnO}_2$ . It should be noted that adding excess water to the solvent may cause the deactivation of  $\text{MnO}_2$ . Using apolar organic solvents is easy to get the best results because the solvent will not compete with the reactants for adsorption on the  $\text{MnO}_2$  particles. Petroleum ether, pentane, hexane, or cyclohexane are commonly used apolar organic solvents. However, because these solvents have low solubility for organic compounds, the oxidation of unsaturated alcohols in practical applications is usually carried out in  $\text{CH}_2\text{Cl}_2$  or chloroform, because these solvents can achieve a balance between solubility and apolarity. Although increasing the reaction temperature can shorten the reaction time, it is not recommended to increase the temperature above room temperature, because aliphatic alcohols may be oxidized by  $\text{MnO}_2$  under conditions higher than room temperature. Generally, the reaction requires 1–70 hours. In the oxidation of hindered allylic and benzyl alcohols, a longer reaction time is required. Benzylic alcohols tend to require a longer oxidation time than allylic alcohols. The reaction mixture must be shaken vigorously to reach the maximum reaction rate.

Representative examples of the selective oxidation of unsaturated alcohols by  $\text{MnO}_2$  are shown in **Figure 1-12**. Example 1 is an allylic alcohol regioselectivity oxidized with active  $\text{MnO}_2$  at room temperature in the presence of two saturated alcohols.<sup>[76]</sup> In example 2, a primary allylic alcohol is oxidized in the presence of secondary benzyl alcohol and a primary saturated alcohol.<sup>[77]</sup> Relative to benzylic alcohol, the selectivity of allylic alcohol oxidation is due to steric factors, and active  $\text{MnO}_2$  tends to oxidize allylic alcohols faster than benzylic alcohols. Example 3 is the selective oxidation of secondary benzylic alcohol by active  $\text{MnO}_2$  in the presence of aliphatic primary alcohol and free phenol.<sup>[78]</sup>

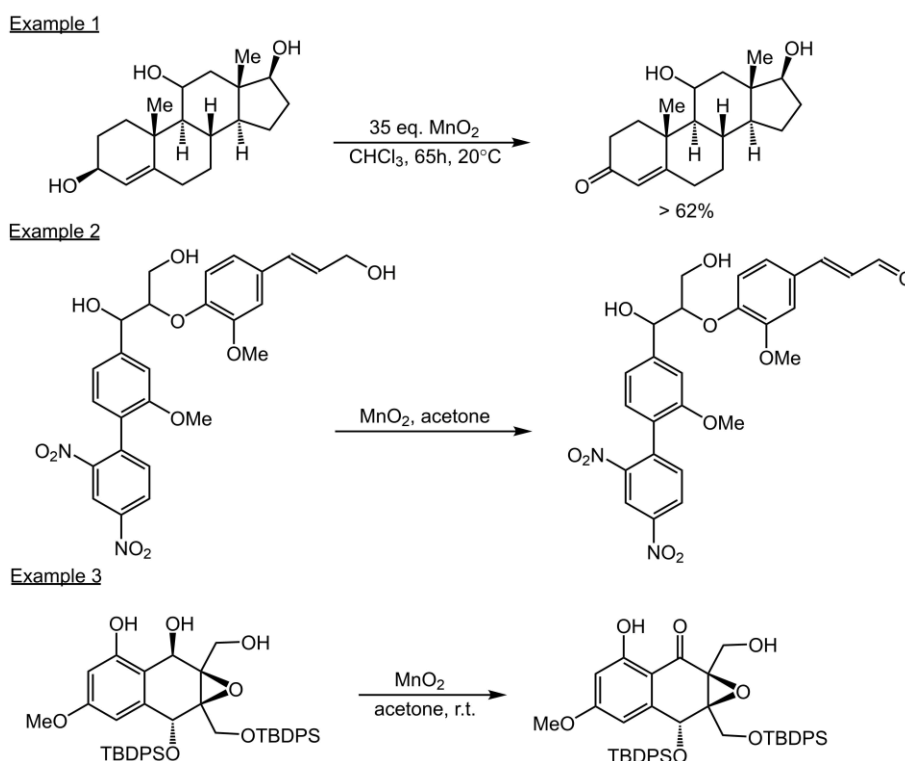


**Figure 1-12** Representative reactions of selective oxidation of unsaturated alcohols by  $\text{MnO}_2$ .

### 1.3.3.3 Functional group sensitivity to oxidation with $\text{MnO}_2$ <sup>[75,79-81]</sup>

Undoubtedly, the oxidation capacity of active  $\text{MnO}_2$  depends largely on temperature. Therefore, at high temperatures, active  $\text{MnO}_2$  behaves as a very strong oxidant but has no obvious selectivity. It should be emphasized that only when used at room temperature, it has high selectivity to the oxidation of allylic and benzylic alcohols. Many studies show that  $\text{MnO}_2$  can oxidize many functional groups, including amines and alkenes. When the reaction temperature is not high,  $\text{MnO}_2$  can selectively oxidize allylic and benzylic alcohols without affecting most other functional groups.

The order of the reactivity of  $\text{MnO}_2$  oxidation of amines is as follows: primary > secondary > tertiary amine. Therefore, usually, tertiary amines do not interfere with the selective oxidation of allylic and benzylic alcohols unless the alcohols are very hindered. Secondary amines commonly do not interfere with the selective oxidation of allylic and benzylic alcohols by  $\text{MnO}_2$ , although some cases show that secondary amines can be selectively oxidized by active  $\text{MnO}_2$  in the presence of these alcohols.

Example 1 in **Figure 1-13** is an interesting example. Due to the tendency of aniline to aromatize to indole, the secondary amine is more sensitive than the benzylic alcohol under  $\text{MnO}_2$  oxidation conditions in this reaction.<sup>[79]</sup> In example 2, two benzylic alcohols are selectively oxidized by active  $\text{MnO}_2$  in the presence of two secondary amines to generate dialdehydes. The selective oxidation of allylic or benzylic alcohols with active  $\text{MnO}_2$  in the presence of primary amines has rarely been published.<sup>[80]</sup> Example 3 is an example of successful selective oxidation involving primary aromatic amine with electron-poor ring. This is a case of selective oxidation of alcohol involves primary amine that possesses less sensitive to oxidation.<sup>[81]</sup>

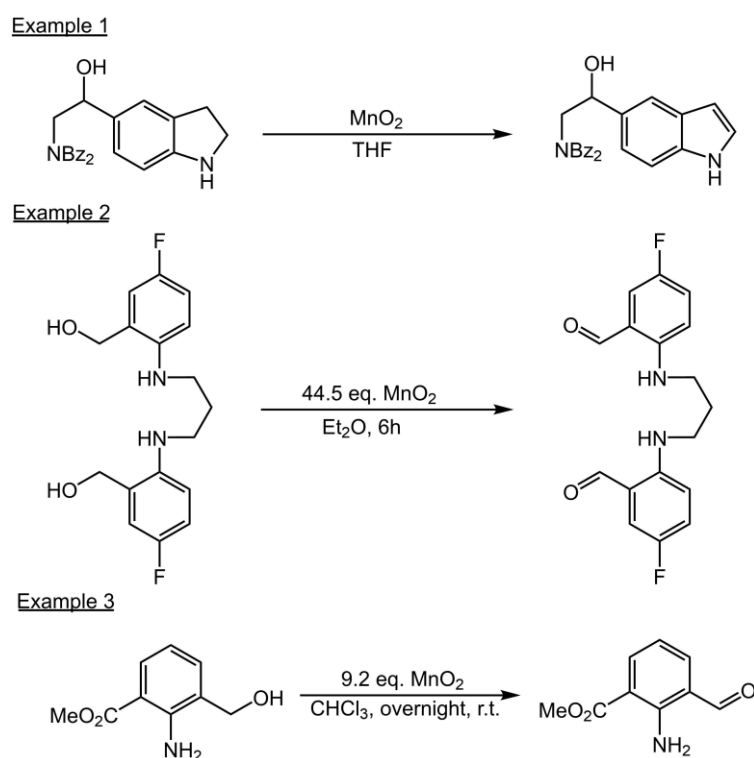


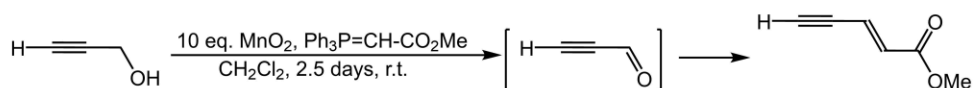
**Figure 1-13** Representative reactions of unsaturated alcohols with functional group sensitivity to oxidation with  $\text{MnO}_2$ .

#### 1.3.3.4 Reactions performed *in-situ* during oxidations with $\text{MnO}_2$ <sup>[75,82-84]</sup>

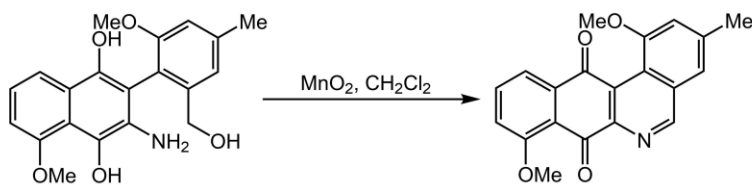
Since  $\text{MnO}_2$  is a mild oxidant, it is possible that the aldehydes and ketones obtained by oxidation of  $\text{MnO}_2$  can undergo subsequent reactions in the same tank. The aldehyde obtained

using  $\text{MnO}_2$  in example 1 in **Figures 1-14** can react with stabilized phosphoranes *in-situ*.<sup>[82]</sup> The process avoids the need to isolate propynal, which is a lachrymator. Similarly, they also found that allylic, propargylic and benzylic primary alcohols can also be directly converted into unsaturated esters in one pot by the oxidation of active  $\text{MnO}_2$ . Moreover, during the oxidation of active  $\text{MnO}_2$  to form aldehydes or ketones, there may also exist intramolecular condensation reactions of amines. Example 2 illustrates the selective oxidation of benzylic alcohol by  $\text{MnO}_2$  in the presence of primary amine.<sup>[83]</sup> The amine condenses intramolecularly with the aldehyde resulting from  $\text{MnO}_2$  oxidation, leading to the formation of an imine. Furthermore,  $\text{MnO}_2$  oxidizes a hydroquinone to generate *p*-benzoquinone. Example 3 is an effective scheme for the oxidation of aldehydes to esters.<sup>[84]</sup> Treatment of unsaturated aldehydes with a mixture of  $\text{NaCN}$  and  $\text{MnO}_2$  in the  $\text{AcOH-MeOH}$  system resulted in the initial formation of cyanohydrin, which was further oxidized with active  $\text{MnO}_2$  to acyl cyanide, and then further hydrolyzed to form methyl ether.

**Example 1**



**Example 2**



**Example 3**

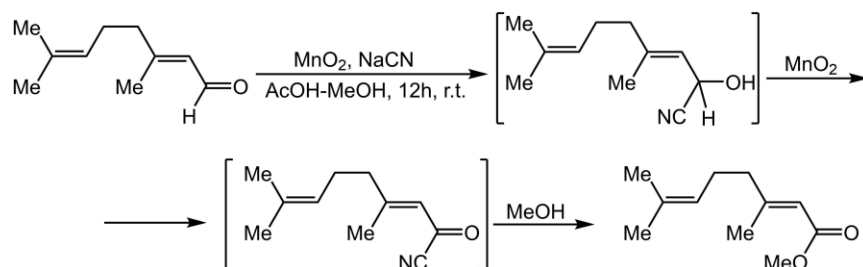
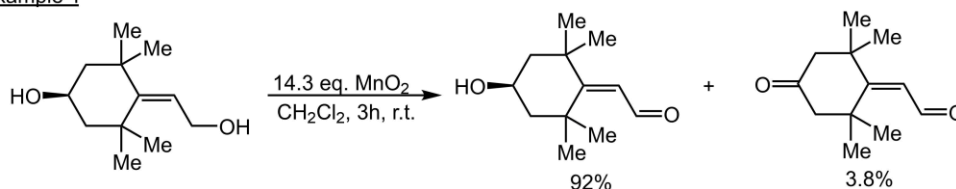


**Figure 1-14** Representative reactions of unsaturated alcohols performed *in-situ* during oxidations with  $\text{MnO}_2$ .

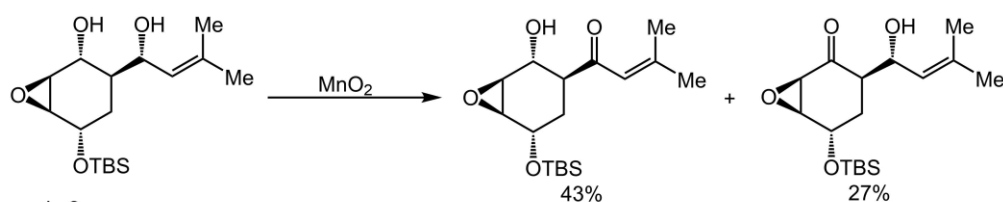
### 1.3.3.5 Side reactions<sup>[75,85-87]</sup>

Although the active  $\text{MnO}_2$  has higher selectivity for unsaturated alcohols than saturated alcohols under mild conditions, sometimes saturated alcohols are oxidized to produce a small amount of aldehydes or ketones. Example 1 in **Figures 1-15**,  $\text{MnO}_2$  selectively oxidizes allylic alcohol, and a small amount of the product from oxidation with saturated alcohol is also obtained.<sup>[85]</sup> In example 2, due to the steric hindrance at the allylic alcohol position, 27% of the aliphatic alcohol oxidation product was finally obtained. Sometimes, enones obtained by the oxidation of allylic alcohols with active  $\text{MnO}_2$  will be subjected to intramolecular conjugated addition from alcohols positioned inside the same molecule.<sup>[86]</sup> Example 3 is to oxidize diol with active  $\text{MnO}_2$ , and the intramolecular conjugate addition reaction occurs.<sup>[87]</sup> The main reaction pathway is the selective oxidation of allylic alcohol. The yield of the product obtained by oxidation of both alcohols is 10-20%, and the intramolecular attack of an alcohol on enone will produce 5% of a product.

Example 1



Example 2



Example 3

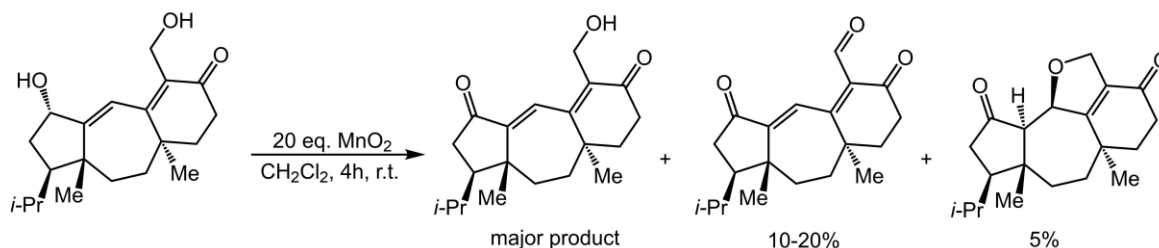


**Figure 1-15** Representative side reactions of unsaturated alcohols during oxidations with  $\text{MnO}_2$ .

## 1.4 Objectives in this study

MnO<sub>2</sub> is stable under alkaline conditions and exists as precipitates. It has the potential to catalyze decomposition of H<sub>2</sub>O<sub>2</sub> and organic peroxides to oxygen and water, and oxygen and alcohols, respectively, without the generation of active oxygen species under oxygen-alkali bleaching conditions, thereby inhibiting the decrease in pulp viscosity caused by the reaction of active oxygen species with carbohydrates, as described in the previous sections. On the other hand, it is commonly reduced to Mn<sup>2+</sup> under acidic conditions to oxidize allylic or benzylic alcohols. Because lignin contains benzylic hydroxy groups, MnO<sub>2</sub> is expected to work as an oxidant of lignin under acidic conditions. However, the catalytic activity of MnO<sub>2</sub> in oxygen delignification and its potential as a delignification agent have still been unclear. In this study, MnO<sub>2</sub> was added to prebleaching (oxygen delignification) stage to examine whether or not the addition suppressed the degradation of carbohydrates, or utilized in prebleaching stage as an oxidative delignification agent to examine whether or not MnO<sub>2</sub> oxidatively delignified unbleached kraft pulp. The mechanism of MnO<sub>2</sub> oxidation was furthermore examined in detail by employing non-phenolic lignin model compounds.

Therefore, targets of this work are as follows.

1. To investigate the utilization of MnO<sub>2</sub> as a pulp bleaching agent during oxygen-alkali bleaching, and as an oxidant to oxidize residual lignin in pulp. (Chapter 2)
2. To investigate the differences in the mechanisms of MnO<sub>2</sub> oxidation between C<sub>6</sub>-C<sub>1</sub>-type monomeric lignin model compounds with the *p*-hydroxyphenyl, guaiacyl, and syringyl nuclei. (Chapter 3)
3. To further investigate the oxidation mechanisms of MnO<sub>2</sub> by using C<sub>6</sub>-C<sub>2</sub>-type monomeric lignin model compounds with *p*-hydroxyphenyl, guaiacyl and syringyl nuclei. (Chapter 4)
4. To investigate the mechanisms of MnO<sub>2</sub> oxidative degradation of lignin by using dimeric non-phenolic  $\beta$ -O-4-type lignin model compounds. (Chapter 5)

## 1.5 References

- [1] Ericsson, B.; Lindgren, B. O. Factors influencing the carbohydrate degradation under oxygen-alkali bleaching. *Svensk Papperstidning* **1971**, 74 (22), 757-765.
- [2] Gierer, J.; Imsgard, F. The reaction of lignins with oxygen and hydrogen peroxide in alkaline media. *Svensk Papperstidning* **1977**, 80 (16), 510-518.
- [3] Gierer, J. Chemistry of delignification part 2: Reactions of lignins during bleaching. *Wood Science and Technology* **1986**, 20 (1), 1-33.
- [4] Ljunggren, S. Kinetic aspects of some lignin reactions in oxygen bleaching. *Journal of Pulp and Paper Science* **1986**, 12 (2), J54-J57.
- [5] Ek, M.; Gierer, J.; Jansbo, K.; Reitberger, T. Study on the selectivity of bleaching with oxygen-containing species. *Holzforschung* **1989**, 43 (6), 391-396.
- [6] Ljunggren, S. The kinetic of lignn reactions during oxygen bleaching part 1: The reactivity of *p,p'*- dihydroxystilbene. *Nordic Pulp & Paper Research Journal* **1990**, 5 (1), 38-43.
- [7] Ljunggren, S.; Johansson, E. The kinetic of lignn reactions during oxygen bleaching part 2: The reactivity of 4,4'-dihydroxy-3,3'-dimethoxystilbene. *Nordic Pulp & Paper Research Journal* **1990**, 5 (3), 148-154.
- [8] Ljunggren, S.; Johansson, E. The kinetic of lignn reactions during oxygen bleaching part 3: The reactivity of *n*-propylguaiacol and 4,4'-di-*n*-porpyl-6,6'-biguaiacol. *Holzforschung* **1990**, 44 (4), 291-296.
- [9] Gierer, J. Basic principles of beaching part 1: Cationic and radical processes. *Holzforschung* **1990**, 44 (5), 387-394.
- [10] Gierer, J. Basic principles of beaching part 2: Anionic processes. *Holzforschung* **1990**, 44 (6), 395-400.
- [11] Sultanov, V. S.; Wallis, A. F. A. Reactivities of guaiacyl and syringyl lignin model phenols towards oxidation with oxygen-alkali. *Journal of Wood Chemistry and Technology* **1991**, 11 (3), 291-305.

- [12] Gierer, J.; Yang, E.; Reitberger, T. The reactions of hydroxyl radicals with aromatic rings in lignins studied with creasol and 4-methylveratrol. *Holzforschung* **1992**, *46* (6), 495-504.
- [13] Gierer, J.; Jansbo, K.; Reitberger, T. Formation of hydroxyl radicals from hydrogen peroxide and their effect on bleaching of mechanical pulps. *Journal of Wood Chemistry and Technology* **1993**, *13* (4), 561-581.
- [14] Gierer, J.; Yang, E.; Reitberger, T. On the significance of the superoxide radical ( $O_2^{\bullet-}/HO_2^{\bullet}$ ) in oxidative delignification studied with 4-*t*-butylsyringol and 4-*t*-butylguaiacol. *Holzforschung* **1994**, *48* (5), 405-414.
- [15] Johansson, E.; Ljunggren, S. The kinetic of lignin reactions during oxygen bleaching part 4: The reactivities of different lignin model compounds and the influence of metal ions on the rate of degradation. *Journal of Wood Chemistry and Technology* **1994**, *14* (4), 507-525.
- [16] Yasumoto, M.; Matsumoto, Y.; Ishizu, A. The role of peroxide species in the carbohydrate degradation during oxygen bleaching part 1: Factors influencing the reaction selectivity between carbohydrate and lignin model compounds. *Journal of Wood Chemistry and Technology* **1996**, *16* (1), 95-107.
- [17] Yokoyama, T.; Matsumoto, Y.; Yasumoto, M.; Meshitsuka, G. The role of peroxide species in the carbohydrate degradation during oxygen bleaching part 2: Effect of oxygen pressure on the degradation of lignin and carbohydrate model compounds and on the reaction selectivity. *Journal of Pulp and Paper Science* **1996**, *22* (5), J151-J154.
- [18] Gierer, J.; Yang, E.; Reitberger, T. The reactions of chromophores of the stilbene type with hydroxyl radical ( $HO^{\bullet}$ ) and superoxide radical ( $O_2^{\bullet-}/HO_2^{\bullet}$ ) part 1: The cleavage of the conjugated double bond. *Holzforschung* **1996**, *50* (4), 342-352.
- [19] Gierer, J.; Yang, E.; Reitberger, T. The reactions of chromophores of the stilbene type with hydroxyl radical ( $HO^{\bullet}$ ) and superoxide radical ( $O_2^{\bullet-}/HO_2^{\bullet}$ ) part 2: Reactions other than cleavage of the conjugated double bond. *Holzforschung* **1996**, *50* (4), 353-359.
- [20] Gierer, J. Formation and involvement of superoxide ( $O_2^{\bullet-}/HO_2^{\bullet}$ ) and hydroxyl ( $HO^{\bullet}$ ) radicals in TCF bleaching processes: A review. *Holzforschung* **1997**, *51* (1), 34-46.

- [21] Yokoyama, T.; Maekawa, I.; Matsumoto, Y.; Meshitsuka, G. Reaction selectivity of active oxygen species produced by oxygen-alkali oxidation of a phenolic compound. *Journal of Wood Science* **1998**, *44* (5), 421-422.
- [22] Yokoyama, T.; Matsumoto, Y.; Meshitsuka, G. The role of peroxide species in the carbohydrate degradation during oxygen bleaching part 3: Effect of metal ions on the reaction selectivity between lignin and carbohydrate model compounds. *Journal of Pulp and Paper Science* **1999**, *25* (2), 42-46.
- [23] Yokoyama, T.; Matsumoto, Y.; Meshitsuka, G. Reaction selectivity of active oxygen speices in oxygen-alkali bleaching. *Journal of Wood Chemistry and Technology* **1999**, *19* (3), 187-202.
- [24] Tong, G.; Yokoyama, T.; Matsumoto, Y.; Meshitsuka, G. Analysis of progress of oxidation reaction during oxygen-alkali treatment I: Method and its application to lignin oxidation. *Journal of Wood Science* **2000**, *46* (1), 32-39.
- [25] Guay, D. F.; Cole, B. J. W.; Fort Jr., R. C.; Genco, J. M.; Hausman, M. C. Mechanisms of oxidative degradation of carbohydrates during oxygen delignification part 1: Reaction of photochemically generated hydroxyl radical with methyl  $\beta$ -D-glucoside. *Journal of Wood Chemistry and Technology* **2000**, *20* (3), 375-394.
- [26] Gierer, J.; Yang, E.; Reitberger, T. Formation and involvement radicals in oxygen delignification studied by the autoxidation of lignin and carbohydrate model compounds. *Journal of Wood Chemistry and Technology* **2001**, *21* (4), 313-341.
- [27] Yokoyama, T.; Matsumoto, Y.; Meshitsuka, G. Characterization of active oxygen species under oxygen-alkali bleaching conditions. *Holzforschung* **2005**, *59* (3), 269-275.
- [28] Yokoyama, T.; Matsumoto, Y.; Meshitsuka, G. Detailed examination of the degradation of phenol derivatives under oxygen delignification conditions. *Journal of Agricultural and Food Chemistry* **2007**, *55* (4), 1301-1307.
- [29] Imai, A.; Yokoyama, T.; Matsumoto, Y.; Meshitsuka, G. Significant lability of guaiacylglycerol- $\beta$ -phenacyl ether under alkaline conditions. *Journal of Agricultural and*

*Food Chemistry* **2007**, 55 (22), 9043-9046.

[30] Imai, A.; Tomoda, I.; Yokoyama, T.; Matsumoto, Y.; Meshitsuka, G.; Tong, G. Application of the amount of oxygen consumption to the investigation of the oxidation mechanism of lignin during oxygen-alkali treatment. *Journal of Wood Science* **2008**, 54 (1), 62-67.

[31] Konishi, F.; Yokoyama, T.; Matsumoto, Y. Investigation on the hydrogen abstraction from methyl glucoside by active oxygen species under oxygen delignification conditions part 1: Study on the anomeric position. *Holzforschung* **2009**, 63 (1), 52-60.

[32] Yokoyama, T.; Nakagawa, A.; Konishi, F.; Matsumoto, Y. Investigation on the hydrogen abstraction from methyl glucoside by active oxygen species under oxygen delignification conditions III: Effect of the origin of active oxygen species. *Journal of Wood Science* **2011**, 57 (6), 512-519.

[33] Nakagawa, A.; Yokoyama, T.; Matsumoto, Y. Investigation on the hydrogen abstraction from methyl glucoside by active oxygen species under oxygen delignification conditions part 2: Study on the C-2 position. *Journal of Wood Chemistry and Technology* **2012**, 32 (1), 10-22.

[34] Ohmura, S.; Yokoyama, T.; Matsumoto, Y. Progress of oxidation of non-phenolic lignin moiety in an oxygen bleaching process via the conversion of non-phenolic into phenolic lignin moiety. *Journal of Wood Science* **2012**, 58 (3), 243-250.

[35] Nakagawa, A.; Yokoyama, T.; Matsumoto, Y. Investigation on the hydrogen abstraction from methyl glucoside by active oxygen species under oxygen delignification conditions IV: Appearance of kinetic isotope effect in the reaction between methyl glucoside and deuterated methyl glucoside. *Journal of Wood Science* **2012**, 58 (6), 563-569.

[36] Ohmura, S.; Yokoyama, T.; Matsumoto, Y. Significance of benzylic hydroxymethylene group in the reaction of lignin side-chain with active oxygen species under oxygen bleaching conditions. *Journal of Wood Science* **2013**, 59 (4), 337-343.

[37] Yokoyama, T.; Nakagawa, A.; Matsumoto, Y. Investigation on the hydrogen abstraction from methyl glucoside by active oxygen species under oxygen delignification conditions part

- 5: Comprehensive results on experiments using deuterium labeled methyl glucosides. *Journal of Wood Chemistry and Technology* **2015**, 35 (6), 450-463.
- [38] Nakagawa, A.; Yokoyama, T.; Matsumoto, Y. Effect of stereo-configurational difference of carbohydrate model compound on the reaction with active oxygen species under oxygen delignification conditions. *Journal of Wood Science* **2015**, 61 (5), 510-516.
- [39] Colodette, J. L.; Rothenberg, S.; Dence, C. W. Factors affecting hydrogen peroxide stability in the brightening of mechanical and chemimechanical pulps part 3: Hydrogen peroxide stability in the presence of magnesium and combination of stabilizers. *Journal of Pulp and Paper Science* **1989**, 15 (2), J45-J51.
- [40] Abbot, J.; Brown, D. G. Stabilization of iron-catalyzed hydrogen peroxide decomposition by magnesium. *Canadian Journal of Chemistry* **1990**, 68 (9), 1537-1543.
- [41] Brown, D. G.; Abbot, J. Effects of metal ions and stabilizers on peroxide decomposition during bleaching. *Journal of Wood Chemistry and Technology* **1995**, 15 (1), 85-111.
- [42] Posoknistakul, P.; Akiho, S.; Akiyama, T.; Yokoyama, T.; Matsumoto, Y. Stereo-preference in the degradation of the *erythro* and *threo* isomers of  $\beta$ -O-4-type lignin model compounds in oxidation processes III: In the reaction with chlorine- and manganese-based oxidants. *Journal of Wood Science* **2018**, 64 (4), 451-457.
- [43] Kratzl, K.; Gratzl, J.; Claus, P. Formation and degradation of biphenyl structures during alkaline oxidation of phenols with oxygen. In *Lignin Structure and Reactions*, American Chemical Society: **1966**; Vol. 59, pp 157-176.
- [44] Kratzl, K.; Claus, P.; Lonsky, W.; Gratzl, J. S. Model studies on reactions occurring in oxidations of lignin with molecular oxygen in alkaline media. *Wood Science and Technology* **1974**, 8 (1), 35-49.
- [45] Hayyan, M.; Hashim, M. A.; AlNashef, I. M. Superoxide ion: Generation and chemical implications. *Chemical Reviews* **2016**, 116 (5), 3029-3085.
- [46] T., S. D. *Oxygen Chemistry*. Oxford University Press: New York, **1991**.
- [47] Gellerstedt, G.; Lindfors, E. Structural changes in lignin during kraft cooking. Part 4.

Phenolic hydroxyl groups in wood and kraft pulps. *Svensk Papperstidning* **1984**, *15*, R115-R117.

[48] Kratzl, K.; Claus, P.; Lonsky, W.; Gratzl, J. S. Model studies on reactions occurring in oxidations of lignin with molecular oxygen in alkaline media. *Wood Science and Technology* **1974**, *8*, 35-49.

[49] Gierer, J.; Imsgard, F.; Noren, I. Studies on the degradation of phenolic lignin units of the  $\beta$ -aryl ether type with oxygen in alkaline media. *Acta chemica scandinavica B* **1977**, *31*, 561-572.

[50] Meller, A. The chemistry of alkaline degradation of cellulose and oxidized celluloses I. *Holzforschung* **1960**, *14* (3), 78.

[51] Meller, A. The chemistry of alkaline degradation of cellulose and oxidized celluloses II. *Holzforschung* **1960**, *14* (5), 129.

[52] Ishizu, A. Behavior of carbohydrates to oxygen-alkali. *Japan Tappi Journal* **1973**, *27* (8), 371-377.

[53] Gilbert, A. F.; Pavlovova, E.; Rapson, W. H. Mechanism of magnesium retardation of cellulose degradation during oxygen bleaching. *Tappi* **1973**, *56* (6), 95-99.

[54] Samuelson, O.; Ojteg, U. Manganese and magnesium during oxygen bleaching of wood pulp. *Nordic Pulp & Paper Research Journal* **1994**, *9* (4), 259-266.

[55] Brown, D. G.; Abbot, J. Effects of metal ions and stabilisers on peroxide decomposition during bleaching. *Journal of Wood Chemistry and Technology* **1995**, *15* (1), 85-111.

[56] Johansson, E.; Ljunggren, S. The kinetics of lignin reactions during oxygen bleaching. IV. The reactivities of different lignin model compounds and the influence of metal ions on the rate of degradation. *Journal of Wood Chemistry and Technology* **1994**, *14* (4), 507-525.

[57] Gevert, B. S.; Lohmander, S. F. Influence of sulfur compounds, manganese, and magnesium on oxygen bleaching of kraft pulp. *Tappi Journal* **1997**, *80* (10), 263-268.

[58] Gyenge, E. L.; Oloman, C. W. *In situ* electrochemically mediated oxygen delignification of wood pulp with a manganese (III) aminopolycarboxylate complex. *Tappi Journal* **1997**, *80*

(1), 194-202.

[59] Gibson, Y. A.; Wajer, M. The use of magnesium hydroxide as an alkali and cellulose protector in chemical pulp bleaching. *Pulp & Paper Canada* **2003**, *104* (11), 28-32.

[60] Tebo, B. M.; Bargar, J. R.; Clement, B. G.; Dick, G. J.; Murray, K. J.; Parker, D.; Verity, R.; Webb, S. M. Biogenic manganese oxides: Properties and mechanisms of formation. *Annual Review of Earth and Planetary Sciences* **2004**, *32* (1), 287-328.

[61] Chen, Z.; Jiao, Z.; Pan, D.; Li, Z.; Wu, M.; Shek, C.-H.; Wu, C. M. L.; Lai, J. K. L. Recent advances in manganese oxide nanocrystals: Fabrication, characterization, and microstructure. *Chemical Reviews* **2012**, *112* (7), 3833-3855.

[62] Brock, S. L.; Duan, N.; Tian, Z. R.; Giraldo, O.; Zhou, H.; Suib, S. L. A review of porous manganese oxide materials. *Chemistry of Materials* **1998**, *10* (10), 2619-2628.

[63] Julien, C.; Massot, M.; Baddour-Hadjean, R.; Franger, S.; Bach, S.; Pereira-Ramos, J. P. Raman spectra of birnessite manganese dioxides. *Solid State Ionics* **2003**, *159* (3), 345-356.

[64] Robinson, D. M.; Go, Y. B.; Mui, M.; Gardner, G.; Zhang, Z.; Mastrogiovanni, D.; Garfunkel, E.; Li, J.; Greenblatt, M.; Dismukes, G. C. Photochemical water oxidation by crystalline polymorphs of manganese oxides: Structural requirements for catalysis. *Journal of the American Chemical Society* **2013**, *135* (9), 3494-3501.

[65] Miao, L.; Wang, J.; Zhang, P. Review on manganese dioxide for catalytic oxidation of airborne formaldehyde. *Applied Surface Science* **2019**, *466*, 441-453.

[66] Fei, J. B.; Cui, Y.; Yan, X. H.; Qi, W.; Yang, Y.; Wang, K. W.; He, Q.; Li, J. B. Controlled preparation of MnO<sub>2</sub> hierarchical hollow nanostructures and their application in water treatment. *Advanced Materials* **2008**, *20* (3), 452-456.

[67] Ball, S.; Goodwin, T. W.; Morton, R. A. Studies on vitamin A: 5. The preparation of retinene1—vitamin A aldehyde. *Biochemical Journal* **1948**, *42* (4), 516-523.

[68] Fatiadi, A. J. Evidence for adsorption as the first step in the solid-state oxidation of benzenehexol with active manganese dioxide. *Journal of the Chemical Society B: Physical Organic* **1971**, *1971*, 889-894.

- [69] Evans, R. M. Oxidations by manganese dioxide in neutral media. *Quarterly Reviews, Chemical Society* **1959**, *13* (1), 61-70.
- [70] Birkofer, L.; Erlenbach, L.  $\beta$ -Aminoaldehyde. *Chemische Berichte* **1958**, *91* (11), 2383-2387.
- [71] Gritter, R. J.; Dupre, G. D.; Wallace, T. J. Oxidation of benzyl alcohols with manganese dioxide. *Nature* **1964**, *202* (4928), 179-181.
- [72] Pratt, E. F.; Van de castle, J. F. Oxidation by solids. I. Oxidation of selected alcohols by manganese dioxide. *The Journal of Organic Chemistry* **1961**, *26*, 2973-2975.
- [73] Hall, T. K.; Story, P. R. Novel oxidative rearrangement with manganese dioxide. *Journal of the American Chemical Society* **1967**, *89* (25), 6759-6761.
- [74] Kwart, H.; George, T. J. Primary deuterium isotope effects in the oxidation of benzyl-a-d alcohol by transition elements and related reagents: Mechanisms of electron transfer. *Journal of Organic Chemistry* **1979**, *44* (1), 162-164.
- [75] Tojo, G.; Fernández, M. I. Selective oxidations of allylic and benzylic alcohols in the presence of saturated alcohols. In *Oxidation of Alcohols to Aldehydes and Ketones: A Guide to Current Common Practice*, Springer US: **2006**; pp 289-330.
- [76] Mancera, O.; Rosenkranz, G.; Sondheimer, F. Steroids. Part XLVI. Synthesis of 11 $\beta$ -hydroxytestosterone and 11-keto testosterone. *Journal of the Chemical Society* **1953**, *1953*, 2189-2191.
- [77] Adler, E.; Becker, H.-D. Zur selektiven oxydation von benzylalkoholen. *Acta Chemica Scandinavica* **1961**, *15* (4), 849-852.
- [78] Uchiyama, M.; Kimura, Y.; Ohta, A. Stereoselective total syntheses of ( $\pm$ )-arthrinone and related natural compounds. *Tetrahedron Letters* **2000**, *41* (51), 10013-10017.
- [79] Steffan, R. J.; Ashwell, M. A.; Solvibile, W. R.; Matelan, E.; Largis, E.; Han, S.; Tillet, J.; Mulvey, R. Novel substituted 4-aminomethylpiperidines as potent and selective human  $\beta_3$ -agonists. Part 2: Arylethanolaminomethylpiperidines. *Bioorganic & Medicinal Chemistry Letters* **2002**, *12* (20), 2963-2967.

- [80] Black, D.; Brockway, D.; Moss, G. Metal template reactions. XXII. General-synthesis of dibenzocorromins and related nickel(II) complexes. *Australian Journal of Chemistry* **1986**, *39* (8), 1231-1247.
- [81] Bu, X.; Deady, L. W. A preparation of methyl 2-amino-3-formylbenzoate and its use in friedlander synthesis. *Synthetic Communications* **1999**, *29* (23), 4223-4233.
- [82] Wei, X.; Taylor, R. J. K. *In situ* alcohol oxidation-wittig reactions. *Tetrahedron Letters* **1998**, *39* (22), 3815-3818.
- [83] Mohri, S.-i.; Stefinovic, M.; Snieckus, V. Combined directed *ortho*-, remote-metalation and cross-coupling strategies. Concise syntheses of the kinamycin biosynthetic grid antibiotics phenanthroviridin aglycon and kinobscurinone. *The Journal of Organic Chemistry* **1997**, *62* (21), 7072-7073.
- [84] Corey, E. J.; Gilman, N. W.; Ganem, B. E. New methods for the oxidation of aldehydes to carboxylic acids and esters. *Journal of the American Chemical Society* **1968**, *90* (20), 5616-5617.
- [85] Madhava Reddy, S.; Goedken, V. L.; Walborsky, H. M. Chiroptical properties of planar acyclic 1, 3-dienes and  $\alpha,\beta$ -unsaturated aldehydes: The planar diene rule. *Journal of the American Chemical Society* **1986**, *108* (10), 2691-2699.
- [86] Shimizu, H.; Okamura, H.; Iwagawa, T.; Nakatani, M. Asymmetric synthesis of (-)- and (+)-eutipoxide B using a base-catalyzed Diels–Alder reaction. *Tetrahedron* **2001**, *57* (10), 1903-1908.
- [87] Shi, B.; Hawryluk, N. A.; Snider, B. B. Formal synthesis of ( $\pm$ )-guanacastepene A. *The Journal of Organic Chemistry* **2003**, *68* (3), 1030-1042.



## **2 Utilization of Recyclable MnO<sub>2</sub> in Prebleaching Stage as a Catalyst for Oxygen Delignification or as a Delignifying Agent**

## 2.1 Introduction

As mentioned in Chapter 1, severe carbohydrate damage accompanied by oxygen delignification is a serious problem during oxygen-alkali bleaching. To overcome this problem, some researches have been conducted to understand the basic chemistry in oxygen delignification. According to these studies, the degradation of carbohydrate is caused by active oxygen species, which are mainly generated from reactions between phenolic units in lignin and molecular oxygen.<sup>[1-3]</sup>

In previous studies, a phenolic lignin model compound (2,4,6-trimethylphenol or 4-hydroxy-3-methoxybenzyl alcohol) was used as the origin of active oxygen species under oxygen-alkali bleaching conditions, although there may exist various active oxygen species.<sup>[4-7]</sup> In these reaction systems, at least a specific active oxygen species generated using phenolic lignin model compounds is confirmed to abstract the anomeric and C-2 hydrogens of carbohydrate. A possible reaction scheme for these reaction systems is shown in **Figure 2-1**.<sup>[8]</sup> The one-electron oxidation of the phenolic lignin model compound by  $O_2$  affords  $O_2^{\bullet-}$  and the corresponding phenoxyl radical, and then  $O_2^{\bullet-}$  and phenoxyl radical is combined to afford the peroxide. The peroxide can generate the relatively stable primary degradation product through ring cleavage reaction. Moreover, the peroxide can also generate active oxygen species, which is the main substance leading to the degradation of carbohydrates. Because  $MnO_2$  catalyzes the self-decomposition of  $H_2O_2$  to be  $H_2O$  and  $O_2$  without formation of any active oxygen species,  $MnO_2$  is also expected to catalyze decomposition of peroxides without any formation of active oxygen species in oxygen-alkali bleaching. Furthermore, it is also mentioned in Chapter 1 that as an oxidant,  $MnO_2$  has the potential to oxidize residual lignin in pulp.

In this chapter, the delignification efficiencies were examined and discussed when  $MnO_2$  was added to a common oxygen delignification process or when a  $MnO_2$  delignification process was substituted for the latter half of this common process.  $MnO_2$  is a recyclable chemical mainly due to its insolubility and oxidation-reduction interconversion with soluble

$\text{Mn}^{2+}$ , so the possibility of  $\text{MnO}_2$  recycling is also discussed.

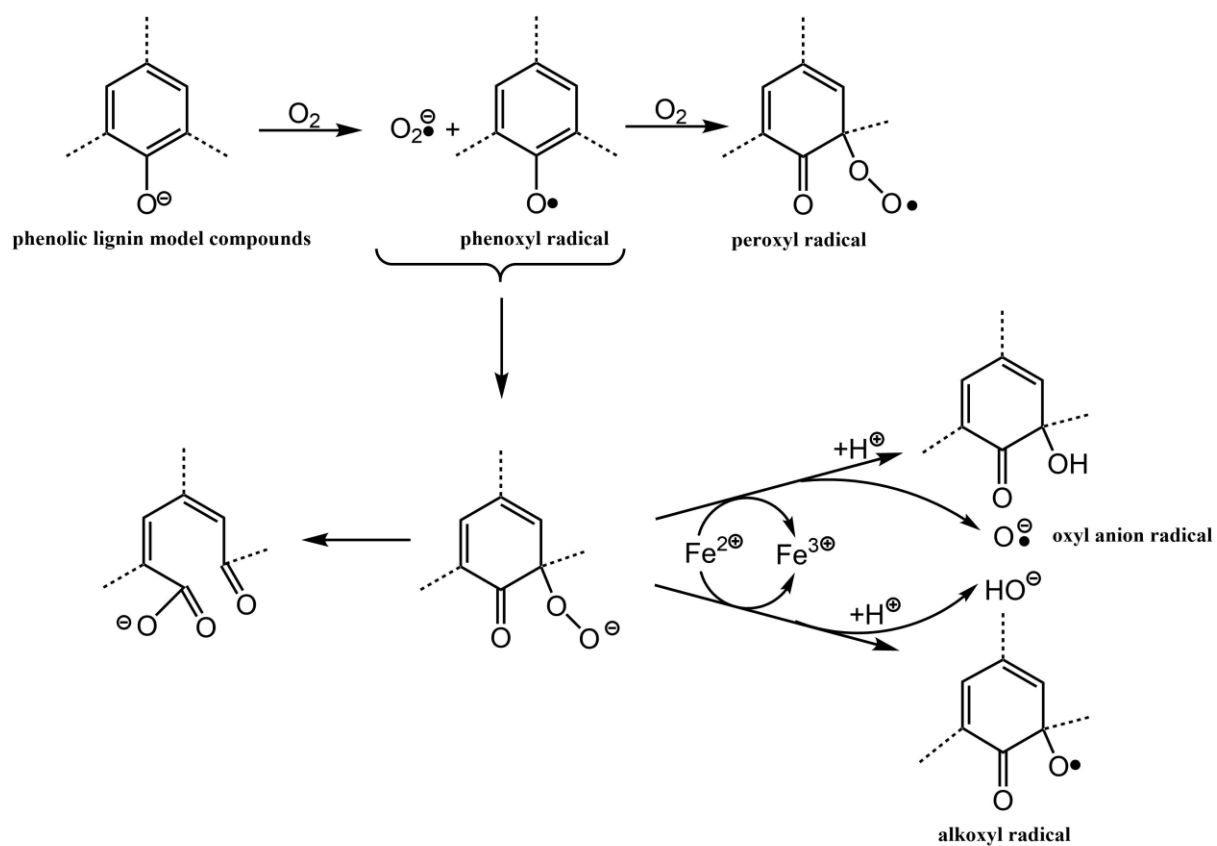


**Figure 2-1** Possible reaction scheme for a phenolic compound under oxygen delignification conditions.

## 2.2 Materials and methods

### 2.2.1 Materials

MGP and a phenolic lignin model compound, 4-hydroxy-3-methoxybenzyl alcohol (vanillyl alcohol, Valc), were purchased from Tokyo Chemical Industry Co. Ltd. (Tokyo, Japan) and recrystallized from C<sub>2</sub>H<sub>5</sub>OH before use. Hardwood unbleached kraft pulp (kappa number: 14.2, viscosity: 21.5 mPa • s) was obtained from Oji Holdings Co. (Tokyo, Japan). All other chemicals used in this study were purchased from FUJIFILM Wako Pure Chemical Co., Ltd. (Osaka, Japan), Tokyo Chemical Industry Co., Ltd., or Sigma-Aldrich Japan K. K. (Tokyo, Japan). Ultrapure H<sub>2</sub>O purified by an ultrapure H<sub>2</sub>O generator, Puric-Z (Organo Co., Tokyo, Japan), was used in all the experiments. Semiconductor grades of NaOH and MnSO<sub>4</sub> • 5 H<sub>2</sub>O were used.

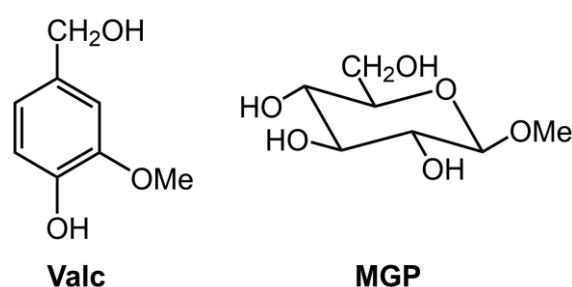


**Figure 2-2** Chemical structures of a phenolic compound of vanillyl alcohol (Valc) as an active oxygen species generator and a carbohydrate model compound of methyl β-D-glucopyranoside (MGP).

### 2.2.2 Methods

#### 2.2.2.1 Reaction of model compound

A reaction solution (300 mL) was prepared to contain MGP (4.0 mmol/L), Valc (9.0 mmol/L), NaOH (0.50 mol/L), and MnSO<sub>4</sub> • 5 H<sub>2</sub>O (0.36 mmol/L). The reaction solution was transferred into a Teflon-coated stainless steel autoclave (500 mL, Taiatsu Techno<sup>®</sup> Co., Tokyo, Japan). The vessel was introduced to a pressure of 1.1 MPa (1.0 MPa as gauge level)

of O<sub>2</sub>, heated to 95°C for 10 min, and then stirred for 300 min. A portion of the reaction solution was withdrawn periodically to quantify residual MGP and Valc. The reaction was run twice to confirm its reproducibility.

#### **2.2.2.2 Preparation of MnO<sub>2</sub> for reaction**

##### **Aging of commercially available MnO<sub>2</sub> (commercial MnO<sub>2</sub>)**

Commercial MnO<sub>2</sub> (FUJIFILM Wako Pure Chemical Co., Ltd.) was ground into powder in a mortar and aged in a solution of 1.0 mol/L H<sub>2</sub>SO<sub>4</sub> for 120 min at room temperature followed by filtration under reduced pressure. The aged MnO<sub>2</sub> on the filter paper was washed with H<sub>2</sub>O until washings were free from SO<sub>4</sub><sup>2-</sup>. The washings were checked by mixing with a BaCl<sub>2</sub> solution. The aged MnO<sub>2</sub> was air-dried for further use. Because the commercial MnO<sub>2</sub> did not consist only of MnO<sub>2</sub>, the oxidation power was measured by iodometric titration after grinding the aged MnO<sub>2</sub> into powder. The content was 90.2% of the theoretical value.

##### **O<sub>2</sub> oxidation of Mn<sup>2+</sup> to synthesize MnO<sub>2</sub> (synthetic MnO<sub>2</sub>)**

MnO<sub>2</sub> was synthesized from Mn<sup>2+</sup> (MnSO<sub>4</sub>) by O<sub>2</sub> oxidation under alkaline conditions. To a solution (700 mL) of MnSO<sub>4</sub> • H<sub>2</sub>O (0.20 mol) was added drop-wise a solution (100 mL) of 4.0 mol/L NaOH. The resultant solution was subjected to O<sub>2</sub> bubbling for 60 min with stirring at room temperature. The suspension was neutralized with a solution (150 mL) of 1.0 mol/L H<sub>2</sub>SO<sub>4</sub> with stirring for 30 min. The drop-wise addition of 4.0 mol/L NaOH and successive O<sub>2</sub> bubbling were then repeated to further advance the oxidation. The obtained precipitates (mostly MnO<sub>2</sub>) were collected by filtration under reduced pressure, and washed with H<sub>2</sub>O until the filtrate became neutral. The obtained precipitates were air-dried for further use. To examine the oxidation power, the precipitates were ground into powder in a mortar and iodometrically titrated. The content was 84.9% of the theoretical value, calculated on the basis of an assumption that all the applied Mn<sup>2+</sup> was completely oxidized to MnO<sub>2</sub>.

#### **2.2.2.3 Oxygen delignification in the presence of MnO<sub>2</sub>**

To a suspension of hardwood unbleached kraft pulp (12.0 g, OD basis) was added the commercial or synthetic  $\text{MnO}_2$  (300 mg, OD basis). A NaOH solution and  $\text{H}_2\text{O}$  were added to the pulp suspension to adjust the pH to 12.5 or 11.5 and the pulp consistency to 4.0%. A carbonate buffer solution was added to the suspension when a lower initial pH (10.5 or 9.2) was applied. After the pulp slurry was transferred into the Teflon-coated stainless steel vessel,  $\text{O}_2$  was introduced to the reactor at a pressure of 0.60 MPa (0.50 MPa as gauge level), and then the vessel was heated to 95°C. After reactions, the vessel was cooled with ice water. The obtained pulp slurry was washed thoroughly with  $\text{H}_2\text{O}$  and air-dried for further use.

For the preparation of a reference pulp, oxygen delignification without adding any  $\text{MnO}_2$  was also carried out under the same conditions.

#### **2.2.2.4 Oxygen delignification in the presence of $\text{MnO}_2$ generated *in-situ* in pulp fibers**

$\text{MnSO}_4 \cdot \text{H}_2\text{O}$  (6.0 mmol) was added to a suspension of the hardwood unbleached kraft pulp (12.0 g, OD basis). A  $\text{H}_2\text{SO}_4$  solution was added to adjust the pH to 2.0, and then stirred at 50°C for 120 min. A NaOH solution and  $\text{H}_2\text{O}$  were used to adjust the pH and pulp consistency to 12.5 and 4.0%, respectively. After the pulp slurry was transferred into the Teflon-coated stainless steel vessel,  $\text{O}_2$  bubbling was performed at room temperature for 120 min to generate  $\text{MnO}_2$  in the pulp fibers *in-situ*. The procedure of this *in-situ* generation of  $\text{MnO}_2$  was similar as described in section 2.2.2.2. Oxygen delignification was then carried out under the same conditions as described in section 2.2.2.3.

#### **2.2.2.5 Successive stages of oxygen delignification and $\text{MnO}_2$ oxidation**

The hardwood unbleached kraft pulp was primarily oxygen-delignified without addition of  $\text{MnO}_2$  at a pH of 12.5 for 120 min, following the procedure described above for the reference pulp. The synthetic  $\text{MnO}_2$  (300 mg, OD basis) was added to a suspension of the oxygen delignified pulp (12.0 g, OD basis), and then a  $\text{H}_2\text{SO}_4$  or sulfate buffer solution and  $\text{H}_2\text{O}$  were added to adjust the pH and consistency of the suspension to specific values and 4.0%, respectively. The prepared pulp slurry was transferred into the Teflon-coated stainless steel vessel, and the vessel was heated to 70°C. After reactions, the vessel was cooled with ice

water. The obtained pulp slurry was washed thoroughly with H<sub>2</sub>O and air-dried for further use.

#### **2.2.2.6 Quantification of model compound**

For quantification of MGP and Valc, a portion of the reaction solution was withdrawn (2.0 mL) at prescribed reaction times and neutralized with acetic acid. A solution of an internal standard compound (*myo*-inositol) was added and the resulting mixture was dried under a vacuum. The dried sample was acetylated with pyridine (2.0 mL) and acetic anhydride (3.0 mL) at 100°C for 60 min and then injected into a gas-chromatograph (GC-2010 plus, Shimadzu Co., Ltd., Kyoto, Japan) equipped with a flame ionization detector and a capillary column (TC-17, 0.25 mm × 30 m, GL Science Inc., Tokyo, Japan).

Conditions of GC were as follows; carrier gas: He, split ratio: 15, flow rate: 1.55 mL/min, injection temperature: 220°C, detector temperature: 230°C. The oven temperature was increased from 195°C to 200°C at 1°C/min and then from 200°C to 220°C at 4°C/min, holding for 10 min. The total running time was 20 min.

#### **2.2.2.7 Determination of kappa number and viscosity of obtained pulp**

The kappa numbers and viscosities of obtained pulps were determined according to TAPPI Methods T236 and T230, respectively. The amount of MnO<sub>2</sub> remaining in the obtained pulps was separately determined iodometrically, and was taken into consideration in the calculation of the kappa numbers.

## 2.3 Results and discussion

### 2.3.1 Reaction of model compound

As described in the Introduction section, addition of  $\text{MnO}_2$  can potentially suppress the degradation of carbohydrates during oxygen delignification. A model experiment was conducted to confirm this suppression using not 2,4,6-trimethylphenol but a phenolic ‘lignin’ model compound, Valc. MGP and Valc were co-treated under conditions simulating oxygen delignification, where active oxygen species were generated by reactions between Valc and  $\text{O}_2$ , and degrade MGP. Hydroxyl radical ( $\text{HO}\cdot$ ,  $\text{pK}_a = 11.9$ ) and its conjugate base, oxyl anion radical ( $\text{O}\cdot^-$ ), are believed to be the active oxygen species most responsible for the degradation of carbohydrates.<sup>[2-3,9]</sup>

In previous study, this model experiment was conducted in the presence or absence of  $\text{FeCl}_3$  under similar conditions to those employed in this study.<sup>[10-11]</sup> MGP was degraded significantly to be a residual yield of 57% at a reaction time of 300 min under the same conditions as those employed in this study, although a different reactor was used and it took a longer period (30 min) to raise the temperature to the target degree ( $95^\circ\text{C}$ ). The recovery yield of MGP was 82% at a reaction time of 300 min when no metal ion was intentionally added at an oxygen pressure of 0.4 MPa (0.3 MPa as a gauge level) using this different reactor. At the lower oxygen pressure, Valc disappeared completely from the reaction solution just before a reaction time of 300 min.

**Figure 2-3** shows the time course of the changes in the residual yields of MGP and Valc when these compounds were treated together under conditions simulating oxygen delignification in the presence of  $\text{MnO}_2$ . Although  $\text{Mn}^{2+}$  was primarily applied, its oxidation to  $\text{MnO}_2$  probably completed in the early stage of the reaction. The degradation of MGP was not great. The residual yield was more than 95% at a reaction time of 300 min, which suggests that the addition of  $\text{MnO}_2$  suppresses the degradation of carbohydrates. This result also suggests that the amount of active oxygen species generated by decomposition of peroxides

controls the degree of the degradation of carbohydrates in an oxygen delignification system.

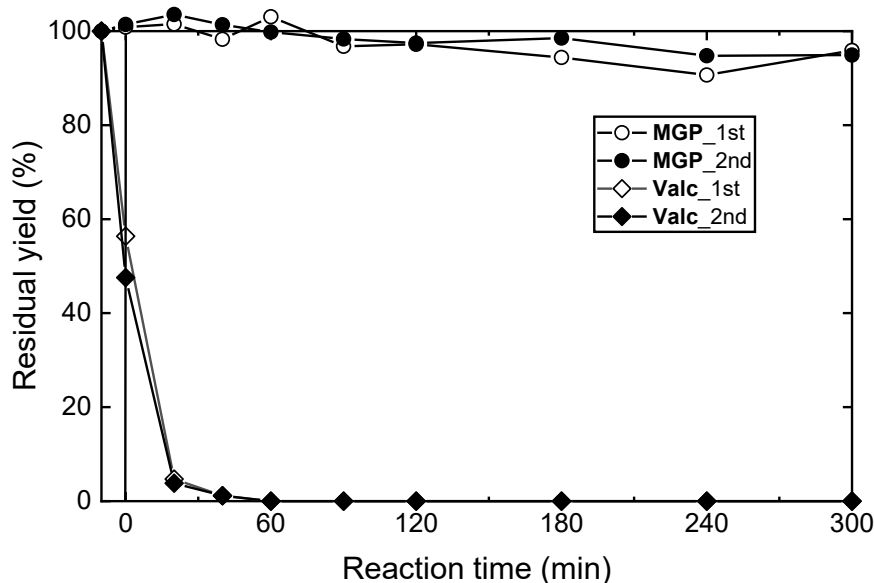


**Figure 2-3** Time course of changes in the residual yields of MGP (white and black circles) and Valc (white and black diamonds) when treated together under conditions simulating oxygen delignification in the presence of  $\text{MnO}_2$ . (white marks: 1st trial, black marks: 2nd trial)

### 2.3.2 Oxygen delignification in the presence of $\text{MnO}_2$

On the basis of the results of the model experiment, hardwood unbleached kraft pulp was oxygen-delignified in the presence of the commercial or synthetic  $\text{MnO}_2$ . The kappa numbers and viscosities of delignified pulps were compared with those of the reference pulp prepared by oxygen delignification without the addition of  $\text{MnO}_2$ . **Figure 2-4** shows the correlations between the viscosities and kappa numbers for the pulps obtained when the hardwood unbleached pulp was oxygen-delignified in the absence of  $\text{MnO}_2$  (reference) or in the presence of the commercial or synthetic  $\text{MnO}_2$ . This correlation is defined as the ‘reaction selectivity’. The reaction selectivity of a delignification process conducted here is desirably high when it prepares pulps with high viscosities at a constant kappa number. **Table 2-1** lists all the data used to plot **Figure 2-4**.

Although the reaction selectivity was slightly different between three oxygen

delignification processes and lower in the presence of either commercial or synthetic  $\text{MnO}_2$  than in the reference treatment before their late stages, these delignification processes showed similar degrees of the reaction selectivity in the late stage. This confirmed that the presence of  $\text{MnO}_2$  does not increase the reaction selectivity, although this was contrary to our expectation based on the results of the model experiment. These small effects of the  $\text{MnO}_2$  addition can be explained if we assume that the added  $\text{MnO}_2$  was present only on the outside of the pulp fibers, and thus its catalytic activity to decompose peroxides without formation of any active oxygen species was not available within the fibers.

**Table 2-2** lists the kappa numbers and viscosities of the pulps that were oxygen-delignified at an initial pH of 11.5, 10.5, or 9.2 under otherwise the same conditions described in the caption of **Figure 2-4** with the final pH values. The alkaline source was NaOH at an initial pH of 11.5 or a carbonate buffer solution at a pH of 10.5 or 9.2. The effect of the addition of the synthetic  $\text{MnO}_2$  was also small at these lower pH values, which can also be attributed to the added  $\text{MnO}_2$  existing only outside of the pulp fibers.

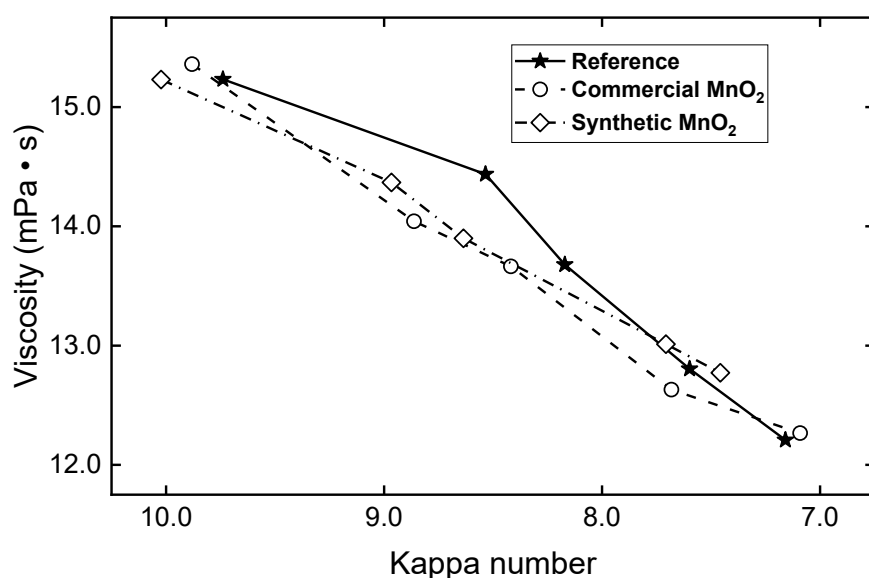


**Figure 2-4** Correlation between viscosities and kappa numbers of pulps obtained when hardwood unbleached kraft pulp was oxygen-delignified in the absence of  $\text{MnO}_2$  (reference, black stars), or in the presence of commercial  $\text{MnO}_2$  (white circles) or synthesized  $\text{MnO}_2$

(white diamonds) at an oxygen pressure of 0.6 MPa, initial pH of 12.5, pulp consistency of 4.0%, and 95°C for 40, 80, 120, 240, or 360 min.

**Table 2-1** Kappa number and viscosity of the pulps employed for the preparation of **Figure 2-4** with the final pH.

Type of delignification	Reaction period	Kappa number			Viscosity <sup>a</sup>			Final pH
		1st	2nd	Mean <sup>b</sup>	1st	2nd	Mean <sup>b</sup>	
Reference	40 min	9.7	9.8	9.8	15.4	15.1	15.3	12.3
	80 min	8.6	8.5	8.6	14.5	14.3	14.4	12.2
	120 min	8.2	8.2	8.2	13.7	13.6	13.7	12.1
	240 min	7.6	7.6	7.6	12.7	12.9	12.8	12.0
	360 min	7.2	7.1	7.2	12.3	12.2	12.3	11.8
Commercial MnO <sub>2</sub>	40 min	9.9	9.9	9.9	15.4	15.3	15.4	11.8
	80 min	8.8	8.9	8.9	13.9	14.1	14.0	11.8
	120 min	8.3	8.5	8.4	13.7	13.6	13.7	11.7
	240 min	7.7	7.6	7.7	12.6	12.7	12.7	11.5
	360 min	7.1	7.1	7.1	12.3	12.2	12.3	11.3
Synthetic MnO <sub>2</sub>	40 min	10.0	10.0	10.0	15.2	15.2	15.2	11.8
	80 min	8.8	9.1	9.0	14.4	14.4	14.4	11.7
	120 min	8.6	8.6	8.6	13.9	13.9	13.9	11.6
	240 min	7.7	7.7	7.7	13.1	13.0	13.1	11.2
	360 min	7.5	7.4	7.5	12.9	12.7	12.8	10.5

<sup>a</sup>Unit: mPa • s. <sup>b</sup>These mean values were used for the preparation of **Figure 2-4**.

**Table 2-2** Kappa number and viscosity of the pulps obtained by oxygen delignification at pHs lower than 12.5, with the initial and final pH.

Initial pH <sup>a</sup>	MnO <sub>2</sub> <sup>b</sup>	Reaction period	Kappa number			Viscosity <sup>c</sup>			Final pH <sup>d</sup>
			1st	2nd	Mean	1st	2nd	Mean	
11.5	×	80 min	10.7	10.8	10.8	18.1	18.4	18.3	8.8
	○		10.7	10.6	10.7	17.9	18.0	18.0	8.4
10.5	×	80 min	9.3	9.4	9.4	14.8	15.0	14.9	—
	○		9.3	9.3	9.3	14.1	14.1	14.1	—
9.2	×	40 min	11.7	11.7	11.7	17.9	17.8	17.9	—
	○		11.7	11.7	11.7	17.1	17.4	17.3	—
	×	80 min	10.7	10.8	10.8	16.9	16.9	16.9	—
	○		10.4	10.5	10.5	16.7	16.8	16.8	—
	×	180 min	10.1	10.1	10.1	16.2	16.3	16.3	—
	○		9.9	10.0	10.0	15.9	15.9	15.9	—

<sup>a</sup>Alkaline source was NaOH for pH 11.5 or carbonate buffer for the others. <sup>b</sup>×: No addition of MnO<sub>2</sub> (reference), ○: Addition of synthetic MnO<sub>2</sub>. <sup>c</sup>Unit: mPa • s. <sup>d</sup>Final pH values are not shown when carbonate buffer was used as the alkaline source.

### 2.3.3 Oxygen delignification in the presence of MnO<sub>2</sub> generated *in-situ* in pulp fibers

To confirm whether or not the presence of MnO<sub>2</sub> in pulp fibers increases the reaction selectivity, the *in-situ* generation of MnO<sub>2</sub> in pulp fibers was carried out before the oxygen delignification. Mn<sup>2+</sup> was primarily infused into pulp fibers under mildly acidic conditions, and then oxidized to MnO<sub>2</sub> by O<sub>2</sub> bubbling under alkaline conditions. Both the kappa number and viscosity slightly decreased from 14.2 to 13.2 and from 21.5 to 20.4 mPa • s, respectively, during the Mn<sup>2+</sup> infusion under mildly acidic conditions. Both also further decreased slightly from 13.2 to 12.7 and from 20.4 to 18.8 mPa • s, respectively, during the O<sub>2</sub> bubbling under alkaline conditions. **Figure 2-5** shows the reaction selectivities of the oxygen delignification

processes in the reference treatment and with the *in-situ* generated  $\text{MnO}_2$ .

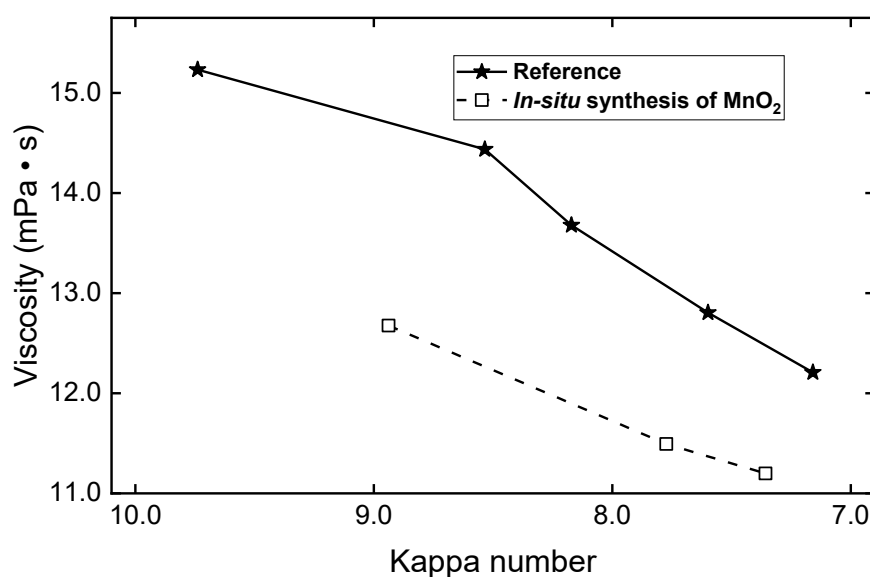


**Figure 2-5** Correlation between viscosities and kappa numbers of pulps obtained when hardwood unbleached kraft pulp was oxygen-delignified in the presence of  $\text{MnO}_2$  generated *in-situ* in pulp fibers at an oxygen pressure of 0.6 MPa, initial pH of 12.5, pulp consistency of 4.0%, and 95°C for 40, 80, or 120 min (white squares). (Black stars are the reference, and the same as those shown in **Figure 2-4**.)

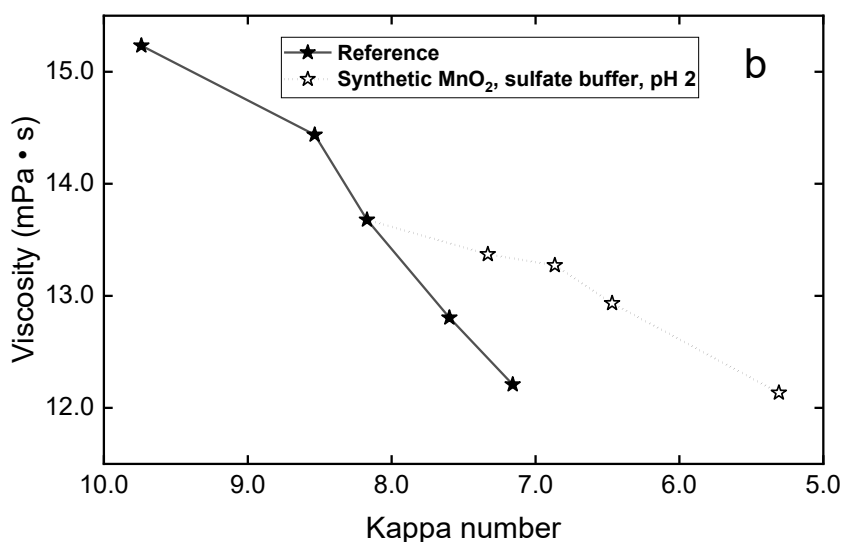
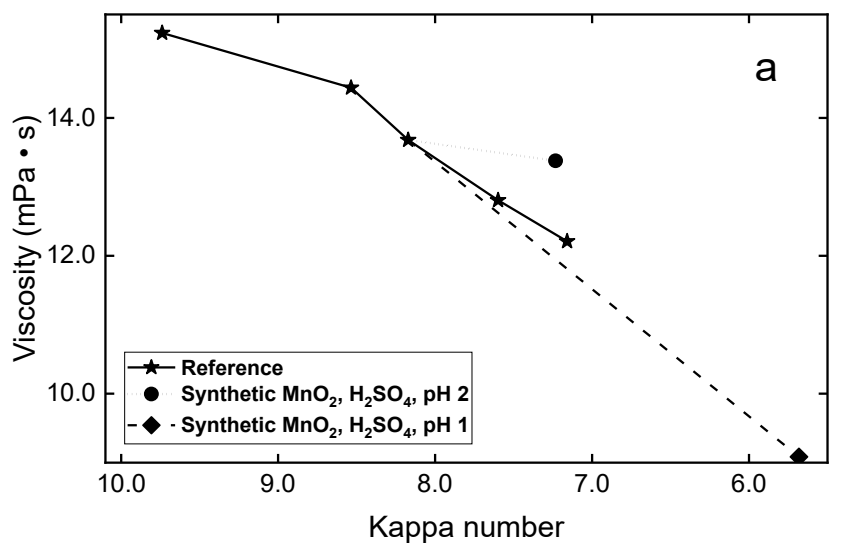
The reaction selectivity in the presence of the  $\text{MnO}_2$  generated *in-situ* in pulp fibers was surprisingly much lower than that in its absence (reference). This result suggests that active oxygen species were efficiently generated in pulp fibers and mainly degraded carbohydrates as well as lignin. A possible explanation for this result is that the oxidation of  $\text{Mn}^{2+}$  within the pulp fibers was not sufficient for complete conversion to  $\text{MnO}_2$ , and hence, not only  $\text{MnO}_2$  but also trivalent Mn species, among others, were generated *in-situ*. This incomplete oxidation may have resulted from some interactions between  $\text{Mn}^{2+}$  and hydroxy groups in the pulp components. These incompletely oxidized Mn species must have been able to generate active oxygen species efficiently, which is quite different from the catalytic activity of  $\text{MnO}_2$ . Because the result did not change when the  $\text{O}_2$  bubbling was prolonged, the oxidation of  $\text{Mn}^{2+}$  must have reached a maximum by the method employed in this study.

It was thus confirmed, contrary to the expectation based on the result of the model experiment, that the addition of any type of  $\text{MnO}_2$  does not improve the reaction selectivity in oxygen delignification.

#### 2.3.4 Successive stages of oxygen delignification and $\text{MnO}_2$ oxidation

Because  $\text{MnO}_2$  can degrade lignin as an oxidant under acidic conditions,<sup>[12]</sup> we tried to substitute a later stage of oxygen delignification with a  $\text{MnO}_2$  oxidation stage under acidic conditions, to examine the reaction selectivity of this strategy and compare it with that of the reference oxygen delignification process.

**Figure 2-6 (a)** shows the reaction selectivity of the reference oxygen delignification process (black stars) and successive stages of the oxygen delignification for 120 min, which was terminated at the third data point, and oxidation by synthetic  $\text{MnO}_2$  at a pH of 2 (black circle) or 1 (black diamond) prepared by a  $\text{H}_2\text{SO}_4$  solution for 60 or 180 min, respectively. **Table 2-3** lists all the data on the kappa numbers and viscosities of the pulps obtained in the successive stages and used for preparing **Figures 2-6**. The reaction selectivity of the successive stages was higher than that of the reference oxygen delignification when the synthetic  $\text{MnO}_2$  oxidation was conducted at a pH of 2. However, the amount of acid was not sufficient to continue the reaction at this pH, because at a reaction time of 60 min the pH increased to 3.7, where  $\text{MnO}_2$  does not sufficiently oxidize organic matter. Although the kappa number greatly decreased when the synthetic  $\text{MnO}_2$  oxidation was conducted at a pH of 1, the reaction selectivity was not high. This lower reaction selectivity must have resulted from the extensive hydrolysis of carbohydrates at this pH.



**Figures 2-6** Correlation between viscosities and kappa numbers of pulps obtained in the reference oxygen delignification (black stars), in the successive stages of oxygen delignification for 120 min, and in the synthetic MnO<sub>2</sub> oxidation. (a) The synthetic MnO<sub>2</sub> oxidation stage was conducted at a pH of 2 (black circle) or 1 (black diamond) prepared by H<sub>2</sub>SO<sub>4</sub>. (b) The synthetic MnO<sub>2</sub> oxidation stage was conducted at a pH of 2 prepared by sulfate buffer (white stars). (Black stars are the reference and the same as those shown in **Figure 2-4**.)

**Table 2-3** Kappa number and viscosity of the pulps employed for the preparation of **Figures 2-6** with the final pH.

Initial pH	Reaction period	Kappa number			Viscosity <sup>a</sup>			Final pH <sup>b</sup>
		1st	2nd	Mean <sup>c</sup>	1st	2nd	Mean <sup>c</sup>	
2.0 <sup>d</sup>	60 min	7.2	7.3	7.3	13.3	13.4	13.4	3.7
1.0 <sup>d</sup>	180 min	5.6	5.7	5.7	9.13	9.04	9.09	1.3
2.0 <sup>e</sup>	30 min	7.3	7.4	7.4	13.3	13.5	13.4	—
	90 min	6.8	6.9	6.9	13.2	13.3	13.3	—
	180 min	6.4	6.5	6.5	12.8	13.1	13.0	—
	360 min	5.3	5.3	5.3	12.0	12.2	12.1	—

<sup>a</sup>Unit: mPa • s. <sup>b</sup>Final pH values are shown only when H<sub>2</sub>SO<sub>4</sub> solution was used. <sup>c</sup>These mean values were used for the preparation of **Figures 2-6**. <sup>d</sup>H<sub>2</sub>SO<sub>4</sub> solution was used to prepare the reaction solution. <sup>e</sup>Sulfate buffer solution was used to prepare the reaction solution.

To continue the reaction and confirm the high selectivity at a pH of 2, the synthetic MnO<sub>2</sub> oxidation stage was carried out in sulfate buffer solution. This solution contained sufficient acid to continue the reaction. **Figure 2-6 (b)** shows the reaction selectivity of the successive stages of the reference oxygen delignification terminated at a reaction time of 120 min and synthetic MnO<sub>2</sub> oxidation at a pH of 2 using sulfate buffer. The data points of the synthetic MnO<sub>2</sub> oxidation stage were obtained at reaction times of 30, 90, 180, and 360 min. The reaction selectivity of the successive stages was much higher than the reference oxygen delignification when the pH of the synthetic MnO<sub>2</sub> oxidation stage was made to be 2 by sulfate buffer. The kappa number decreased from about 5 to 3 with almost the same viscosity by the substitution of the later stage of the common oxygen delignification with the synthetic MnO<sub>2</sub> oxidation at a pH of 2 using sulfate buffer. The degree of this improvement is rather surprising.

Because the successive stages showed much higher reaction selectivity than the reference oxygen delignification, the latter synthetic MnO<sub>2</sub> oxidation stage seems to be very

effective for increasing the reaction selectivity. In this context, the hardwood unbleached kraft pulp was directly treated with the synthetic  $\text{MnO}_2$  oxidation at a pH of 2 in the sulfate buffer solution without the common oxygen delignification. Contrarily to the expectation, however, the delignification did not proceed in this synthetic  $\text{MnO}_2$  oxidation, despite a slight viscosity drop. The synthetic  $\text{MnO}_2$  may not have penetrated into pulp fibers when the unbleached pulp was directly treated with the synthetic  $\text{MnO}_2$ . Similar experiments were also carried out in a buffer solution with a pH of 1. The kappa number and viscosity decreased rapidly, but the bleaching selectivity was significantly lower than that of common oxygen delignification (data not shown).

### **2.3.5 Possibility on the recycle of $\text{MnO}_2$**

Because  $\text{MnO}_2$  is reduced to  $\text{Mn}^{2+}$  in the synthetic  $\text{MnO}_2$  stage, almost all the  $\text{MnO}_2$  can be converted to soluble  $\text{Mn}^{2+}$  when  $\text{MnO}_2$  is applied in an appropriate amount. After filtration and washing of the pulp, all the  $\text{Mn}^{2+}$  is present in the filtrate (effluent) with organic matter. The  $\text{Mn}^{2+}$  can be reconverted to precipitates of  $\text{MnO}_2$  by  $\text{O}_2$  bubbling under alkaline conditions, and the  $\text{MnO}_2$  can be isolated by filtration. Most co-present organic matter in the effluent would not precipitate even under alkaline conditions.

$\text{MnO}_2$  can be added before the initial oxygen delignification process because, as shown in **Figure 2-4**, the addition of  $\text{MnO}_2$  does not have a large effect on the reaction selectivity. In this context, it is possible to filter the reconverted  $\text{MnO}_2$  not with filter paper but by using unbleached pulp, which can then be subjected to the successive stages.

## 2.4 Conclusions

The addition of  $\text{MnO}_2$  suppressed the degradation of a carbohydrate model compound, MGP, when it was treated under oxygen delignification conditions together with a phenolic lignin model compound, Valc. This result is attributed to the catalytic action of  $\text{MnO}_2$  to decompose peroxides without the formation of any active oxygen species.

The addition of  $\text{MnO}_2$  did not have any meaningful effect on the reaction selectivity in oxygen delignification of hardwood unbleached pulp. This is because the  $\text{MnO}_2$  was present not within but only outside of the pulp fibers.

When  $\text{MnO}_2$  was generated *in-situ* in pulp fibers and the fibers were subjected to oxygen delignification, the reaction selectivity was much worse than the oxygen delignification without the addition of  $\text{MnO}_2$ . This is because the *in-situ* generation of  $\text{MnO}_2$  was not complete, and not only  $\text{MnO}_2$  but also trivalent Mn species, among others, were generated in the pulp fibers, catalyzing the decomposition of peroxides to generate active oxygen species.

The successive stages of common oxygen delignification for 120 min followed by synthetic  $\text{MnO}_2$  oxidation at a pH of 2.0 using a sulfate buffer solution showed a much higher reaction selectivity than that of the common oxygen delignification. This result indicates that  $\text{MnO}_2$  can work as an oxidant to oxidatively degrade residual lignin in pulp. However, its oxidation mechanisms are rarely reported.

## 2.5 References

- [1] Ericsson, B.; Lindgren, B. O. Factors influencing the carbohydrate degradation under oxygen-alkali bleaching. *Svensk Papperstidning* **1971**, 74 (22), 757–765.
- [2] Gierer, J.; Imsgard, F. The reaction of lignins with oxygen and hydrogen peroxide in alkaline media. *Svensk Papperstidning* **1977**, 80 (16), 510-518.
- [3] Yokoyama, T.; Matsumoto, Y.; Yasumoto, M.; Meshitsuka, G. The role of peroxide species in the carbohydrate degradation during oxygen bleaching part 2: Effect of oxygen pressure on the degradation of lignin and carbohydrate model compounds and on the reaction selectivity. *Journal of Pulp and Paper Science* **1996**, 22 (5), J151-J154.
- [4] Konishi, F.; Yokoyama, T.; Matsumoto, Y. Investigation of hydrogen abstraction from methyl glucoside by active oxygen species under oxygen delignification conditions. Part 1: Study on the anomeric position. *Holzforschung* **2009**, 63 (1), 52-60.
- [5] Nakagawa, A.; Yokoyama, T.; Matsumoto, Y. Investigation on the hydrogen abstraction from methyl glucoside by active oxygen species under oxygen delignification conditions. Part 2: Study on the C-2 position. *Journal of Wood Chemistry and Technology* **2012**, 32 (1), 10-22.
- [6] Yokoyama, T.; Nakagawa, A.; Konishi, F.; Matsumoto, Y. Investigation on hydrogen abstraction from methyl glucoside by active oxygen species under oxygen delignification conditions III: effects of the origin of active oxygen species. *Journal of Wood Science* **2011**, 57 (6), 512-519.
- [7] Nakagawa, A.; Yokoyama, T.; Matsumoto, Y. Investigation on the hydrogen abstraction from methyl glucoside by active oxygen species under oxygen delignification conditions IV: appearance of kinetic isotope effect in the reaction between methyl glucoside and deuterated methyl glucoside. *Journal of Wood Science* **2012**, 58 (6), 563-569.
- [8] Yokoyama, T.; Nakagawa, A.; Matsumoto, Y. Investigation on the hydrogen abstraction from methyl glucoside by active oxygen species under oxygen delignification conditions part 5: Comprehensive results on experiments using deuterium labeled methyl glucosides. *Journal*

*of Wood Chemistry and Technology* **2015**, 35 (6), 450-463.

[9] Yokoyama, T.; Matsumoto, Y.; Meshitsuka, G. Characterization of active oxygen species under oxygen-alkali bleaching conditions. *Holzforschung* **2005**, 59 (3), 269-275.

[10] Yasumoto, M.; Matsumoto, Y.; Ishizu, A. The role of peroxide species in the carbohydrate degradation during oxygen bleaching part 1: Factors influencing the reaction selectivity between carbohydrate and lignin model compounds. *Journal of Wood Chemistry and Technology* **1996**, 16 (1), 95-107.

[11] Yokoyama, T.; Nakagawa, A.; Konishi, F.; Matsumoto, Y. Investigation on the hydrogen abstraction from methyl glucoside by active oxygen species under oxygen delignification conditions III: Effect of the origin of active oxygen species. *Journal of Wood Science* **2011**, 57 (6), 512-519.

[12] Posoknistakul, P.; Akiho, S.; Akiyama, T.; Yokoyama, T.; Matsumoto, Y. Stereo-preference in the degradation of the *erythro* and *threo* isomers of  $\beta$ -O-4-type lignin model compounds in oxidation processes III: in the reaction with chlorine- and manganese-based oxidants. *Journal of Wood Science* **2018**, 64 (4), 451-457.

**3 Differences in the Mechanisms of MnO<sub>2</sub> Oxidation  
between C<sub>6</sub>-C<sub>1</sub>-type Monomeric Lignin Model  
Compounds with the *p*-Hydroxyphenyl, Guaiacyl, and  
Syringyl Nuclei**

### 3.1 Introduction

Lignin is commonly depolymerized and degraded to isolate a portion with inevitable structural alteration, to promote delignification and allow isolation of the other components, the carbohydrates, or to obtain lignin-based fine chemicals in a biomass conversion process of woody raw materials, including chemical pulping for paper making. Oxidation is one of the most common methods for these purposes, together with acidic and alkaline treatments. In an oxidation process, lignin should be selectively oxidized while minimizing degradation of the carbohydrates as far as possible. Establishment of a process to realize this requirement is desirable; the oxidation processes currently in practical use do not show satisfactory selectivity.

In Chapter 2, manganese dioxide ( $\text{MnO}_2$ ) was employed in an oxidation process as an oxidant at a pH of 2 (in a sulfate buffer solution) and temperature of  $70^\circ\text{C}$  to the prebleaching (oxygen delignification) stage of chemical pulping. The latter half of the oxygen delignification stage was substituted with the  $\text{MnO}_2$  oxidation process, which promoted delignification while suppressing the degradation of the carbohydrates relative to that observed in the common oxygen delignification stage without the substitution. The  $\text{MnO}_2$  oxidation process therefore is the potential to satisfy the above-described requirement.  $\text{MnO}_2$  is a recyclable oxidant because it is reduced to  $\text{Mn}^{2+}$  in the oxidation process and  $\text{Mn}^{2+}$  can be reconverted to  $\text{MnO}_2$  by oxygen oxidation under alkaline conditions. This recyclability is another advantage of the  $\text{MnO}_2$  oxidation process.

$\text{MnO}_2$  oxidation of lignin has been examined in only a few studies, at least from a pure chemistry viewpoint,<sup>[1-2]</sup> although non-recyclable permanganate ( $\text{MnO}_4^-$ ) oxidation of lignin has been reported fairly widely.<sup>[3-13]</sup> It is generally known that  $\text{MnO}_2$  oxidizes allyl and benzyl alcohols selectively among various types of alcohol to afford the corresponding conjugate and aromatic carbonyls, respectively, with the oxidation rates being higher in non-polar organic solvents than in polar solvents.<sup>[14-21]</sup>  $\text{MnO}_2$  oxidation of other alcohols progresses only under

sever conditions.<sup>[16,22]</sup> However, if MnO<sub>2</sub> had oxidized only benzyl alcohols in the residual lignin, and consequently the corresponding  $\alpha$ -carbonyl groups had just formed in the study of Chapter 2, in accordance with this general knowledge, sufficient delignification must not have been attained. Just introducing  $\alpha$ -carbonyl groups does not contribute to delignification at the employed pH and temperature.

The aim of this study is to examine the mechanism of MnO<sub>2</sub> oxidation of lignin using model compounds. This paper is the first in a series, and focuses mainly on the mechanism of MnO<sub>2</sub> oxidation of simple non-phenolic lignin model compounds consisting of the *p*-hydroxyphenyl (**H**), guaiacyl (**G**), and syringyl (**S**) nuclei. **Figure 3-1** shows the **H**-, **G**-, and **S**-type lignin model compounds as well as *p*-ethylphenyl-type (**E**-type) compounds employed in this study. They are analogues of benzene (methoxybenzene (**H**-type, **I<sub>H</sub>**), 1,2-dimethoxybenzene (**G**-type, **I<sub>G</sub>**), 1,2,3-trimethoxybenzene (**S**-type, **I<sub>S</sub>**), and ethylbenzene (**E**-type, **I<sub>E</sub>**)), benzyl alcohol (4-methoxybenzyl alcohol (**H**-type, **II<sub>H</sub>**), 3,4-dimethoxybenzyl alcohol (**G**-type, **II<sub>G</sub>**), 3,4,5-trimethoxybenzyl alcohol (**S**-type, **II<sub>S</sub>**), and 4-ethylbenzyl alcohol (**E**-type, **II<sub>E</sub>**)), and benzyl alcohol deuterated at the methylene of the benzylic hydroxymethyl group (1-hydroxy(<sup>2</sup>H<sub>2</sub>)methyl-4-methoxybenzene (**H**-type, **III<sub>H</sub>**), 1-hydroxy(<sup>2</sup>H<sub>2</sub>)methyl-3,4-dimethoxybenzene (**G**-type, **III<sub>G</sub>**), 1-hydroxy(<sup>2</sup>H<sub>2</sub>)methyl-3,4,5-trimethoxybenzene (**S**-type, **III<sub>S</sub>**), and 1-ethyl-4-hydroxy(<sup>2</sup>H<sub>2</sub>)methylbenzene (**E**-type, **III<sub>E</sub>**)).

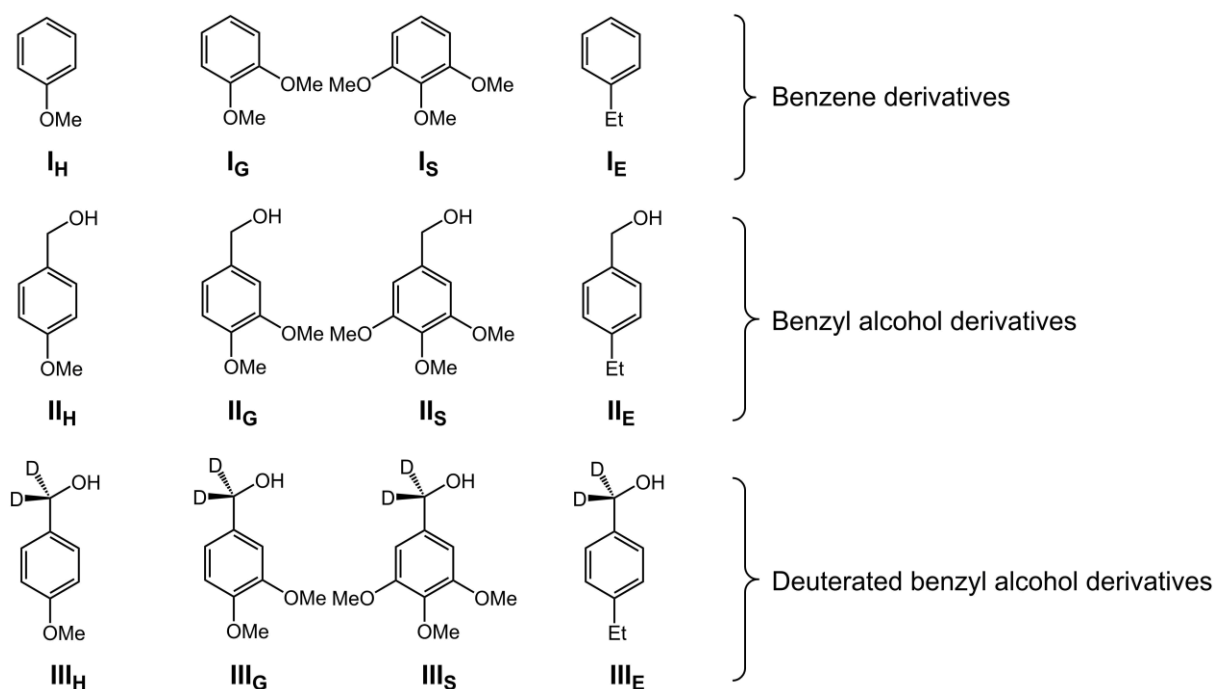


**Figure 3-1** Non-phenolic lignin model compounds (the **H**-, **G**-, and **S**-types) and *p*-ethylphenyl type compounds (the **E**-types) employed in this study.

## 3.2 Materials and methods

### 3.2.1 Materials

All chemicals used in this study except for the organic compounds described below were purchased from FUJIFILM Wako Pure Chemical Industries, Ltd. (Osaka, Japan), Tokyo Chemical Industry Co., Ltd. (Tokyo, Japan), or Sigma-Aldrich Japan K. K. (Tokyo, Japan), and used without further purification. Ultrapure H<sub>2</sub>O prepared by a generator, Puric-Z (Organo Co., Tokyo, Japan), was used in all the experiments.

#### 3.2.1.1 Preparation of model compounds and authentic compounds of reaction products

Compounds **I** (all the **H**-, **G**-, **S**- and **E**-types) and **II** were commercially available and purified by silica gel chromatography (Isolera<sup>TM</sup>, Biotage Japan Ltd., Tokyo, Japan). Compounds **III<sub>H</sub>**, **III<sub>G</sub>**, and **III<sub>E</sub>** were synthesized from commercially available 4-methoxybenzoic acid, 3,4-dimethoxybenzoic acid, and 4-ethylbenzoic acid, respectively, by

direct reduction with  $\text{LiAlD}_4$  in dry THF, and purified by silica gel chromatography. Compound **III**s was synthesized from commercially available 3,4,5-trimethoxybenzoic acid by ethyl esterification in  $\text{C}_2\text{H}_5\text{OH}$  containing  $\text{H}_2\text{SO}_4$  and successive reduction with  $\text{NaBD}_4$  and  $\text{LiCl}$  in dry THF, and then purified by silica gel chromatography.

**Figure 3-2** shows the quantified reaction products and another reaction product possibly generated in spite of no detection. The formers are analogues of benzaldehyde (**H**-type (**A<sub>H</sub>**), **G**-type (**A<sub>G</sub>**), **S**-type (**A<sub>S</sub>**), and **E**-type (**A<sub>E</sub>**)), 1,4-benzoquinone (**G**-type (**B<sub>G</sub>**) and **S**-type (**B<sub>S</sub>**)), and benzaldehyde deuterated at the benzylic formyl group (**H**-type (**A<sub>H</sub>'**), **G**-type (**A<sub>G</sub>'**), **S**-type (**A<sub>S</sub>'**), and **E**-type (**A<sub>E</sub>'**)). The latter is 1,4-benzoquinone (**H**-type (**B<sub>H</sub>**)). Products **A** were purchased and purified by silica gel chromatography for use as authentic compounds for identification, for preparing their calibration lines for quantification, and for reacting them as starting materials in the  $\text{MnO}_2$  oxidations described below. Products **B<sub>G</sub>** and **B<sub>S</sub>** were isolated from reaction solutions of the  $\text{MnO}_2$  oxidations of compounds **I<sub>G</sub>** and **II<sub>S</sub>**, respectively, and purified by silica gel chromatography for the same purposes. Product **B<sub>H</sub>** was purchased and purified by silica gel chromatography for the same purposes. Products **A'** were obtained from the corresponding compounds **III** by oxidizing them with  $\text{MnO}_2$  in  $\text{CH}_2\text{Cl}_2$  at room temperature, and purified by silica gel chromatography for the same purposes.

All the reaction products shown in **Figure 3-2** except for product **B<sub>H</sub>** were identified on the basis of their  $^1\text{H}$ - and  $^{13}\text{C}$ -NMR (JNM-A500, 500MHz, JEOL Ltd., Tokyo Japan) and gas chromatography-mass spectrometry (GC/MS, (electron ionization, 70 eV) was run on a Shimadzu GC2010/PARVUM2 (Shimadzu Co., Ltd., Kyoto, Japan) equipped with a capillary column (TC-17, 0.25 mm i.d.  $\times$  30 m, GL Science Inc., Tokyo, Japan).

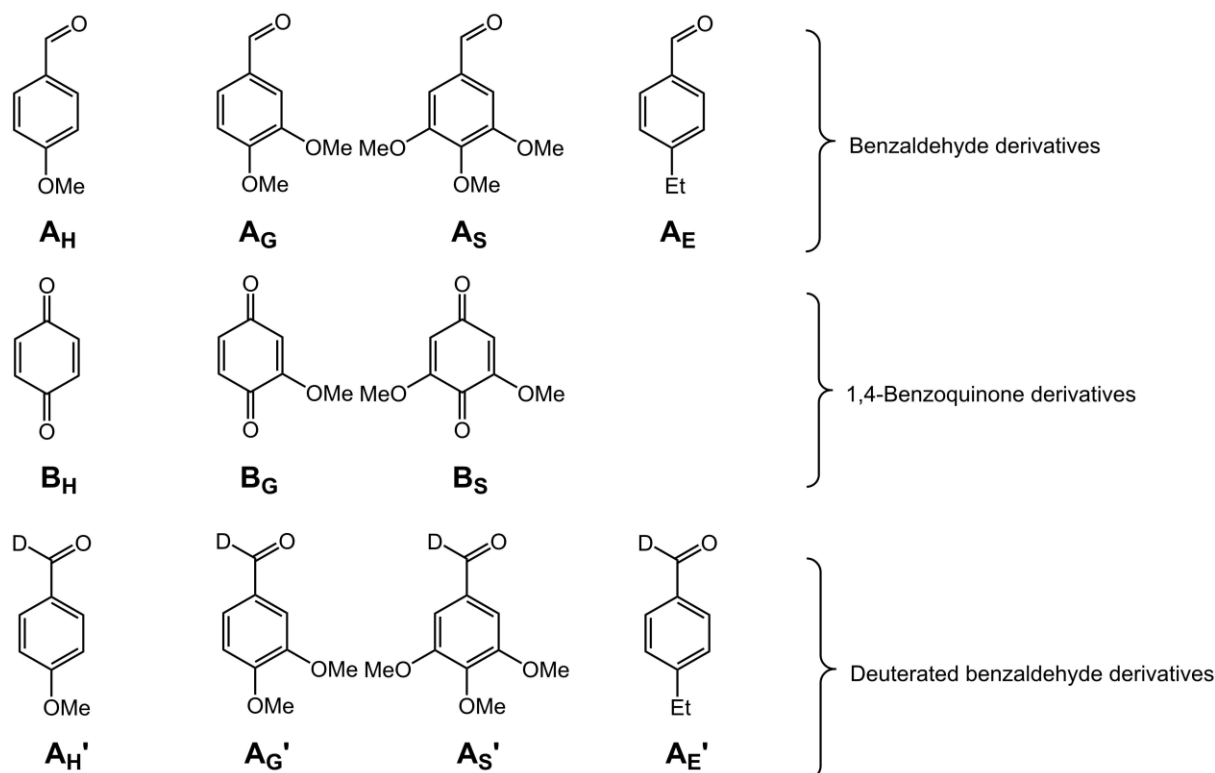
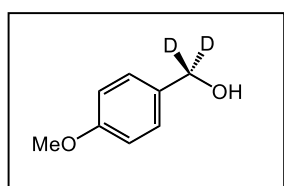


**Figure 3-2** Quantified reaction products as well as another possible one without detection (product **B<sub>H</sub>**) in the MnO<sub>2</sub> oxidation.

### 3.2.1.2 Synthetic processes of model compounds and reaction products

#### Synthesis of 1-hydroxy(<sup>2</sup>H<sub>2</sub>)methyl-4-methoxybenzene (**III<sub>H</sub>**)

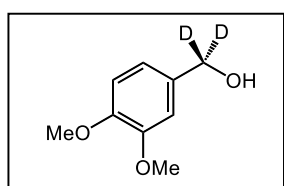


To a solution of dry tetrahydrofuran (THF, 5 mL) containing lithium aluminum hydride-*d*<sub>4</sub> (LiAlD<sub>4</sub>, 100 mg, 2.38 mmol) was added another dry THF (5 mL) with 4-methoxybenzoic acid (150 mg, 0.99 mmol). The reaction mixture was stirred at room temperature for 4 h. The completion of the reaction was monitored by TLC [EtOAc-hexane = 50:50, R<sub>f</sub> (starting material) = 0.38, R<sub>f</sub> (target material) = 0.50], quenched by addition of the mixture of methanol and H<sub>2</sub>O (10 mL, 1:1) and extracted with CH<sub>2</sub>Cl<sub>2</sub> (2 × 50 mL), dried over anhydrous Na<sub>2</sub>SO<sub>4</sub>, evaporated under vacuum and purified by PTLC [CH<sub>2</sub>Cl<sub>2</sub>-EtOAc = 90:10] to give **III<sub>H</sub>** as a colorless liquid (125.7 mg, 91%).

Compound **III<sub>H</sub>**: <sup>1</sup>H-NMR (solvent: CD<sub>2</sub>Cl<sub>2</sub> + aliquot of D<sub>2</sub>O): δ 3.79 (s, 3H, OCH<sub>3</sub>),

6.88 (broad d, 2H,  $J = 9$  Hz, aromatic C<sub>3</sub>-H & C<sub>5</sub>-H), 7.28 (broad d, 2H,  $J = 9$  Hz, aromatic C<sub>2</sub>-H & C<sub>6</sub>-H). <sup>13</sup>C-NMR:  $\delta$  55.6 (OCH<sub>3</sub>), 64.2 (CD<sub>2</sub>OH), 114.1 (aromatic C<sub>3</sub> & C<sub>5</sub>), 128.9 (aromatic C<sub>2</sub> & C<sub>6</sub>), 133.6 (aromatic C<sub>1</sub>), 159.6 (aromatic C<sub>4</sub>). MS m/z (rel. int.): 140 (M<sup>+</sup>, 100), 123 (88), 110 (91), 95 (47), 78 (69), 77 (40), 63 (40), 51 (48), 40 (47).

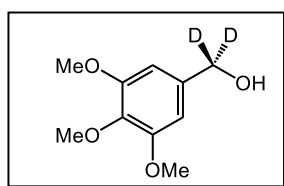
### Synthesis of 1-hydroxy(<sup>2</sup>H<sub>2</sub>)methyl-3,4-dimethoxybenzene (III<sub>G</sub>)



LiAlD<sub>4</sub> (100 mg, 2.38 mmol) was added to a solution of dry THF (5 mL). After mixing for 5 min, the mixture was added another dry THF (5 mL) containing 3,4-dimethoxybenzoic acid (150 mg, 0.82 mmol) and stirred at room temperature for 4 h. The progress of the reaction was monitored by TLC [EtOAc-hexane = 50:50, R<sub>f</sub> (starting material) = 0.21, R<sub>f</sub> (target material) = 0.31], quenched by addition of the mixture of methanol and H<sub>2</sub>O (10 mL, 1:1). The mixture was extracted with CH<sub>2</sub>Cl<sub>2</sub> (2 × 50 mL), the organic fractions were combined, dried over anhydrous Na<sub>2</sub>SO<sub>4</sub>, condensed under vacuum and purified by PTLC [CH<sub>2</sub>Cl<sub>2</sub>-EtOAc = 90:10] to give III<sub>G</sub> as a colorless liquid (98.1 mg, 70%).

Compound III<sub>G</sub>: <sup>1</sup>H-NMR (solvent: CDCl<sub>3</sub> + aliquot of D<sub>2</sub>O):  $\delta$  3.89 (s, 3H, aromatic C<sub>3</sub>- or C<sub>4</sub>-OCH<sub>3</sub>), 3.89 (s, 3H, aromatic C<sub>3</sub>- or C<sub>4</sub>-OCH<sub>3</sub>), 6.85 (d, 1H,  $J = 8.0$  Hz, aromatic C<sub>5</sub>-H), 6.89 (dd, 1H,  $J = 8.0, 2.0$  Hz, aromatic C<sub>6</sub>-H), 6.93 (d, 1H,  $J = 2.0$  Hz, aromatic C<sub>2</sub>-H). <sup>13</sup>C-NMR:  $\delta$  56.0 (aromatic C<sub>3</sub>- or C<sub>4</sub>-OCH<sub>3</sub>), 56.1 (aromatic C<sub>3</sub>- or C<sub>4</sub>-OCH<sub>3</sub>), 64.7 (CD<sub>2</sub>OH), 110.7 (aromatic C<sub>2</sub>), 111.2 (aromatic C<sub>5</sub>), 119.6 (aromatic C<sub>6</sub>), 133.6 (aromatic C<sub>1</sub>), 148.8 (aromatic C<sub>4</sub>), 149.3 (aromatic C<sub>3</sub>). MS m/z (rel. int.): 170 (M<sup>+</sup>, 100), 153 (39), 140 (47), 122 (14), 111 (34), 99 (53), 79 (60), 67 (73), 51 (54), 40 (44).

### Synthesis of 1-hydroxy(<sup>2</sup>H<sub>2</sub>)methyl-3,4,5-trimethoxybenzene (III<sub>S</sub>)

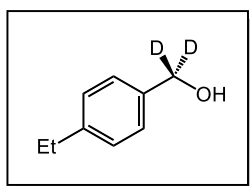


To a solution of 3,4,5-trimethoxybenzoic acid (S<sub>3</sub>, 500 mg, 2.35 mmol) in C<sub>2</sub>H<sub>5</sub>OH (100 mL) was slowly added 12 mL sulfuric acid (98%). The reaction mixture was heated at 50°C for 12 h. Na<sub>2</sub>CO<sub>3</sub> was added to neutralize the reaction mixture. The mixture was

extracted with EtOAc (2 × 100 mL), dried over anhydrous Na<sub>2</sub>SO<sub>4</sub>, concentrated under vacuum to afford ethyl 3,4,5-trimethoxybenzoate as a white solid and purified by silica gel chromatography [EtOAc-hexane = 50:50] (380.3 mg, 67%). Ethyl 3,4,5-Trimethoxybenzoate (120 mg, 0.50 mmol) was reduced in dry THF (25 mL) containing sodium borodeuteride (NaBD<sub>4</sub>, 100 mg, 2.39 mmol) and lithium chloride (LiCl, 100 mg, 2.36 mmol) to synthesize **III<sub>S</sub>**. The reaction mixture was refluxed at 80°C for 2 days. The progress of the reaction was monitored by TLC [EtOAc-hexane = 50:50, R<sub>f</sub> (starting material) = 0.15, R<sub>f</sub> (target material) = 0.31], quenched by addition of the mixture of methanol and H<sub>2</sub>O (10 mL, 1:1) and extracted with CH<sub>2</sub>Cl<sub>2</sub> (2 × 50 mL). The organic phase was combined, dried over anhydrous Na<sub>2</sub>SO<sub>4</sub>, concentrated under vacuum and the crude material was purified by PTLC [CH<sub>2</sub>Cl<sub>2</sub>-EtOAc = 90:10] to give **III<sub>S</sub>** as a colorless liquid (38.0 mg, 38%).

Compound **III<sub>S</sub>**: <sup>1</sup>H-NMR (solvent: CDCl<sub>3</sub> + aliquot of D<sub>2</sub>O): δ 3.82 (s, 3H, aromatic C<sub>4</sub>-OCH<sub>3</sub>), 3.84 (s, 6H, aromatic C<sub>3</sub>- & C<sub>5</sub>-OCH<sub>3</sub>), 6.57 (s, 2H, aromatic C<sub>2</sub>-H & C<sub>6</sub>-H). <sup>13</sup>C-NMR: δ 56.2 (aromatic C<sub>3</sub>- & C<sub>5</sub>-OCH<sub>3</sub>), 61.0 (aromatic C<sub>4</sub>-OCH<sub>3</sub>), 64.9 (CD<sub>2</sub>OH), 104.0 (aromatic C<sub>2</sub> & C<sub>6</sub>), 136.8 (aromatic C<sub>1</sub>), 136.9 (aromatic C<sub>4</sub>), 153.4 (aromatic C<sub>3</sub> & C<sub>5</sub>). MS m/z (rel. int.): 200 (M<sup>+</sup>, 100), 185 (28), 170 (9), 157 (20), 139 (19), 129 (96), 125 (42), 112 (19), 97 (65), 83 (30), 66 (43), 53 (52), 43 (40), 40 (37).

### Synthesis of 1-ethyl-4-hydroxy(<sup>2</sup>H<sub>2</sub>)methylbenzene (**III<sub>E</sub>**)



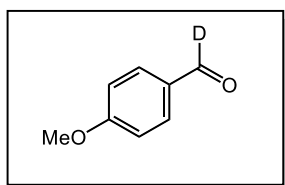
To a solution of dry tetrahydrofuran (THF, 10 mL) containing lithium aluminum hydride-*d*<sub>4</sub> (LiAlD<sub>4</sub>, 200 mg, 4.76 mmol) was added another dry THF (10 mL) with 4-ethylbenzoic acid (300 mg, 2.00 mmol). The reaction mixture was stirred at room temperature for 4 h.

The completion of the reaction was monitored by TLC [EtOAc-hexane = 50:50, R<sub>f</sub> (starting material) = 0.40, R<sub>f</sub> (target material) = 0.68], quenched by addition of the mixture of methanol and H<sub>2</sub>O (10 mL, 1:1) and extracted with CH<sub>2</sub>Cl<sub>2</sub> (2 × 50 mL), dried over anhydrous Na<sub>2</sub>SO<sub>4</sub>, evaporated under vacuum and purified by PTLC [CH<sub>2</sub>Cl<sub>2</sub>-EtOAc = 90:10] to give **III<sub>E</sub>** as a

colorless liquid (234.9 mg, 85%).

Compound **III<sub>E</sub>**: <sup>1</sup>H-NMR (solvent: CD<sub>3</sub>OD): δ 1.23 (t, 3H, *J* = 7.5 Hz, CH<sub>2</sub>-CH<sub>3</sub>), 2.64 (q, 2H, *J* = 7.5 Hz, CH<sub>2</sub>-CH<sub>3</sub>), 7.19 (d, 2H, *J* = 8.0 Hz, aromatic C<sub>3</sub>-H & C<sub>5</sub>-H), 7.27 (d, 2H, *J* = 8.0 Hz, aromatic C<sub>2</sub>-H & C<sub>6</sub>-H). <sup>13</sup>C-NMR: δ 16.6 (CH<sub>2</sub>-CH<sub>3</sub>), 29.9 (CH<sub>2</sub>-CH<sub>3</sub>), 64.7 (CD<sub>2</sub>OH), 128.6 (aromatic C<sub>2</sub> & C<sub>6</sub>), 129.1 (aromatic C<sub>3</sub> & C<sub>5</sub>), 140.1 (aromatic C<sub>1</sub>), 144.9 (aromatic C<sub>4</sub>). MS *m/z* (rel. int.): 138 (M<sup>+</sup>, 62), 123 (16), 109 (100), 92 (25), 81 (85), 77 (26), 63 (11), 51 (22), 40 (10).

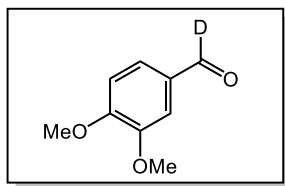
### Synthesis of 4-methoxybenzaldehyde-*α*-*d* (**A<sub>H</sub>'**)



To a solution of **III<sub>H</sub>** (50 mg, 0.36 mmol) in CH<sub>2</sub>Cl<sub>2</sub> (20 mL) was added MnO<sub>2</sub> (500 mg, 5.75 mmol) and stirred at room temperature for 1 day. The completion of the reaction was monitored by TLC [EtOAc-hexane = 50:50, R<sub>f</sub> (starting material) = 0.50, R<sub>f</sub> (target material) = 0.73]. The crude mixture was filtered, and the filtrate was evaporated under vacuum, purified by PTLC [CH<sub>2</sub>Cl<sub>2</sub>-EtOAc = 95:5] to give **A<sub>H</sub>'** as a colorless liquid (39.6 mg, 80%).

Product **A<sub>H</sub>'**: <sup>1</sup>H-NMR (solvent: CDCl<sub>3</sub> + aliquot of D<sub>2</sub>O): δ 3.90 (s, 3H, OCH<sub>3</sub>), 7.01 (dd, 2H, *J* = 6.9, 2.0 Hz, aromatic C<sub>3</sub>-H & C<sub>5</sub>-H), 7.85 (dd, 2H, *J* = 6.9, 2.0 Hz, aromatic C<sub>2</sub>-H & C<sub>6</sub>-H). <sup>13</sup>C-NMR: δ 55.8 (OCH<sub>3</sub>), 114.5 (aromatic C<sub>3</sub> & C<sub>5</sub>), 130.1 (aromatic C<sub>1</sub>), 132.2 (aromatic C<sub>2</sub> & C<sub>6</sub>), 164.8 (aromatic C<sub>4</sub>), 190.9 (CDH). MS *m/z* (rel. int.): 137 (M<sup>+</sup>, 69), 135 (100), 119 (1), 107 (19), 92 (29), 77 (52), 66 (34), 50 (20), 40 (27).

### Synthesis of veratraldehyde-*α*-*d* (**A<sub>G</sub>'**)

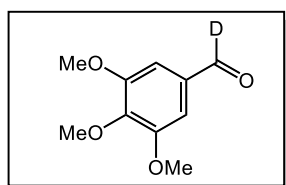


To a solution of **III<sub>G</sub>** (50 mg, 0.29 mmol) in CH<sub>2</sub>Cl<sub>2</sub> (20 mL) was added MnO<sub>2</sub> (500 mg, 5.75 mmol) at room temperature. The reaction mixture was stirred for 1 day at the same temperature. The completion of the reaction was monitored by TLC [EtOAc-hexane = 50:50, R<sub>f</sub> (starting material) = 0.31, R<sub>f</sub> (target material) = 0.60], The crude mixture was

filtered and the filtrate was evaporated under vacuum, purified by PTLC [ $\text{CH}_2\text{Cl}_2$ -EtOAc = 95:5] to give **AG'** as a light yellow liquid (31.2 mg, 64%).

Product **AG'**:  $^1\text{H}$ -NMR (solvent:  $\text{CDCl}_3$  + aliquot of  $\text{D}_2\text{O}$ ):  $\delta$  3.95 (s, 3H, aromatic  $\text{C}_3$ - $\text{OCH}_3$ ), 3.97 (s, 3H, aromatic  $\text{C}_4$ - $\text{OCH}_3$ ), 6.98 (d, 1H,  $J$  = 8.3 Hz, aromatic  $\text{C}_5$ - $\text{H}$ ), 7.42 (d, 1H,  $J$  = 1.4 Hz, aromatic  $\text{C}_2$ - $\text{H}$ ), 7.47 (dd, 1H,  $J$  = 8.3, 1.4 Hz, aromatic  $\text{C}_6$ - $\text{H}$ ).  $^{13}\text{C}$ -NMR:  $\delta$  56.2 (aromatic  $\text{C}_3$ - $\text{OCH}_3$ ), 56.4 (aromatic  $\text{C}_4$ - $\text{OCH}_3$ ), 109.1 (aromatic  $\text{C}_5$ ), 110.6 (aromatic  $\text{C}_2$ ), 127.1 (aromatic  $\text{C}_6$ ), 130.3 (aromatic  $\text{C}_1$ ), 149.8 (aromatic  $\text{C}_3$ ), 154.7 (aromatic  $\text{C}_4$ ). 190.7 ( $\text{CDO}$ ). MS  $m/z$  (rel. int.): 167 ( $\text{M}^+$ , 100), 152 (20), 137 (6), 119 (12), 107 (9), 96 (95), 78 (57), 66 (42), 63 (23), 51 (63), 42 (32).

### Synthesis of 3,4,5-trimethoxybenzaldehyde- $\alpha$ - $d$ (**As'**)

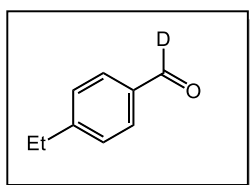


$\text{MnO}_2$  (100 mg, 1.15 mmol) was added to a solution of **III**s (10 mg, 0.05 mmol) in  $\text{CH}_2\text{Cl}_2$  (10 mL). The reaction mixture was stirred at room temperature for 1 day. The completion of the reaction was monitored by TLC [EtOAc-hexane = 50:50,  $R_f$  (starting material) = 0.31,  $R_f$  (target material) = 0.65]. The crude mixture was filtered, and the filtrate was evaporated under vacuum, purified by PTLC [ $\text{CH}_2\text{Cl}_2$ -EtOAc = 95:5] to give **As'** as a white solid (7.8 mg, 79%).

Product **As'**:  $^1\text{H}$ -NMR (solvent:  $\text{CDCl}_3$  + aliquot of  $\text{D}_2\text{O}$ ):  $\delta$  3.94 (s, 6H, aromatic  $\text{C}_3$ - &  $\text{C}_5$ - $\text{OCH}_3$ ), 3.95 (s, 3H, aromatic  $\text{C}_4$ - $\text{OCH}_3$ ), 7.14 (s, 2H, aromatic  $\text{C}_2$ - $\text{H}$  &  $\text{C}_6$ - $\text{H}$ ),  $^{13}\text{C}$ -NMR:  $\delta$  56.5 (aromatic  $\text{C}_3$ - &  $\text{C}_5$ - $\text{OCH}_3$ ), 61.2 (aromatic  $\text{C}_4$ - $\text{OCH}_3$ ), 106.9 (aromatic  $\text{C}_2$  &  $\text{C}_6$ ), 131.8 (aromatic  $\text{C}_1$ ), 143.8 (aromatic  $\text{C}_4$ ), 153.8 (aromatic  $\text{C}_3$  &  $\text{C}_5$ ), 190.8 ( $\text{CDO}$ ). MS  $m/z$  (rel. int.): 197 ( $\text{M}^+$ , 60), 182 (29), 167 (2), 154 (7), 137 (9), 126 (52), 124 (10), 111 (59), 96 (47), 78 (20), 66 (48), 52 (36), 40 (100).

### Synthesis of 4-ethylbenzaldehyde- $\alpha$ - $d$ (**AE'**)

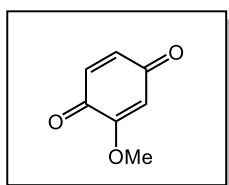
$\text{MnO}_2$  (500 mg, 5.75 mmol) was added to a solution of **III**E (100 mg, 0.72 mmol) in  $\text{CH}_2\text{Cl}_2$  (50 mL). The reaction mixture was stirred at room temperature for 1 day. The



completion of the reaction was monitored by TLC [EtOAc-hexane = 50:50,  $R_f$  (starting material) = 0.68,  $R_f$  (target material) = 0.85]. The crude mixture was filtered, and the filtrate was evaporated under vacuum, purified by PTLC [ $\text{CH}_2\text{Cl}_2$ -EtOAc = 95:5] to give **A<sub>E</sub>'** as a colorless liquid (43.3 mg, 44%).

Product **A<sub>E</sub>'**:  $^1\text{H-NMR}$  (solvent:  $\text{CDCl}_3$ ):  $\delta$  1.28 (t, 3H,  $J = 7.5$  Hz,  $\text{CH}_2\text{-CH}_3$ ), 2.74 (q, 2H,  $J = 7.5$  Hz,  $\text{CH}_2\text{-CH}_3$ ), 7.37 (d, 2H,  $J = 8.0$  Hz, aromatic  $\text{C}_3\text{-H}$  &  $\text{C}_5\text{-H}$ ), 7.27 (d, 2H,  $J = 8.0$  Hz, aromatic  $\text{C}_2\text{-H}$  &  $\text{C}_6\text{-H}$ ).  $^{13}\text{C-NMR}$ :  $\delta$  15.5 ( $\text{CH}_2\text{-CH}_3$ ), 29.6 ( $\text{CH}_2\text{-CH}_3$ ), 128.8 (aromatic  $\text{C}_3$  &  $\text{C}_5$ ), 130.2 (aromatic  $\text{C}_2$  &  $\text{C}_6$ ), 134.6 (aromatic  $\text{C}_1$ ), 152.1 (aromatic  $\text{C}_4$ ), 191.8 ( $\text{CDH}$ ). MS  $m/z$  (rel. int.): 135 ( $\text{M}^+$ , 99), 133 (86), 120 (23), 105 (66), 92 (100), 77 (39), 63 (17), 51 (35), 40 (10).

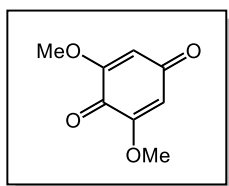
### Synthesis of methoxybenzoquinone (**B<sub>G</sub>**)



To 1,2-dimethoxybenzene (**I<sub>G</sub>**, 1 g, 7.24 mmol) dissolved in  $\text{H}_2\text{SO}_4$  solution (1 mol/L)/1,4-dioxane (200 mL, v:v = 2:1) was added  $\text{MnO}_2$  (5 g, 57.5 mmol). The mixture was stirred at room temperature for 6 days. The progress of the reaction was monitored by TLC [EtOAc-hexane = 50:50,  $R_f$  (starting material) = 0.78,  $R_f$  (target material) = 0.67], quenched by addition of sodium carbonate (2 g). The crude mixture was filtered, and the filtrate was extracted with EtOAc (2  $\times$  100 mL). The combined organic fraction was dried over anhydrous  $\text{Na}_2\text{SO}_4$  and evaporated under vacuum. The crude **B<sub>G</sub>** (63.7 mg, 6%) was separated from the mixture by silica gel chromatography using EtOAc-hexane = 10:90. The pure **B<sub>G</sub>** (yellow solid) was obtained by multiple purification with PTLC [EtOAc-hexane = 50:50 and  $\text{CH}_2\text{Cl}_2$ -methanol = 90:1].

Product **B<sub>G</sub>**:  $^1\text{H-NMR}$  (solvent:  $\text{CDCl}_3$ ):  $\delta$  3.85 (s, 3H,  $\text{OCH}_3$ ), 5.96 (d, 1H,  $J = 1.4$  Hz,  $\text{C}_2\text{-H}$ ), 6.71-6.77 (m, 2H, aromatic  $\text{C}_5\text{-H}$  &  $\text{C}_6\text{-H}$ ).  $^{13}\text{C-NMR}$ :  $\delta$  56.5 ( $\text{OCH}_3$ ), 107.9 ( $\text{C}_2$ ), 134.7 ( $\text{C}_5$  &  $\text{C}_6$ ), 137.5 ( $\text{C}_3$ ), 182.0 ( $\text{C}_1$ ), 187.7 ( $\text{C}_4$ ). MS  $m/z$  (rel. int.): 138 ( $\text{M}^+$ , 14), 123 (4), 110 (28), 108 (22), 95 (26), 82 (24), 69 (100), 54 (51), 41 (25).

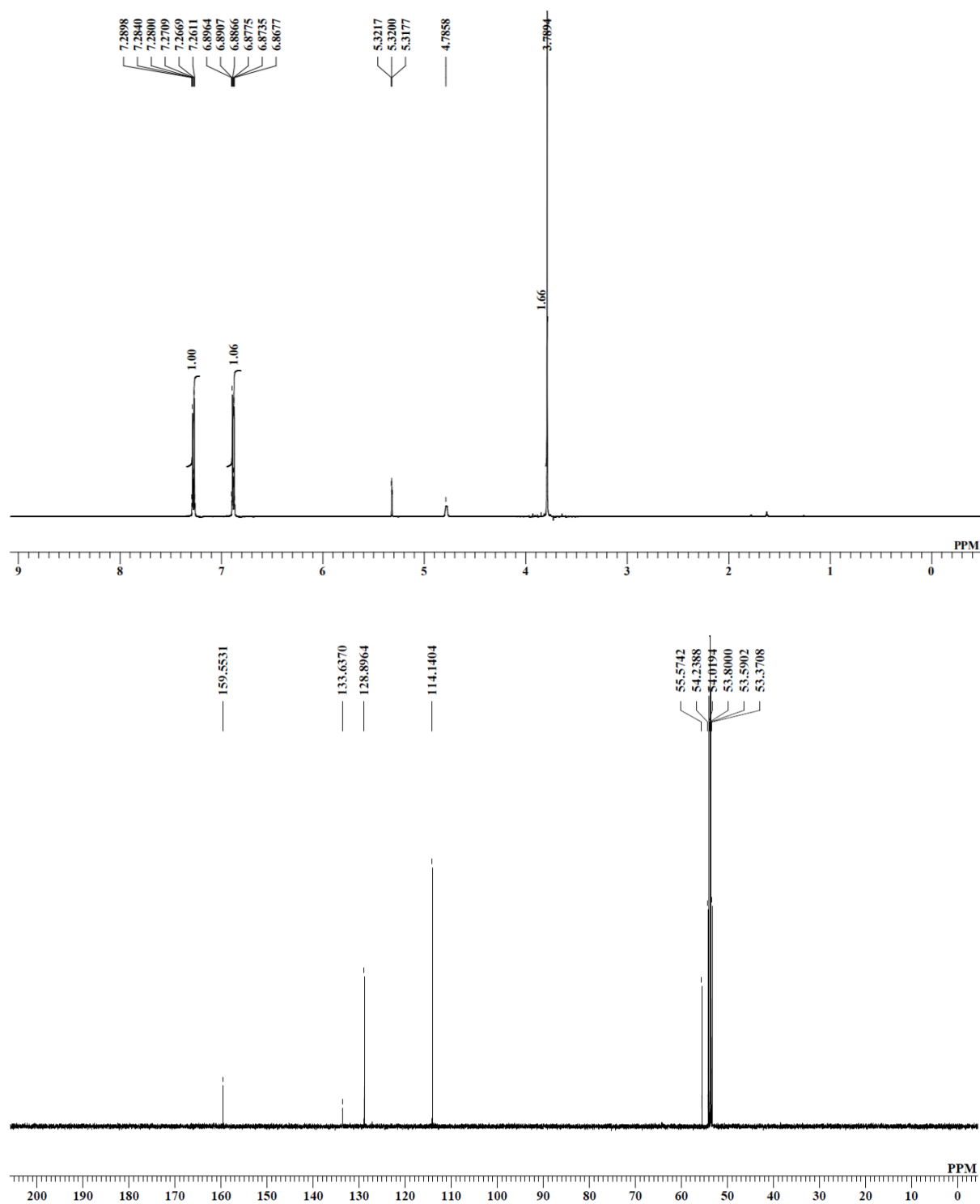
## Synthesis of 2,6-dimethoxy-1,4-benzoquinone (**Bs**)



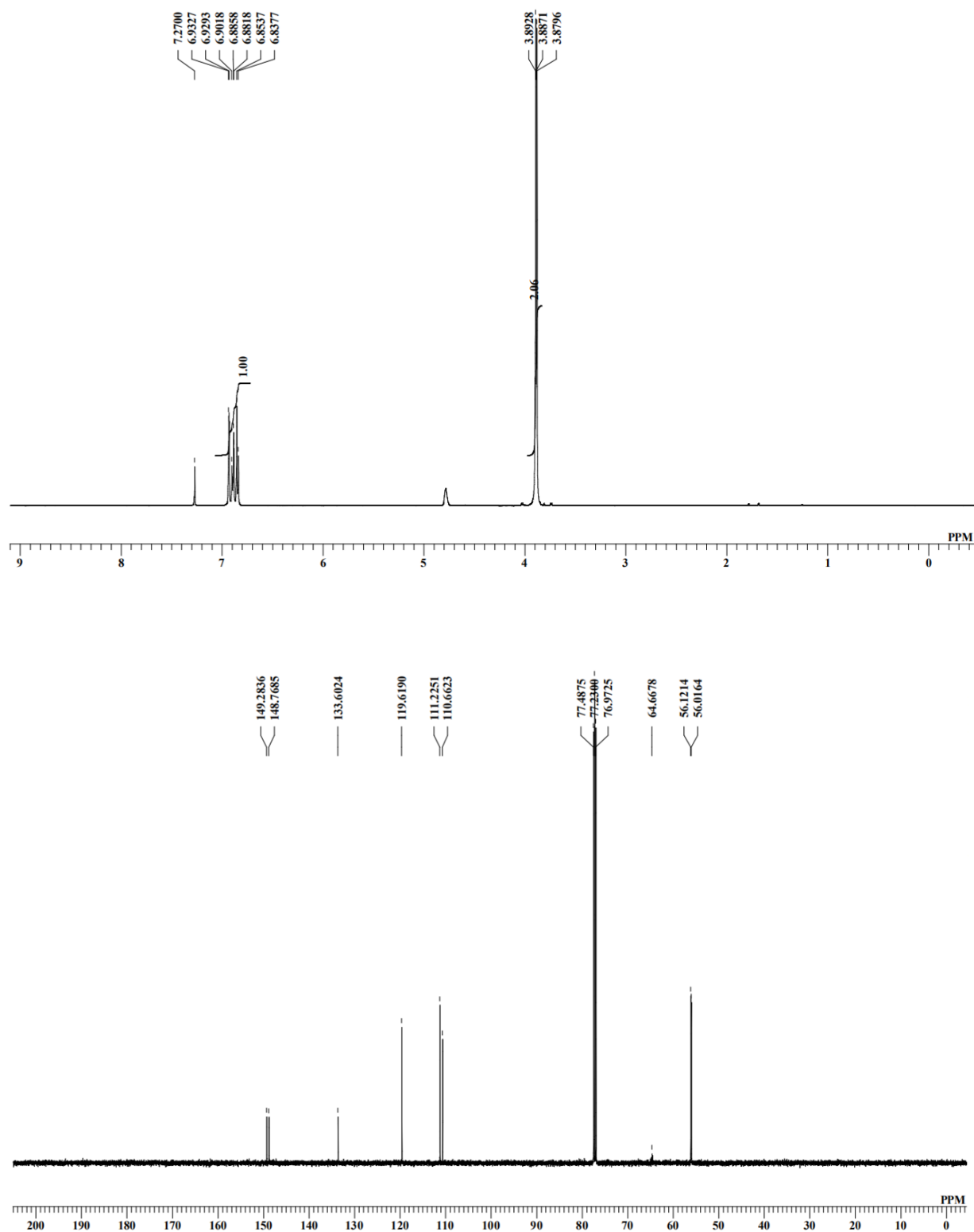
To 3,4,5-trimethoxybenzyl alcohol (**II**<sub>s</sub>, 1 g, 5.04 mmol) dissolved in H<sub>2</sub>SO<sub>4</sub> solution (1 mol/L)/1,4-dioxane (200 mL, v:v = 2:1) was added MnO<sub>2</sub> (5 g, 57.5 mmol). The mixture was stirred for 72 h at room temperature. The progress of the reaction was monitored by TLC [EtOAc-hexane = 50:50, R<sub>f</sub> (starting material) = 0.30, R<sub>f</sub> (target material) = 0.44], quenched by addition of sodium carbonate (2 g). The crude mixture was filtered, and the filtrate was extracted with EtOAc (2 × 100 mL). The combined organic fraction was dried over anhydrous Na<sub>2</sub>SO<sub>4</sub> and evaporated under vacuum. Then the crude **Bs** was separated from the mixture by silica gel chromatography (41.3 mg, 5%) using EtOAc-hexane = 50:50 at multiple times. The pure **Bs** (bright yellow solid) was obtained by multiple purifications with PTLC [CH<sub>2</sub>Cl<sub>2</sub>-methanol = 90:3].

Product **Bs**: <sup>1</sup>H-NMR (solvent: CDCl<sub>3</sub>): δ 3.82 (s, 6H, OCH<sub>3</sub>), 5.86 (s, 2H, C<sub>2</sub>-H & C<sub>6</sub>-H). <sup>13</sup>C-NMR: δ 56.7 (OCH<sub>3</sub>), 107.6 (C<sub>2</sub> & C<sub>6</sub>), 157.5 (C<sub>3</sub> & C<sub>5</sub>), 176.9 (C<sub>1</sub>), 187.1 (C<sub>4</sub>). MS m/z (rel. int.): 168 (M<sup>+</sup>, 9), 153 (1), 138 (4), 125 (6), 112 (4), 97 (8), 80 (17), 69 (100), 59 (13), 53 (27), 41 (12).

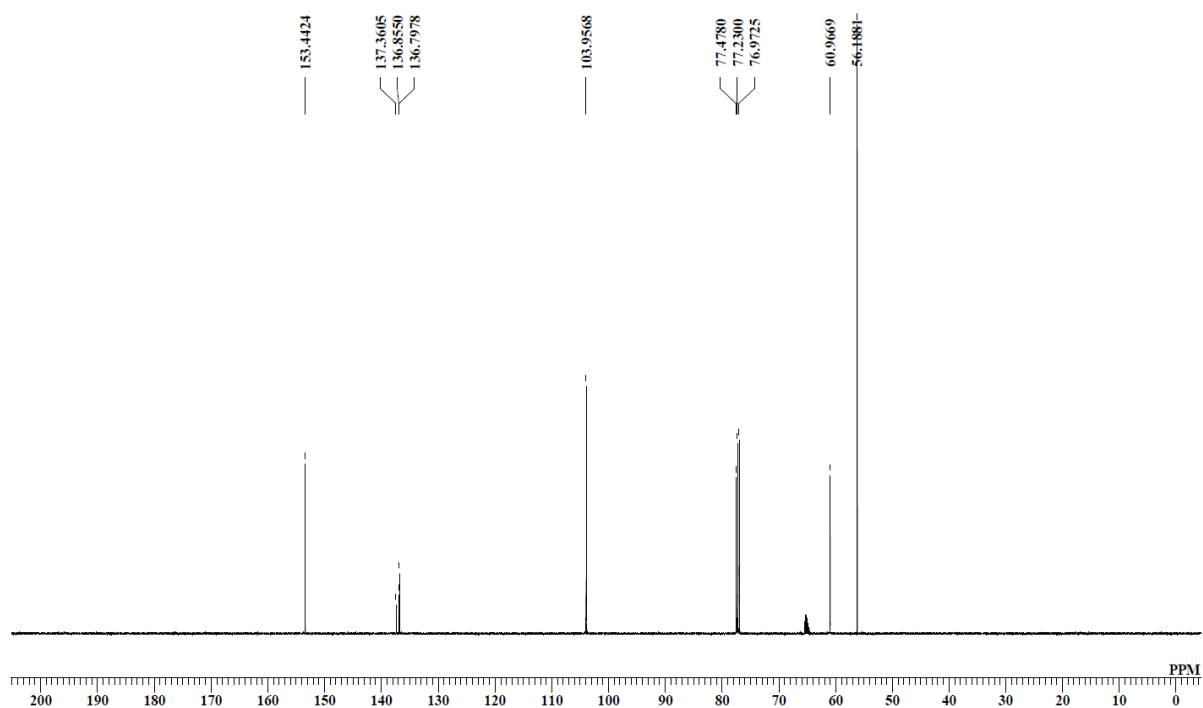
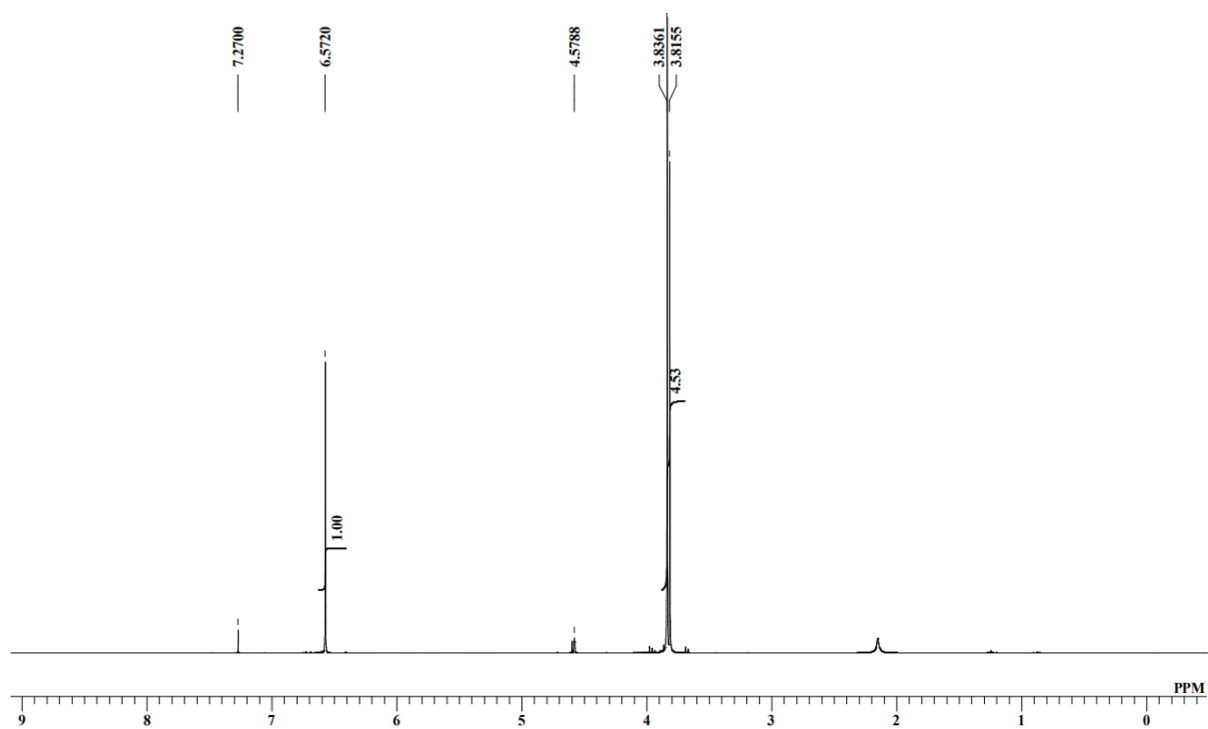
### 3.2.1.3 NMR and GC/MS spectra of synthesized model compounds and reaction products



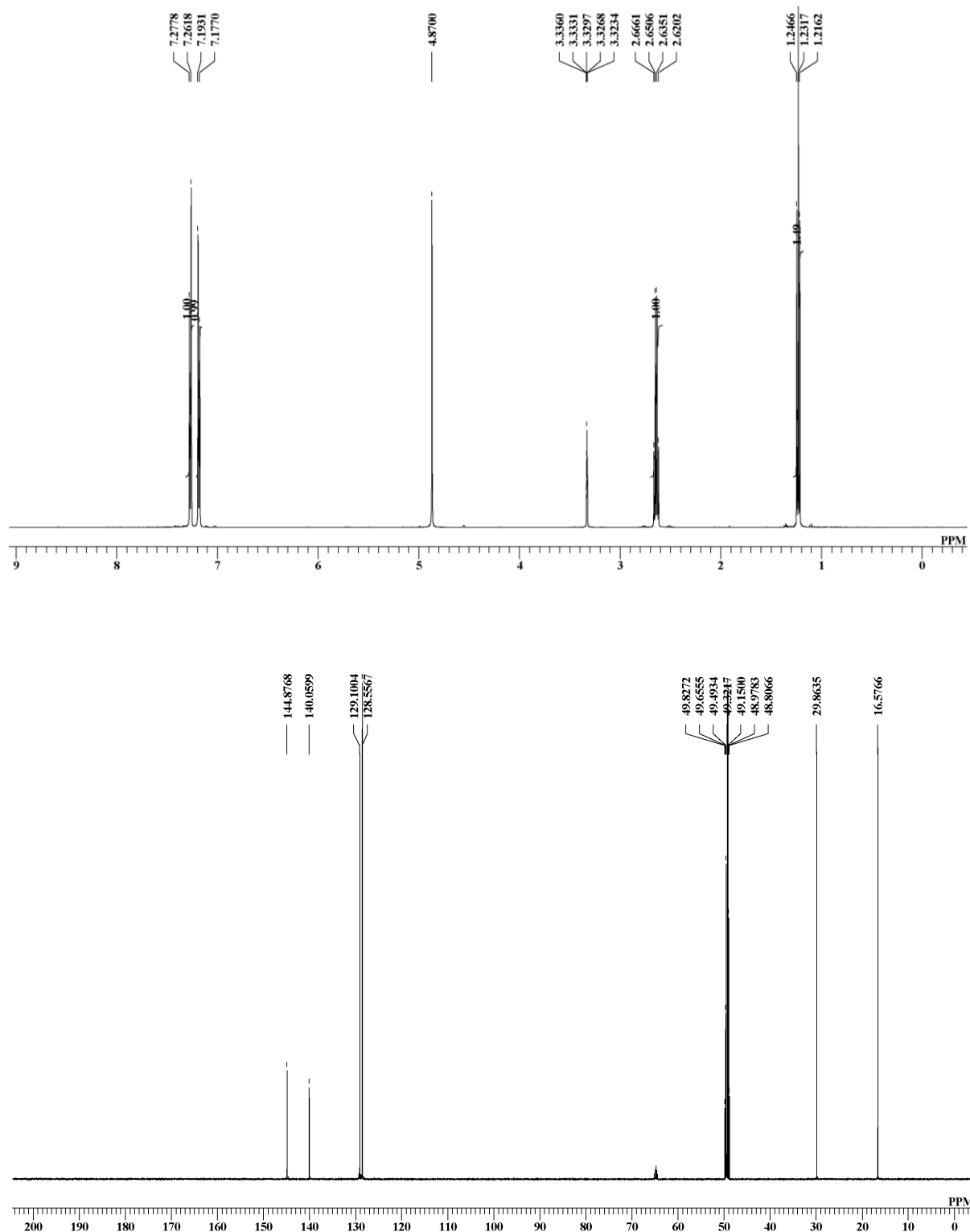
**Figure 3-3**  $^1\text{H}$ -NMR (top) and  $^{13}\text{C}$ -NMR (bottom) spectra of compound **IIIH**.



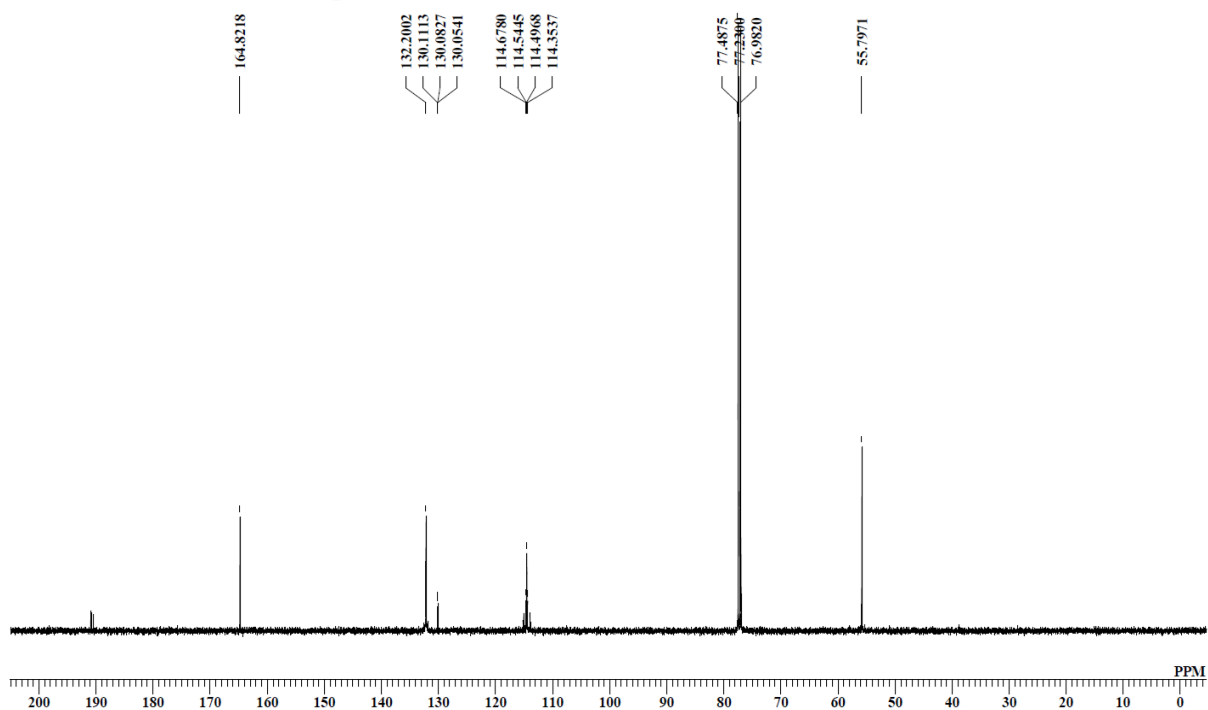
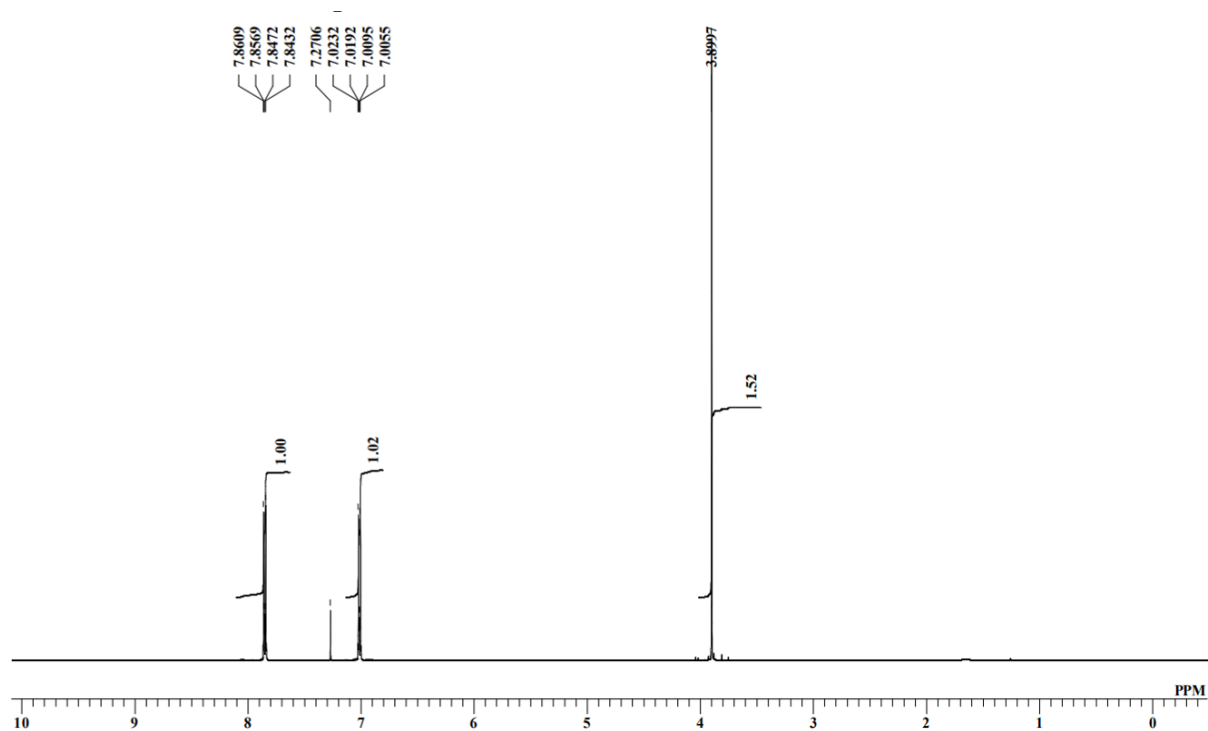
**Figure 3-4** <sup>1</sup>H-NMR (top) and <sup>13</sup>C-NMR (bottom) spectra of compound **IIIc**.



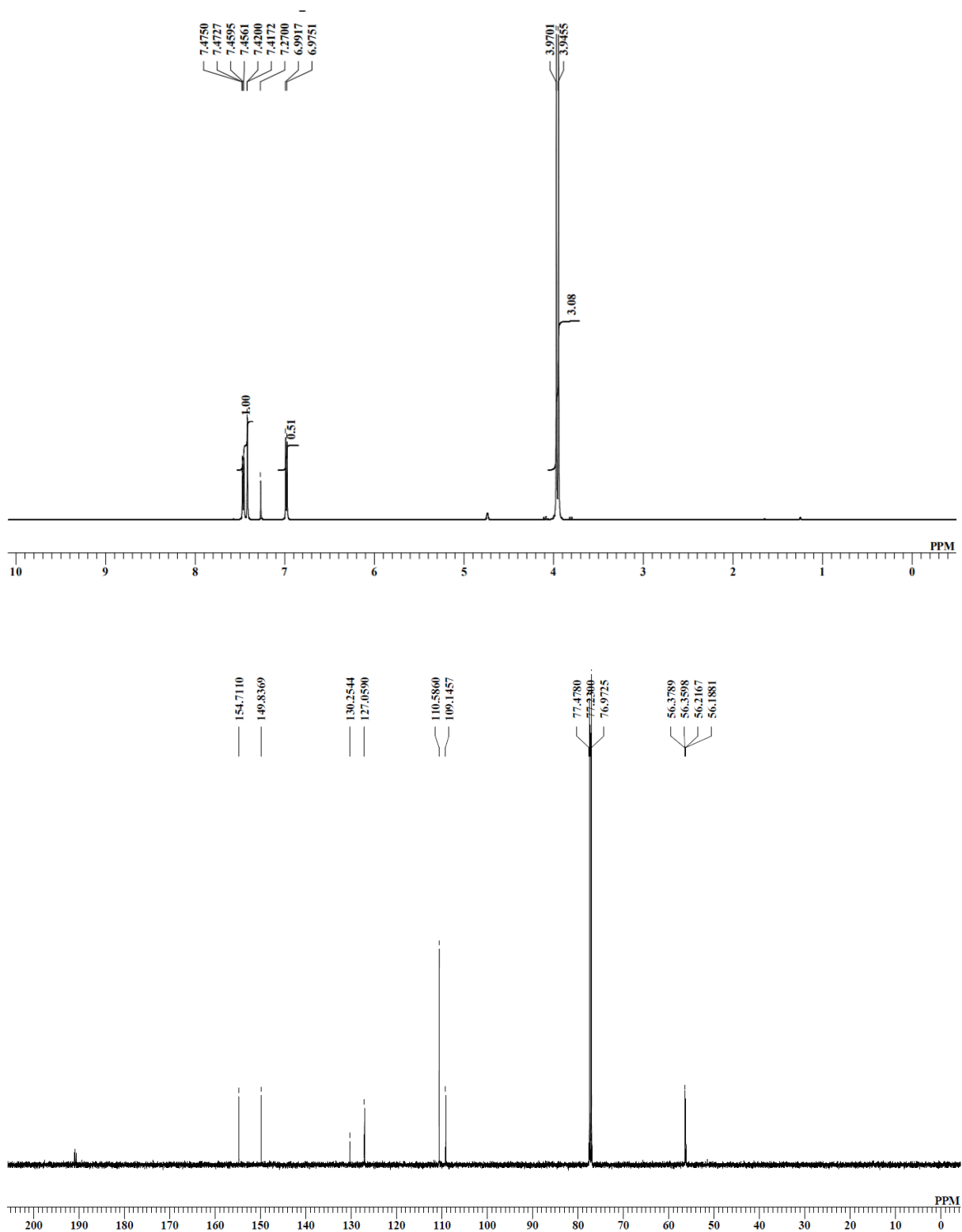
**Figure 3-5**  $^1\text{H}$ -NMR (top) and  $^{13}\text{C}$ -NMR (bottom) spectra of compound **III**s.



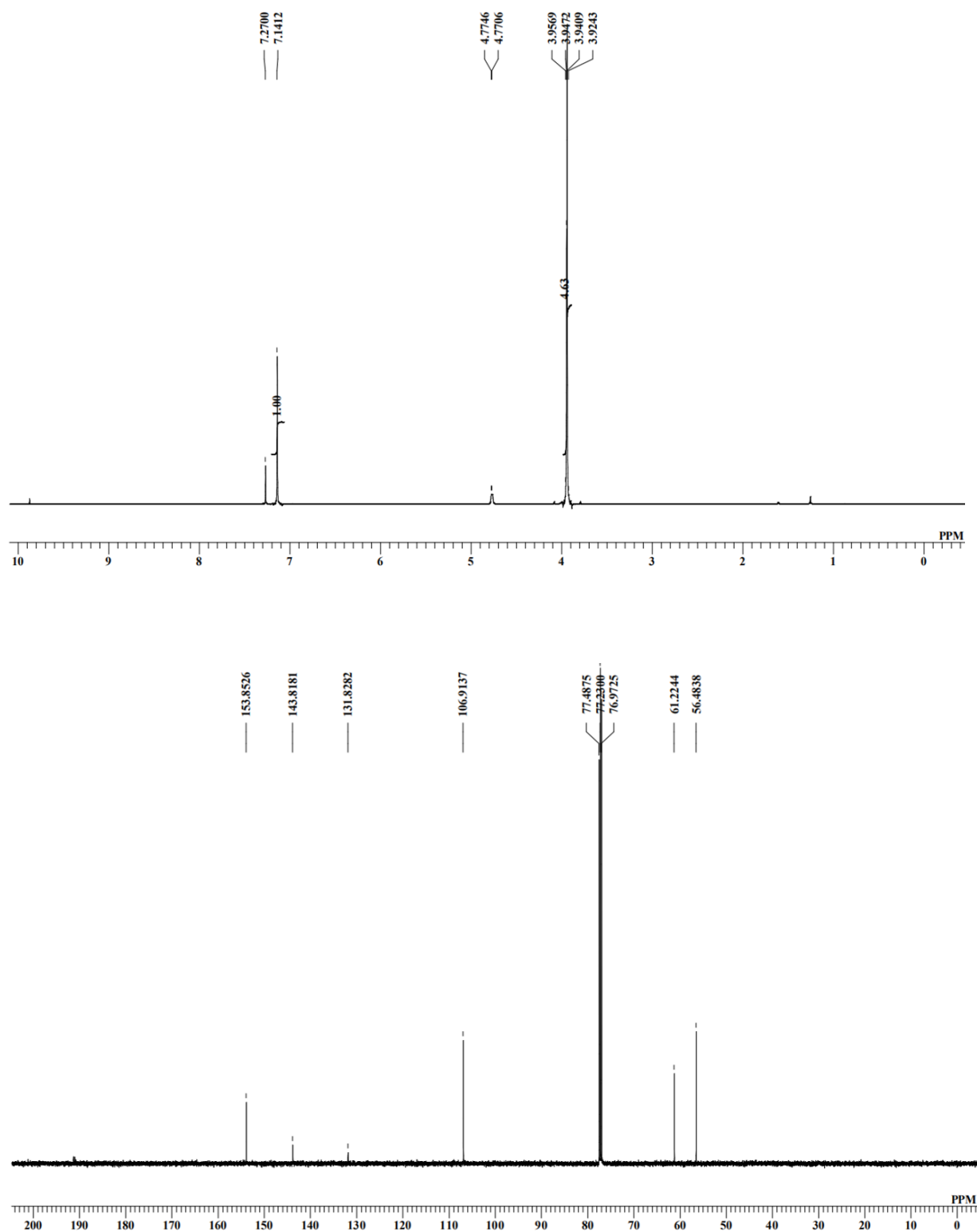
**Figure 3-6**  $^1\text{H}$ -NMR (top) and  $^{13}\text{C}$ -NMR (bottom) spectra of compound **III<sub>E</sub>**.



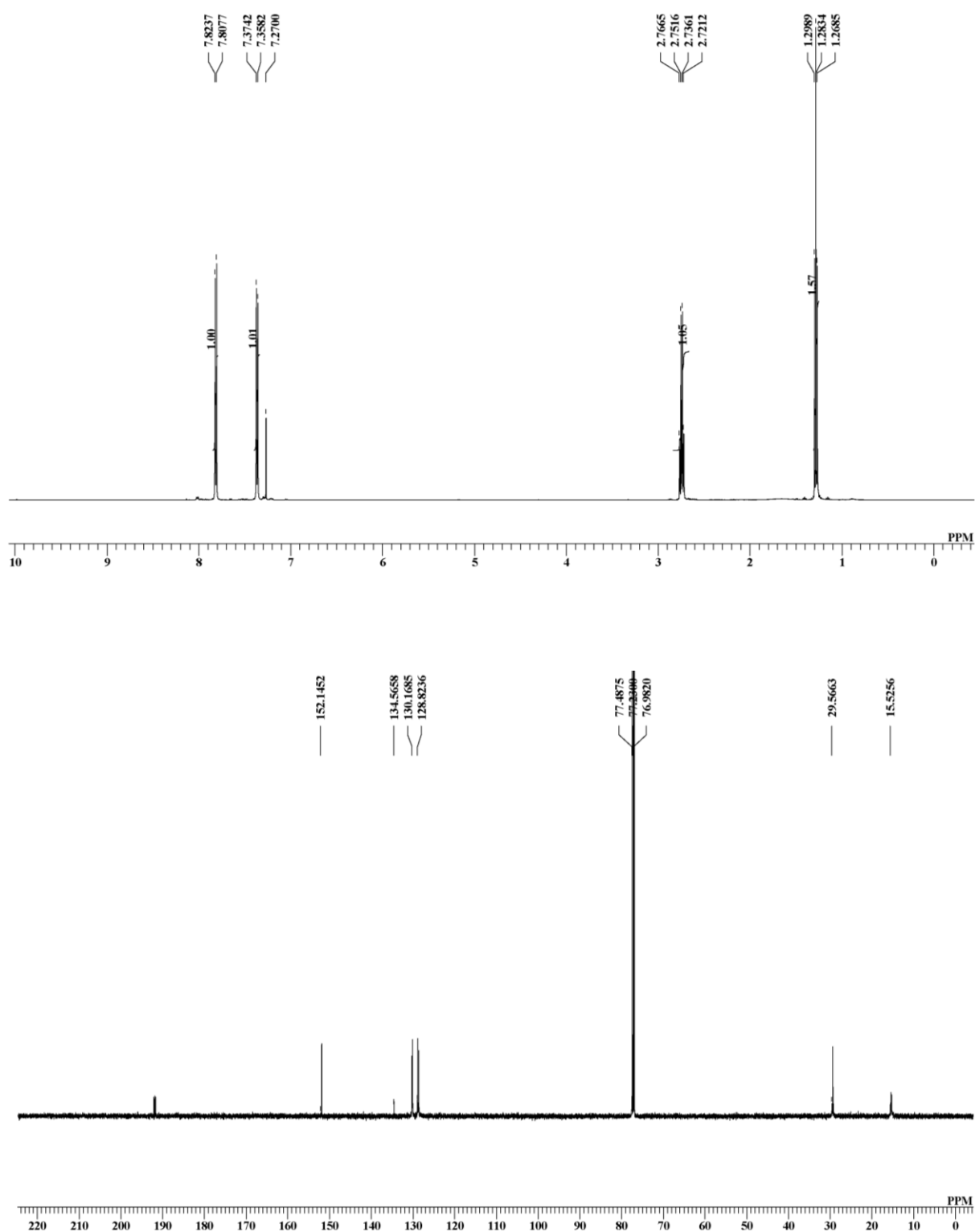
**Figure 3-7** <sup>1</sup>H-NMR (top) and <sup>13</sup>C-NMR (bottom) spectra of product A'H.



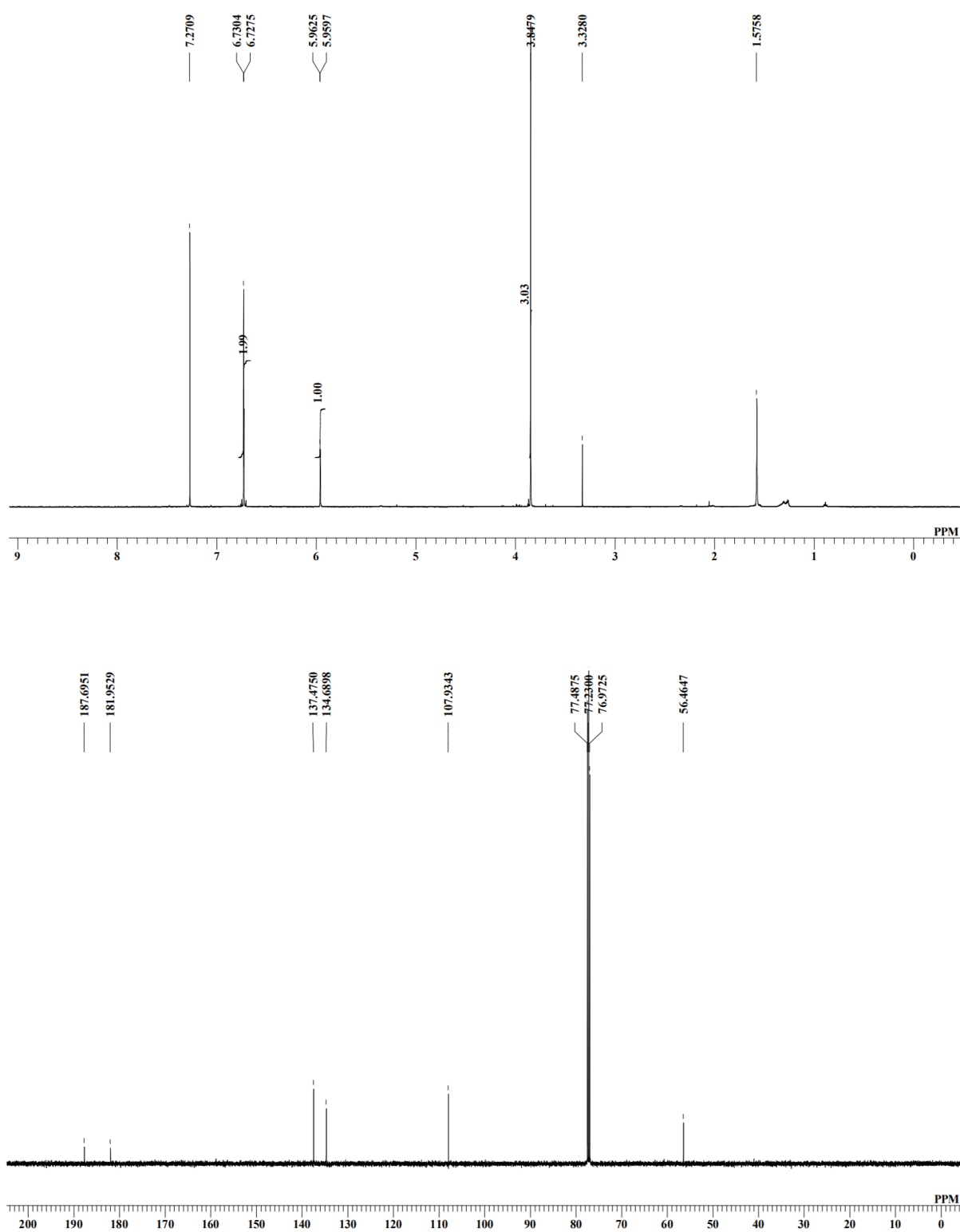
**Figure 3-8** <sup>1</sup>H-NMR (top) and <sup>13</sup>C-NMR (bottom) spectra of product A'G.



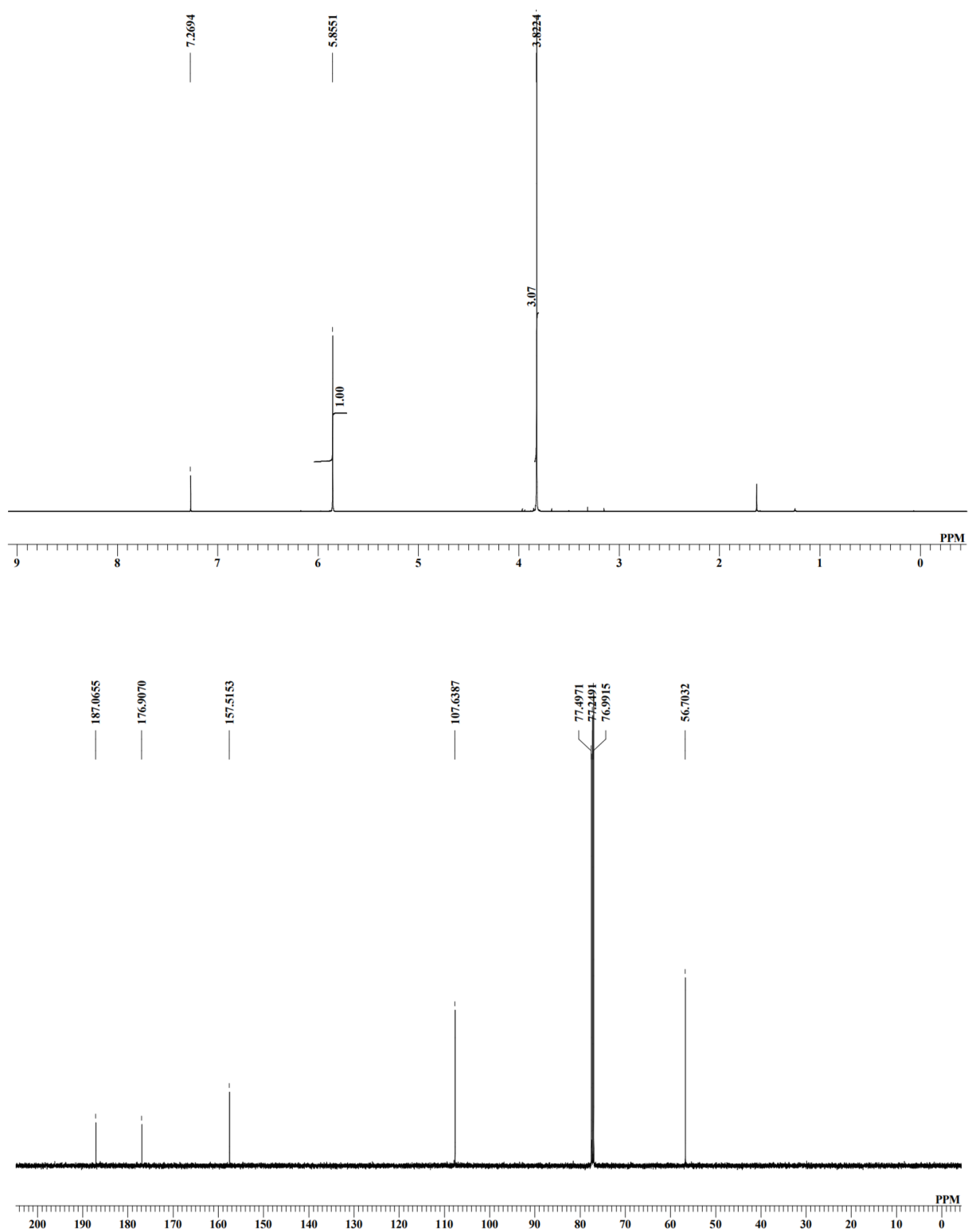
**Figure 3-9**  $^1\text{H}$ -NMR (top) and  $^{13}\text{C}$ -NMR (bottom) spectra of product A's.



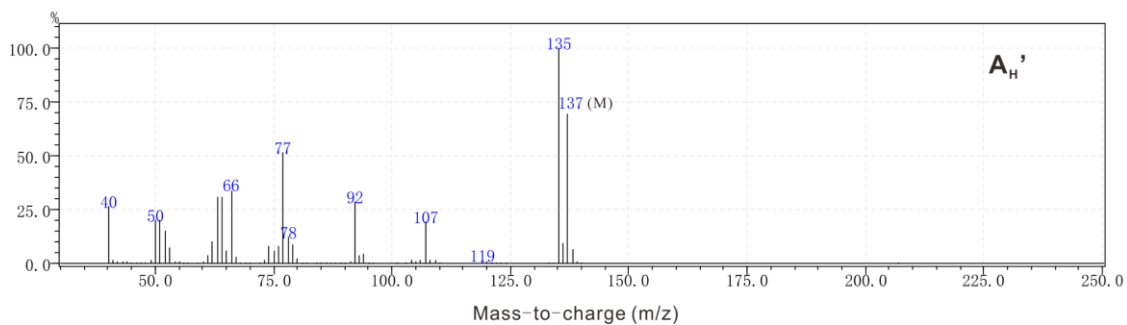
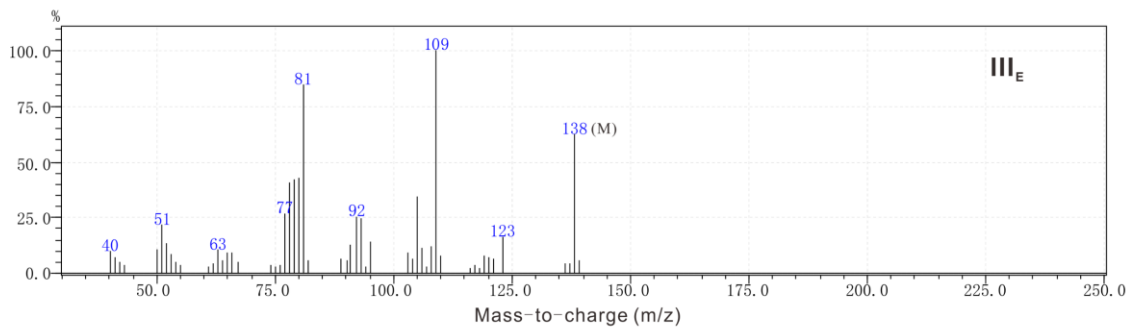
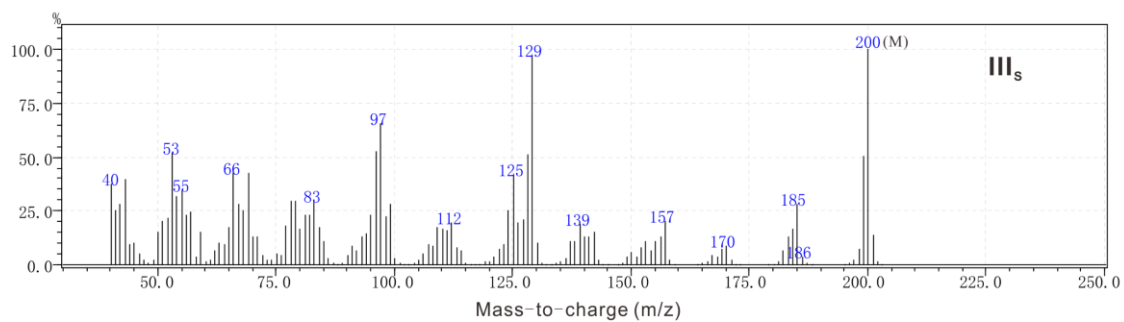
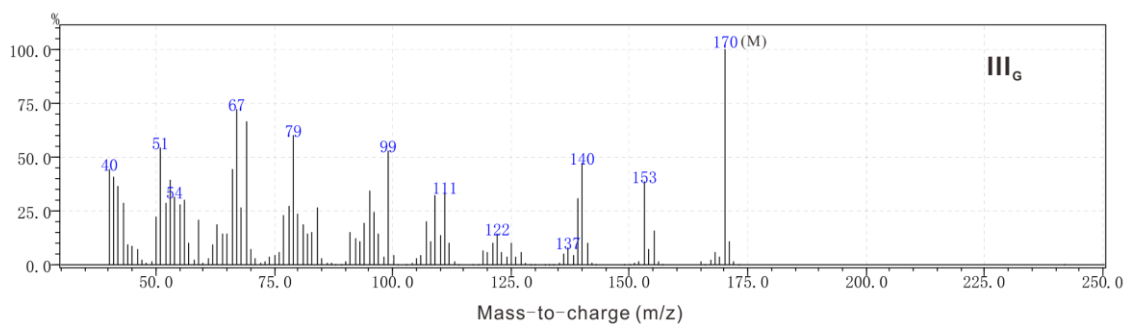
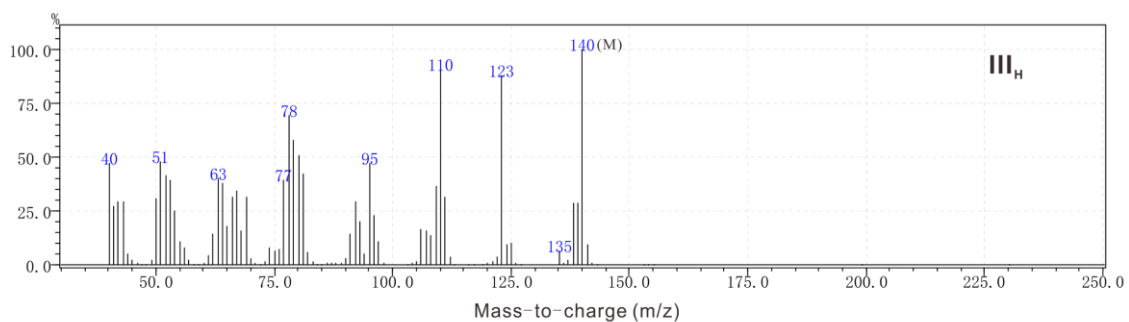
**Figure 3-10** <sup>1</sup>H-NMR (top) and <sup>13</sup>C-NMR (bottom) spectra of product A'E.



**Figure 3-11**  $^1\text{H}$ -NMR (top) and  $^{13}\text{C}$ -NMR (bottom) spectra of product **BG**.



**Figure 3-12**  $^1\text{H}$ -NMR (top) and  $^{13}\text{C}$ -NMR (bottom) spectra of product **Bs**.



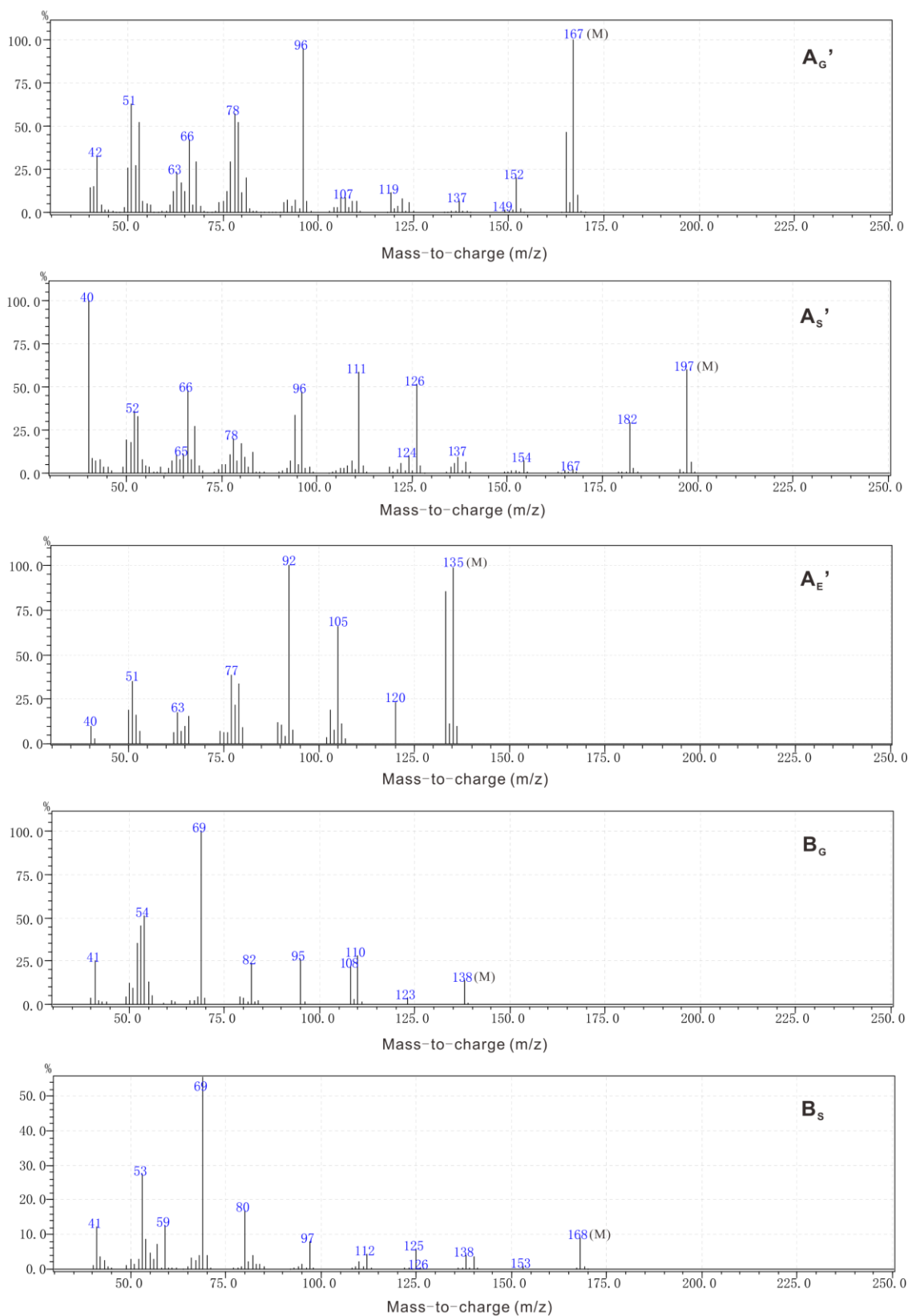


**Figure 3-13** GC/MS spectra of synthesized model compounds and reaction products employed in this chapter.

## 3.2.2 Methods

### 3.2.2.1 MnO<sub>2</sub> oxidation reaction

All reactions were conducted in a bottom-round glass flask (200 mL volume) equipped with a magnetic stirrer. A sulfate buffer solution (0.50 mol/L, pH 1.5) was prepared in advance by mixing Na<sub>2</sub>SO<sub>4</sub> and H<sub>2</sub>SO<sub>4</sub> solutions (0.50 mol/L each).

The MnO<sub>2</sub> powder used in this chapter is the synthetic MnO<sub>2</sub>, and the synthesis process was described in Chapter 2. The powder (1.2 mmol (oxidation power basis:  $1.2 \times 84.9/100 = 1.02$  mmol), oven-dry basis) was aged in sulfate buffer solution (50 mL) for 120 min in a glass flask at room temperature. Another sulfate buffer solution (10 mL) consisting of the same sulfate components and containing one of the compounds shown in **Figure 3-1** or **3-2** (12 μmol) as a starting material was added to the sulfate buffer solution containing the MnO<sub>2</sub> powder to initiate the reaction at room temperature. The initial concentrations of the compound and MnO<sub>2</sub> (insoluble solid) were 0.20 and 20 mmol/L, respectively. Each reaction was conducted three times to confirm the reproducibility.

### 3.2.2.2 Quantification

A specific amount of the reaction solution was withdrawn at prescribed reaction times, and poured into a glass tube to which a saturated NaHCO<sub>3</sub> solution had already been added for neutralization. The mixture was extracted with CH<sub>2</sub>Cl<sub>2</sub> containing an internal standard compound, 1,2,3-trimethoxybenzene or 3,4-dimethoxybenzaldehyde (veratraldehyde), and further twice (without the internal standard compound) in the glass tube. The organic layers were combined, dried over anhydrous Na<sub>2</sub>SO<sub>4</sub>, filtered with a membrane filter, and injected into an HPLC instrument with an ultraviolet-visible (UV-Vis) absorption detector (LC-2010CHT, Shimadzu Co., Ltd., Kyoto, Japan) for quantification based on absorbance at 280 nm.

In HPLC analyses, an HPLC column, Luna 5 u C18(2) 100 Å (length: 150 mm, inner diameter: 2.0 mm, particle size: 5.0 μm, Phenomenex, Inc., Torrance, CA, USA), was used at

an oven temperature of 40°C with a solvent flow rate of 0.2 mL/min. The types of solvent and gradients were as follows. For the reactions of the **H**-, **G**-, and **S**-type compounds, the gradient of CH<sub>3</sub>OH/H<sub>2</sub>O (v/v) was from 30/70 to 40/60 for 30 min, and then maintained for 10 min. For the reactions of the **E**-type compounds except for compound **I<sub>E</sub>**, the gradient of CH<sub>3</sub>OH/H<sub>2</sub>O (v/v) was from 30/70 to 50/50 for 10 min, from 50/50 to 60/40 for 15 min, and maintained for 10 min. For the reactions of compound **I<sub>E</sub>**, the gradient of CH<sub>3</sub>OH/H<sub>2</sub>O (v/v) was from 40/60 to 50/50 for 10 min, from 50/50 to 85/15 for 20 min, and maintained for 10 min.

**Table 3-1** HPLC analysis methods for MnO<sub>2</sub> oxidation of lignin model compounds and their respective internal standards for quantification.

Compound	Binary gradient system in HPLC	Internal standard
<b>I<sub>H</sub></b>	gradient CH <sub>3</sub> OH/H <sub>2</sub> O (v/v) from 30/70 to 40/60 for 30 min and maintained for 10 min (total time 40 min), following an equilibration step	3,4-dimethoxybenzaldehyde
<b>I<sub>G</sub></b>	gradient CH <sub>3</sub> OH/H <sub>2</sub> O (v/v) from 30/70 to 40/60 for 30 min and maintained for 10 min (total time 40 min), following an equilibration step	3,4-dimethoxybenzaldehyde
<b>I<sub>S</sub></b>	gradient CH <sub>3</sub> OH/H <sub>2</sub> O (v/v) from 30/70 to 40/60 for 30 min and maintained for 10 min (total time 40 min), following an equilibration step	3,4-dimethoxybenzaldehyde
<b>I<sub>E</sub></b>	gradient CH <sub>3</sub> OH/H <sub>2</sub> O (v/v) from 40/60 to 50/50 for 10 min, from 50/50 to 85/15 for 20 min, and maintained for 10 min (total time 40 min), following an equilibration step	1,2,3-trimethoxybenzene
<b>II<sub>H</sub></b>	gradient CH <sub>3</sub> OH/H <sub>2</sub> O (v/v) from 30/70 to 40/60 for 30 min and maintained for 10 min (total time 40 min), following an equilibration step	1,2,3-trimethoxybenzene
<b>II<sub>G</sub></b>	gradient CH <sub>3</sub> OH/H <sub>2</sub> O (v/v) from 30/70 to 40/60 for 30 min and maintained for 10 min (total time 40 min), following an equilibration step	1,2,3-trimethoxybenzene
<b>II<sub>S</sub></b>	gradient CH <sub>3</sub> OH/H <sub>2</sub> O (v/v) from 30/70 to 40/60 for 30 min and maintained for 10 min (total time 40 min), following an equilibration step	1,2,3-trimethoxybenzene
<b>II<sub>E</sub></b>	gradient CH <sub>3</sub> OH/H <sub>2</sub> O (v/v) from 30/70 to 50/50 for 10 min, from 50/50 to 60/40 for 15 min, and maintained for 10 min (total time 35 min), following an equilibration step	1,2,3-trimethoxybenzene
<b>III<sub>H</sub></b>	gradient CH <sub>3</sub> OH/H <sub>2</sub> O (v/v) from 30/70 to 40/60 for 30 min and maintained for 10 min (total time 40 min), following an equilibration step	1,2,3-trimethoxybenzene
<b>III<sub>G</sub></b>	gradient CH <sub>3</sub> OH/H <sub>2</sub> O (v/v) from 30/70 to 40/60 for 30 min and maintained for 10 min (total time 40 min), following an equilibration step	1,2,3-trimethoxybenzene
<b>III<sub>S</sub></b>	gradient CH <sub>3</sub> OH/H <sub>2</sub> O (v/v) from 30/70 to 40/60 for 30 min and maintained for 10 min (total time 40 min), following an equilibration step	1,2,3-trimethoxybenzene
<b>III<sub>E</sub></b>	gradient CH <sub>3</sub> OH/H <sub>2</sub> O (v/v) from 30/70 to 50/50 for 10 min, from 50/50 to 60/40 for 15 min, and maintained for 10 min (total time 35 min), following an equilibration step	1,2,3-trimethoxybenzene

## 3.3 Results and discussion

### 3.3.1 Description of the reaction system

#### 3.3.1.1 Preparation of MnO<sub>2</sub>

Commercially available active MnO<sub>2</sub> (FUJIFILM Wako Pure Chemical Industries, Ltd.) was ground into powder. The oxidation power was iodometrically titrated to be 90.2% of the theoretical value by the method described above. The MnO<sub>2</sub> powder was applied to the oxidation of compound **II**<sub>G</sub> under conditions identical to those described above. When the logarithmic plot for the disappearance of compound **II**<sub>G</sub> was approximated to a pseudo-first-order reaction, the approximation was rather bad. The disappearance was gradually accelerated when compared with that which was supposed to follow a pseudo-first-order reaction from the initial stage, the rate reached a ceiling level at a reaction time of about 120 min. In contrast, the disappearance followed a pseudo-first-order reaction well from the initial stage at a rate similar to the above ceiling level, when the MnO<sub>2</sub> powder had primarily been aged following the procedure described above. The observed acceleration of the oxidation using the MnO<sub>2</sub> powder without the pre-aging thus suggests that the MnO<sub>2</sub> powder was aged and became more active during the oxidation. This clarified that pre-aging is necessary for the commercial MnO<sub>2</sub>.

MnO<sub>2</sub> was synthesized from Mn<sup>2+</sup> by the method described above, and the obtained precipitates were ground into powder. This synthesized MnO<sub>2</sub> powder was applied to the oxidation of compound **II**<sub>G</sub> with or without pre-aging. The disappearance approximated well to a specific pseudo-first-order reaction from the initial stage, regardless of conducting pre-aging. It was faster than that observed when the above-described commercial MnO<sub>2</sub> powder was used, which was surprising because the synthesized MnO<sub>2</sub> powder had less oxidation power (84.9%) than the commercial powder (90.2%). This clarified that pre-aging is not necessary for the synthesized MnO<sub>2</sub> powder.

The observed difference between the commercial and the synthesized  $\text{MnO}_2$  powders must have arisen from their physical properties. Physical property of commercially available  $\text{MnO}_2$  is often dependent on vender. Thus, the synthesized  $\text{MnO}_2$  powder, whose physical property is possibly prepared to be constant anytime, was employed in this study. Because any aging and the consequent activity change during the  $\text{MnO}_2$  oxidation process interfere with ready analysis, furthermore, the pre-aging was applied to the synthesized  $\text{MnO}_2$  powder in spite of its unnecessary.

### 3.3.1.2 Choice of the E-Type compounds

Reactivity at the benzyl position of an aromatic compound with functional groups on the aromatic nucleus in a chemical reaction commonly correlates well with their Hammett's substituent constants ( $\sigma$  values), when they locate at the *para*- and/or *meta*- of the benzyl carbon and the reactivity is relatively compared with that of an analogous aromatic compound with other or no functional groups present at both positions. The E-type compounds were employed in this context. The total  $\sigma$  value of two methoxy groups of the G-type compounds is  $-0.153$  ( $= -0.268$  (*para*)  $+ 0.115$  (*meta*)), which is close to that of the ethyl group of the E-type compounds,  $-0.151$ . Each E-type compound can thus be expected to have similar reactivity to the corresponding G-type compound in a reaction occurring at their benzyl positions, provided that the reaction is affected only by the electronic factors that originate in the functional groups and appear locally at the benzyl positions. Thus, the reactivities of the G- as well as the other types are compared with those of the E-types in the following sections.

### 3.3.2 $\text{MnO}_2$ oxidation of benzene analogues (compounds I)

Although  $\text{MnO}_2$  is an oxidant that selectively oxidizes an analogue of allyl or benzyl alcohol, as described in the Introduction section, it was examined by employing compounds **I** whether or not  $\text{MnO}_2$  can oxidize the aromatic nucleus of an aromatic compound without benzylic hydroxy group and a substructure corresponding to the side-chain portion in lignin, and whether the progress of this oxidation is dependent on the type of aromatic nucleus.

Compound **I<sub>H</sub>** disappeared in the MnO<sub>2</sub> oxidation and remained with a recovery yield ( $\pm$  standard deviation calculated from three duplicated runs) of  $81.0 \pm 2.0\%$  at a reaction time of 660 min, although no other peaks of any size appeared on the HPLC chromatogram. These results were considered to indicate that the aromatic nucleus of compound **I<sub>H</sub>** was degraded to afford reaction products that do not exhibit the absorbance at around 280 nm and/or that it just volatilized. When compound **I<sub>H</sub>** was reacted in the absence of MnO<sub>2</sub> under otherwise exactly the same conditions, where it must stably have existed, it disappeared and remained with the same recovery yield as for the MnO<sub>2</sub> oxidation. Compound **I<sub>H</sub>** must therefore have volatilized and not have been oxidized by MnO<sub>2</sub>. Because exactly the same phenomena were observed in the reactions of compound **I<sub>E</sub>** with and without MnO<sub>2</sub>, it must also have volatilized and not been oxidized by MnO<sub>2</sub>. Incidentally, because product **B<sub>H</sub>** was afforded when compound **I<sub>H</sub>** was subjected to the MnO<sub>2</sub> oxidation applying 1.0 mol/L H<sub>2</sub>SO<sub>4</sub> under otherwise the same conditions, the oxidation power of MnO<sub>2</sub> is dependent on the system acidity. It can be excluded from an explanation for these observed phenomena that polymers formed but they were not detected by the HPLC analysis, when the employed conditions are taken into consideration.

Compound **I<sub>G</sub>** or **I<sub>S</sub>** disappeared in the MnO<sub>2</sub> oxidation and remained with a recovery yield of  $60.8 \pm 1.1\%$  or  $60.0 \pm 1.2\%$ , respectively, at a reaction time of 660 min, although neither compound disappeared in the reaction without MnO<sub>2</sub>. Product **B<sub>G</sub>** or **B<sub>S</sub>** was afforded as the exclusive major reaction product with a yield of  $20.9 \pm 1.1\%$  or  $13.2 \pm 0.1\%$ , respectively, at the same reaction time. Many small peaks in addition to the large peak of product **B<sub>G</sub>** or **B<sub>S</sub>**, respectively, appeared on the HPLC chromatogram of the reaction solution withdrawn at this reaction time, indicating the formation of many minor reaction products. The proportion of the amount of afforded product **B<sub>G</sub>** or **B<sub>S</sub>** to that of disappearing compound **I<sub>G</sub>** or **I<sub>S</sub>**, respectively, did not vary largely during the reaction. Product **B<sub>G</sub>** or **B<sub>S</sub>** was stable under the employed conditions when subjected to MnO<sub>2</sub> oxidation as a starting compound. The disappearance of compound **I<sub>G</sub>** or **I<sub>S</sub>** and concomitant formation of product **B<sub>G</sub>** or **B<sub>S</sub>**,

respectively, are shown in **Figure 3-14** and **Figure 3-15**.

The above observations confirm that  $\text{MnO}_2$  cannot oxidize the **H**- and **E**- but can oxidize the **G**- and **S**-type aromatic nuclei to afford products **B<sub>G</sub>** and **B<sub>S</sub>**, respectively, as the exclusive major reaction products under the employed conditions in spite of the slow progresses. The labilities of the **G**- and **S**-type aromatic nuclei do not seem to be different.

The disappearance of compound **I<sub>G</sub>** or **I<sub>S</sub>** was approximated to a pseudo-first-order reaction to obtain the pseudo-first-order reaction rate constant  $k_{\text{obs}}$ , which is listed in **Table 3-2**. The approximations were fairly good in most of the six runs (2 compounds  $\times$  3 duplications, see the  $R^2$  values in **Table 3-2**).

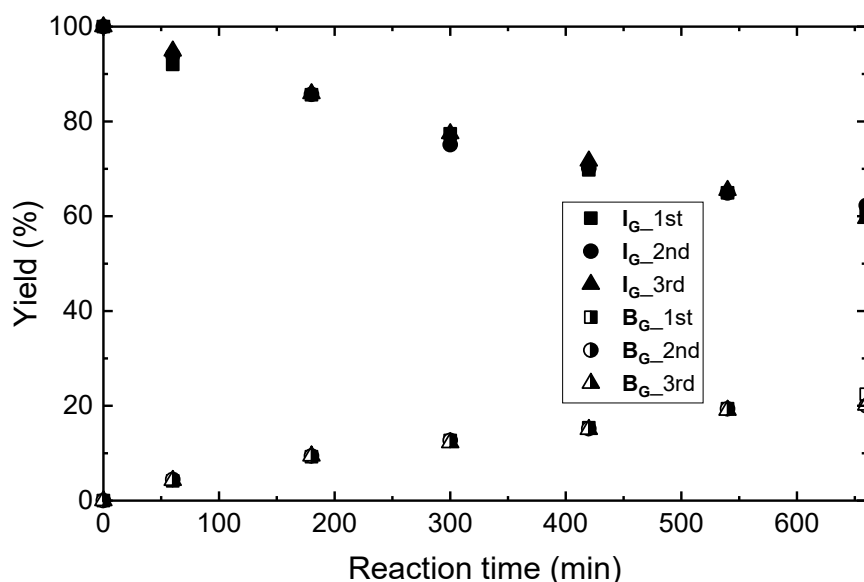


**Figure 3-14** Time course of the changes in the recovery yield of compound **I<sub>G</sub>** and yield of product **B<sub>G</sub>** in the  $\text{MnO}_2$  oxidation of compound **I<sub>G</sub>**.

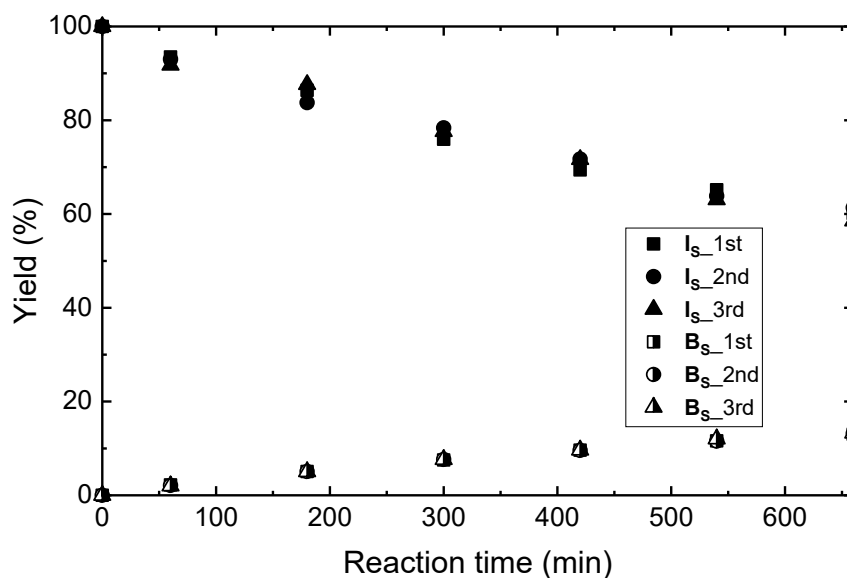


**Figure 3-15** Time course of the changes in the recovery yield of compound **Is** and yield of product **Bs** in the  $\text{MnO}_2$  oxidation of compound **Is**.

**Table 3-2** Observed pseudo-first-order reaction rate constants ( $k_{\text{obs}}$ ), squares of the correlation coefficients ( $R^2$ ) in the approximations, and ratios of  $k_{\text{obs}}$  values between compounds **II** and **III** ( $k_{\text{obs}}(\text{II})/k_{\text{obs}}(\text{III})$ ) for estimation of the magnitudes of the kinetic isotope effects.

C.I <sup>a</sup>	$k_{\text{obs}}^b$	$R^{2c}$	C.II <sup>d</sup>	$k_{\text{obs}}^b$	$R^{2c}$	C.III <sup>e</sup>	$k_{\text{obs}}^b$	$R^{2c}$	$k_{\text{obs}}(\text{II})/k_{\text{obs}}(\text{III})$
<b>I<sub>H</sub></b>	—	—	<b>II<sub>H</sub></b>	$14.7 \pm 0.1$	0.995	<b>III<sub>H</sub></b>	$3.13 \pm 0.09$	0.995	4.7 ( <b>H</b> )
					0.997			0.986	
					0.995			0.987	
<b>I<sub>G</sub></b>	$7.96 \pm 0.05$	0.986	<b>II<sub>G</sub></b>	$911 \pm 23$	0.999	<b>III<sub>G</sub></b>	$227 \pm 8$	1.00	4.0 ( <b>G</b> )
		0.972			0.985			1.00	
		0.998			0.988			1.00	
<b>I<sub>S</sub></b>	$8.08 \pm 0.14$	0.987	<b>II<sub>S</sub></b>	$343 \pm 18$	0.962	<b>III<sub>S</sub></b>	$127 \pm 2$	0.983	2.7 ( <b>S</b> )
		0.983			0.968			0.985	
		0.991			0.994			0.983	
<b>I<sub>E</sub></b>	—	—	<b>II<sub>E</sub></b>	$2.09 \pm 0.06$	0.995	<b>III<sub>E</sub></b>	$0.244 \pm 0.008$	0.961	8.6 ( <b>E</b> )
					0.992			0.958	
					0.991			0.941	

<sup>a</sup>Compounds **I**. <sup>b</sup>Unit:  $\times 10^{-4} \text{ min}^{-1}$ . The values after the ‘ $\pm$ ’ marks are the standard deviations of three duplicated runs. <sup>c</sup>The value obtained from each of three duplicated runs. <sup>d</sup>Compounds

## II. <sup>e</sup>Compounds III.

### 3.3.3 MnO<sub>2</sub> oxidation of benzyl alcohol analogues (compounds II)

Compound **II<sub>H</sub>** was oxidized in the MnO<sub>2</sub> oxidation, and product **A<sub>H</sub>** formed as the exclusive major reaction product. The recovery yield and yield of product **A<sub>H</sub>** were  $52.7 \pm 0.1\%$  and  $39.3 \pm 0.7\%$ , respectively, at a reaction time of 660 min. The total of these was 92.0%, indicating that side reactions contributed only slightly. Few small peaks appeared on the HPLC chromatogram of the reaction solution withdrawn at this reaction time. Compound **II<sub>H</sub>** was stable in the absence of MnO<sub>2</sub> under otherwise the same conditions. Product **A<sub>H</sub>** was stable under the employed conditions when it was subjected to the MnO<sub>2</sub> oxidation as a starting compound.

All the observed phenomena in the MnO<sub>2</sub> oxidation of compound **II<sub>G</sub>** were the same as those of compound **II<sub>H</sub>** except for the remarkably higher rate. The recovery yield and yield of product **A<sub>G</sub>** were  $4.3 \pm 0.4\%$  and  $87.2 \pm 8.7\%$ , respectively, at a reaction time of 30 min. The total of these was thus 91.5%. Product **A<sub>G</sub>** was stable under the employed conditions when subjected to MnO<sub>2</sub> oxidation as a starting compound.

In contrast, compound **II<sub>S</sub>** afforded products **A<sub>S</sub>** and **B<sub>S</sub>** as the exclusive major and prominent secondary reaction product, respectively, although all of the other phenomena were the same as those of compound **II<sub>G</sub>** except for the slower oxidation. The **S** nucleus of compound **II<sub>S</sub>** was oxidized in the MnO<sub>2</sub> oxidation. The recovery yield and yields of products **A<sub>S</sub>** and **B<sub>S</sub>** were  $3.5 \pm 0.7\%$ ,  $66.0 \pm 1.2\%$ , and  $7.8 \pm 0.2\%$ , respectively, at a reaction time of 120 min. The total of these was thus 77.3%, which was lower than those of compounds **II<sub>H</sub>** and **II<sub>G</sub>**. The oxidation of the aromatic nucleus (**S**-nucleus) may thus increase reactions affording unidentified reaction products. Because few small peaks appeared on the HPLC chromatogram, the oxidation of the aromatic nucleus must have afforded aliphatic reaction products accompanying the degradation of the **S**-nucleus. Product **A<sub>S</sub>** or **B<sub>S</sub>** was stable under the employed conditions when subjected to MnO<sub>2</sub> oxidation as a starting compound.

All the observed phenomena in the MnO<sub>2</sub> oxidation of compound **II<sub>E</sub>** were the same as

those of compound **II<sub>H</sub>** except for the slower oxidation. The recovery yield and yield of product **A<sub>E</sub>** were  $87.0 \pm 0.1\%$  and  $13.2 \pm 0.1\%$ , respectively, at a reaction time of 660 min. The total of these was 100.2%, indicating that this oxidation reaction was quantitative. Product **A<sub>E</sub>** was stable under the employed conditions when subjected to  $\text{MnO}_2$  oxidation as a starting compound. Each disappearance of compounds **II** and concomitant formation of the reaction products are shown in **Figure 3-16** to **Figure 3-19**.

Each disappearance of compounds **II** was approximated to a pseudo-first-order reaction, and the value of  $k_{\text{obs}}$  is listed in **Table 3-2**. The approximations were good in most of the twelve runs (4 compounds  $\times$  3 duplications, see the  $R^2$  values in **Table 3-2**). The rates were in the order of: compounds **II<sub>G</sub>** > **II<sub>S</sub>** >> **II<sub>H</sub>** > **II<sub>E</sub>**. If the  $\text{MnO}_2$  oxidations had been affected only by the electronic effects originating in the functional groups on their aromatic nuclei and appearing locally only at their benzyl positions, the rates should have been in the order of: compound **II<sub>H</sub>** > **II<sub>G</sub>**  $\geq$  **II<sub>E</sub>** > **II<sub>S</sub>** on the basis of their Hammett's  $\sigma$  values, which are  $-0.268$ ,  $-0.153$ ,  $-0.151$ , and  $-0.038$ , respectively. This inconsistency suggests that the  $\text{MnO}_2$  oxidations are affected by not only the electronic effects on the benzyl positions but also some other factors.

These other factors are discussed here. Previous studies proposed that allyl or benzyl alcohols can form the  $\pi$ -complex type of interactions with Lewis acid sites on the surface of  $\text{MnO}_2$  aggregates, and hence these alcohols are oxidized by  $\text{MnO}_2$  much more readily than other types of alcohol.<sup>[17,23-24]</sup> On the basis of this proposal,  $\text{MnO}_2$  is presumed to readily oxidize an analogue of benzyl alcohol with high electron density in its aromatic nucleus owing to the ready formation of the  $\pi$ -complex type of an interaction with it. In this context, the slowest  $\text{MnO}_2$  oxidation of compound **II<sub>E</sub>** can be explained as follows. Compounds **II<sub>H</sub>**, **II<sub>G</sub>**, and **II<sub>S</sub>** with the methoxy group substituent(s) have the aromatic nuclei with the electron densities higher than that of compound **II<sub>E</sub>** with the ethyl group substituent, resulting in rapid or ready formation of the  $\pi$ -complex type of interactions with  $\text{MnO}_2$ . The methoxy groups resonantly donate their lone pairs to the  $\pi$ -electron systems of their aromatic nuclei, which

consequently increase their electron densities higher than that of compound **II<sub>E</sub>** elevated only inductively by the ethyl group. The faster MnO<sub>2</sub> oxidations of compounds **II<sub>G</sub>** and **II<sub>S</sub>** than that of compound **II<sub>H</sub>** can result from the high electron densities of their aromatic nuclei owing to the presence of plural methoxy groups. Because the MnO<sub>2</sub> oxidation of the benzyl position of compound **II<sub>S</sub>** is relatively suppressed by the electron-withdrawal inductive effect originating in two *meta*-substituted methoxy groups, however, the MnO<sub>2</sub> oxidation of compound **II<sub>S</sub>** must have been suppressed and slower than that of compound **II<sub>G</sub>**. Instead, the oxidation of the aromatic S-nucleus of compound **II<sub>S</sub>** progressed to afford product **B<sub>S</sub>** as the secondary prominent reaction product, owing to the quite high electron density of the S-nucleus.

Although MnO<sub>2</sub> can oxidize the aromatic nucleus of not only the S-type (compound **I<sub>S</sub>**) but also G-type (compound **I<sub>G</sub>**), as shown in the previous section, product **B<sub>G</sub>** was not detected in the MnO<sub>2</sub> oxidation of compound **II<sub>G</sub>**. This is probably because the oxidation of the benzyl position of compound **II<sub>G</sub>** is fast enough to be exclusive in competing with the oxidation of the G-nucleus.

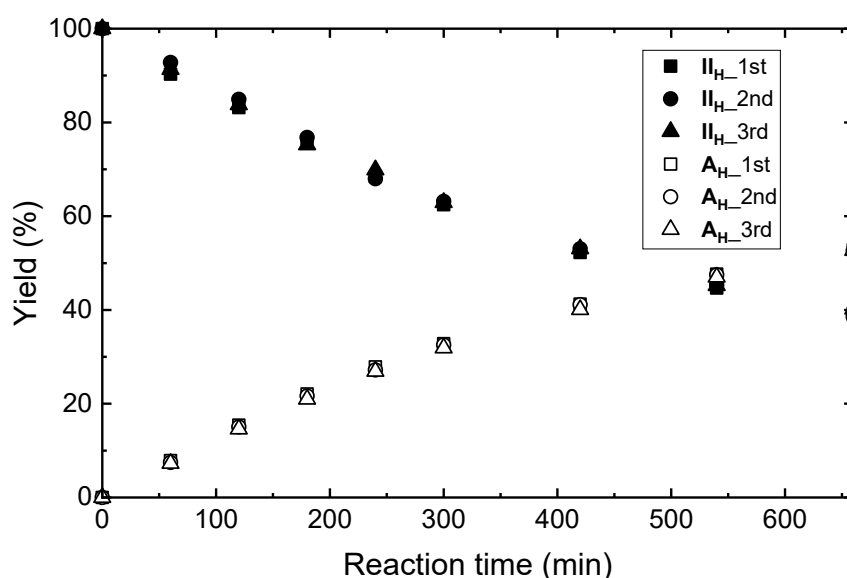


**Figure 3-16** Time course of the changes in the recovery yield of compound **II<sub>H</sub>** and yield of product **A<sub>H</sub>** in the MnO<sub>2</sub> oxidation of compound **II<sub>H</sub>**.

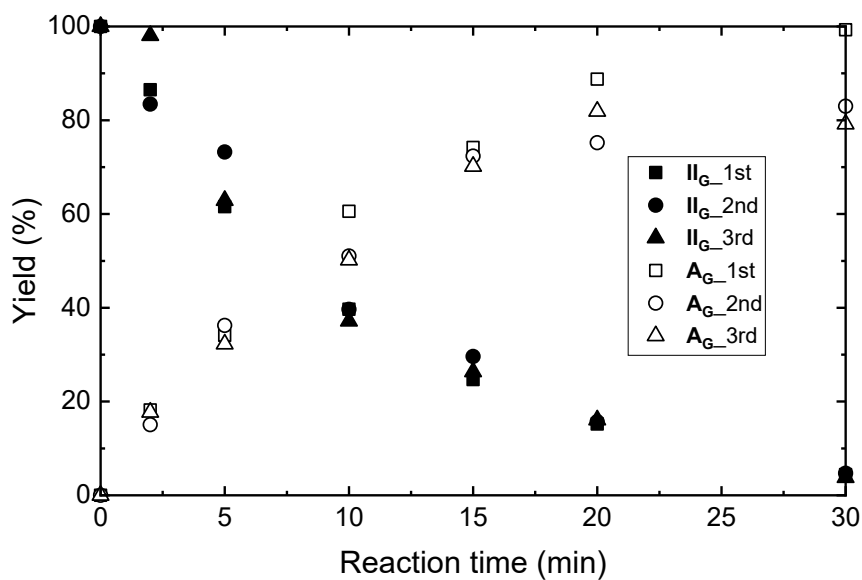


**Figure 3-17** Time course of the changes in the recovery yield of compound **II<sub>G</sub>** and yield of product **A<sub>H</sub>** in the MnO<sub>2</sub> oxidation of compound **II<sub>G</sub>**.

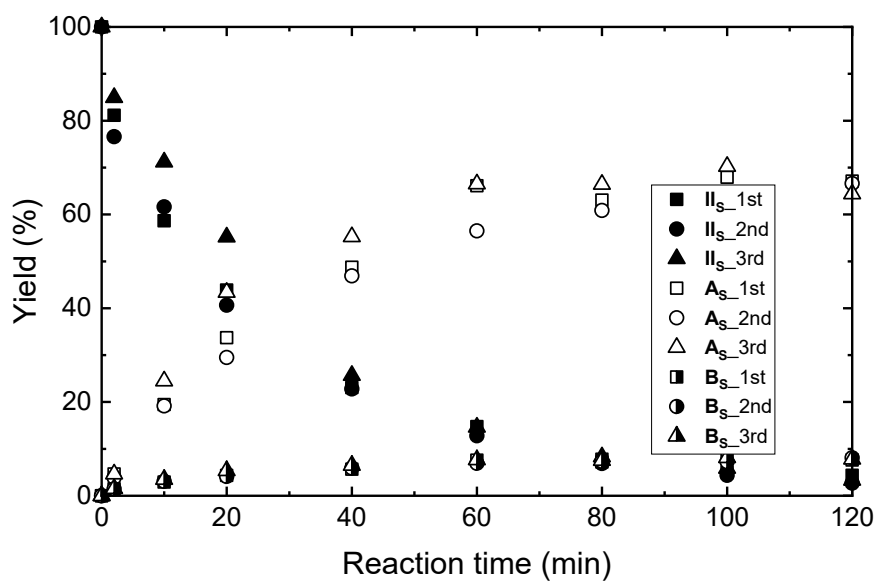


**Figure 3-18** Time course of the changes in the recovery yield of compound **II<sub>s</sub>** and yields of products **A<sub>s</sub>** and **B<sub>s</sub>** in the MnO<sub>2</sub> oxidation of compound **II<sub>s</sub>**.

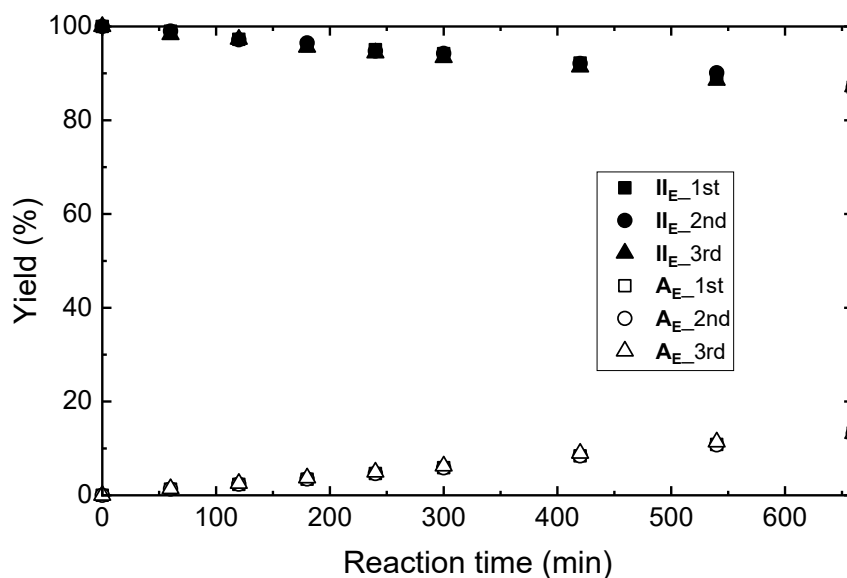


**Figure 3-19** Time course of the changes in the recovery yield of compound **II<sub>E</sub>** and yield of product **A<sub>E</sub>** in the MnO<sub>2</sub> oxidation of compound **II<sub>E</sub>**.

### 3.3.4 MnO<sub>2</sub> oxidation of deuterated benzyl alcohol analogues (compounds **III**)

The observed phenomena in the MnO<sub>2</sub> oxidation of each of compounds **III** were mostly the same as those of the corresponding compounds **II** except that the rate was lower due to the appearance of the primary kinetic isotope effect (**Table 3-2**). The recovery yield of compound **III<sub>H</sub>** and yield of product **A<sub>H</sub>'** were  $81.7 \pm 0.5\%$  and  $16.9 \pm 0.3\%$ , respectively, at a reaction time of 660 min. The total of these was 98.6%. Those of compound **III<sub>G</sub>** and product **A<sub>G</sub>'** were  $1.9 \pm 0.2\%$  and  $86.6 \pm 0.2\%$ , respectively, at a reaction time of 180 min. The total of these was 88.5%. In the MnO<sub>2</sub> oxidation of compound **III<sub>S</sub>**, products **A<sub>S</sub>'** and **B<sub>S</sub>** formed as the exclusive major and secondary prominent reaction products, respectively. The recovery yield of compound **III<sub>S</sub>** and yields of products **A<sub>S</sub>'** and **B<sub>S</sub>** were  $11.5 \pm 0.4\%$ ,  $31.0 \pm 0.2\%$ , and  $18.1 \pm 0.0\%$ , respectively, at a reaction time of 180 min. The total of these was 60.6%. The recovery yield of compound **III<sub>E</sub>** and yield of product **A<sub>E</sub>'** were  $98.4 \pm 0.0\%$  and  $1.3 \pm 0.0\%$ , respectively, at a reaction time of 660 min. The total of these was 99.7%. Each disappearance

of compounds **III** and concomitant formation of the reaction products are shown in **Figure 3-20** to **Figure 3-23**.

Regarding the observed aspects other than the rates, it should be noted that only the S-type compounds showed significant difference between compounds **III** and **II**. The amount of afforded product **As'** was smaller than twice that of product **Bs** in the MnO<sub>2</sub> oxidation of compound **III**<sub>s</sub>, while product **As** was afforded in an amount about 7~9 times as large as that of product **Bs** in the reaction of compound **II**<sub>s</sub>. This significant difference in the S-type compounds suggests that in the oxidation of compound **III**<sub>s</sub> the S-nucleus oxidation is competitively and alternatively enhanced by suppressing the oxidation of the benzyl position due to the presence of the deuteriums and appearance of the kinetic isotope effect.

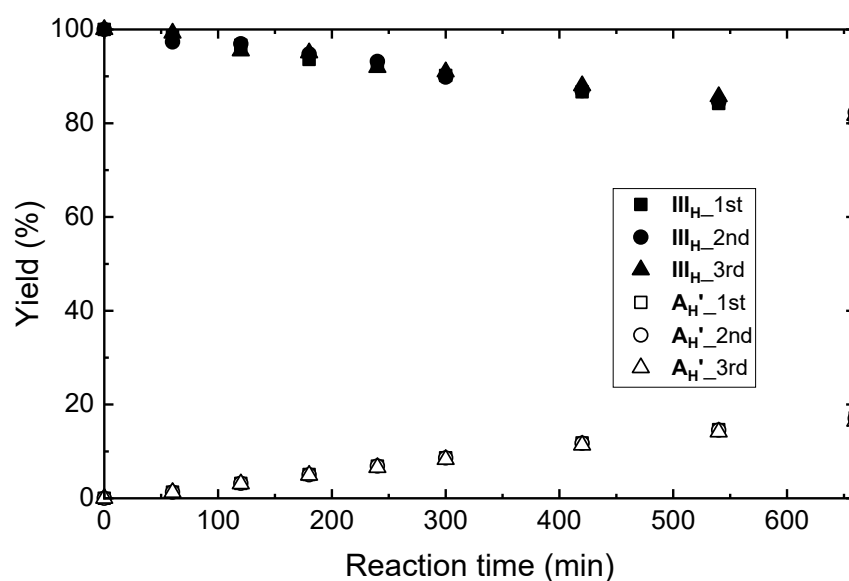


**Figure 3-20** Time course of the changes in the recovery yield of compound **III<sub>H</sub>** and yield of product **A<sub>H</sub>'** in the MnO<sub>2</sub> oxidation of compound **III<sub>H</sub>**.

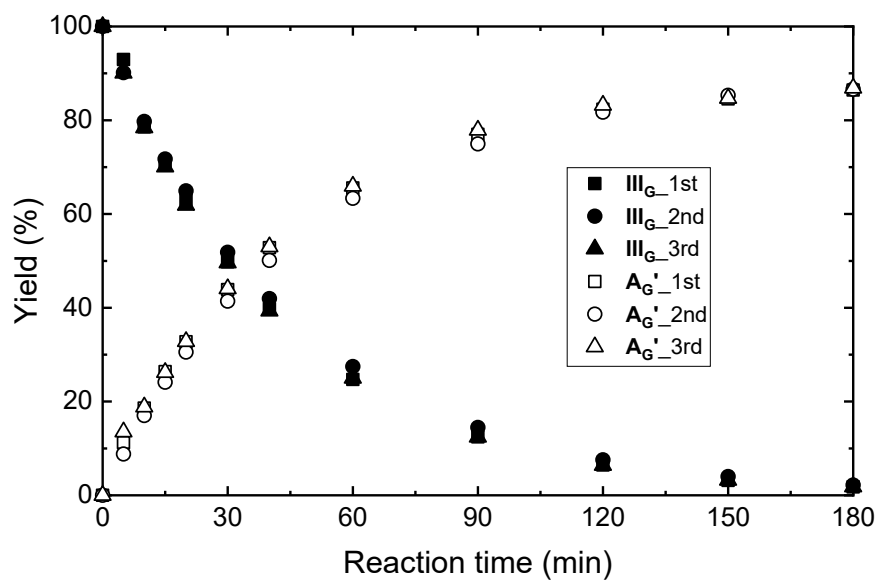


**Figure 3-21** Time course of the changes in the recovery yield of compound **III<sub>G</sub>** and yield of product **A<sub>G</sub>'** in the MnO<sub>2</sub> oxidation of compound **III<sub>G</sub>**.

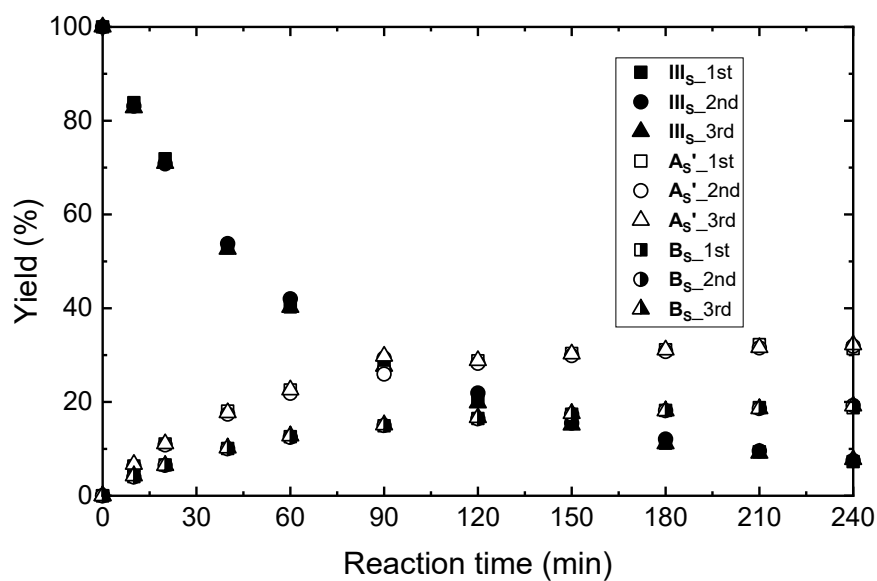


**Figure 3-22** Time course of the changes in the recovery yield of compound **III<sub>s</sub>** and yields of products **A<sub>s</sub>'** and **B<sub>s</sub>** in the MnO<sub>2</sub> oxidation of compound **III<sub>s</sub>**.

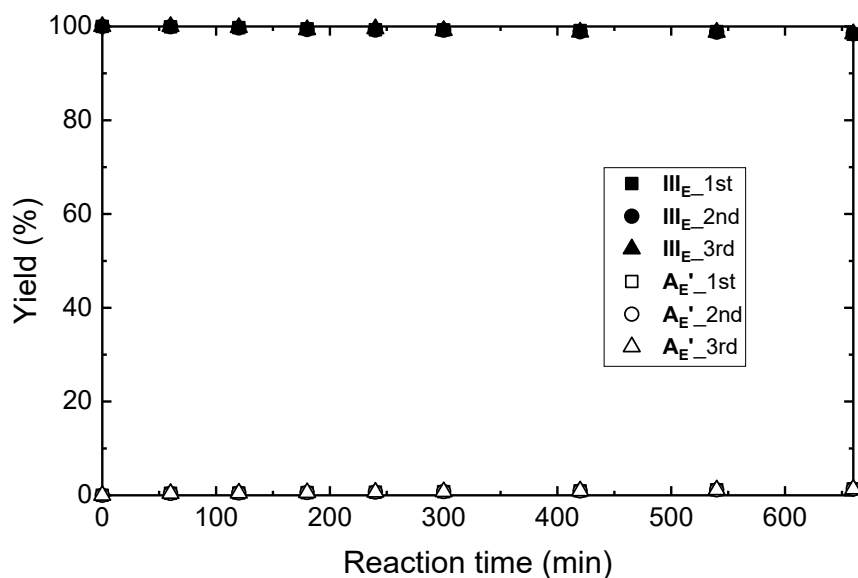


**Figure 3-23** Time course of the changes in the recovery yield of compound **III<sub>E</sub>** and yield of product **A<sub>E</sub>'** in the MnO<sub>2</sub> oxidation of compound **III<sub>E</sub>**.

### 3.3.5 Possible reaction modes of C<sub>6</sub>-C<sub>1</sub>-type monomeric lignin model compounds in MnO<sub>2</sub> oxidation

Although MnO<sub>2</sub> commonly oxidizes alcohol groups present at the benzyl position,<sup>[17]</sup> it certainly oxidized the **G**- and **S**-nuclei of compounds **I<sub>G</sub>** and **I<sub>S</sub>**, respectively, which do not have the benzyl position and substructures corresponding to the side-chain portion of lignin, under the employed conditions. On the basis of this observation, three possible reaction modes can be proposed for the MnO<sub>2</sub> oxidation of compounds **II** and **III**, as shown in **Figure 3-24**.

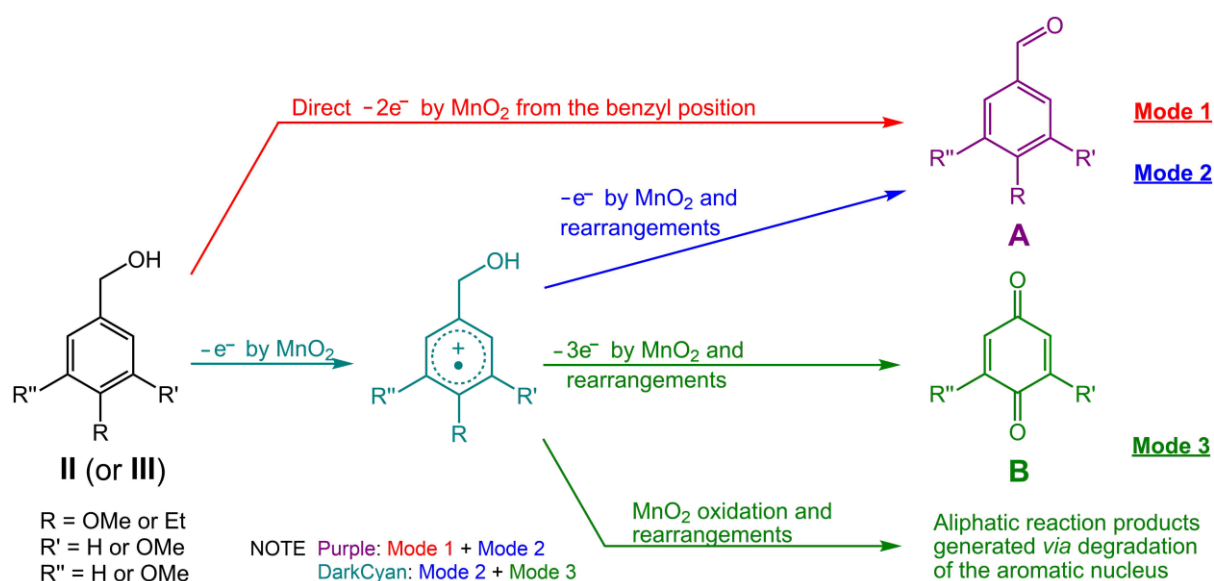


**Figure 3-24** Three possible reaction modes in the  $\text{MnO}_2$  oxidations of the benzyl alcohol analogues, compounds **II** and **III**. The former is representatively described although the latter also undergoes these modes.

Mode **1** is direct oxidation of the benzyl position to afford the corresponding benzaldehyde-type products **A** or **A'**, respectively, which is the general mode of  $\text{MnO}_2$  oxidation. Mode **2** begins with the oxidation of the aromatic nucleus, but finally results in the oxidation of the benzyl position to afford products **A** or **A'**, respectively. In this mode, the aromatic cation radical must be the primary intermediate, which is generated by the one-electron oxidation of the aromatic nucleus by  $\text{MnO}_2$ . Mode **3** also begins with the oxidation of the aromatic nucleus, and finally results in the oxidative degradation of the aromatic nucleus to afford product **B** as well as other unidentified aliphatic reaction products. It is discussed in the following paragraphs which is the major reaction mode in the  $\text{MnO}_2$  oxidation of the **H**-, **G**-, **S**-, and **E**-type compounds on the basis of the magnitudes of the kinetic isotope effects, which are expressed by the ratios of the  $k_{\text{obs}}$  values of compounds **II** to those of the corresponding compounds **III** ( $k_{\text{obs}}(\text{II})/k_{\text{obs}}(\text{III})$ ) listed in **Table 3-2**, focusing on how dependent the ratio is on the type of the **H**-, **G**-, **S**-, and **E**-nuclei of compounds **II** and **III**. On the other hand, it is not discussed in this study which mechanism the  $\text{MnO}_2$  oxidation follows,

the consecutive two steps of one-electron oxidation or one step of two-electron oxidation, and how primarily generated intermediates are further oxidized by  $\text{MnO}_2$  and rearrange to products **A** and **B**, although the aromatic cation radical is drawn as the intermediate on the way in **Figure 3-24**. Other possible intermediates are not discussed in this study, because any data obtained in this study cannot sufficiently contribute to distinguishing between the above-described two mechanisms of the  $\text{MnO}_2$  oxidation (two steps of one-electron oxidation and one step of two electrons) and tracing further rearrangements. However, it is valuable enough to clarify which mode, **1**, **2**, or **3**, is the major in the  $\text{MnO}_2$  oxidation of the **H**-, **G**-, **S**-, and **E**-type compounds.

The ratio between the **E**-type compounds ( $k_{\text{obs}}(\text{II}_\text{E})/k_{\text{obs}}(\text{III}_\text{E})$ ) is 8.6 and the largest among all types. This ratio seems to be a common magnitude as an expression of the primary kinetic isotope effect. As described in the previous section,  $\text{MnO}_2$  cannot oxidize compound **I**<sub>E</sub>, and the  $\text{MnO}_2$  oxidation of compound **II**<sub>E</sub> or **III**<sub>E</sub> quantitatively affords product **A**<sub>E</sub> or **A**<sub>E</sub>', respectively. On the basis of these facts, the  $\text{MnO}_2$  oxidations of the **E**-type compounds **II**<sub>E</sub> and **III**<sub>E</sub> are presumed to progress exclusively *via* mode **1**.

The ratio between the **H**- or **G**-type compounds is 4.7 ( $k_{\text{obs}}(\text{II}_\text{H})/k_{\text{obs}}(\text{III}_\text{H})$ ) or 4.0 ( $k_{\text{obs}}(\text{II}_\text{G})/k_{\text{obs}}(\text{III}_\text{G})$ ), respectively, which is smaller than that between the **E**-type compounds ( $k_{\text{obs}}(\text{II}_\text{E})/k_{\text{obs}}(\text{III}_\text{E})$ ). Because the rate-determining step is the oxidation of the aromatic nucleus and hence the kinetic isotope effect does not appear when the  $\text{MnO}_2$  oxidation progresses only *via* mode **2**, any contribution of mode **2** to the  $\text{MnO}_2$  oxidation must decrease the ratio. On the basis of this fact, the  $\text{MnO}_2$  oxidations of the **H**-type compounds **II**<sub>H</sub> and **III**<sub>H</sub> must progress *via* not only mode **1** but also mode **2**, although  $\text{MnO}_2$  cannot oxidize the **H**-nucleus in the oxidation of compound **I**<sub>H</sub>. Mode **2** can become progressive in the  $\text{MnO}_2$  oxidations of compounds **II**<sub>H</sub> and **III**<sub>H</sub> owing to the presence of their benzyl hydroxymethyl groups as an inductively electron-donating group. Similar discussion is possible for the  $\text{MnO}_2$  oxidations of the **G**-type compounds (**II**<sub>G</sub> and **III**<sub>G</sub>). Because  $\text{MnO}_2$  can oxidize compound **I**<sub>G</sub>, the contribution of mode **2** is greater than that in the oxidations of compounds **II**<sub>H</sub> and **III**<sub>H</sub>,

resulting in  $k_{\text{obs}}(\text{II}_\text{G})/k_{\text{obs}}(\text{III}_\text{G})$  being smaller than  $k_{\text{obs}}(\text{II}_\text{H})/k_{\text{obs}}(\text{III}_\text{H})$ .

The ratio between the S-type compounds,  $k_{\text{obs}}(\text{II}_\text{S})/k_{\text{obs}}(\text{III}_\text{S})$ , is 2.7, which is much smaller than the others. As described in the previous section, the  $\text{MnO}_2$  oxidations of compounds  $\text{II}_\text{S}$  and  $\text{III}_\text{S}$  afford products  $\text{B}_\text{S}$ , which clearly shows that  $\text{MnO}_2$  oxidizes their S-nuclei to afford the products. Thus, mode **3** contributes substantially to the  $\text{MnO}_2$  oxidations of compounds  $\text{II}_\text{S}$  and  $\text{III}_\text{S}$ . The kinetic isotope effect does not naturally appear in mode **3**, and hence the contribution of mode **3** to the  $\text{MnO}_2$  oxidation decreases the ratio. The electron-withdrawal inductive effects of the two *meta*-methoxy groups ( $\sigma$  value:  $+ 0.115 \times 2$ ) of compounds  $\text{II}_\text{S}$  and  $\text{III}_\text{S}$  decrease the contribution of mode **1**, which further decreases the ratio. These facts indicate that modes **1**, **2**, and **3** all contribute to the  $\text{MnO}_2$  oxidations of compounds  $\text{II}_\text{S}$  and  $\text{III}_\text{S}$ . Compounds  $\text{II}_\text{S}$  and  $\text{III}_\text{S}$  thus progress to mode **3** contrarily to the lack of mode **3** in the  $\text{MnO}_2$  oxidations of compounds  $\text{II}_\text{G}$  and  $\text{III}_\text{G}$ , although both the S- and G-type compounds are oxidized to be the cation radicals as the primary intermediates. This relative preference of mode **3** in the oxidations of the S-type compounds is based on its higher electron density as well as relative resistance in the rearrangement of the aromatic cation radical to the benzyl radical accompanying the deprotonation from the benzyl position. The  $\text{MnO}_2$  oxidation of the benzyl radical must readily progress to afford products **A**.

### 3.4 Conclusions

MnO<sub>2</sub> oxidized the **G**- and **S**-nuclei of compounds **I<sub>G</sub>** and **I<sub>S</sub>**, respectively, which do not have substructures corresponding to the side-chain of lignin, although MnO<sub>2</sub> commonly oxidizes alcohol groups present at the benzyl positions. MnO<sub>2</sub> oxidized compounds **II**, the analogues of benzyl alcohol, with the rate in the order **G**- > **S**- >> **H**- > **E**-type. This order suggests that their reactivity is determined by the electronic effects of their methoxy and ethyl groups on not only their benzyl positions but also their aromatic  $\pi$ -electron systems. The magnitudes of the kinetic isotope effects in the MnO<sub>2</sub> oxidations were estimated from the ratios of the  $k_{\text{obs}}$  values between compounds **II** and **III**, the non-deuterated and deuterated analogues of benzyl alcohol, respectively. Because the kinetic isotope effect did not appear when the MnO<sub>2</sub> oxidation began with their aromatic nuclei, the ratio decreased with increasing contribution of the oxidation of the aromatic nuclei. The observed ratios were in the order of **E**- >> **H**- > **G**- >> **S**-type, which suggests that the contribution of the oxidations of the aromatic nuclei increases in the reverse order.

Because any carbon-carbon bond does not cleave in modes **1** and **2**, these modes may not contribute to delignification in a bleaching process of actual chemical pulp. Because mode **3** does not contribute to the oxidation of the **G**-type compounds, the MnO<sub>2</sub> oxidation may not be effective in a bleaching process of softwood pulp in contrast to that of hardwood pulp examined in Chapter 2. These will be examined in next coming chapters.

### 3.5 References

- [1] Posoknistakul, P.; Akiho, S.; Akiyama, T.; Yokoyama, T.; Matsumoto, Y. Stereo-preference in the degradation of the *erythro* and *threo* isomers of  $\beta$ -O-4-type lignin model compounds in oxidation processes III: in the reaction with chlorine- and manganese-based oxidants. *Journal of Wood Science* **2018**, *64* (4), 451-457.
- [2] Dai, J.; Patti, A. F.; Styles, G. N.; Nanayakkara, S.; Spiccia, L.; Arena, F.; Italiano, C.; Saito, K. Lignin oxidation by MnO<sub>2</sub> under the irradiation of blue light. *Green Chemistry* **2019**, *21* (8), 2005-2014.
- [3] Freudenberg, K.; Janson, A.; Knopf, E.; Haag, A. Zur kenntnis des lignins (15. mitteil.). *Berichte der Deutschen Chemischen Gesellschaft (A and B Series)* **1936**, *69* (6), 1415-1425.
- [4] Berzins, V. Kappa number of pulp. *Tappi* **1965**, *48* (1), 15-20.
- [5] Lindner, A.; Wegener, G. Characterization of lignins from organosolv pulping according to the organocell process part 4. molecular weight determination and investigation of fractions isolated by GPC. *Journal of Wood Chemistry and Technology* **1990**, *10* (3), 351-363.
- [6] Tsutsumi, Y.; Islam, A.; Anderson, C., D.; Sarkanen, K., V. Acidic permanganate oxidations of lignin and model compounds: Comparison with ozonolysis. *Holzforschung* **1990**, *44* (1), 59-66.
- [7] Gellerstedt, G. Chemical degradation methods: Permanganate oxidation. In *Methods in Lignin Chemistry*, Lin, S. Y.; Dence, C. W., Eds. Springer-Verlag: Heidelberg, Germany, **1992**; pp 322-333.
- [8] Bose, S. K.; Wilson, K. L.; Francis, R. C.; Aoyama, M. Lignin analysis by permanganate oxidation I. Native spruce lignin. *Holzforschung* **1998**, *52* (3), 297.
- [9] Li, J.; Gellerstedt, G. Kinetics and mechanism of kappa number determination. *Nordic Pulp & Paper Research Journal* **1998**, *13* (2), 147-152.
- [10] Bose, S. K.; Wilson, K. L.; Hausch, D. L.; Francis, R. C. Lignin analysis by permanganate oxidation II. Lignins in acidic organosolv pulps. *Holzforschung* **1999**, *53* (6),

603.

- [11] Tong, G.; Yokoyama, T.; Matsumoto, Y.; Meshitsuka, G. Analysis of progress of oxidation reaction during oxygen-alkali treatment of lignin I: method and its application to lignin oxidation. *Journal of Wood Science* **2000**, *46* (1), 32-39.
- [12] Tong, G.; Matsumoto, Y.; Meshitsuka, G. Analysis of progress of oxidation reaction during oxygen-alkali treatment of lignin 2: significance of oxidation reaction of lignin during oxygen delignification. *Journal of Wood Science* **2000**, *46* (5), 371-375.
- [13] Parkås, J.; Brunow, G.; Lundquist, K. Quantitative lignin analysis based on permanganate oxidation. *BioResources* **2007**, *2* (2), 169-178.
- [14] Harfenist, M.; Bavley, A.; Lazier, W. A. The oxidation of allyl and benzyl alcohols to the aldehydes. *Journal of Organic Chemistry* **1954**, *19* (10), 1608-1616.
- [15] Barakat, M. Z.; Abdelwahab, M. F.; Elsadr, M. M. Oxidation of organic compounds by solid manganese dioxide. *Journal of the Chemical Society* **1956**, *1956*, 4685-4687.
- [16] Evans, R. M. Oxidations by manganese dioxide in neutral media. *Quarterly Reviews, Chemical Society* **1959**, *13* (1), 61-70.
- [17] Gritter, R. J.; Wallace, T. J. The manganese dioxide oxidation of allylic alcohols. *Journal of Organic Chemistry* **1959**, *24* (8), 1051-1056.
- [18] Papadopoulos, E. P.; Jarrar, A. I., C. H. Oxidations with manganese dioxide. *Journal of Organic Chemistry* **1966**, *31* (2), 615-616.
- [19] Fatiadi, A. J. Active manganese dioxide oxidation in organic chemistry part I. *Synthesis* **1976**, *1976* (2), 65-104.
- [20] Fatiadi, A. J. Active manganese dioxide oxidation in organic chemistry part II. *Synthesis* **1976**, *1976* (3), 133-167.
- [21] Cahiez, G.; Alami, M.; Taylor, R. J. K.; Reid, M.; Foot, J. S. Manganese dioxide. In *Encyclopedia of reagents for organic synthesis*, 2<sup>nd</sup> ed.; Paquette, L. A.; Crich, D.; Puchs, P. L.; Molander, G. A., Eds. Wiley: New York, NY, **2009**; Vol. 8, pp 6378-6392.
- [22] Birkofer, L.; Erlenbach, L.  $\beta$ -Aminoaldehyde. *Chemische Berichte* **1958**, *91* (11), 2383-

2387.

[23] Pratt, E. F.; Castle, J. F. V. D. Oxidation by solids I: Oxidation of selected alcohols by manganese dioxide. *Journal of Organic Chemistry* **1961**, 26 (8), 2973-2975.

[24] Dollimore, D.; Tonge, K. H. Calculated and observed oxidising capacities of manganese oxides in the oxidation of cinnamyl alcohol in neutral solution. *Journal of the Chemical Society B: Physical Organic* **1967**, 1967, 1380-1384.



**4 Further Investigation of the Mechanisms of MnO<sub>2</sub>  
Oxidation using C<sub>6</sub>-C<sub>2</sub>-type Monomeric Lignin Model  
Compounds with the *p*-Hydroxyphenyl, Guaiacyl, and  
Syringyl Nuclei**

## 4.1 Introduction

In Chapter 3, it was investigated how the reaction rates and mechanisms of MnO<sub>2</sub> oxidation differ between the *p*-hydroxyphenyl (**H**), guaiacyl (**G**), and syringyl (**S**) types of lignin model compounds as well as the *p*-ethylphenyl (**E**) type compounds. The oxidation was conducted using an excess amount of MnO<sub>2</sub> in a sulfate buffer solution at a pH of 1.5 and room temperature. It was shown that MnO<sub>2</sub> oxidizes at least the **G**- and **S**-nuclei without any side-chain structure affording the corresponding benzoquinone derivatives, although it commonly oxidizes benzyl alcohols to benzaldehydes. The oxidation rates of the benzyl alcohol derivatives were in the order of **G**- > **S**- >> **H**- > **E**-type, which suggests that the rates are determined by the electronic effects of their methoxy and ethyl functional groups on not only their benzyl positions but also their aromatic  $\pi$ -electron systems. The kinetic isotope effect was observed in the MnO<sub>2</sub> oxidations of the same derivatives deuterated at their benzyl hydroxymethyl groups. The observed magnitudes were in the order of **E**- >> **H**- > **G**- >> **S**-type, suggesting that the contribution of oxidation of their aromatic nuclei becomes greater with the reverse order.

It should be noted that benzyl hydroxy groups in any lignin sample commonly exist in the form of secondary alcohols,<sup>[1-5]</sup> rather than primary alcohols like the C<sub>6</sub>-C<sub>1</sub>-type monomeric lignin model compounds used in Chapter 3. In this chapter, representative C<sub>6</sub>-C<sub>2</sub>-type monomeric lignin model compounds, in which the benzyl hydroxy groups exist in the form of secondary alcohols, were subjected to the MnO<sub>2</sub> oxidation under the same conditions as those in Chapter 3 to compare the differences in the reactions between C<sub>6</sub>-C<sub>2</sub>-type monomeric lignin model compounds with the **H**-, **G**-, and **S**- nuclei. The results obtained in this chapter were compared with in Chapter 3 to understand the reaction mechanisms further. **Figure 4-1** shows the structures of C<sub>6</sub>-C<sub>2</sub>-type monomeric lignin model compounds (**H**-, **G**-, and **S**-types) as well as *p*-ethylphenyl-type compounds (**E**-types) employed in this chapter. They are 1-(4-methoxyphenyl)ethanol (**H**-type, **IV<sub>H</sub>**), 1-(3,4-dimethoxyphenyl)ethanol (**G**-

type, **IV<sub>G</sub>**), 1-(3,4,5-trimethoxyphenyl)ethanol (**S**-type, **IV<sub>S</sub>**), and 1-(4-ethylphenyl)ethanol (**E**-type, **V<sub>E</sub>**), and their deuterated compounds, 1-(4-methoxyphenyl)(1-<sup>2</sup>H)ethanol (**H**-type, **V<sub>H</sub>**), 1-(3,4-dimethoxyphenyl)(1-<sup>2</sup>H)ethanol (**G**-type, **V<sub>G</sub>**), 1-(3,4,5-trimethoxyphenyl)(1-<sup>2</sup>H)ethanol (**S**-type, **V<sub>S</sub>**), and 1-(4-ethylphenyl)(1-<sup>2</sup>H)ethanol (**E**-type, **V<sub>E</sub>**).

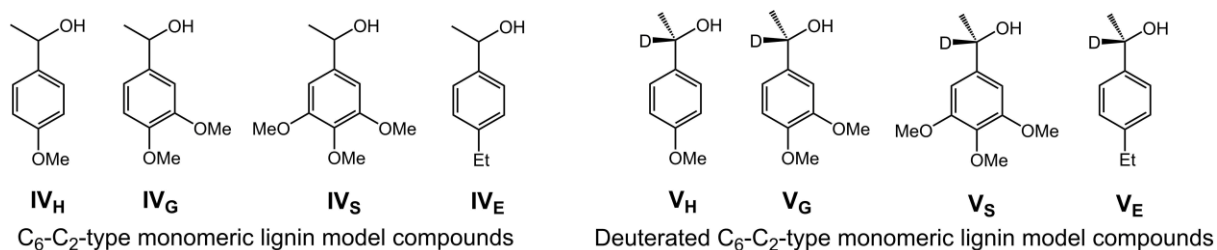


**Figure 4-1** Non-phenolic C<sub>6</sub>-C<sub>2</sub>-type monomeric lignin model compounds (the **H**-, **G**-, and **S**-types) and *p*-ethylphenyl type compounds (the **E**-types) employed in this chapter.

## 4.2 Materials and methods

### 4.2.1 Materials

All chemicals used in this study except for the organic compounds described below were purchased from FUJIFILM Wako Pure Chemical Industries, Ltd. (Osaka, Japan), Tokyo Chemical Industry Co., Ltd. (Tokyo, Japan), or Sigma-Aldrich Japan K. K. (Tokyo, Japan), and used without further purification. Ultrapure H<sub>2</sub>O used in all the experiments was prepared by a generator, Puric-Z (Organo Co., Tokyo, Japan). MnO<sub>2</sub> was synthesized from Mn<sup>2+</sup> (MnSO<sub>4</sub>) by O<sub>2</sub> oxidation under alkaline conditions; the synthesis procedure was described in Chapter 2. Sulfate buffer solution (0.50 mol/L, pH 1.5) prepared with Na<sub>2</sub>SO<sub>4</sub> and H<sub>2</sub>SO<sub>4</sub> solutions (0.5 mol/L each) was used in all the experiments.

#### 4.2.1.1 Preparation of model compounds and authentic compounds of reaction products

Compounds **IV** (all the **H**-, **G**-, **S**- and **E**-types) were commercially available and purified by silica gel chromatography (Isolera<sup>TM</sup>, Biotage Japan Ltd., Tokyo, Japan) before use. Compounds **V<sub>H</sub>**, **V<sub>G</sub>**, **V<sub>S</sub>**, and **V<sub>E</sub>** were synthesized from commercially available acetophenone derivatives, 1-acetyl-4-methoxybenzene, 1-acetyl-3,4-dimethoxybenzene, 1-acetyl-3,4,5-trimethoxybenzene and 1-acetyl-4-ethylbenzene, respectively, by reduction with NaBD<sub>4</sub> in C<sub>2</sub>H<sub>5</sub>OH, and then purified by silica gel chromatography.

**Figure 4-2** shows all the quantified reaction products as well as two products possibly generated despite no detection. The left three products are analogues of 1,4-benzoquinone (**B<sub>H</sub>** (**H**-type), **B<sub>G</sub>** (**G**-type), and **B<sub>S</sub>** (**S**-type)), two of which (products **B<sub>H</sub>** and **B<sub>G</sub>**) were not detected. Product **B<sub>H</sub>** was commercially available, and products **B<sub>G</sub>** and **B<sub>S</sub>** were synthesized by the method described in Chapter 3. The right four products are analogues of acetophenone (acetylbenzene, **C<sub>H</sub>** (**H**-type), **C<sub>G</sub>** (**G**-type), **C<sub>S</sub>** (**S**-type), and **C<sub>E</sub>** (**E**-type)). All of the products **C** were commercially available and purified by silica gel chromatography for use as authentic compounds for identification and preparation of their calibration lines for quantification.

Products **C** also were reacted with  $\text{MnO}_2$  as starting materials to confirm the stability under the reaction conditions employed in this study.

The structure and purity of synthetic compounds mentioned above were confirmed by  $^1\text{H}$ -NMR,  $^{13}\text{C}$ -NMR (JNM-A500, 500MHz, JEOL Ltd.), and gas chromatography-mass spectrometry (GC/MS, (electron ionization, 70 eV). The GC/MS analysis was done on GC2010/PARVUM2 (Shimadzu Co., Ltd., Kyoto, Japan) equipped with a capillary column (TC-17, 0.25 mm i.d.  $\times$  30 m, GL Science Inc., Tokyo, Japan).

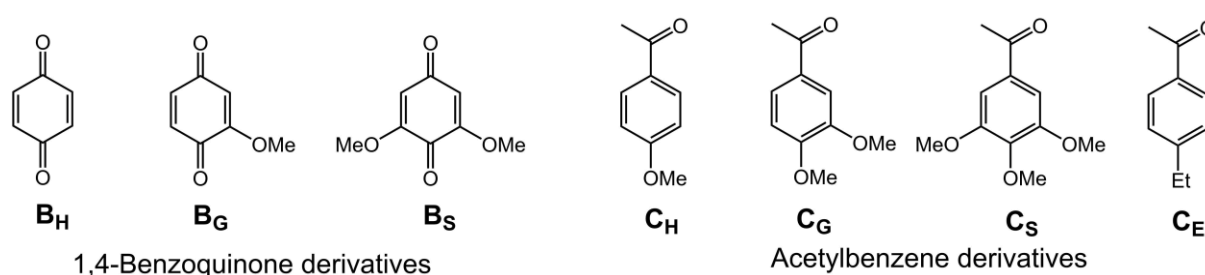
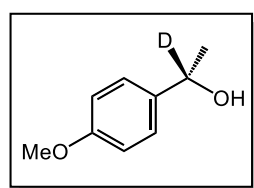


**Figure 4-2** Quantified reaction products and possible two without detection (product **B<sub>H</sub>** and **B<sub>G</sub>**) in the  $\text{MnO}_2$  oxidation.

#### 4.2.1.2 Synthetic processes of model compounds

##### Synthesis of 1-(4-methoxyphenyl)(1- $^2\text{H}$ )ethanol (**V<sub>H</sub>**)

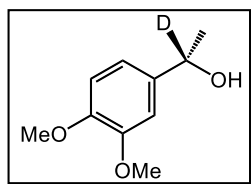


To a solution of ethanol ( $\text{C}_2\text{H}_5\text{OH}$ , 50 mL) containing 4-methoxyacetophenone (**C<sub>H</sub>**, 300 mg, 2.00 mmol) was added  $\text{NaBD}_4$  (150 mg, 3.58 mmol). The reaction mixture was stirred at room temperature overnight. After the completion of the reaction was confirmed by TLC [EtOAc-hexane = 50:50,  $R_f$  (starting material) = 0.71,  $R_f$  (target material) = 0.60], the remaining  $\text{NaBD}_4$  was quenched by addition of  $\text{CH}_3\text{COOH}$ . The volume of the solution was reduced by a rotary evaporation followed by addition of 10 ml of deionized  $\text{H}_2\text{O}$ . Then, the mixture was extracted with  $\text{CH}_2\text{Cl}_2$  (2  $\times$  50 mL). The organic layers were combined, dried over anhydrous  $\text{Na}_2\text{SO}_4$ , and evaporated under vacuum. The remaining  $\text{CH}_3\text{COOH}$  was

removed azeotropically with C<sub>6</sub>H<sub>5</sub>CH<sub>3</sub>. Then the obtained crude product was purified by silica gel chromatography to give **V<sub>H</sub>** as a colorless liquid (265 mg, 87%).

Compound **V<sub>H</sub>**: <sup>1</sup>H-NMR (solvent: CD<sub>2</sub>Cl<sub>2</sub> + aliquot of D<sub>2</sub>O): δ 1.42 (s, 3H, CDOH-CH<sub>3</sub>), 3.78 (s, 3H, OCH<sub>3</sub>), 6.87 (broad d, 2H, *J* = 8.3 Hz, aromatic C<sub>3</sub>-H & C<sub>5</sub>-H), 7.28 (broad d, 2H, *J* = 8.6 Hz, aromatic C<sub>2</sub>-H & C<sub>6</sub>-H). <sup>13</sup>C-NMR: δ 25.2 (CDOH-CH<sub>3</sub>), 55.6 (OCH<sub>3</sub>), 69.5 (CDOH), 114.1 (aromatic C<sub>3</sub> & C<sub>5</sub>), 127.0 (aromatic C<sub>2</sub> & C<sub>6</sub>), 138.6 (aromatic C<sub>1</sub>), 159.3 (aromatic C<sub>4</sub>). MS *m/z* (rel. int.): 153 (M<sup>+</sup>, 23), 138 (87), 135 (100), 120 (53), 110 (46), 92 (61), 78 (24), 66 (29), 43 (21).

### Synthesis of 1-(3,4-dimethoxyphenyl)(1-<sup>2</sup>H)ethanol (**V<sub>G</sub>**)



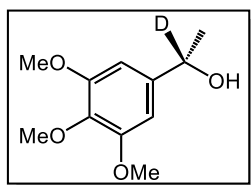
1-Acetyl-3,4-dimethoxybenzene (**C<sub>G</sub>**, 300 mg, 1.66 mmol) was added to 50 mL of C<sub>2</sub>H<sub>5</sub>OH. To the solution was added NaBD<sub>4</sub> (150 mg, 3.58 mmol), and the mixture was stirred at room temperature overnight.

The progress of the reaction was monitored by TLC [EtOAc-hexane = 50:50, R<sub>f</sub> (starting material) = 0.54, R<sub>f</sub> (target material) = 0.38]. After the completion of the reduction, the remaining NaBD<sub>4</sub> was quenched by addition of CH<sub>3</sub>COOH. The volume of the solution was reduced by a rotary evaporation followed by addition of 10 ml of deionized H<sub>2</sub>O. Then, the mixture was extracted with CH<sub>2</sub>Cl<sub>2</sub> (2 × 50 mL). The organic layers were combined, dried over anhydrous Na<sub>2</sub>SO<sub>4</sub>, and evaporated under vacuum. The remaining CH<sub>3</sub>COOH was removed azeotropically with C<sub>6</sub>H<sub>5</sub>CH<sub>3</sub>. The obtained product was purified by silica gel chromatography to give **V<sub>G</sub>** as a colorless liquid (267 mg, 88%).

Compound **V<sub>G</sub>**: <sup>1</sup>H-NMR (solvent: CDCl<sub>3</sub> + aliquot of D<sub>2</sub>O): δ 1.49 (s, 3H, CDOH-CH<sub>3</sub>), 3.88 (s, 3H, aromatic C<sub>3</sub>- or C<sub>4</sub>-OCH<sub>3</sub>), 3.90 (s, 3H, aromatic C<sub>3</sub>- or C<sub>4</sub>-OCH<sub>3</sub>), 6.84 (d, 1H, *J* = 8.0 Hz, aromatic C<sub>5</sub>-H), 6.89 (d, 1H, *J* = 8.1 Hz, aromatic C<sub>6</sub>-H), 6.95 (s, 1H, aromatic C<sub>2</sub>-H). <sup>13</sup>C-NMR: δ 25.0 (CDOH-CH<sub>3</sub>), 56.0 (aromatic C<sub>3</sub>- or C<sub>4</sub>-OCH<sub>3</sub>), 56.1 (aromatic C<sub>3</sub>- or C<sub>4</sub>-OCH<sub>3</sub>), 69.7 (CDOH), 108.8 (aromatic C<sub>2</sub>), 111.1 (aromatic C<sub>5</sub>), 117.6 (aromatic C<sub>6</sub>), 138.7 (aromatic C<sub>1</sub>), 148.4 (aromatic C<sub>4</sub>), 149.1 (aromatic C<sub>3</sub>). MS *m/z* (rel. int.): 183 (M<sup>+</sup>,

28), 165 (100), 150 (41), 140 (58), 122 (19), 104 (23), 92 (40), 78 (29), 65 (8), 43 (25).

### Synthesis of 1-(3,4,5-trimethoxyphenyl)(1-<sup>2</sup>H)ethanol (**V<sub>S</sub>**)

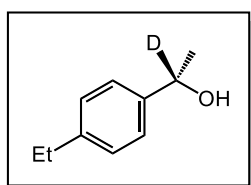


To a solution of 1-acetyl-3,4,5-trimethoxybenzene (**C<sub>S</sub>**, 300 mg, 1.43 mmol) in C<sub>2</sub>H<sub>5</sub>OH (50 mL) was added NaBD<sub>4</sub> (150 mg, 3.58 mmol). The reaction mixture was stirred at room temperature overnight.

The progress of the reaction was monitored by TLC [EtOAc-hexane = 50:50, R<sub>f</sub> (starting material) = 0.58, R<sub>f</sub> (target material) = 0.33]. CH<sub>3</sub>COOH was added to quench the reaction. The volume of the solution was reduced by a rotary evaporation followed by addition of 10 ml of deionized H<sub>2</sub>O. Then, the mixture was extracted with CH<sub>2</sub>Cl<sub>2</sub> (2 × 50 mL). The organic phases were combined, dried over anhydrous Na<sub>2</sub>SO<sub>4</sub>, and concentrated under vacuum. The remaining CH<sub>3</sub>COOH was removed azeotropically with C<sub>6</sub>H<sub>5</sub>CH<sub>3</sub>. The crude material was purified by silica gel chromatography to give **V<sub>S</sub>** as a colorless liquid (245 mg, 80%).

Compound **V<sub>S</sub>**: <sup>1</sup>H-NMR (solvent: CDCl<sub>3</sub> + aliquot of D<sub>2</sub>O): δ 1.49 (s, 3H, CDOH-CH<sub>3</sub>), 3.84 (s, 3H, aromatic C<sub>4</sub>-OCH<sub>3</sub>), 3.88 (s, 6H, aromatic C<sub>3</sub>- & C<sub>5</sub>-OCH<sub>3</sub>), 6.61 (s, 2H, aromatic C<sub>2</sub>-H & C<sub>6</sub>-H). <sup>13</sup>C-NMR: 25.2 (CDOH-CH<sub>3</sub>), δ 56.2 (aromatic C<sub>3</sub>- & C<sub>5</sub>-OCH<sub>3</sub>), 61.0 (aromatic C<sub>4</sub>-OCH<sub>3</sub>), 70.1 (CDOH), 102.4 (aromatic C<sub>2</sub> & C<sub>6</sub>), 137.2 (aromatic C<sub>1</sub>), 141.9 (aromatic C<sub>4</sub>), 153.4 (aromatic C<sub>3</sub> & C<sub>5</sub>). MS m/z (rel. int.): 213 (M<sup>+</sup>, 48), 198 (40), 195 (100), 180 (87), 170 (57), 152 (43), 137 (38), 120 (21), 109 (12), 92 (39), 78 (24), 66 (47), 43 (41).

### Synthesis of 1-(4-ethylphenyl)(1-<sup>2</sup>H)ethanol (**V<sub>E</sub>**)



To a solution of C<sub>2</sub>H<sub>5</sub>OH (50 mL) containing 1-acetyl-4-ethylbenzene (**C<sub>E</sub>**, 300 mg, 2.02 mmol) was added NaBD<sub>4</sub> (150 mg, 3.58 mmol). The reaction mixture was stirred at room temperature overnight. After the completion of the reaction was confirmed by TLC [EtOAc-hexane = 50:50, R<sub>f</sub> (starting material) = 0.85, R<sub>f</sub> (target material) = 0.75], the remaining NaBD<sub>4</sub> was quenched by addition of the CH<sub>3</sub>COOH. The volume of the solution

was reduced by a rotary evaporation followed by addition of 10 ml of deionized H<sub>2</sub>O, and the mixture was extracted with CH<sub>2</sub>Cl<sub>2</sub> (2 × 50 mL). The organic layers were combined, dried over anhydrous Na<sub>2</sub>SO<sub>4</sub>, and evaporated under vacuum. The remaining CH<sub>3</sub>COOH was removed azeotropically with C<sub>6</sub>H<sub>5</sub>CH<sub>3</sub>. The crude material was purified by silica gel chromatography to give **V<sub>E</sub>** as a colorless liquid (234.9 mg, 77%).

Compound **V<sub>E</sub>**: <sup>1</sup>H-NMR (solvent: CD<sub>2</sub>Cl<sub>2</sub> + aliquot of D<sub>2</sub>O): δ 1.24 (t, 3H, *J* = 7.4 Hz, CH<sub>2</sub>-CH<sub>3</sub>), 1.44 (s, 3H, CDOH-CH<sub>3</sub>), 2.64 (q, 2H, *J* = 7.8 Hz, CH<sub>2</sub>-CH<sub>3</sub>), 7.19 (d, 2H, *J* = 7.8 Hz, aromatic C<sub>3</sub>-H & C<sub>5</sub>-H), 7.28 (d, 2H, *J* = 8.1 Hz, aromatic C<sub>2</sub>-H & C<sub>6</sub>-H). <sup>13</sup>C-NMR: δ 15.9 (CH<sub>2</sub>-CH<sub>3</sub>), 25.2 (CDOH-CH<sub>3</sub>), 28.9 (CH<sub>2</sub>-CH<sub>3</sub>), 69.8 (CDOH), 125.7 (aromatic C<sub>2</sub> & C<sub>6</sub>), 128.2 (aromatic C<sub>3</sub> & C<sub>5</sub>), 143.7 (aromatic C<sub>1</sub>), 143.8 (aromatic C<sub>4</sub>). MS *m/z* (rel. int.): 151 (M<sup>+</sup>, 25), 136 (83), 118 (32), 108 (15), 92 (15), 80 (100), 65 (6), 43 (40).

#### 4.2.1.3 NMR spectra and GC/MS spectra of synthesized model compounds

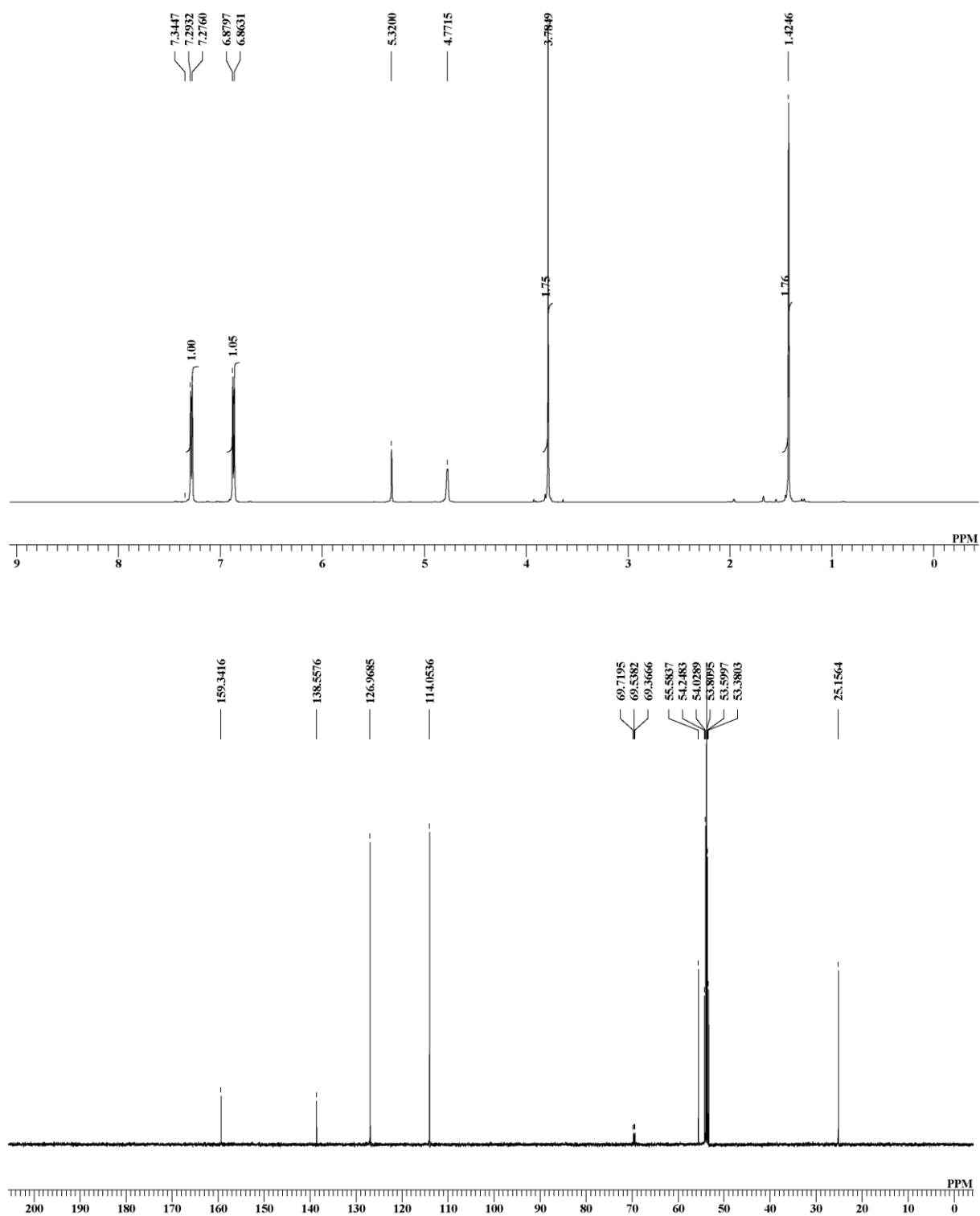


**Figure 4-3** <sup>1</sup>H-NMR (top) and <sup>13</sup>C-NMR (bottom) spectra of compound V<sub>H</sub>.

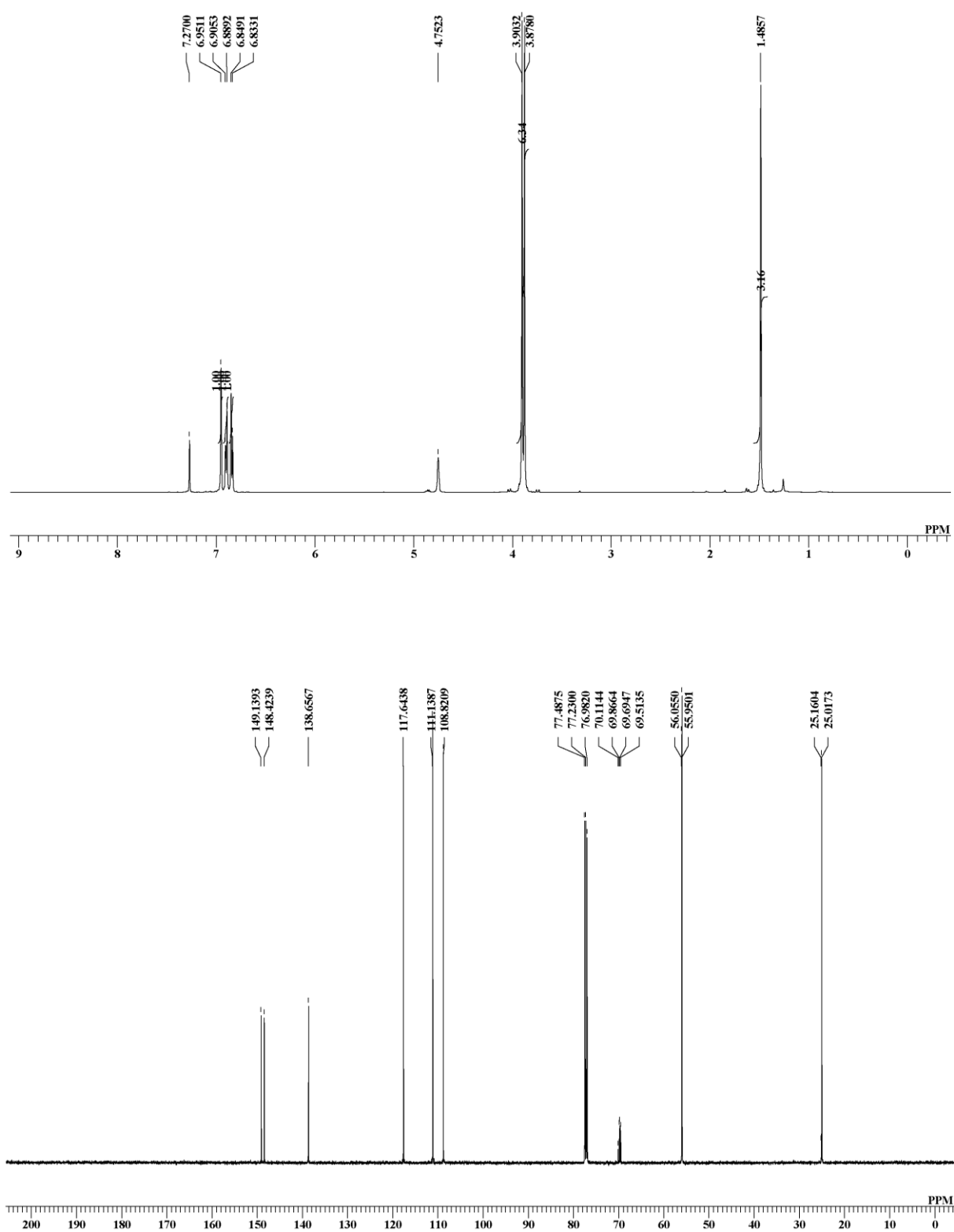


**Figure 4-4** <sup>1</sup>H-NMR (top) and <sup>13</sup>C-NMR (bottom) spectra of compound VG.

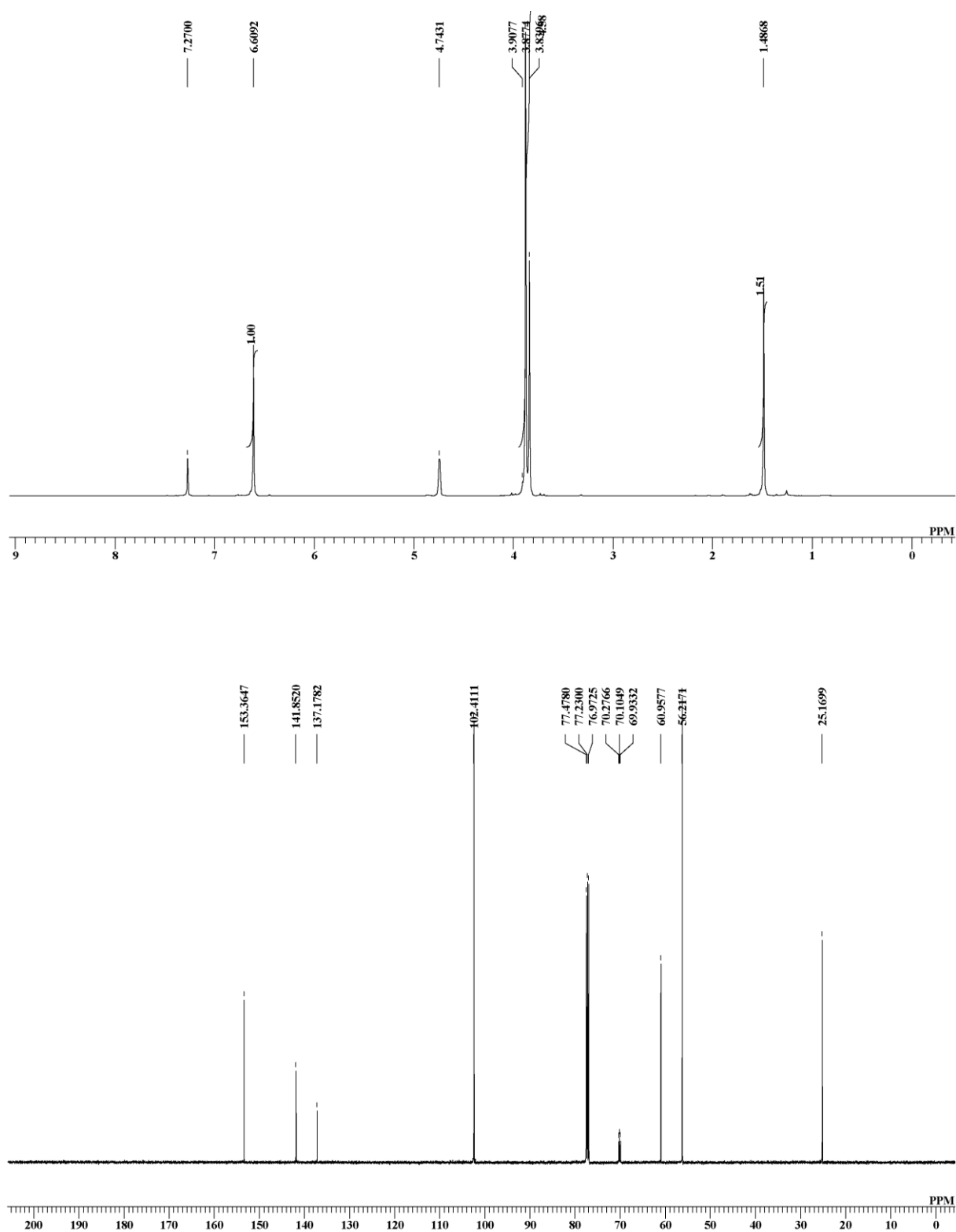


**Figure 4-5**  $^1\text{H}$ -NMR (top) and  $^{13}\text{C}$ -NMR (bottom) spectra of compound Vs.

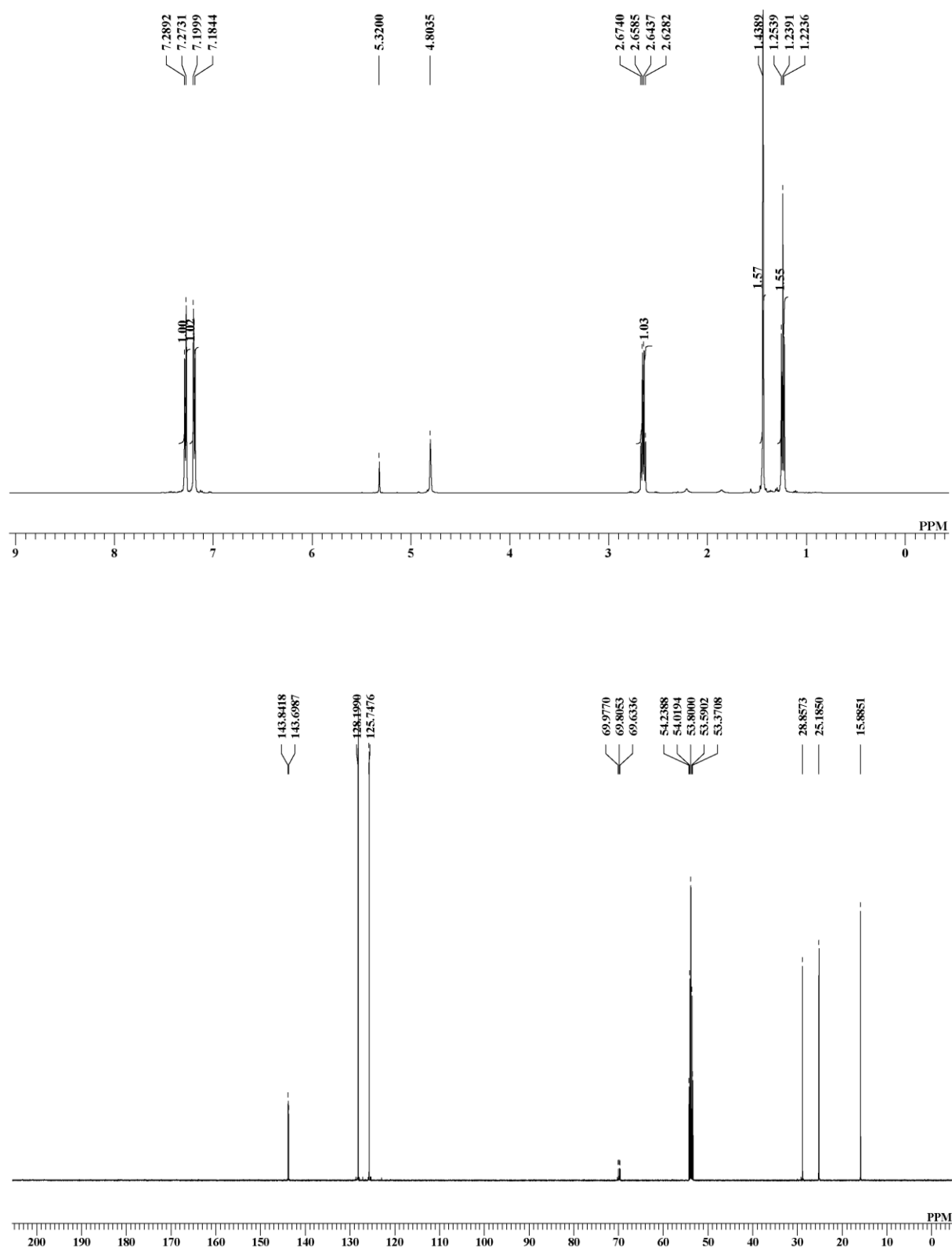


**Figure 4-6**  $^1\text{H}$ -NMR (top) and  $^{13}\text{C}$ -NMR (bottom) spectra of compound **VE**.

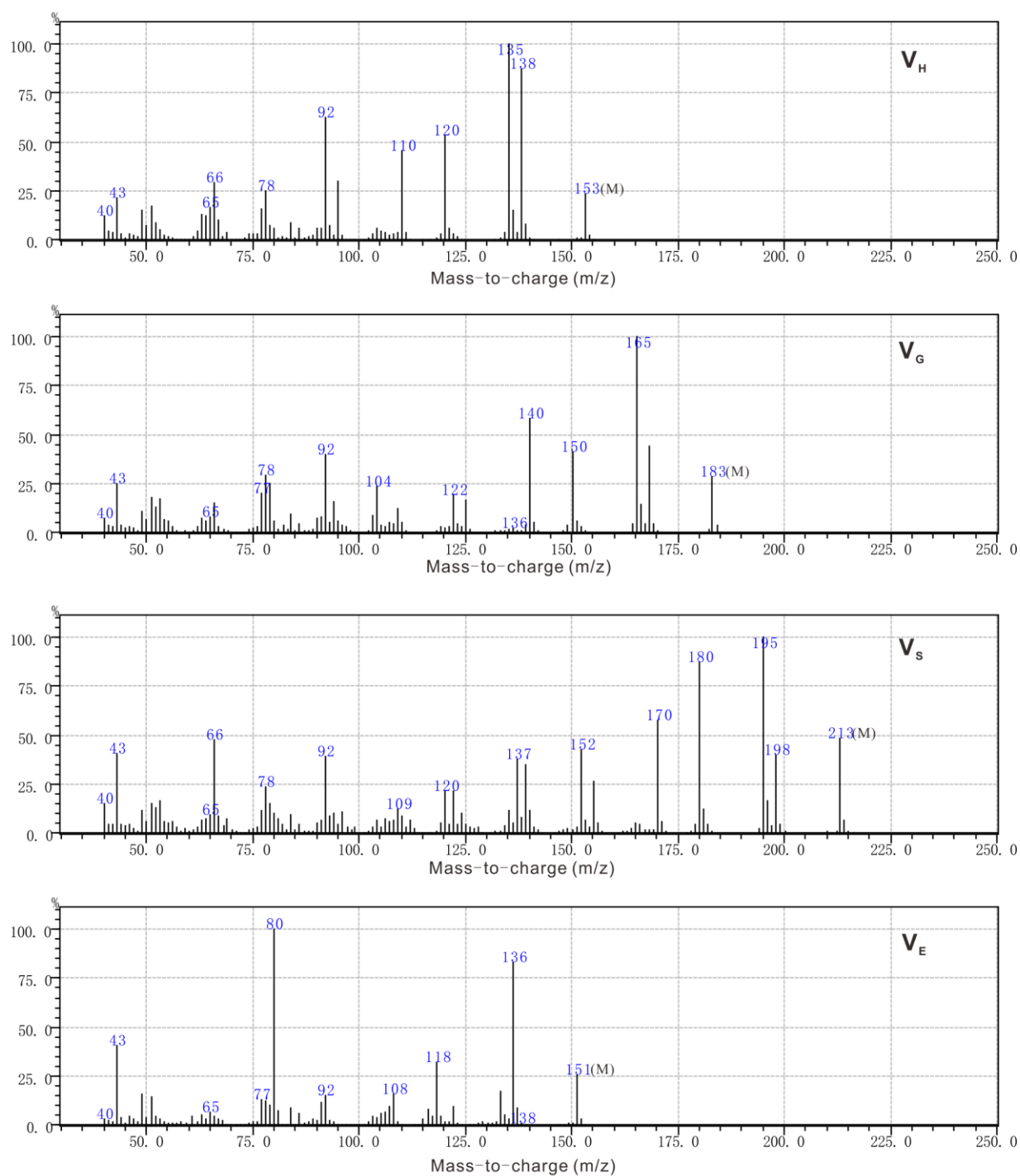


**Figure 4-7** GC/MS spectra of synthesized model compounds employed in this chapter.

## 4.2.2 Methods

### 4.2.2.1 MnO<sub>2</sub> oxidation reaction

All the oxidations were conducted in a bottom-round glass flask (200 mL volume) equipped with a magnetic stirrer. The MnO<sub>2</sub> powder used in this chapter is the synthetic MnO<sub>2</sub> (the synthesis process was described in Chapter 2) with theoretical oxidation power of 84.9%. The powder (1.2 mmol (oxidation power basis:  $1.2 \times 84.9/100 = 1.02$  mmol), oven-dry basis) was aged in a sulfate buffer solution (50 mL, 0.50 mol/L, pH 1.5) for 120 min in the glass flask at room temperature.

Another sulfate buffer solution (10 mL, 0.50 mol/L, pH 1.5) containing each starting material (12  $\mu$ mol) was added to the buffer solution containing the aged MnO<sub>2</sub> powder to initiate the reaction. The initial concentration of each starting material was 0.20 mmol/L, and MnO<sub>2</sub> (insoluble solid) was 20 mmol/L. Each reaction was conducted three times to confirm the reproducibility.

### 4.2.2.2 Quantification

A specific amount of the reaction solution was withdrawn at prescribed reaction times to quantify the residual starting material and reaction products. The withdrawn solution was rapidly neutralized with an excess amount of a saturated NaHCO<sub>3</sub> solution, and mixed with methanol containing an internal standard compound (1,2,3-trimethoxybenzene or 3,4-dimethoxybenzaldehyde (veratraldehyde)). The mixture was filtrated with a membrane filter and injected into an HPLC instrument equipped with an ultraviolet-visible (UV-VIS) absorption detector (LC-2010C<sub>HT</sub>, Shimadzu Co., Ltd.) using the absorbance at 280 nm for quantification. The conditions of HPLC were as follows. An HPLC column, Luna 5  $\mu$  C18(2), 100 Å (length: 150 mm, inner diameter: 2.0 mm, particle size: 5.0  $\mu$ m, Phenomenex, Inc., Torrance, CA, USA) was used at an oven temperature of 40°C with a solvent flow rate of 0.2 mL/min.

The types of solvent and gradients were as follows: For the reactions of the **H**-, and **G**-type compounds, the gradient of CH<sub>3</sub>OH/H<sub>2</sub>O (v/v) was from 30/70 to 40/60 for 30 min, and then maintained for 10 min. For the reactions of compound **IV**s, the gradient of CH<sub>3</sub>OH/H<sub>2</sub>O (v/v) was from 30/70 to 50/50 for 30 min, and then maintained for 10 min. For the reactions of compound **V**s, the gradient of CH<sub>3</sub>OH/H<sub>2</sub>O (v/v) was from 30/70 to 65/35 for 30 min, and then maintained for 10 min. For the reactions of the **E**-type compounds, the gradient of CH<sub>3</sub>OH/H<sub>2</sub>O (v/v) was from 30/70 to 50/50 for 10 min, from 50/50 to 60/40 for 15 min, and maintained for 10 min.

**Table 4-1** HPLC analysis methods for MnO<sub>2</sub> oxidation of C<sub>6</sub>-C<sub>2</sub>-type monomeric lignin model compounds and their respective internal standards for quantification.

Compound	Binary gradient system in HPLC	Internal standard
<b>IV<sub>H</sub></b>	gradient CH <sub>3</sub> OH/H <sub>2</sub> O (v/v) from 30/70 to 40/60 for 30 min and maintained for 10 min (total time 40 min), following an equilibration step	3,4-dimethoxybenzaldehyde
<b>IV<sub>G</sub></b>	gradient CH <sub>3</sub> OH/H <sub>2</sub> O (v/v) from 30/70 to 40/60 for 30 min and maintained for 10 min (total time 40 min), following an equilibration step	1,2,3-trimethoxybenzene
<b>IV<sub>S</sub></b>	gradient CH <sub>3</sub> OH/H <sub>2</sub> O (v/v) from 30/70 to 50/50 for 30 min and maintained for 10 min (total time 40 min), following an equilibration step	1,2,3-trimethoxybenzene
<b>IV<sub>E</sub></b>	gradient CH <sub>3</sub> OH/H <sub>2</sub> O (v/v) from 30/70 to 50/50 for 10 min, from 50/50 to 60/40 for 15 min, and maintained for 10 min (total time 35 min), following an equilibration step	1,2,3-trimethoxybenzene
<b>V<sub>H</sub></b>	gradient CH <sub>3</sub> OH/H <sub>2</sub> O (v/v) from 30/70 to 40/60 for 30 min and maintained for 10 min (total time 40 min), following an equilibration step	3,4-dimethoxybenzaldehyde
<b>V<sub>G</sub></b>	gradient CH <sub>3</sub> OH/H <sub>2</sub> O (v/v) from 30/70 to 40/60 for 30 min and maintained for 10 min (total time 40 min), following an equilibration step	1,2,3-trimethoxybenzene
<b>V<sub>S</sub></b>	gradient CH <sub>3</sub> OH/H <sub>2</sub> O (v/v) from 30/70 to 65/35 for 30 min and maintained for 10 min (total time 40 min), following an equilibration step	1,2,3-trimethoxybenzene
<b>V<sub>E</sub></b>	gradient CH <sub>3</sub> OH/H <sub>2</sub> O (v/v) from 30/70 to 50/50 for 10 min, from 50/50 to 60/40 for 15 min, and maintained for 10 min (total time 35 min), following an equilibration step	1,2,3-trimethoxybenzene

## 4.3 Results and discussion

### 4.3.1 MnO<sub>2</sub> oxidation of C<sub>6</sub>-C<sub>2</sub>-type monomeric lignin model compounds (compounds IV)

The synthetic MnO<sub>2</sub> was used in this chapter under the same reaction conditions as those described in Chapter 3. The reason for choosing E-type compounds (**IV<sub>E</sub>** and **V<sub>E</sub>**) is the same as that described in Chapter 3. The total  $\sigma$  value of two methoxy groups of the G-type compounds is  $-0.153$  ( $= -0.268$  (*para*) +  $0.115$  (*meta*)), which is close to that of the ethyl group of the E-type compounds,  $-0.151$ . **Figures 4-8, 4-9, 4-10, and 4-11** show the oxidation of compounds **IV** (**IV<sub>H</sub>**, **IV<sub>G</sub>**, **IV<sub>S</sub>**, and **IV<sub>E</sub>**) when each of the compounds was individually treated at a pH of 1.5 and room temperature.

In Chapter 3, I presented the following three models of MnO<sub>2</sub> oxidation. Mode **1** is the direct oxidation of the benzyl position to afford the corresponding benzaldehyde-type products. Mode **2** begins with the oxidation of the aromatic nucleus, but finally results in the oxidation of the benzyl position to afford the corresponding benzaldehyde-type products. Mode **3** also begins with the oxidation of the aromatic nucleus, and finally results in the oxidative degradation of the aromatic nucleus to afford the 1,4-benzoquinone-type products as well as other unidentified aliphatic reaction products *via* degradation of the aromatic nucleus.

In this chapter, the C<sub>6</sub>-C<sub>2</sub>-type monomeric lignin model compounds shown in **Figure 4-1** were oxidized by MnO<sub>2</sub> under the same condition as those described in Chapter 3. Possible reaction products are the acetylbenzene-type products (**C-types**) afforded by the oxidation of the benzyl hydroxy groups and/or the 1,4-benzoquinone-type products (**B-types**) afforded by the oxidation of the aromatic nuclei on the basis of the reaction modes presented in Chapter 3.

Compound **IV<sub>H</sub>** disappeared in the MnO<sub>2</sub> oxidation, and product **C<sub>H</sub>** formed as the only exclusive reaction product. The recovery yield of **IV<sub>H</sub>** and yield of product **C<sub>H</sub>** were  $80.1 \pm 0.4\%$  and  $19.5 \pm 0.53\%$ , respectively, at a reaction time of 660 min. The MnO<sub>2</sub> oxidation of compound **IV<sub>G</sub>** showed the same phenomena as those of compound **IV<sub>H</sub>**. The recovery

yield of **IV<sub>G</sub>** and yield of product **C<sub>G</sub>** were  $2.5 \pm 0.8\%$  and  $95.3 \pm 0.9\%$ , respectively, at a reaction time of 120 min. Product **C<sub>H</sub>** or **C<sub>G</sub>** was stable under the employed conditions when subjected to the MnO<sub>2</sub> oxidation as a starting compound. The total of the recovery yield of **IV<sub>H</sub>** and yield of product **C<sub>H</sub>** were 99.6%, and those of **IV<sub>G</sub>** and **C<sub>G</sub>** were 97.8%, which indicated that almost no side reactions occurred.

In contrast, the aromatic nucleus (**S**-nucleus) of compound **IV<sub>S</sub>** was oxidized in the MnO<sub>2</sub> oxidation. The recovery yield of **IV<sub>S</sub>** and yields of products **B<sub>S</sub>** and **C<sub>S</sub>** were  $7.6 \pm 0.4\%$ ,  $9.3 \pm 0.2\%$ , and  $46.9 \pm 1.5\%$ , respectively, at a reaction time of 480 min. The total of these was 63.8%. The oxidation of the aromatic nucleus (**S**-nucleus) affording unidentified aliphatic reaction products may have resulted in why the total of the recovery yield and yield of these products was lower than 100%. Product **B<sub>S</sub>** or **C<sub>S</sub>** was stable under the employed conditions when subjected to the MnO<sub>2</sub> oxidation as a starting compound.

For the MnO<sub>2</sub> oxidation of compound **IV<sub>E</sub>**, the recovery yield of **IV<sub>E</sub>** and yield of product **C<sub>E</sub>** were  $88.2 \pm 0.1\%$  and  $12.0 \pm 0.1\%$ , respectively, at a reaction time of 2880 min. The total of these was 100.2%. These observed phenomena were similar to those in the oxidation of compounds **IV<sub>H</sub>** and **IV<sub>G</sub>**, which indicates that almost no side reactions occurred in the oxidation of compound **IV<sub>E</sub>**. Product **C<sub>E</sub>** was stable under the employed conditions when subjected to the MnO<sub>2</sub> oxidation as a starting compound.

All the disappearance behaviors of compounds **IV** conducted in this chapter were well approximated to pseudo-first-order reactions. The pseudo-first-order reaction rate constants ( $k_{\text{obs}}$ ) and squares of the correlation coefficient ( $R^2$ ) are listed in **Table 4-2**. The rates were in the order of: compounds **IV<sub>G</sub>** > **IV<sub>S</sub>** >> **IV<sub>H</sub>** > **IV<sub>E</sub>**, which is exactly the same as that obtained when the C<sub>6</sub>-C<sub>1</sub>-type monomeric lignin model compounds were used as starting compounds. The rates should have been in the order of: compound **IV<sub>H</sub>** > **IV<sub>G</sub>** ≥ **IV<sub>E</sub>** > **IV<sub>S</sub>** based on their Hammett's  $\sigma$  values, which are - 0.268, - 0.153, - 0.151, and - 0.038, respectively, if the MnO<sub>2</sub> oxidations had only been affected by the electronic effects originating in the functional groups on their aromatic nuclei and appearing locally only at their benzyl positions. This

inconsistency suggests that the contribution of the oxidations of the aromatic nuclei has an influence on the order as described in Chapter 3, and hence, the reaction modes of the  $\text{MnO}_2$  oxidation proposed for the  $\text{C}_6\text{-C}_1$ -type monomeric lignin model compounds are also applicable to that of the  $\text{C}_6\text{-C}_2$  type monomeric lignin model compounds.

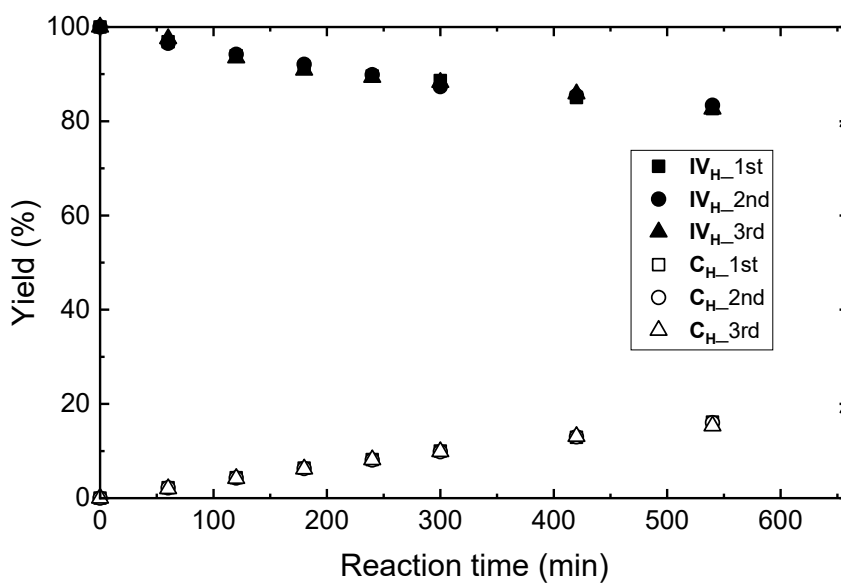


**Figure 4-8** Time course of the changes in the recovery yield of compound  $\text{IV}_\text{H}$  and yield of product  $\text{C}_\text{H}$  in the  $\text{MnO}_2$  oxidation of compound  $\text{IV}_\text{H}$ .

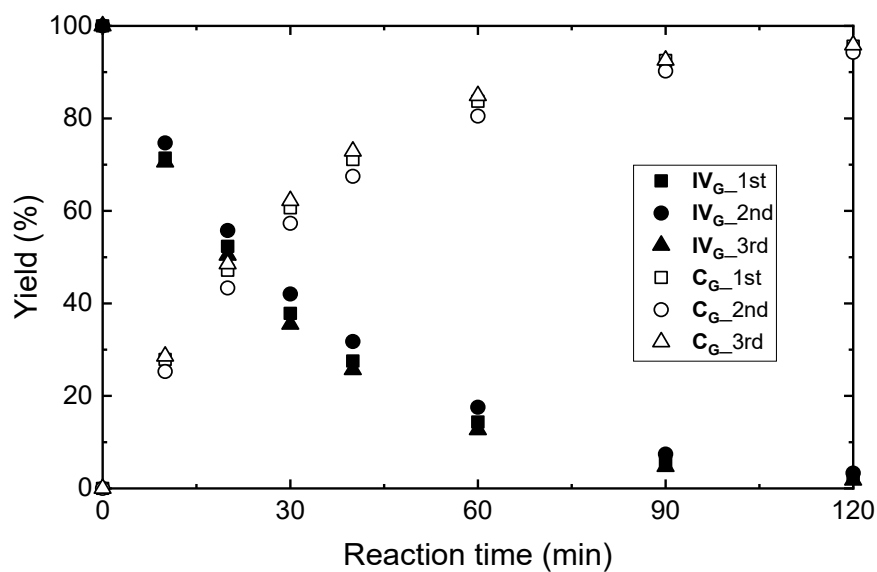


**Figure 4-9** Time course of the changes in the recovery yield of compound **IV<sub>G</sub>** and yield of product **C<sub>G</sub>** in the  $\text{MnO}_2$  oxidation of compound **IV<sub>G</sub>**.

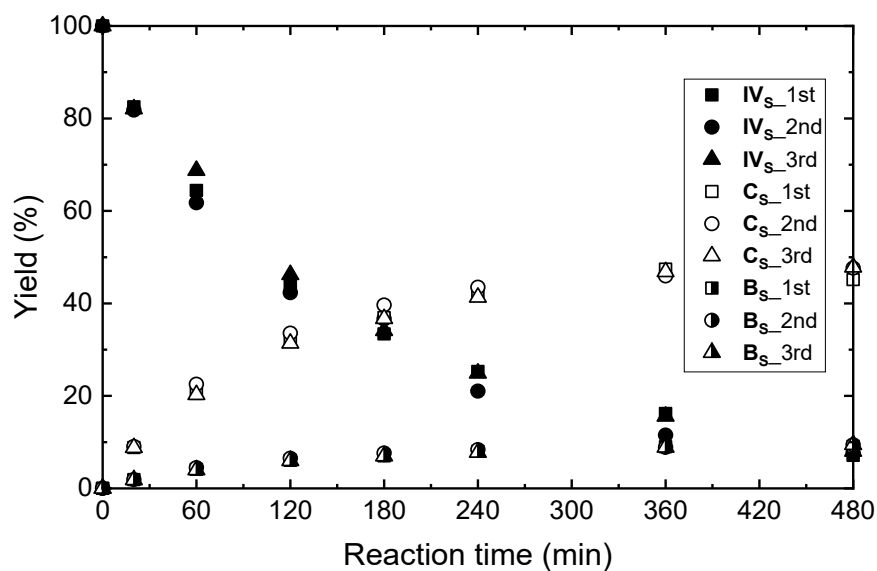


**Figure 4-10** Time course of the changes in the recovery yield of compound **IV<sub>s</sub>** and yields of products **C<sub>s</sub>** and **B<sub>s</sub>** in the  $\text{MnO}_2$  oxidation of compound **IV<sub>s</sub>**.

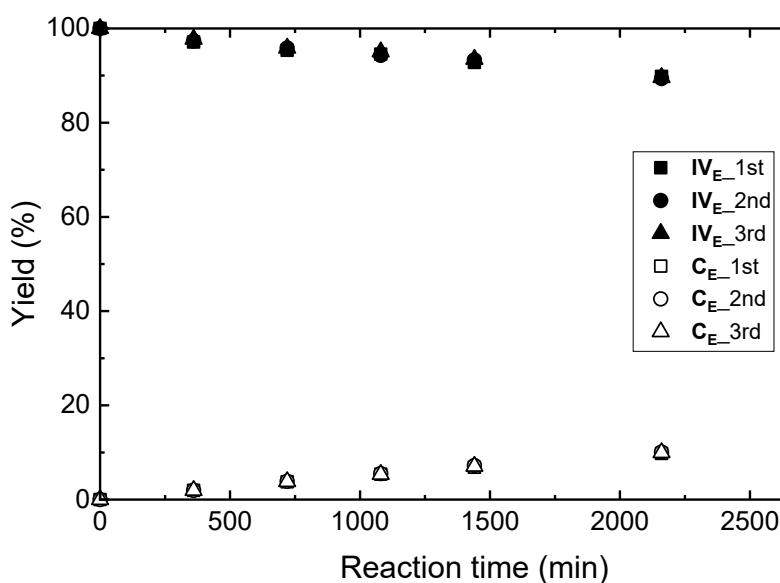


**Figure 4-11** Time course of the changes in the recovery yield of compound **IV<sub>E</sub>** and yield of product **C<sub>E</sub>** in the MnO<sub>2</sub> oxidation of compound **IV<sub>E</sub>**.

**Table 4-2** Observed pseudo-first-order reaction rate constants ( $k_{\text{obs}}$ ), squares of the correlation coefficients ( $R^2$ ) in the approximations, and ratios of  $k_{\text{obs}}$  values between compounds **IV** and **V** ( $k_{\text{obs}}(\text{IV})/k_{\text{obs}}(\text{V})$ ) for estimation of the magnitudes of the kinetic isotope effects.

<b>C.IV<sup>a</sup></b>	$k_{\text{obs}}^b$	$R^{2c}$	<b>C.V<sup>d</sup></b>	$k_{\text{obs}}^b$	$R^{2c}$	$k_{\text{obs}}(\text{IV})/k_{\text{obs}}(\text{V})$
<b>IV<sub>H</sub></b>	3.66±0.01	0.942	<b>V<sub>H</sub></b>	0.867±0.013	0.984	4.2 ( <b>H</b> )
		0.946			0.982	
		0.939			0.957	
<b>IV<sub>G</sub></b>	315±21	1.00	<b>V<sub>G</sub></b>	96.2±0.7	0.999	3.3 ( <b>G</b> )
		1.00			0.998	
		1.00			0.999	
<b>IV<sub>S</sub></b>	55.6±2.0	0.984	<b>V<sub>S</sub></b>	28.9±1.1	0.960	1.9 ( <b>S</b> )
		0.978			0.980	
		0.989			0.974	
<b>IV<sub>E</sub></b>	0.478±0.008	0.952	<b>V<sub>E</sub></b>	0.0627±0.0005	0.978	7.6 ( <b>E</b> )
		0.968			0.984	
		0.978			0.989	

<sup>a</sup>Compounds **IV**. <sup>b</sup>Unit:  $\times 10^{-4} \text{ min}^{-1}$ . The values after the '±' marks are the standard deviations of three duplicated runs. <sup>c</sup>The value obtained from each of three duplicated runs. <sup>d</sup>Compounds **V**.

### 4.3.2 MnO<sub>2</sub> oxidation of deuterated C<sub>6</sub>-C<sub>2</sub>-type monomeric lignin model compounds (compounds V)

Figures 4-12, 4-13, 4-14, and 4-15 show the oxidation of compound V (V<sub>H</sub>, V<sub>G</sub>, V<sub>S</sub>, and V<sub>E</sub>) when each of the compounds was individually treated at the same conditions as those of the oxidation of compounds IV. Each disappearance of compounds V was approximated well to a pseudo-first-order reaction. The pseudo-first-order reaction rate constants ( $k_{\text{obs}}$ ) and squares of the correlation coefficient ( $R^2$ ) are also listed in Table 4-2. The MnO<sub>2</sub> oxidations of deuterated compounds V showed similar phenomena to those of the corresponding compounds IV, except that the oxidation rate was lower due to the primary kinetic isotope effect.

The recovery yield of compound V<sub>H</sub> and yield of product C<sub>H</sub> were  $94.3 \pm 0.3\%$  and  $5.3 \pm 0.1\%$ , respectively, at a reaction time of 660 min. The total of these was 99.6%. The recovery yield of compound V<sub>G</sub> and product C<sub>G</sub> were  $31.8 \pm 0.5\%$  and  $67.2 \pm 0.4\%$ , respectively, at a reaction time of 120 min. The total of these was 99.0%. These indicated that almost no side reactions occurred in the MnO<sub>2</sub> oxidation of compound V<sub>H</sub> or V<sub>G</sub>. In the MnO<sub>2</sub> oxidation of compound V<sub>S</sub>, products C<sub>S</sub> and B<sub>S</sub> formed as the exclusive primary and secondary prominent reaction products, respectively. The recovery yield of compound V<sub>S</sub> and yields of products C<sub>S</sub> and B<sub>S</sub> were  $27.7 \pm 1.3\%$ ,  $8.2 \pm 0.2\%$ , and  $5.3 \pm 0.1\%$ , respectively, at a reaction time of 480 min. The total of these was 41.2%. The recovery yield of compound V<sub>E</sub> and yield of product C<sub>E</sub> were  $98.2 \pm 0.1\%$  and  $1.5 \pm 0.0\%$ , respectively, at a reaction time of 2880 min. The total of these was 99.7%.

In the MnO<sub>2</sub> oxidation of compound IV<sub>S</sub>, it should be noted that the yield of product C<sub>S</sub> was more than five times higher than that of product B<sub>S</sub>. However, when compound V<sub>S</sub> was oxidized, there was almost no difference in the yields of the products C<sub>S</sub> and B<sub>S</sub>. This difference indicates that in the oxidation of compound V<sub>S</sub> the presence of the deuterium at the benzyl position decelerated the oxidation of the benzyl position, and hence, more S-nucleus was oxidized to afford product B<sub>S</sub>.

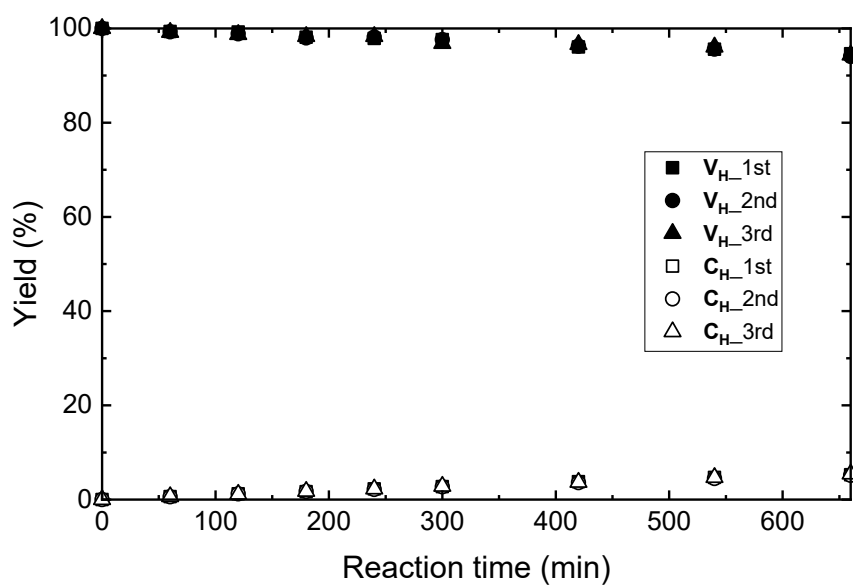


**Figure 4-12** Time course of the changes in the recovery yield of compound V<sub>H</sub> and yield of product C<sub>H</sub> in the MnO<sub>2</sub> oxidation of compound V<sub>H</sub>.

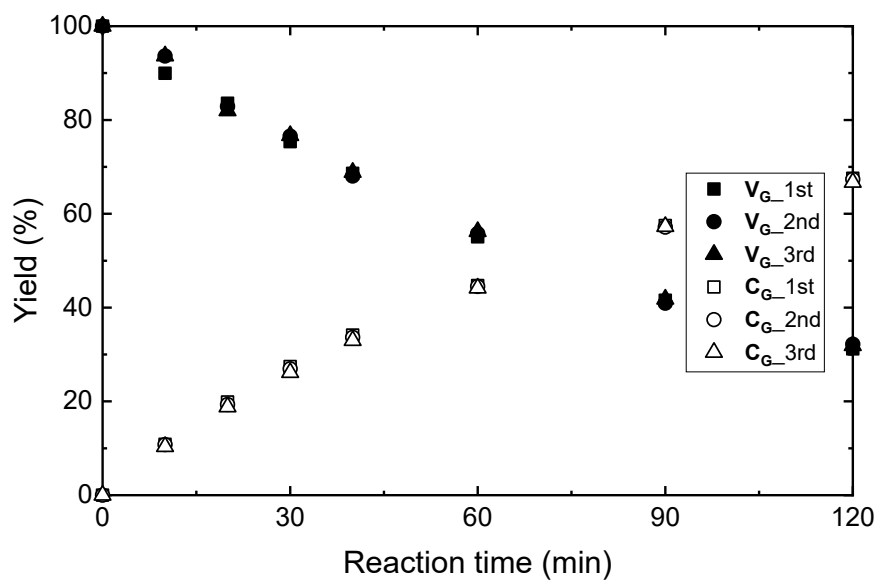


**Figure 4-13** Time course of the changes in the recovery yield of compound V<sub>G</sub> and yield of product C<sub>G</sub> in the MnO<sub>2</sub> oxidation of compound V<sub>G</sub>.

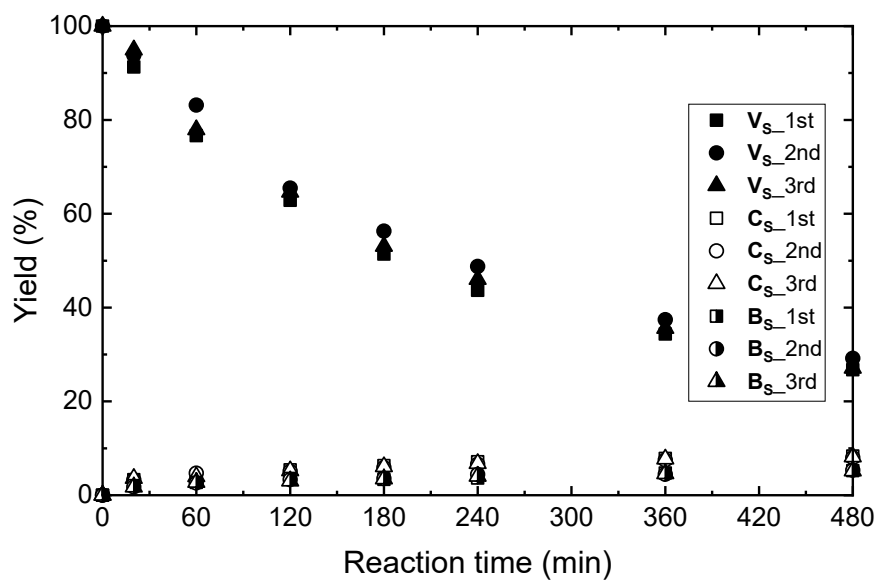


**Figure 4-14** Time course of the changes in the recovery yield of compound  $V_s$  and yields of products  $C_s$  and  $B_s$  in the  $MnO_2$  oxidation of compound  $V_s$ .

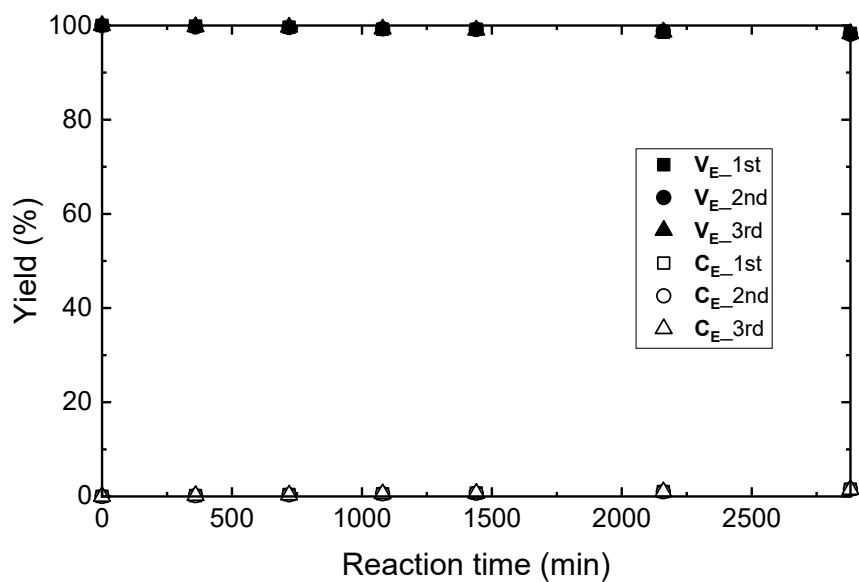


**Figure 4-15** Time course of the changes in the recovery yield of compound  $V_E$  and yield of product  $C_E$  in the  $MnO_2$  oxidation of compound  $V_E$ .

### 4.3.3 Possible reaction modes of C<sub>6</sub>-C<sub>2</sub>-type monomeric lignin model compounds in the MnO<sub>2</sub> oxidation and the comparison with C<sub>6</sub>-C<sub>1</sub>-type compounds

Based on the results observed in this chapter, three possible reaction modes can be proposed for the MnO<sub>2</sub> oxidation of compounds **IV** and **V**, as shown in **Figure 4-16**, which are the same as those proposed for that of the C<sub>6</sub>-C<sub>1</sub>-type monomeric lignin model compounds in Chapter 3.

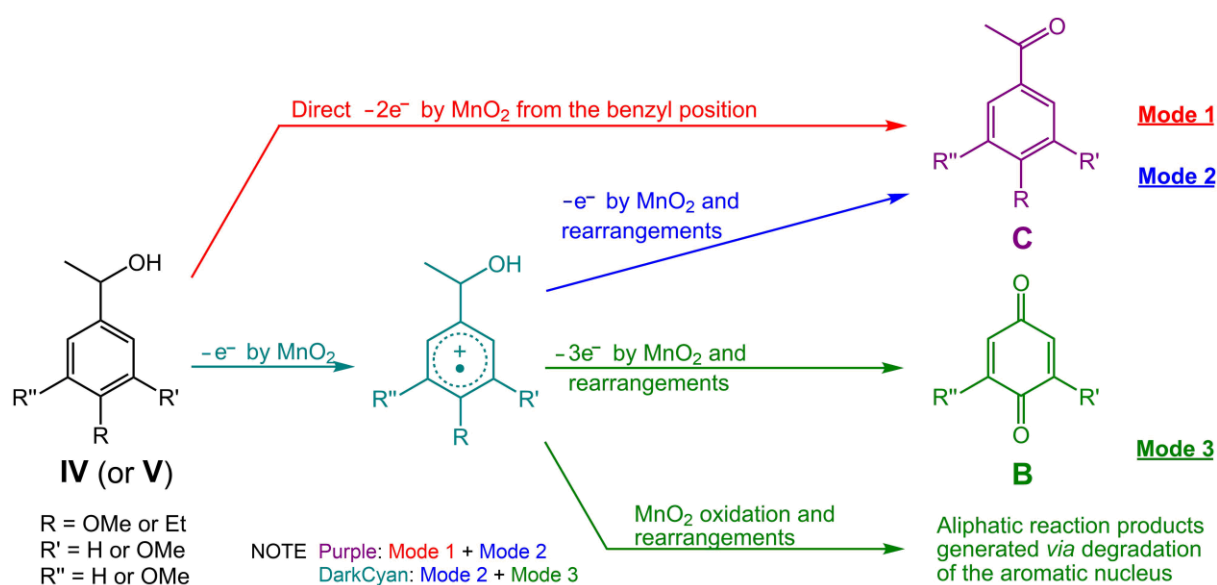


**Figure 4-16** Three possible reaction modes in the MnO<sub>2</sub> oxidations of the C<sub>6</sub>-C<sub>2</sub>-type monomeric lignin model compounds **IV** and **V**. The former is representatively described although the latter also undergoes these modes.

**Table 4-2** listed the ratios of the  $k_{\text{obs}}$  values of compounds **IV** to those of the corresponding compounds **V** ( $k_{\text{obs}}(\text{IV})/k_{\text{obs}}(\text{V})$ ). The major reaction modes in the MnO<sub>2</sub> oxidation of the **H**-, **G**-, **S**-, and **E**-type compounds based on the magnitudes of the kinetic isotope effects are discussed. The ratio between the **E**-type compounds ( $k_{\text{obs}}(\text{IV}_\text{E})/k_{\text{obs}}(\text{V}_\text{E})$ ) is 7.6. This ratio between the **E**-type compounds is a common magnitude of the primary kinetic isotope effect. The ratio between the **H**- or **G**-type compounds is 4.2 ( $k_{\text{obs}}(\text{IV}_\text{H})/k_{\text{obs}}(\text{V}_\text{H})$ ) or 3.3 ( $k_{\text{obs}}(\text{IV}_\text{G})/k_{\text{obs}}(\text{V}_\text{G})$ ), respectively. The MnO<sub>2</sub> oxidations of the **E**-type compounds (**IV**<sub>E</sub>

and **V<sub>E</sub>**) may be presumed to progress exclusively *via* mode **1**. The ratio between the **H**- or **G**-type compounds is smaller than that between the **E**-type compounds. Because of the contribution of mode **2** to the MnO<sub>2</sub> oxidation of the **H**- or **G**-type compounds, the kinetic isotope effect was suppressed when the MnO<sub>2</sub> oxidation progresses partly *via* mode **2**. The MnO<sub>2</sub> oxidations of the **H**-type compounds **IV<sub>H</sub>** and **V<sub>H</sub>** must progress *via* not only mode **1** but also mode **2**. The contribution of mode **2** of the **G**-type compounds (**IV<sub>G</sub>** and **V<sub>G</sub>**) is greater than that in the oxidations of compounds **IV<sub>H</sub>** and **V<sub>H</sub>**, because  $k_{\text{obs}}(\text{IV}_G)/k_{\text{obs}}(\text{V}_G)$  is smaller than  $k_{\text{obs}}(\text{IV}_H)/k_{\text{obs}}(\text{V}_H)$ .

The ratio between the **S**-type compounds,  $k_{\text{obs}}(\text{IV}_S)/k_{\text{obs}}(\text{V}_S)$ , is 1.9, which is smallest than the others. The affording of products **B<sub>S</sub>** indicated that MnO<sub>2</sub> could oxidize the **S**-nuclei, and hence, compounds **IV<sub>S</sub>** and **V<sub>S</sub>** progress to mode **3**. Because the kinetic isotope effect does not naturally appear in mode **3**, the contribution of mode **3** to the MnO<sub>2</sub> oxidation decreases the ratio leading to the smallest ratio of  $k_{\text{obs}}(\text{IV}_S)/k_{\text{obs}}(\text{V}_S)$  compared with the others.

**Table 4-3** Ratios observed pseudo-first-order reaction rate constants ( $k_{\text{obs}}$  values) between compounds **II** and **III** ( $k_{\text{obs}}(\text{II})/k_{\text{obs}}(\text{III})$ ), and the ratios between compounds **IV** and **V** ( $k_{\text{obs}}(\text{IV})/k_{\text{obs}}(\text{V})$ ) for estimation of the magnitudes of the kinetic isotope effects. Ratios between compound **II** and **IV** ( $k_{\text{obs}}(\text{II})/k_{\text{obs}}(\text{IV})$ ), and the ratios between compounds **III** and **V** ( $k_{\text{obs}}(\text{III})/k_{\text{obs}}(\text{V})$ ) for estimation of the differences between C<sub>6</sub>-C<sub>2</sub>- and C<sub>6</sub>-C<sub>1</sub>-type monomeric lignin model compounds.

C. <sup>a</sup>	$k_{\text{obs}}(\text{II})/k_{\text{obs}}(\text{III})^b$	$k_{\text{obs}}(\text{IV})/k_{\text{obs}}(\text{V})^c$	$k_{\text{obs}}(\text{II})/k_{\text{obs}}(\text{IV})$	$k_{\text{obs}}(\text{III})/k_{\text{obs}}(\text{V})$
<b>H</b> -type	4.7	4.2	4.0	3.6
<b>G</b> -type	4.0	3.3	2.9	2.4
<b>S</b> -type	2.7	1.9	6.2	4.4
<b>E</b> -type	8.6	7.6	4.4	3.9

<sup>a</sup>Compounds with the *p*-hydroxyphenyl (**H**-type), guaiacyl (**G**-type), and syringyl (**S**-type) nuclei, and *p*-ethylphenyl type (**E**-type) compounds. <sup>b</sup>Reported in **Table 3-2**. <sup>c</sup>Reported in **Table 4-2**.

**Table 4-3** shows the ratios between C<sub>6</sub>-C<sub>1</sub>-type compounds **II** and **III** ( $k_{\text{obs}}(\text{II})/k_{\text{obs}}(\text{III})$ ), and between C<sub>6</sub>-C<sub>2</sub>-type compounds **IV** and **V** ( $k_{\text{obs}}(\text{IV})/k_{\text{obs}}(\text{V})$ ) for estimation of the magnitudes of the kinetic isotope effects. The ratios between compounds **II** and **III** were 4.7,

4.0, 2.7, and 8.6, respectively. The ratios between compounds **IV** and **V** were 4.2, 3.3, 1.9, and 7.6, respectively. The order of observed ratios between C<sub>6</sub>-C<sub>2</sub>-type compounds and those between C<sub>6</sub>-C<sub>1</sub>-type compounds were the same, in the order of **E**- >> **H**- > **G**- >> **S**-type, which suggests that the contribution of the oxidations of the aromatic nuclei increases in the reverse order as described in Chapter 3. There is an obvious phenomenon that the ratio between the C<sub>6</sub>-C<sub>2</sub>-type compounds consisting of each type of aromatic nucleus is smaller than that between the corresponding C<sub>6</sub>-C<sub>1</sub>-type compounds, respectively. These smaller kinetic isotope effects observed in the reactions of the C<sub>6</sub>-C<sub>2</sub>-type compounds suggests that, compared with the C<sub>6</sub>-C<sub>1</sub>-type compounds, the steric effect of the  $\beta$ -methyl group at the benzyl position in the C<sub>6</sub>-C<sub>2</sub>-type compounds suppresses the MnO<sub>2</sub> oxidation *via* mode **1** and the more contribution of modes **2** and **3**. Because the ratio of the **E**-type compounds also decreases, their oxidation may progress *via* mode **1** as well as **2** (and **3**).

The ratios between compounds **II** and **IV** ( $k_{\text{obs}}(\text{II})/k_{\text{obs}}(\text{IV})$ ), and the ratios between compounds **III** and **V** ( $k_{\text{obs}}(\text{III})/k_{\text{obs}}(\text{V})$ ) are also listed in **Table 4-3** for estimation of the differences between C<sub>6</sub>-C<sub>2</sub>- and C<sub>6</sub>-C<sub>1</sub>-type monomeric lignin model compounds. The ratios between compounds **II** and **IV** were 4.0, 2.9, 6.2, and 4.4 for the **H**-, **G**-, **S**-, and **E**-type compounds, respectively. The ratio between deuterated compounds **III** and **V** were 3.6, 2.4, 4.4, and 3.9, respectively. Both ratios were in the order of **S**- >> **E**- > **H**- >> **G**-type, which indicates that the presence of the  $\beta$ -methyl group affects the reactions of compounds **IV** and **V** most and least greatly in the **S**- and **G**-type compounds, respectively. This order cannot be clearly explained. It is another noticeable phenomenon that the ratios between compounds **III** and **V** are smaller than those between compounds **II** and **IV**, regardless of the type of compound. This is explained by the following two rationally presumed phenomena: i) The contribution of modes **2** and **3** is greater in the reactions of the deuterated compounds **III** and **V** than in those of the corresponding compounds **II** and **IV**. ii) The steric factor of the  $\beta$ -methyl group of compounds **IV** and **V** must decrease the oxidation rate *via* mode **1** more than those *via* modes **2** and **3**.

## 4.4 Conclusions

MnO<sub>2</sub> oxidized compounds **IV**, the C<sub>6</sub>-C<sub>2</sub>-type monomeric lignin model compounds, with the rates in the order **G**- > **S**- >> **H**- > **E**-type, which is the same as that of the C<sub>6</sub>-C<sub>1</sub>-type compounds. Therefore, their reactivity is determined by the electronic effects of their methoxy and ethyl groups on not only their benzyl positions but also their aromatic  $\pi$ -electron systems.

The magnitudes of the kinetic isotope effects in the MnO<sub>2</sub> oxidations were estimated from the ratios of the  $k_{\text{obs}}$  values between compounds **IV** and **V**, the non-deuterated and deuterated C<sub>6</sub>-C<sub>2</sub>-type compounds, respectively. The ratios were in the order of **E**- >> **H**- > **G**- >> **S**-type. The result is the same as that of the C<sub>6</sub>-C<sub>1</sub>-type compounds. The contribution of the oxidations of the aromatic nuclei decreases following the reverse order, because no kinetic isotope effect should be observed when the MnO<sub>2</sub> oxidation begins with aromatic nuclei.

The ratios of the  $k_{\text{obs}}$  values between C<sub>6</sub>-C<sub>1</sub>- and C<sub>6</sub>-C<sub>2</sub>-type lignin model compounds were in the order of **S**- >> **E**- > **H**- >> **G**-type, which suggest that the MnO<sub>2</sub> oxidation of C<sub>6</sub>-C<sub>2</sub>-type compounds are not only affected by the reaction modes discussed in previous sections, but also by the steric effects due to the substitution of the methyl group at benzyl position.

## 4.5 References

- [1] Adler, E.; Lindgren, B. O.; Saeden, U. The  $\beta$ -guaiacyl ether of  $\alpha$ -veratrylglycerol as a lignin model. *Svensk Papperstidning* **1952**, 55 (7), 245-254.
- [2] Boerjan, W.; Ralph, J.; Baucher, M. Lignin biosynthesis. In *Annual Review of Plant Biology*, **2003**; Vol. 54, pp 519-546.
- [3] Akiyama, T.; Goto, H.; Nawawi, D. S.; Syafii, W.; Matsumoto, Y.; Meshitsuka, G. *Erythro/threo* ratio of  $\beta$ -O-4 structures as an important structural characteristic of lignin. Part 4: Variation in the *erythro/threo* ratio in softwood and hardwood lignins and its relation to syringyl/guaiacyl ratio. *Holzforschung* **2005**, 59 (3), 276-281.
- [4] Vanholme, R.; Demedts, B.; Morreel, K.; Ralph, J.; Boerjan, W. Lignin biosynthesis and structure. *Plant Physiology* **2010**, 153 (3), 895-905.
- [5] Posoknistakul, P.; Akiho, S.; Akiyama, T.; Yokoyama, T.; Matsumoto, Y. Stereo-preference in the degradation of the *erythro* and *threo* isomers of  $\beta$ -O-4-type lignin model compounds in oxidation processes III: in the reaction with chlorine- and manganese-based oxidants. *Journal of Wood Science* **2018**, 64 (4), 451-457.

**5 MnO<sub>2</sub> Oxidation of  $\beta$ -O-4-type Lignin Model**  
**Compounds with Syringyl or Guaiacyl Nucleus**  
**Focusing on the Difference in the Reactivities between**  
**the *erythro* and *threo* Diastereomers**

## 5.1 Introduction

The potential of  $\text{MnO}_2$  as a pulp bleaching agent was confirmed in Chapter 2. In Chapters 3 and 4,  $\text{MnO}_2$  was confirmed to oxidize **S**-nucleus to afford 2,6-dimethoxy-1,4-benzoquinone and aliphatic reaction products *via* degradation of the nuclei by the model experiments using the monomeric lignin model compounds, which ensures that  $\text{MnO}_2$  oxidation contributes to delignification in a bleaching process of actual chemical pulp.  $\text{MnO}_2$  can also oxidize **G**-nucleus, which is only accompanied by the oxidation of the benzyl position without the cleavage of carbon-carbon bond. Therefore, the oxidation of **G**-nucleus seems to have no contribution to delignification. It is well known that lignin is not simple monomeric structures, as shown in Chapters 3 and 4, but highly complex phenolic polymers. In plant cell walls, lignin is biosynthesized by coupling reactions between three primary precursors, i.e., *p*-coumaryl (4-hydroxycinnamyl), coniferyl (4-hydroxy-3-methoxycinnamyl), and sinapyl (4-hydroxy-3,5-dimethoxycinnamyl) alcohols.<sup>[1-3]</sup> The structural units of lignin after the synthesis are termed as *p*-hydroxyphenyl (**H**), guaiacyl (**G**), and syringyl (**S**) units.<sup>[4]</sup> Softwood lignin belongs to **G** lignin, and hardwood lignin belongs to **S** and **G** lignin. Therefore, the  $\text{MnO}_2$  oxidation may not be effective in a bleaching process of softwood pulp in contrast to that of hardwood pulp examined in Chapter 2.

The internal linkages of lignin macromolecules are also complex, mainly including C-O bonds ( $\beta$ -O-4,  $\alpha$ -O-4,  $\alpha$ -O- $\gamma$ , 4-O-5) and C-C bonds ( $\beta$ -5,  $\beta$ - $\beta$ ,  $\beta$ -1, 5-5).<sup>[5]</sup> Among these bonds, the  $\beta$ -O-4 bonds occupies the highest content in natural lignin.<sup>[6]</sup> The side chain of the  $\beta$ -O-4 structure has both the *erythro* and *threo* stereostructures (**Figure 5-1**), and each has a pair of enantiomers. The ratios between the *erythro* and *threo* structure in different plants are different.<sup>[7]</sup> There are also significant differences in various chemical reactions between these structures.<sup>[8-9]</sup>

In order to study the above-described topics, six dimeric non-phenolic  $\beta$ -O-4-type lignin model compounds with guaiacyl (**G**), and/or syringyl (**S**) nuclei ( $\text{C}_6$ - $\text{C}_3$ -type, **Figure 5-2**)

were oxidized by  $\text{MnO}_2$  under the same conditions as those in the previous chapter. It can be discussed by these oxidation reactions how the mechanisms of  $\text{MnO}_2$  oxidation differ between the lignin model compounds consisting of different A-rings (see **Figure 5-2** for the definition of A- and B- rings) or different stereostructures in the side-chains (*erythro* or *threo*). Besides, dimeric nonphenolic  $\beta$ -O-4-type lignin model compounds without the  $\gamma$ -hydroxymethyl group ( $\text{C}_6$ - $\text{C}_2$ -type, **Figure 5-2**) were employed to eliminate the effect of the presence of the  $\gamma$ -hydroxymethyl group and hence visualize it on the  $\text{MnO}_2$  oxidation reactions.

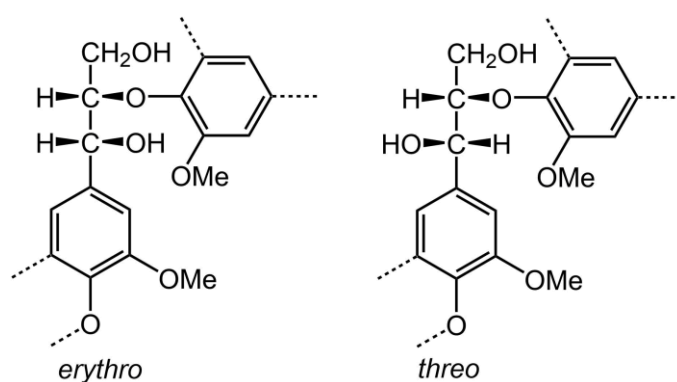
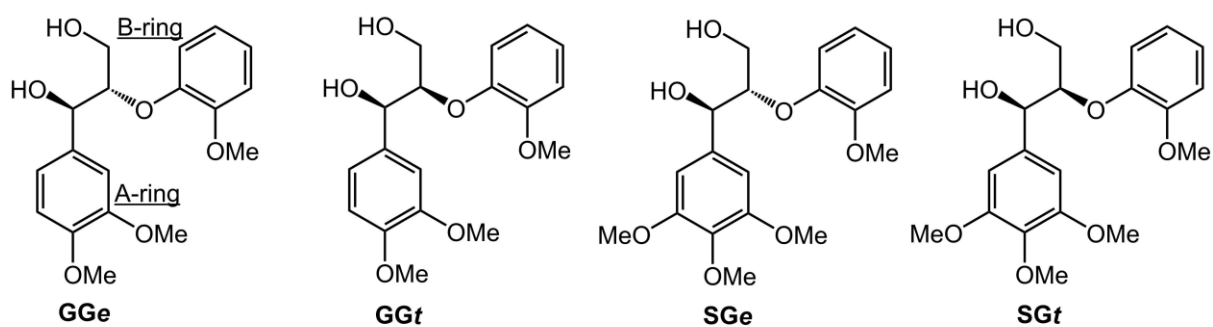
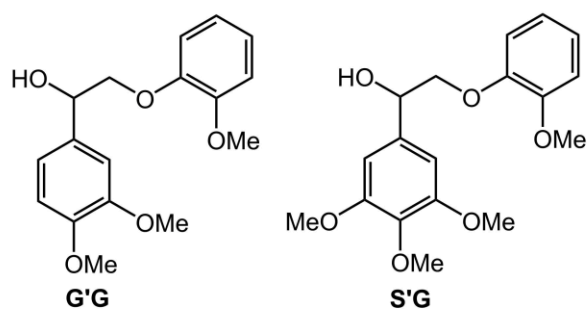


**Figure 5-1** The *erythro* and *threo* stereostructures in the side-chain portion of the  $\beta$ -O-4-type substructure of lignin.



$C_6-C_3$  non-phenolic  $\beta$ -O-4-type compounds



$C_6-C_2$  non-phenolic  $\beta$ -O-4-type compounds

**Figure 5-2** Chemical structures of the dimeric non-phenolic  $\beta$ -O-4-type lignin model compounds employed in this chapter. **GGe** and **GGt**: the *erythro* and *threo* isomers, respectively, of 2-(2-methoxyphenoxy)-1-(3,4-dimethoxyphenyl)propane-1,3-diol; **SGe** and **SGt**: the *erythro* and *threo* isomers, respectively, of 2-(2-methoxyphenoxy)-1-(3,4,5-trimethoxyphenyl)propane-1,3-diol; **G'G**: 2-(2-methoxyphenoxy)-1-(3,4-dimethoxyphenyl)ethanol; **S'G**: 2-(2-methoxyphenoxy)-1-(3,4,5-trimethoxyphenyl)ethanol.

## 5.2 Materials and methods

### 5.2.1 Materials

All chemicals used in this study except for the organic compounds described below were purchased from FUJIFILM Wako Pure Chemical Industries, Ltd. (Osaka, Japan), Tokyo Chemical Industry Co., Ltd. (Tokyo, Japan), or Sigma-Aldrich Japan K. K. (Tokyo, Japan), and used without further purification. Ultrapure H<sub>2</sub>O prepared by a generator, Puric-Z (Organo Co., Tokyo, Japan), was used in all the experiments. MnO<sub>2</sub> was synthesized from Mn<sup>2+</sup> (MnSO<sub>4</sub>) by O<sub>2</sub> oxidation under alkaline conditions; the synthesis procedure was described in Chapter 2. Sulfate buffer solution (0.50 mol/L, pH 1.5) prepared with Na<sub>2</sub>SO<sub>4</sub> and H<sub>2</sub>SO<sub>4</sub> solutions (0.5 mol/L each) was used in all the experiments.

#### 5.2.1.1 Preparation of model compounds and authentic compounds of reactions products

The abbreviations of the model compounds are shown in **Figure 5-2**. **GGe**, **GGt** and **G'G** were previously prepared in the laboratory of wood chemistry, the University of Tokyo. **SGe**, **SGt**, and **S'G** were synthesized according to the method of Adler et al.<sup>[10]</sup> These were obtained as a mixture, which were separated to each using anion exchange chromatography after being converted to the boron complexes in an aqueous C<sub>2</sub>H<sub>5</sub>OH solution containing potassium borate. The structures and purities of these compounds were confirmed by <sup>1</sup>H- and <sup>13</sup>C-NMR (JNM-A500, 500MHz, JEOL Ltd.).

**Figure 5-3** shows the quantified reaction products. **GCHO**, **SCHO**, **GCOMe** and **SCOMe** were commercially available and purified by silica gel chromatography (Isolera<sup>TM</sup>, Biotage Japan Ltd., Tokyo, Japan). The synthetic processes of compounds **GBQ** and **SBQ** were described in Chapter 3. The product **GBQ** may be derived from A-ring and/or B-ring. Products **GGC=O**, **SGC=O**, **G'GC=O** and **S'GC=O** were obtained as the intermediate products of the syntheses of **GG**, **SG**, **G'G** and **S'G**, respectively, and purified by silica gel chromatography before use. In

addition, products **B<sub>1</sub>** and **B<sub>2</sub>** were synthesized, and the processes were described in the following section. The structure and purity of products **B<sub>1</sub>** and **B<sub>2</sub>** were confirmed by <sup>1</sup>H-NMR, <sup>13</sup>C-NMR (JNM-A500, 500MHz, JEOL Ltd.) and gas chromatography-mass spectrometry (GC/MS, (electron ionization, 70 eV) was run on a Shimadzu GC2010/PARVUM2 (Shimadzu Co., Ltd., Kyoto, Japan) equipped with a capillary column (TC-17, 0.25 mm i.d. × 30 m, GL Science Inc., Tokyo, Japan).

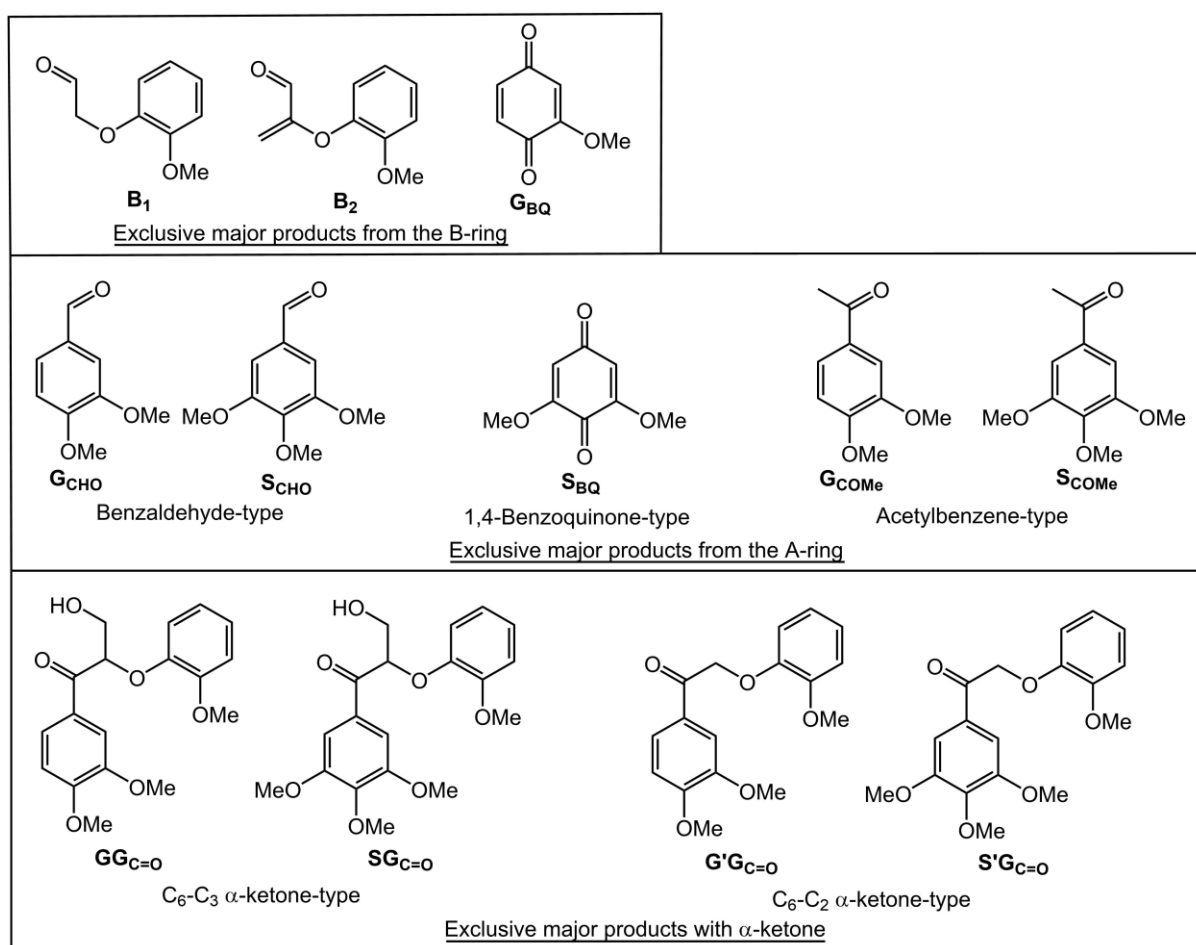


**Figure 5-3** Exclusive major reaction products from the A- and B-rings, and of dimer with the α-ketone.

### 5.2.1.2 Synthetic processes of model compounds and reaction products

#### Syntheses of SG and S'G

The synthetic route of **SG** and **S'G** is shown in **Figure 5-4**.

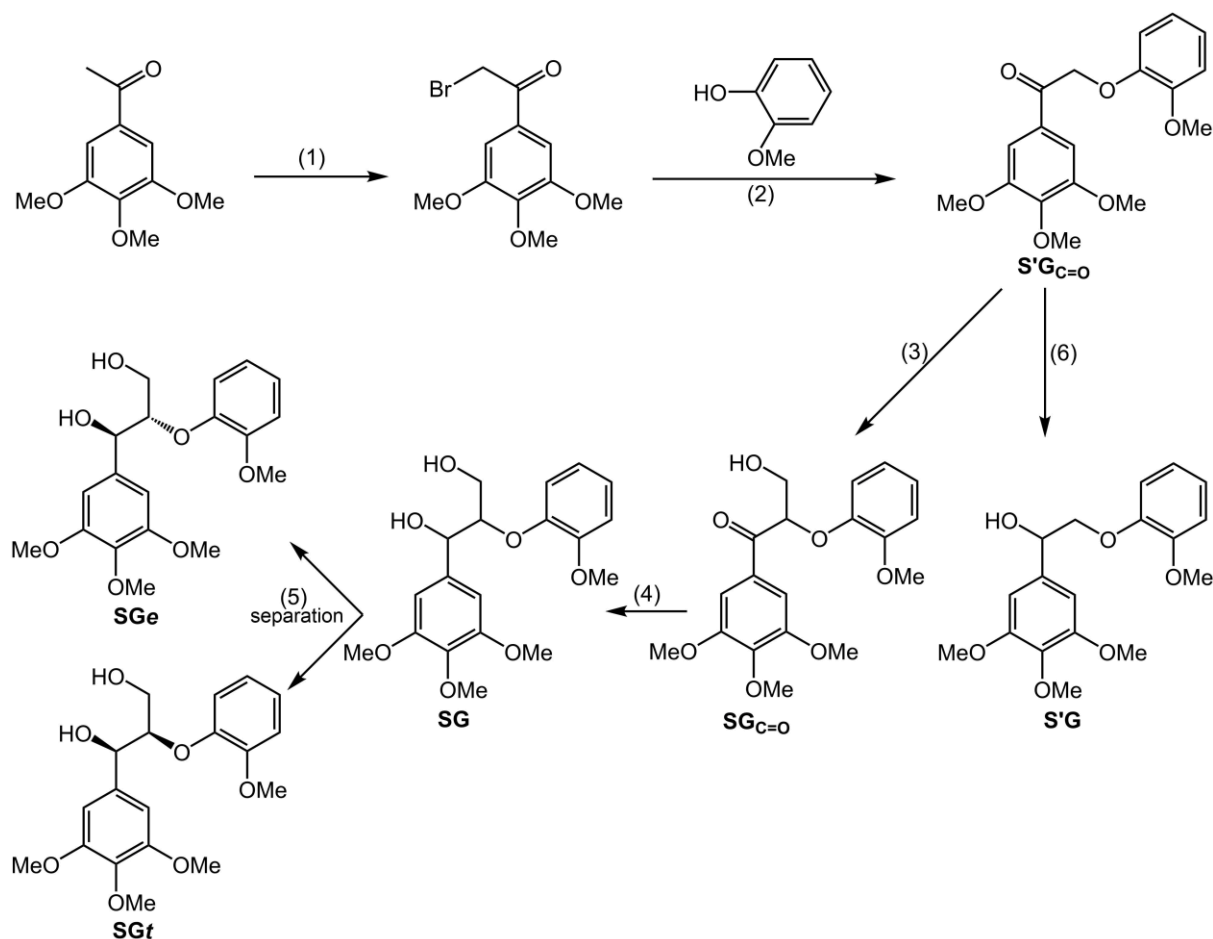


**Figure 5-4** Synthetic route of **SG** and **S'G**. Reagents and conditions were as follows: (1)  $\text{Br}_2$ ,  $\text{C}_2\text{H}_5\text{OH}$ , rt, (2)  $\text{K}_2\text{CO}_3$ , acetone,  $40^\circ\text{C}$ , (3)  $\text{HCHO}$ , THF,  $\text{K}_2\text{CO}_3$ ,  $35^\circ\text{C}$ , (4)  $\text{NaBH}_4$ ,  $\text{C}_2\text{H}_5\text{OH}$ , rt, (5) EtOH solution containing  $\text{K}_2\text{B}_4\text{O}_7$ , anion exchange chromatography, (6)  $\text{NaBH}_4$ ,  $\text{C}_2\text{H}_5\text{OH}$ , rt.

(1) Synthesis of 1-bromoacetyl-3,4,5-trimethoxybenzene (3,4,5-trimethoxy- $\alpha$ -bromoacetophenone)

First of all, 1-acetyl-3,4,5-trimethoxybenzene (3,4,5-trimethoxyacetophenone, 24.0 g, 114.2 mmol) was dissolved in  $\text{C}_2\text{H}_5\text{OH}$  (400 mL) with stirring in a round bottom flask.  $\text{Br}_2$

(20 g, 125.1 mmol) was diluted to twice the volume and then added dropwise to the solution. The completion of reaction was monitored by TLC [EtOAc-hexane = 1:1,  $R_f$  (starting material) = 0.50,  $R_f$  (target material) = 0.63], which took about 30 min. After the starting material completely disappeared, deionized H<sub>2</sub>O (200 mL) was added to the solution. The mixture was extracted with chloroform (3 × 50 mL). The organic fractions were combined, dried over anhydrous Na<sub>2</sub>SO<sub>4</sub> and evaporated under vacuum. The crude product was purified by silica gel chromatography to give 3,4,5-trimethoxy- $\alpha$ -bromoacetophenone as a white solid (20.4 g, 70.6 mmol, 62%).

(2) Synthesis of 1-(2-methoxyphenoxyacetyl)-3,4,5-trimethoxybenzene (3,4,5-trimethoxy- $\alpha$ -(2-methoxyphenoxy)acetophenone) (**S'G<sub>C=O</sub>**)

First of all, 20.4 g (70.6 mmol) of 3,4,5-trimethoxy- $\alpha$ -bromoacetophenone, 10 g (80.6 mmol) of 2-methoxyphenol (guaiacol) and 20 g (144.7 mmol) of K<sub>2</sub>CO<sub>3</sub> were added in 200 mL of acetone in a round bottom flask, and then the flask was placed in a water bath at 40°C with stirring. TLC was used to monitor the progress of the reaction [EtOAc-hexane = 50:50,  $R_f$  (starting material) = 0.63,  $R_f$  (target material) = 0.46]. The reaction took about 150 min and the reaction solution was neutralized with CH<sub>3</sub>COOH. 70% of the solvent was removed using a rotary evaporator. The mixture was added 200 mL deionized H<sub>2</sub>O and extracted with CH<sub>2</sub>Cl<sub>2</sub> (3 × 50 mL), the organic fractions were combined, dried over anhydrous Na<sub>2</sub>SO<sub>4</sub>, condensed under vacuum and purified by silica gel chromatography to give **S'G<sub>C=O</sub>** as a white solid (4.1 g, 12.3 mmol, 17%).

(3) Synthesis of 3-hydroxy-2-(2-methoxyphenoxy)-1-(3,4,5-trimethoxyphenyl)propan-1-one (**SG<sub>C=O</sub>**)

First of all, 4.1 g (12.3 mmol) of the product **S'G<sub>C=O</sub>** was dissolved in 60 mL of THF in a round bottom flask. Then 1.7 g (12.3 mmol) of K<sub>2</sub>CO<sub>3</sub> and 16 mL of formaldehyde solution (37 wt%) were added to the solution. The flask was placed in a water bath at 35°C with stirring. The progress of the reaction was monitored by TLC [EtOAc-hexane = 50:50,  $R_f$  (starting

material) = 0.46,  $R_f$  (target material) = 0.16]. The reaction took about 60 min and then deionized  $H_2O$  (200mL) was added to the reaction solution and then  $CH_3COOH$  was added for neutralization. The mixture was extracted with chloroform ( $3 \times 50$  mL), the organic fractions were combined, dried over anhydrous  $Na_2SO_4$ , condensed under vacuum and purified by silica gel chromatography to give **SG<sub>C=O</sub>** as a white solid (0.9 g, 2.5 mmol, 20%).

#### (4) Synthesis of 2-(2-methoxyphenoxy)-1-(3,4,5-trimethoxyphenyl)propane-1,3-diol (**SG**)

To a stirred solution  $C_2H_5OH$  (100 mL) dissolving **SG<sub>C=O</sub>** (0.9 g, 2.5 mmol), excess of  $NaBH_4$  (1 g, 26.4 mmol) was added slowly over 5 min. The reaction suspension was stirred at room temperature for 1 day and the completion of the reaction was checked by TLC [EtOAc-hexane = 50:50,  $R_f$  (starting material) = 0.16,  $R_f$  (target material) = 0.08].  $CH_3COOH$  was dropwise to quench the reaction. The volume of the solution was reduced by a rotary evaporation followed by addition of 100 mL of deionized  $H_2O$ . Then, the reaction mixture was extracted with  $CH_2Cl_2$  ( $3 \times 50$  mL). The organic fractions were combined, dried over anhydrous  $Na_2SO_4$  and concentrated under vacuum, remaining  $CH_3COOH$  was removed azeotropically with  $C_6H_5CH_3$ . A mixture of **SG<sub>e</sub>** and **SG<sub>t</sub>** was obtained as yellowish syrup, which was purified by silica gel chromatography to afford another mixture of **SG<sub>e</sub>** and **SG<sub>t</sub>** as colorless syrup. (0.9 g, 2.5 mmol, 99%).

#### (5) Separation of **SG<sub>e</sub>** and **SG<sub>t</sub>** *via* anion exchange chromatography

**SG<sub>e</sub>** and **SG<sub>t</sub>** were separated to each *via* anion exchange chromatography in an aqueous  $C_2H_5OH$  solution containing  $K_2B_4O_7$ .<sup>[11-12]</sup> High-performance liquid chromatography (HPLC) was used to check the separation by injecting each separated solute fraction. For neutralization,  $CH_3COOH$  was added to each of the two collected solutes which contained **SG<sub>e</sub>** and **SG<sub>t</sub>**, respectively. Each of the two collected solutes was extracted with  $CH_2Cl_2$  ( $3 \times 50$  mL). The combined organic layers were combined, dried over anhydrous  $Na_2SO_4$  and evaporated to obtain the syrups of the separated **SG<sub>e</sub>** and **SG<sub>t</sub>**.

Conditions for the separation *via* anion exchange chromatography were as follows:

Column material: glass, column length: 500 mm, column diameter: 25 mm, column volume 220 cm<sup>3</sup>, fixed bed: QAE Sephadex A-25 (particle size 40-120 μm), eluent: 20% C<sub>2</sub>H<sub>5</sub>OH (v/v) containing 0.06 mol/L K<sub>2</sub>B<sub>4</sub>O<sub>7</sub>.

Compound **SGe**: <sup>1</sup>H-NMR (solvent: CDCl<sub>3</sub> + aliquot D<sub>2</sub>O): δ 3.67 (dd, 1H, *J* = 12.1, 3.2 Hz, C<sub>γ</sub>-H<sub>a</sub>), 3.82, 3.83, and 3.86 (s, 12H, OCH<sub>3</sub>), 3.92 (dd, *J* = 12.3, 5.7 Hz, 1H, C<sub>γ</sub>-H<sub>b</sub>), 4.15-4.18 (m, 1H, C<sub>β</sub>-H), 4.95 (d, *J* = 4.9 Hz, 1H, C<sub>α</sub>-H), 6.61 (s, 2H, aromatic), 6.90-6.95 (m, 3H, aromatic), 7.03-7.06 (m, 1H, aromatic). <sup>13</sup>C-NMR: δ 56.0, 56.3, 60.8 (OCH<sub>3</sub>), 61.0 (C<sub>γ</sub>), 73.0 (C<sub>α</sub>), 87.0 (C<sub>β</sub>), 103.3, 112.3, 120.7, 121.8, 124.3, 135.8, 137.5, 147.0, 151.6, 153.4 (aromatic).

Compound **SGt**: <sup>1</sup>H-NMR (solvent: CDCl<sub>3</sub> + aliquot D<sub>2</sub>O): δ 3.52 (dd, 1H, *J* = 12.6, 3.7 Hz, C<sub>γ</sub>-H<sub>a</sub>), 3.66 (dd, 1H, *J* = 12.4, 3.2 Hz, C<sub>γ</sub>-H<sub>b</sub>), 3.83, 3.86, and 3.91 (s, 12H, OCH<sub>3</sub>), 4.02-4.05 (m, 1H, C<sub>β</sub>-H), 4.97 (d, *J* = 7.8 Hz, 1H, C<sub>α</sub>-H), 6.68 (s, 2H, aromatic), 6.91-6.96 (m, 2H, aromatic), 7.05-7.12 (m, 2H, aromatic). <sup>13</sup>C-NMR: δ 56.1, 56.3, 61.0 (OCH<sub>3</sub>), 61.1 (C<sub>γ</sub>), 74.2 (C<sub>α</sub>), 89.2 (C<sub>β</sub>), 104.2, 112.4, 121.0, 121.9, 124.4, 135.4, 138.0, 147.7, 151.4, 153.5 (aromatic).

#### (6) Synthesis of 2-(2-methoxyphenoxy)-1-(3,4,5-trimethoxyphenyl)ethanol (**S'G**)

To a stirred solution C<sub>2</sub>H<sub>5</sub>OH (100 mL) dissolving **S'G**-o (1.0 g, 3.0 mmol), excess of NaBH<sub>4</sub> (1 g, 26.4 mmol) was added slowly over 5 min. The reaction suspension was stirred at room temperature for 1 day and the completion of the reaction was checked by TLC [EtOAc-hexane = 50:50, R<sub>f</sub> (starting material) = 0.46, R<sub>f</sub> (target material) = 0.34]. CH<sub>3</sub>COOH was dropwise to quench the reaction. The volume of the solution was reduced by a rotary evaporation followed by addition of 100 mL of deionized H<sub>2</sub>O. Then, the reaction mixture was extracted with CH<sub>2</sub>Cl<sub>2</sub> (3 × 50 mL). The organic fractions were combined, dried over anhydrous Na<sub>2</sub>SO<sub>4</sub> and concentrated under vacuum, remaining CH<sub>3</sub>COOH was removed azeotropically with C<sub>6</sub>H<sub>5</sub>CH<sub>3</sub>. The obtained syrup was purified by silica gel chromatography to afford **S'G** as white solid. (0.9 g, 2.7 mmol, 90%).

Compound **S'G**: <sup>1</sup>H-NMR (solvent: CDCl<sub>3</sub> + aliquot D<sub>2</sub>O): δ 3.84, 3.87, and 3.89 (s, 12H, OCH<sub>3</sub>), 3.95-4.00 (m, 1H, C<sub>β</sub>-H<sub>a</sub>), 4.18 (dd, *J* = 10.1, 2.9 Hz, 1H, C<sub>β</sub>-H<sub>b</sub>), 5.03 (dd, *J* = 9.2,

2.9 Hz, 1H, C $\alpha$ -H), 6.67 (s, 2H, aromatic), 6.91-6.96 (m, 3H, aromatic), 6.96-7.00 (m, 1H, aromatic).  $^{13}\text{C}$ -NMR:  $\delta$  55.9, 56.2, 60.9 (OCH $_3$ ), 72.4 (C $\alpha$ ), 76.1 (C $\beta$ ), 103.3, 112.1, 115.5, 121.2, 122.4, 135.6, 137.6, 148.1, 149.9, 153.4 (aromatic).

### Syntheses of products **B**<sub>1</sub> and **B**<sub>2</sub>

The synthetic route of products **B**<sub>1</sub> and **B**<sub>2</sub> is shown in **Figure 5-5**.

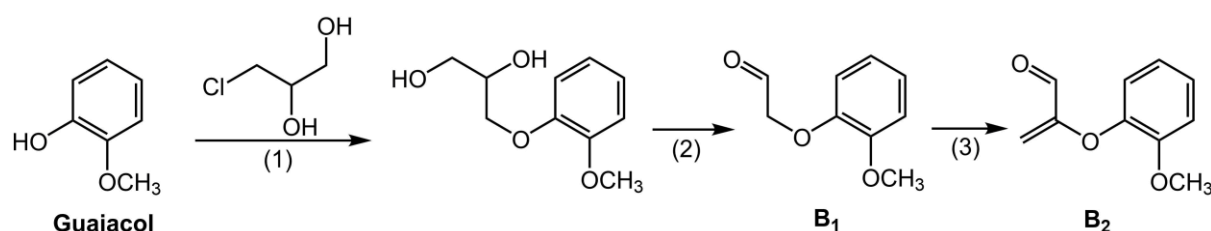


**Figure 5-5** Synthetic route of products **B**<sub>1</sub> and **B**<sub>2</sub>. Reagents and conditions were as follows: (1) NaOH, C $_2$ H $_5$ OH, reflux, (2) NaIO $_4$ , CH $_2$ Cl $_2$ , rt, (3) HCHO, THF, 35°C.

#### (1) Synthesis of 3-(2-methoxyphenoxy)-1,2-propanediol

A solution of guaiacol (3.1 g, 25.0 mmol) in C $_2$ H $_5$ OH (30 mL) was prepared in a 100 mL round bottom with stirring. To this solution was added a solution of NaOH (1.3 g, 32.5 mmol) in 10 mL of H $_2$ O. The mixture was refluxed under water bath and stirring for 10 min. Then a solution 3-chloro-1,2-propanediol (3.3 g, 30.0 mmol) dissolved in C $_2$ H $_5$ OH (10 mL) was added to the mixture, and the mixture was refluxed for 3 h. The completion of the reaction was checked by TLC [EtOAc-hexane = 50:50, R $_f$  (starting material) = 0.79, R $_f$  (target material) = 0.07]. After cooling the solution, 100 mL of H $_2$ O was added into the mixture, and extracted with diethyl ether (3  $\times$  50 mL), the organic fractions were combined, dried over anhydrous Na $_2$ SO $_4$  and condensed under vacuum. The resulting crude mixture (4.5 g) was afforded for the next step.

#### (2) Synthesis of 2-methoxyphenoxyacetaldehyde (**B**<sub>1</sub>)

The crude mixture from the former step was dissolved in CH $_2$ Cl $_2$  (200 mL). A solution of

NaIO<sub>4</sub> (7.0 g, 32.7 mmol) prepared in H<sub>2</sub>O (50 mL) was added to the above reaction mixture with stirring for 1 h at room temperature. The progress of the reaction was monitored by TLC [EtOAc-hexane = 50:50, R<sub>f</sub> (starting material) = 0.07, R<sub>f</sub> (target material) = 0.41]. After the reaction, the solution was extracted with CH<sub>2</sub>Cl<sub>2</sub> (3 × 50 mL). The organic layers were combined, dried over anhydrous Na<sub>2</sub>SO<sub>4</sub> and concentrated under vacuum. Then the crude mixture was purified by silica gel chromatography to afford **B<sub>1</sub>** as white solid (3.5 g, 21.1 mmol, 84%).

Product **B<sub>1</sub>**: <sup>1</sup>H-NMR (solvent: CDCl<sub>3</sub>): δ 3.90 (s, 3H, OCH<sub>3</sub>), 4.61 (s, 2H, Ar-O-CH<sub>2</sub>), 6.83-6.84 (m, 1H, aromatic), 6.85-6.96 (m, 2H, aromatic), 7.01-7.04 (m, 1H, aromatic), 9.91 (s, 1H, CHO). <sup>13</sup>C-NMR: δ 56.0 (OCH<sub>3</sub>), 74.5 (Ar-O-CH<sub>2</sub>), 112.5, 115.1, 121.1, 123.2, 147.5, 149.9 (aromatic), 200.4 (CHO). MS m/z (rel. int.): 166 (M<sup>+</sup>, 49), 137 (26), 122 (78), 109 (11), 92 (32), 77 (100), 65 (31), 52 (41), 41 (20).

### (3) Synthesis of 2-(2-methoxyphenoxy)prop-2-enal (**B<sub>2</sub>**)

1.5 g (9.0 mmol) of **B<sub>1</sub>** was dissolved in 60 mL of THF in a round bottom flask. Then 1.7 g (12.3 mmol) of K<sub>2</sub>CO<sub>3</sub> and 10 mL of formaldehyde solution (37 wt%) were added to the solution. The flask was placed in a water bath at 35°C with stirring. The progress of the reaction was monitored by TLC [EtOAc-hexane = 50:50, R<sub>f</sub> (starting material) = 0.41, R<sub>f</sub> (target material) = 0.79]. The reaction took about 1 h and deionized H<sub>2</sub>O (200 mL) was added to the reaction mixture and then CH<sub>3</sub>COOH was added for neutralization. The mixture was extracted with CH<sub>2</sub>Cl<sub>2</sub> (3 × 50 mL), the organic fractions were combined, dried over anhydrous Na<sub>2</sub>SO<sub>4</sub>, condensed under vacuum and purified by silica gel chromatography to give **B<sub>2</sub>** as a colorless liquid (0.2 g, 1.1 mmol, 12%).

Product **B<sub>2</sub>**: <sup>1</sup>H-NMR (solvent: CDCl<sub>3</sub>): δ 3.82 (s, 3H, OCH<sub>3</sub>), 5.07 (d, *J* = 2.9 Hz, 1H, =CH<sub>a</sub>), 5.26 (d, *J* = 2.9 Hz, 1H, =CH<sub>b</sub>), 6.95-7.00 (m, 2H, aromatic), 7.04-7.06 (m, 1H, aromatic), 7.15-7.20 (m, 1H, aromatic), 9.46 (s, 1H, CHO). <sup>13</sup>C-NMR: δ 56.1 (OCH<sub>3</sub>), 107.5 (=CH<sub>2</sub>), 113.3, 121.4, 122.4, 126.6, 143.0, 151.4 (aromatic), 158.4 (Ar-O-C), 187.2 (CHO). MS m/z (rel. int.): 178 (M<sup>+</sup>, 89), 149 (24), 135 (21), 121 (35), 108 (87), 92 (36), 81 (51), 77 (100), 65 (51), 52 (64), 41 (25).

### 5.2.1.3 NMR and GC/MS spectra of synthesized model compounds and reaction products.

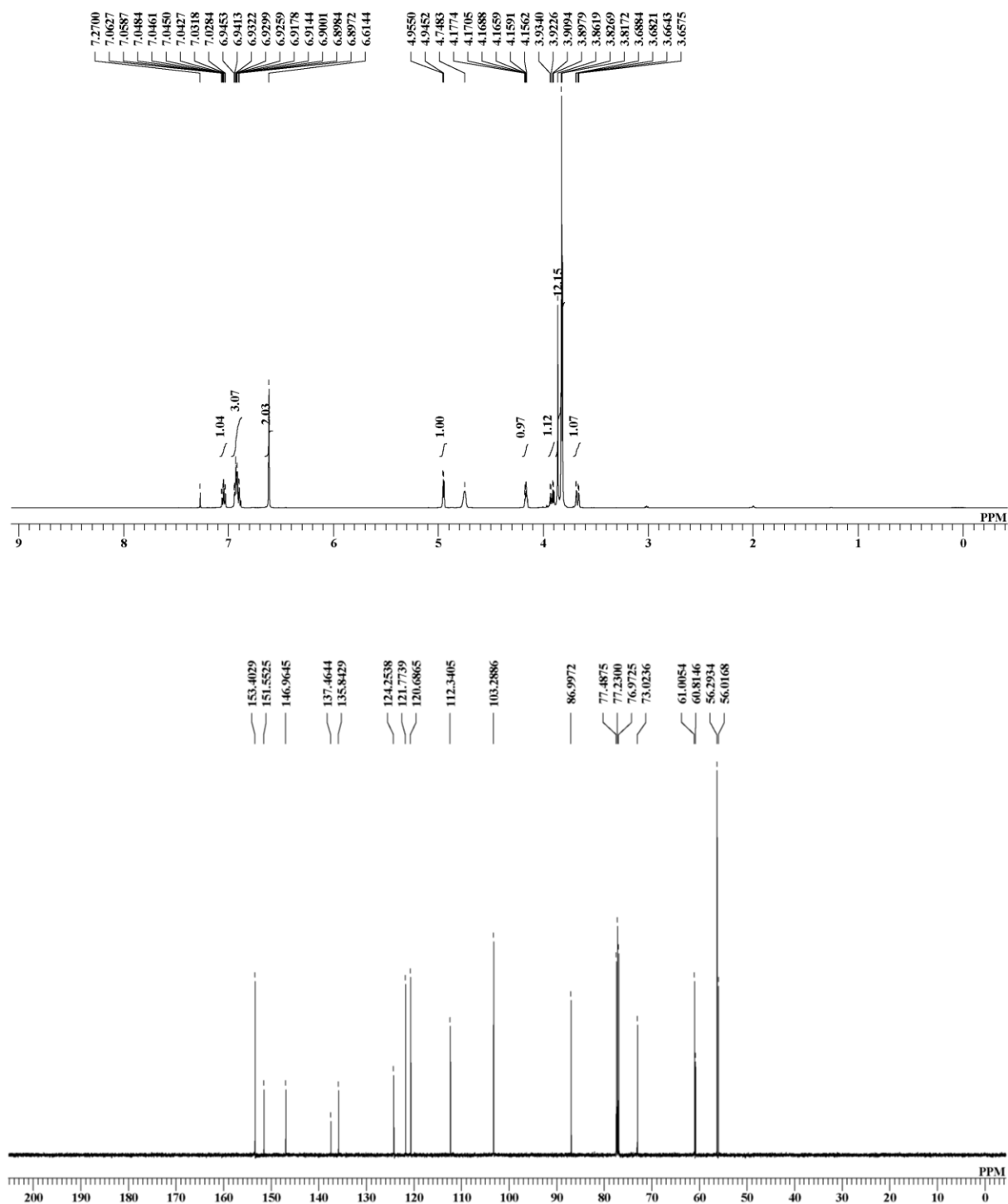


**Figure 5-6**  $^1\text{H}$ -NMR (top) and  $^{13}\text{C}$ -NMR (bottom) spectra of compound *SGe*.

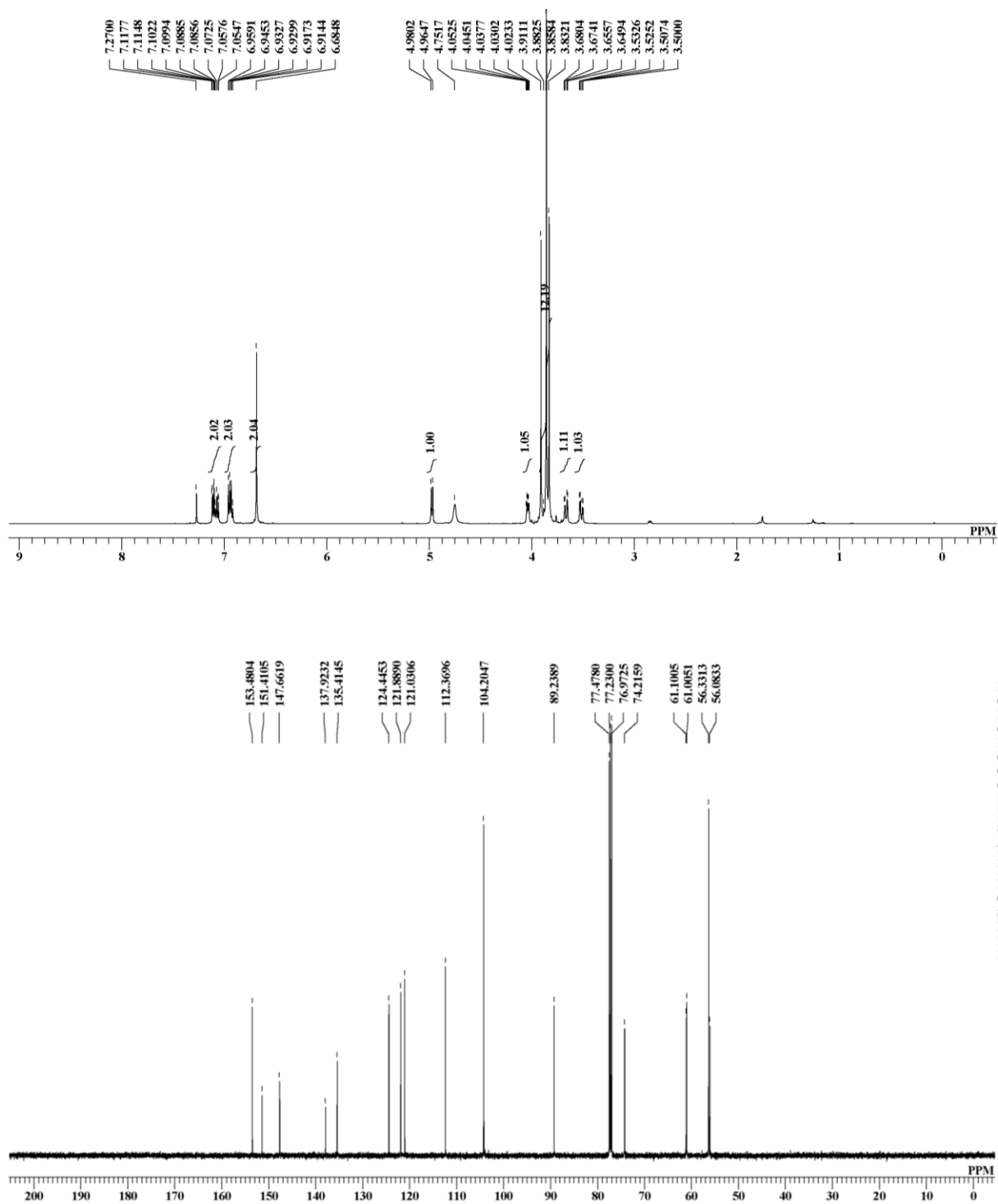


**Figure 5-7** <sup>1</sup>H-NMR (top) and <sup>13</sup>C-NMR (bottom) spectra of compound **SGt**.

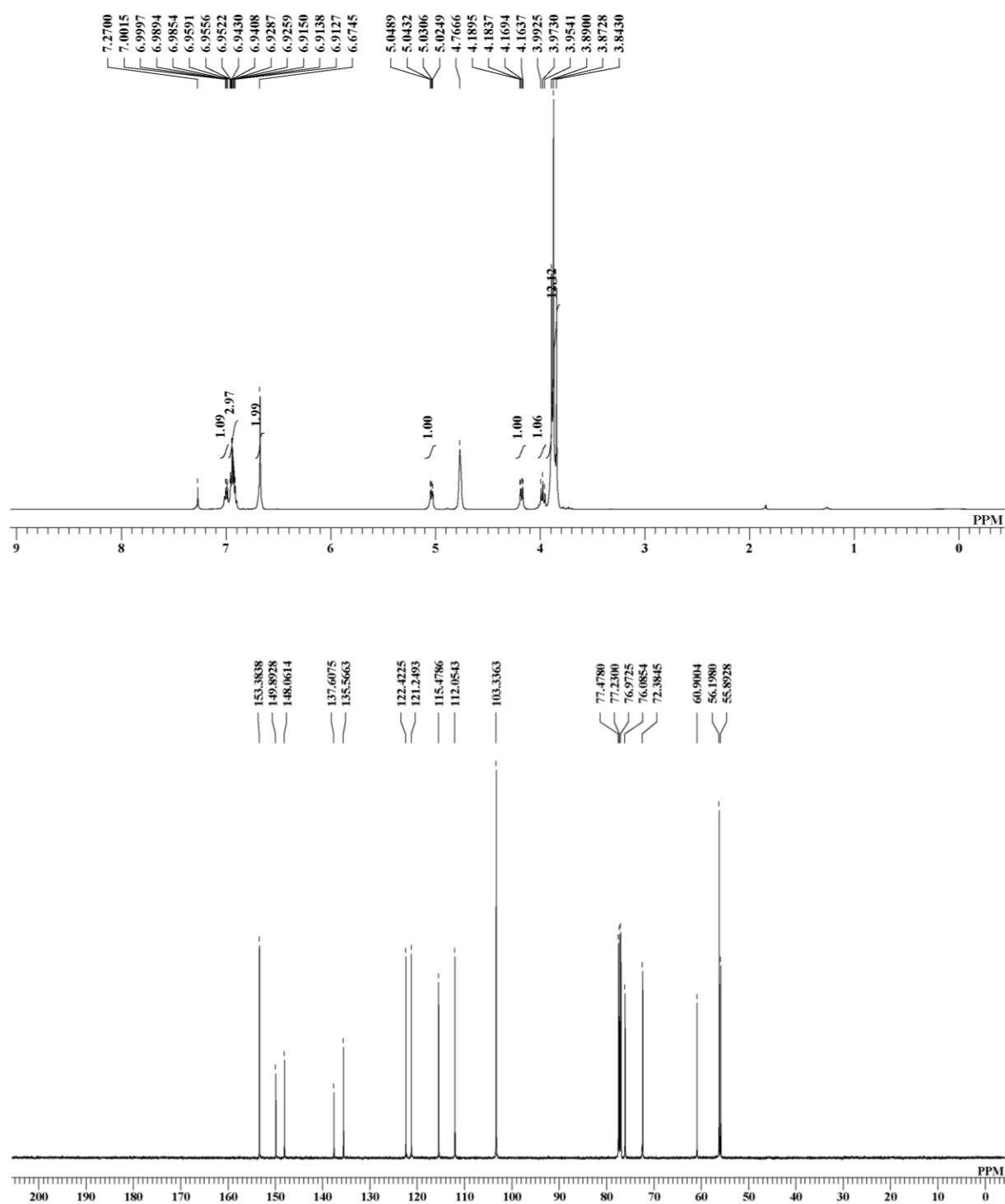


**Figure 5-8** <sup>1</sup>H-NMR (top) and <sup>13</sup>C-NMR (bottom) spectra of compound S'G.

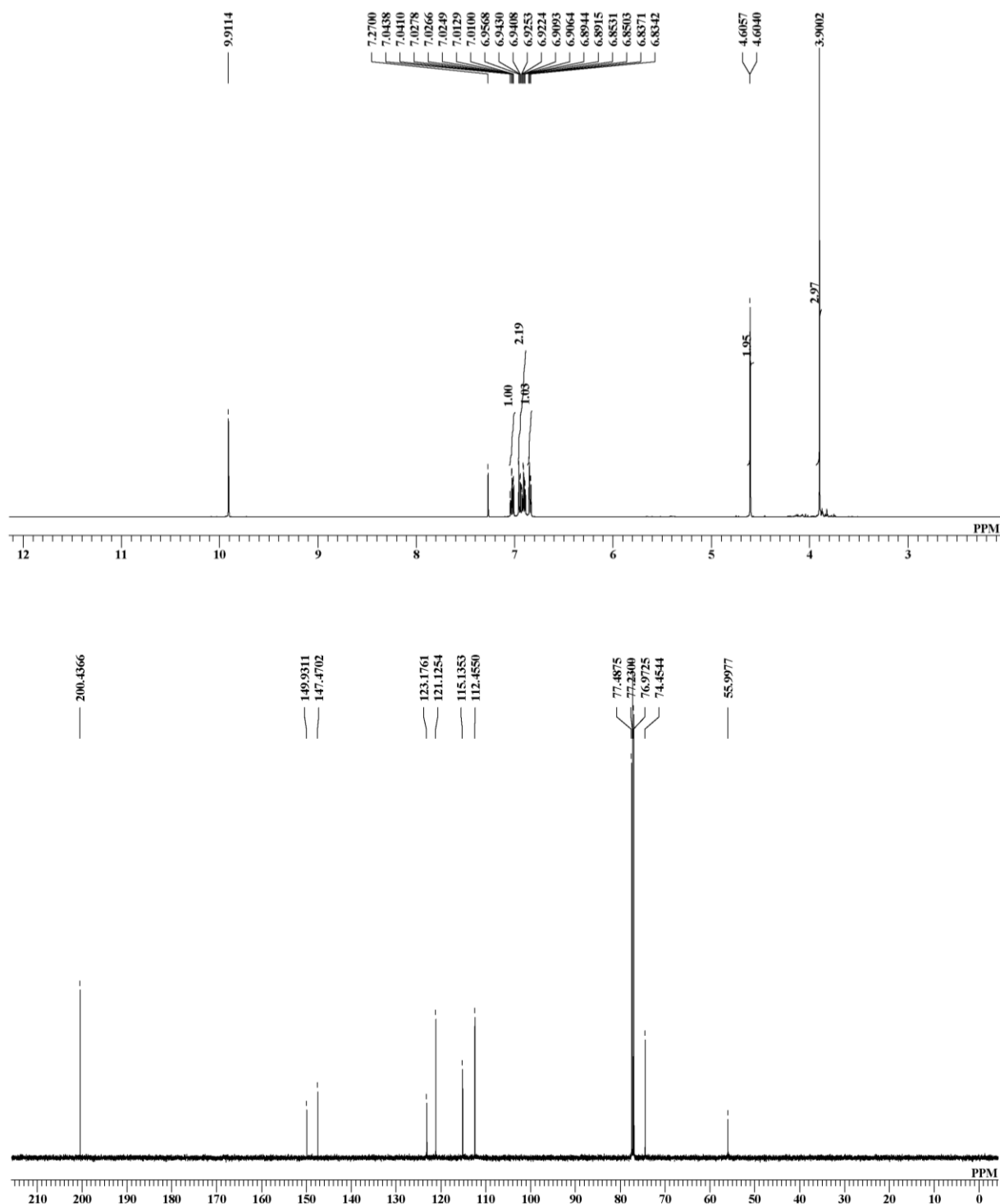


**Figure 5-9**  $^1\text{H}$ -NMR (top) and  $^{13}\text{C}$ -NMR (bottom) spectra of product **B<sub>1</sub>**.

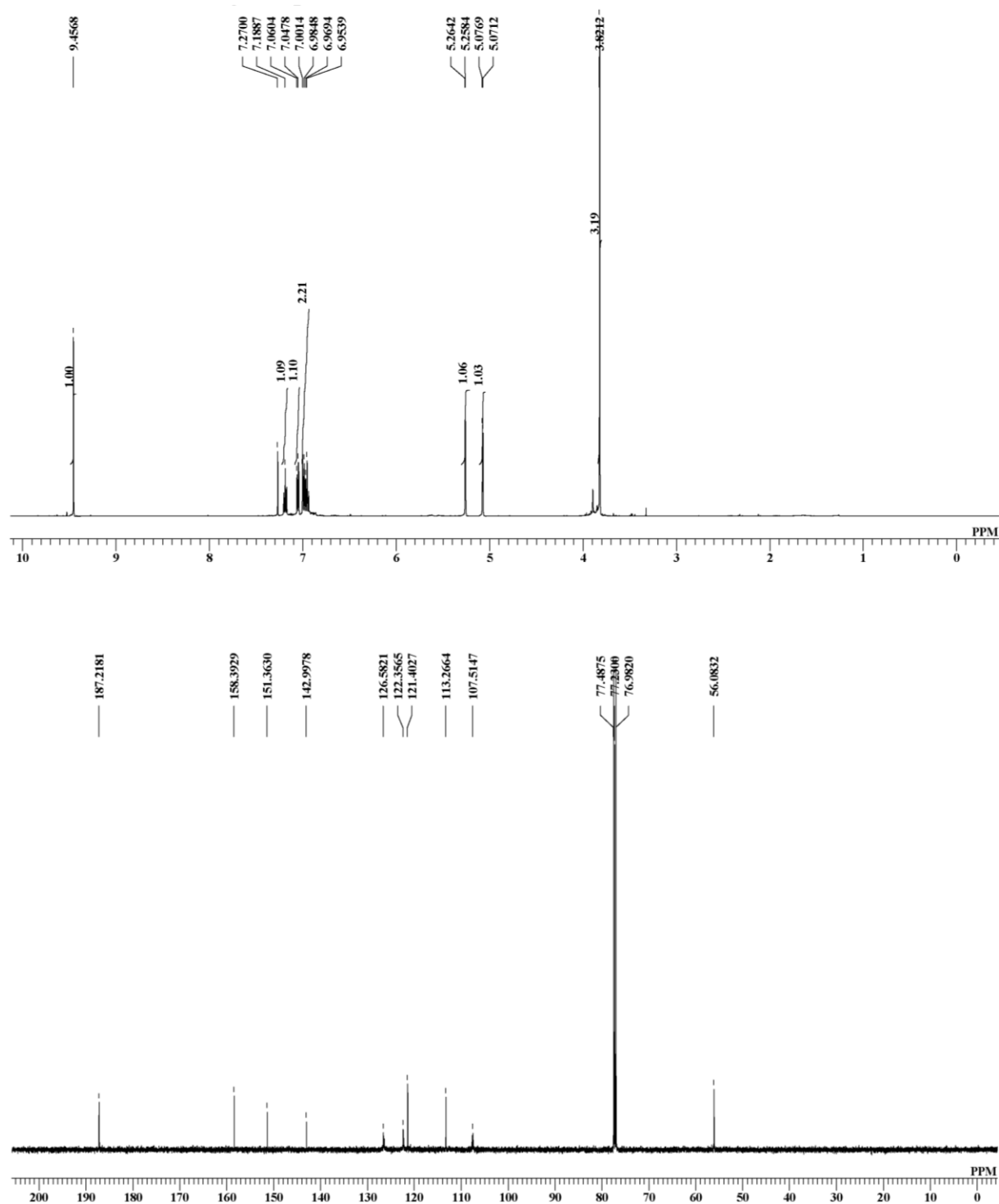


**Figure 5-10** <sup>1</sup>H-NMR (top) and <sup>13</sup>C-NMR (bottom) spectra of product **B<sub>2</sub>**.

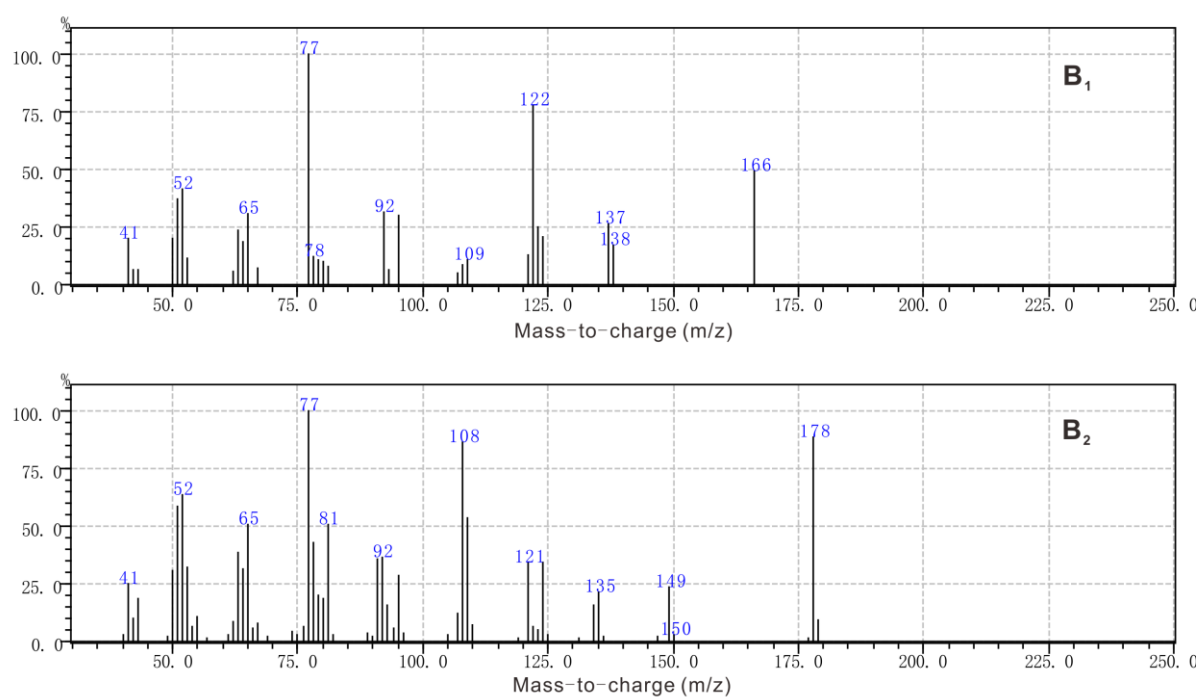


**Figure 5-11** GC/MS spectra of **B<sub>1</sub>** and **B<sub>2</sub>**.

## 5.2.2 Methods

### 5.2.2.1 MnO<sub>2</sub> oxidation reaction

All reactions were conducted in a bottom-round glass flask (200 mL volume) equipped with a magnetic stirrer. The MnO<sub>2</sub> powder used in this chapter is the synthetic MnO<sub>2</sub> (the synthesis process was described in Chapter 2) with theoretical oxidation power of 84.9%. The powder (1.2 mmol (oxidation power basis:  $1.2 \times 84.9/100 = 1.02$  mmol), oven-dry basis) was aged in sulfate buffer solution (50 mL) for 120 min in a glass flask at room temperature. Another sulfate buffer solution (10 mL) consisting of the same sulfate components and containing one of the compounds shown in **Figure 5-2** (12  $\mu$ mol) as a starting material was added to the sulfate buffer solution containing the MnO<sub>2</sub> powder to initiate the reaction at room temperature. The initial concentrations of the compound and MnO<sub>2</sub> (insoluble solid) were 0.20 and 20 mmol/L, respectively. Each reaction was conducted three times to confirm the reproducibility.

### 5.2.2.2 Quantification

Two specific amounts of the reaction solutions were withdrawn at prescribed reaction times to quantify the residual starting material and reaction products. The withdrawn solutions were rapidly neutralized with saturated NaHCO<sub>3</sub>.

One of the neutralized solutions was mixed with methanol containing an internal standard (1,2,3-trimethoxybenzene). The mixture was filtrated with a membrane filter and injected into an HPLC equipped with an ultraviolet-visible (UV-VIS) absorption detector (LC-2010C<sub>HT</sub>, Shimadzu Co., Ltd.), using the absorbance at 280 nm for quantification. In HPLC analyses, an HPLC column, Luna 5 u C18(2) 100 Å (length: 150 mm, inner diameter: 2.0 mm, particle size: 5.0  $\mu$ m, Phenomenex, Inc., Torrance, CA, USA), was used at an oven temperature of 40°C with a solvent flow rate of 0.2 mL/min. The HPLC analyses were used for quantifying residual yield of the starting materials **GG**, **SG**, **G'G** and **S'G**, and products

**GGC=O**, **SGC=O**, **G'GC=O** and **S'GC=O**. Solvent system: gradient CH<sub>3</sub>OH/H<sub>2</sub>O (v/v) from 30/70 to 40/60 for 30 min and maintained for 10 min for a total time of 40 min.

The other one of the neutralized solutions was extracted with CH<sub>2</sub>Cl<sub>2</sub> containing an internal standard (3,4-dimethoxybenzaldehyde (veratraldehyde) or 3,4,5-trimethoxybenzaldehyde), and further twice with CH<sub>2</sub>Cl<sub>2</sub> (without the internal standard compound) in the glass tube. The organic layers were combined, dried over anhydrous Na<sub>2</sub>SO<sub>4</sub>, filtered with a membrane filter. The filtered solution was analyzed by GC (GC-2014, Shimadzu Co., Ltd., Kyoto, Japan) equipped with a flame ionization detector (FID). In GC analyses for quantifying the reaction products, a capillary column of TC-17 (0.25 mm × 30 m, GL Science Inc., Tokyo, Japan) and helium as a carrier were used at injector and detector temperatures of 250°C and 280°C, respectively. The split ratio was 1 and the flow rate was 2.72 mL/min. The oven temperature was raised from 60°C to 100°C at 5°C/min and subsequently raised from 100°C to 220°C at 7.5°C/min, it was again raised to 260°C at 10°C/min and maintained for 37 min, making a total of 65 min.

**Table 5-1** HPLC and GC analysis methods for MnO<sub>2</sub> oxidation of lignin model compounds and their respective internal standard for quantification.

Compound	Binary gradient system in HPLC	Internal standard in HPLC
<b>GGe</b>	gradient CH <sub>3</sub> OH/H <sub>2</sub> O (v/v) from 30/70 to 40/60 for 30 min and maintained for 10 min (total time 40 min), following an equilibration step	1,2,3-trimethoxybenzene
<b>GGt</b>		1,2,3-trimethoxybenzene
<b>G'G</b>		1,2,3-trimethoxybenzene
<b>SGe</b>		1,2,3-trimethoxybenzene
<b>SGt</b>		1,2,3-trimethoxybenzene
<b>S'G</b>		1,2,3-trimethoxybenzene
Compound	Temperature program in GC	Internal standard in GC
<b>GGe</b>	oven temperature was raised from 60°C to 100°C at 5°C/min and subsequently raised from 100°C to 220°C at 7.5°C/min, it was again raised to 260°C at 10°C/min and maintained for 37 min, making a total of 65 min	3,4,5-trimethoxybenzaldehyde
<b>GGt</b>		3,4,5-trimethoxybenzaldehyde
<b>G'G</b>		3,4,5-trimethoxybenzaldehyde
<b>SGe</b>		3,4-dimethoxybenzaldehyde
<b>SGt</b>		3,4-dimethoxybenzaldehyde
<b>S'G</b>		3,4-dimethoxybenzaldehyde

## 5.3 Results and discussion

### 5.3.1 Reaction products derived from the MnO<sub>2</sub> oxidation of $\beta$ -O-4-type lignin model compounds

The reaction conditions were the same as those described in Chapters 3 and 4. **Figures 5-12, 5-13, 5-14, 5-15, 5-16, and 5-17** show the changes in the recovery yields of **GGe**, **GGt**, **G'G**, **SGe**, **SGt**, and **S'G**, respectively, and in the yields of the exclusive major reaction products when each compound was individually oxidized by MnO<sub>2</sub> at a pH of 1.5 (sulfate buffer 0.50 mol/L) and room temperature. All the major reaction products could be identified and quantified. **Figure 5-18** shows these exclusive major reaction products obtained in the MnO<sub>2</sub> oxidation of these lignin model compounds. **Table 5-2** shows the yields of these products at a specific reaction time, when the conversions of the starting materials were larger than or close to 90%.

Not only  $\alpha$ -ketone-type compounds (**GGC=O** from **GGe** and **GGt**; **SGC=O** from **SGe** and **SGt**; **G'GC=O** from **G'G**; **S'GC=O** from **S'G**) obtained by the oxidation of the  $\alpha$ -hydroxy groups, which are common products in the MnO<sub>2</sub> oxidation, but also benzaldehyde-type compounds (**GCHO** from **GGe**, **GGt** and **G'G**; **SCHO** from **SGe**, **SGt** and **S'G**) derived from the cleavage of the C $_{\alpha}$ -C $_{\beta}$  bonds were obtained as major products *via* the oxidation of the  $\alpha$ -hydroxy groups of all the compounds. MnO<sub>2</sub> oxidized only the S-nucleus to afford 2,6-dimethoxy-1,4-benzoquinone (**SBQ**) in the MnO<sub>2</sub> oxidation of the C<sub>6</sub>-C<sub>1</sub>- and C<sub>6</sub>-C<sub>2</sub>-type non-phenolic monomeric lignin model compounds in Chapters 3 and 4, respectively. The oxidations of the S-nuclei also afforded **SBQ** from **SGe**, **SGt** and **S'G**, accompanying the cleavage of the C<sub>aryl</sub>-C $_{\alpha}$  bonds. **GBQ** was also detected as a major product from the B-ring of **SGe**, **SGt** and **S'G**. In the oxidations of **GGe**, **GGt** and **G'G**, **GBQ** was also detected as a major product. According to the previous chapters, the C<sub>6</sub>-C<sub>1</sub>- and C<sub>6</sub>-C<sub>2</sub>-type monomeric compounds with the G-nucleus (**II<sub>G</sub>**, **III<sub>G</sub>**, **IV<sub>G</sub>**, and **V<sub>G</sub>**) were converted only to the corresponding benzaldehyde or acetylbenzene derivatives, without the formation of **GBQ**.

Therefore, the **GBQ** obtained in the oxidations of **GGe**, **GGt**, and **G'G** should come from the oxidations of the B-rings. Because the **G**-nucleus of compound **IG**, which does not have any side-chain similarly to the **G**-nuclei of **GGe**, **GGt**, and **G'G**, was oxidized to **GBQ** in the  $\text{MnO}_2$  oxidation, the B-ring of **GGe**, **GGt**, and **G'G** can be oxidized to afford **GBQ**.

Guaiacol (2-methoxyphenol) is a possible reaction product accompanying the  $\beta$ -O-4 bond cleavage in the oxidation of any compound (including **G'G** and **S'G**), although it was not detected in any reaction system. The oxidation of guaiacol is an alternative formation route of **GBQ**. A separate experiment confirmed that guaiacol is rapidly oxidized to **GBQ** and other unidentified products when it was oxidized as a starting compound in the  $\text{MnO}_2$  oxidation. Acetylbenzene-type compounds were obtained from the oxidations of the  $\text{C}_6\text{-C}_2$ -type compounds (**GCOM<sub>e</sub>** from **G'G**; **SCOM<sub>e</sub>** from **S'G**), which is caused by the cleavage of the  $\beta$ -O-4 bond, although this type was not obtained from the  $\text{C}_6\text{-C}_3$ -type compounds.

**B<sub>1</sub>** and **B<sub>2</sub>** were obtained from the B-ring of all the dimeric compounds except for **G'G** and from the B-ring of **SGe** and **SGt**, respectively. Many small peaks appeared in the HPLC and GC analyses, which shows the formation of various minor reaction products.

Because the formation of all the major reaction products other than the  $\alpha$ -ketone-type compounds (**GGC=O**, **SGC=O**, **G'GC=O** and **S'GC=O**) suggests that lignin macromolecule can be depolymerized by the  $\text{MnO}_2$  oxidation, not only hardwood but also softwood unbleached pulp can potentially be delignified by the  $\text{MnO}_2$  oxidation stage developed in Chapter 2.

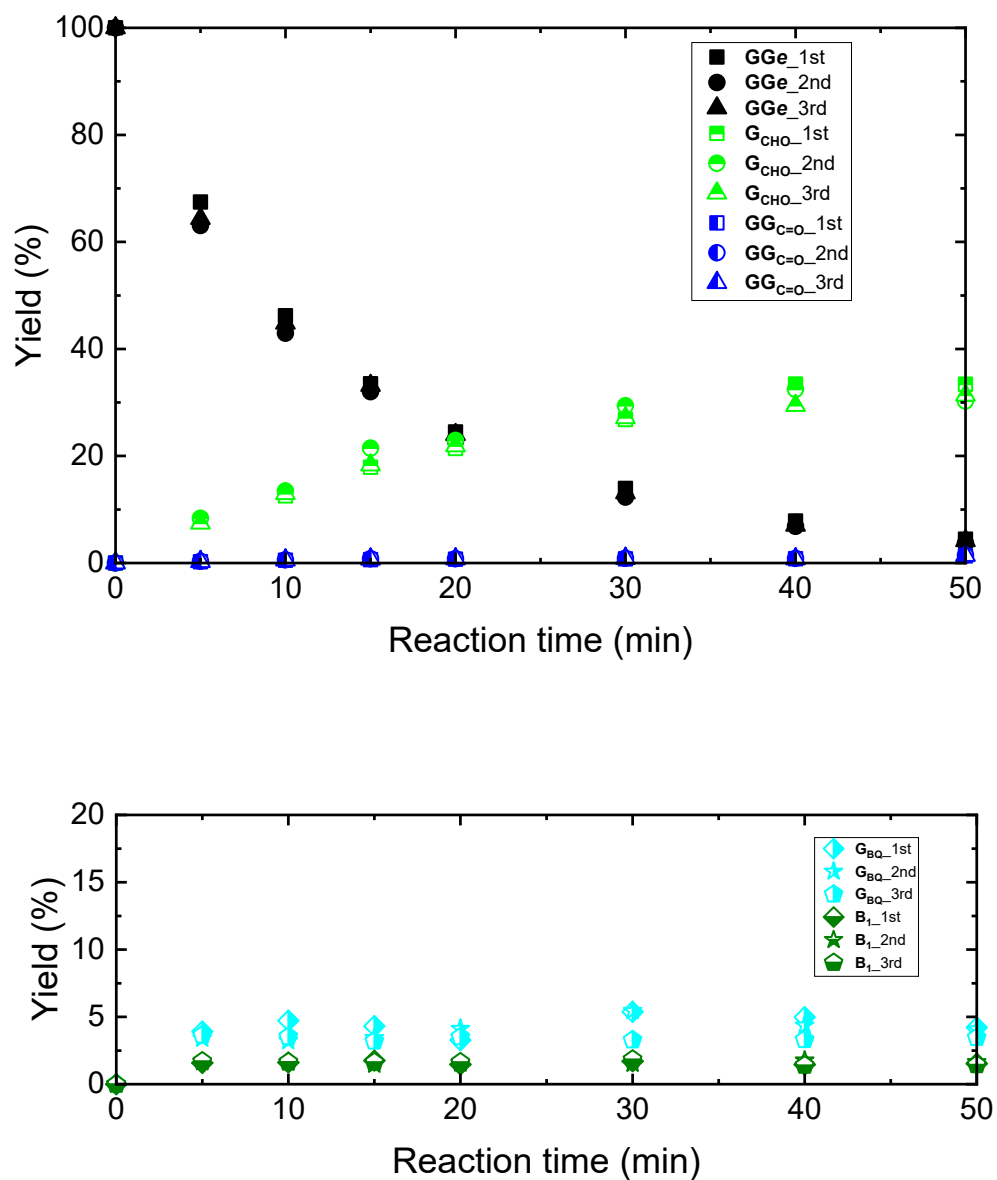


**Figure 5-12** Time course of the changes in the recovery yield of **GGe** and yields of products from A-ring (top) and B-ring (bottom) in the  $\text{MnO}_2$  oxidation of **GGe**.

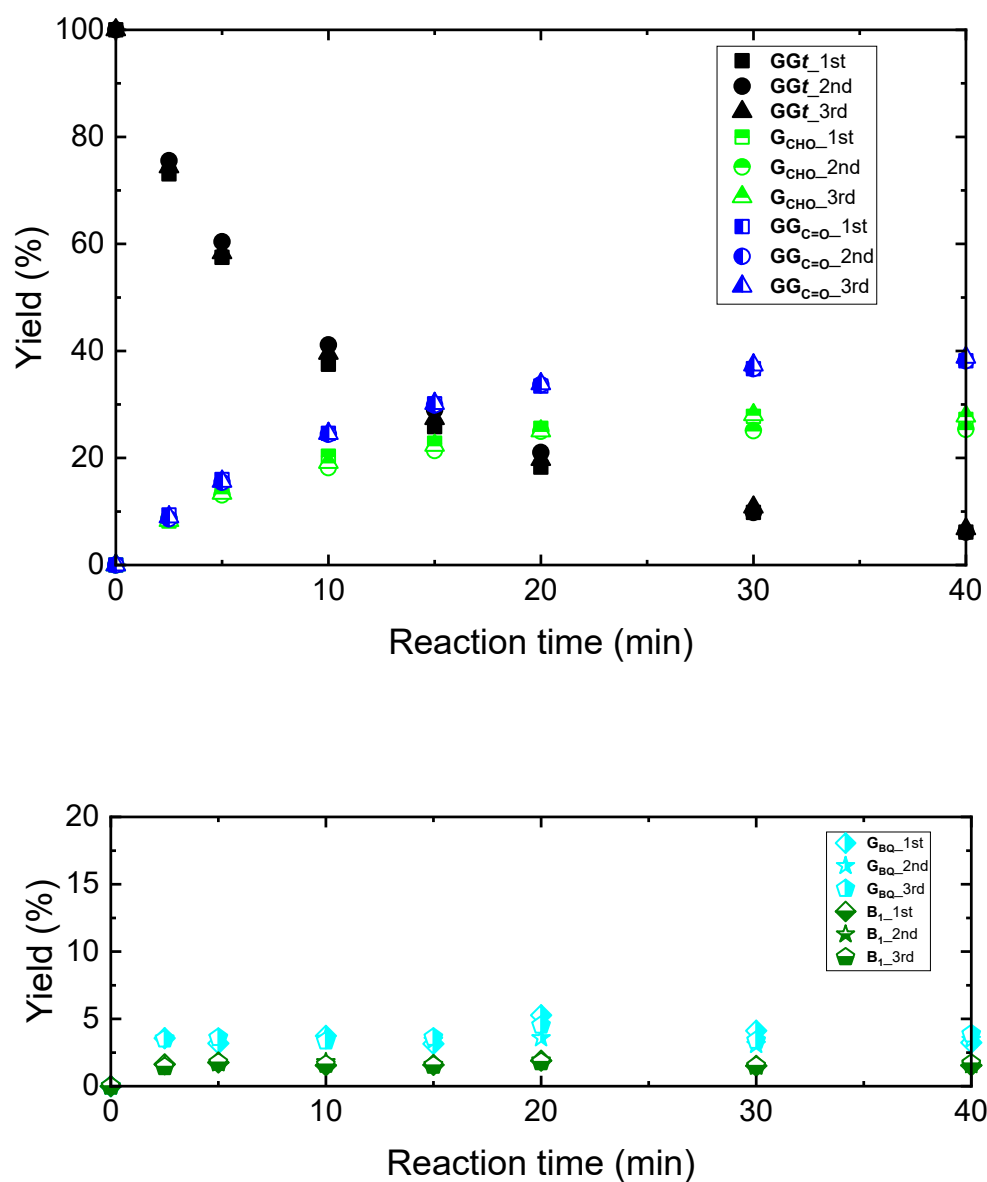


**Figure 5-13** Time course of the changes in the recovery yield of **GGt** and yields of products from A-ring (top) and B-ring (bottom) in the MnO<sub>2</sub> oxidation of **GGt**.

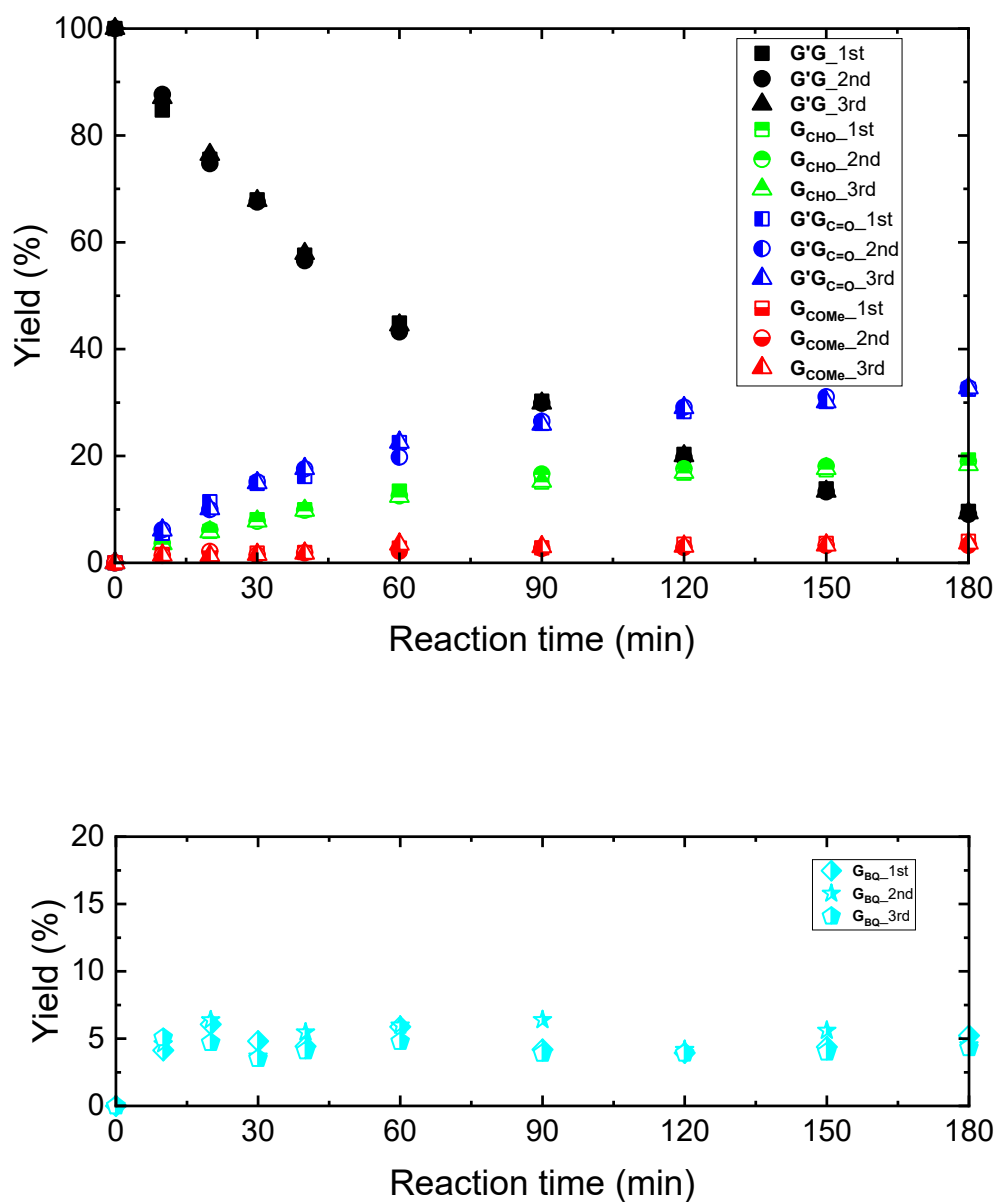


**Figure 5-14** Time course of the changes in the recovery yield of  $G'G$  and yields of products from A-ring (top) and B-ring (bottom) in the  $MnO_2$  oxidation of  $G'G$ .

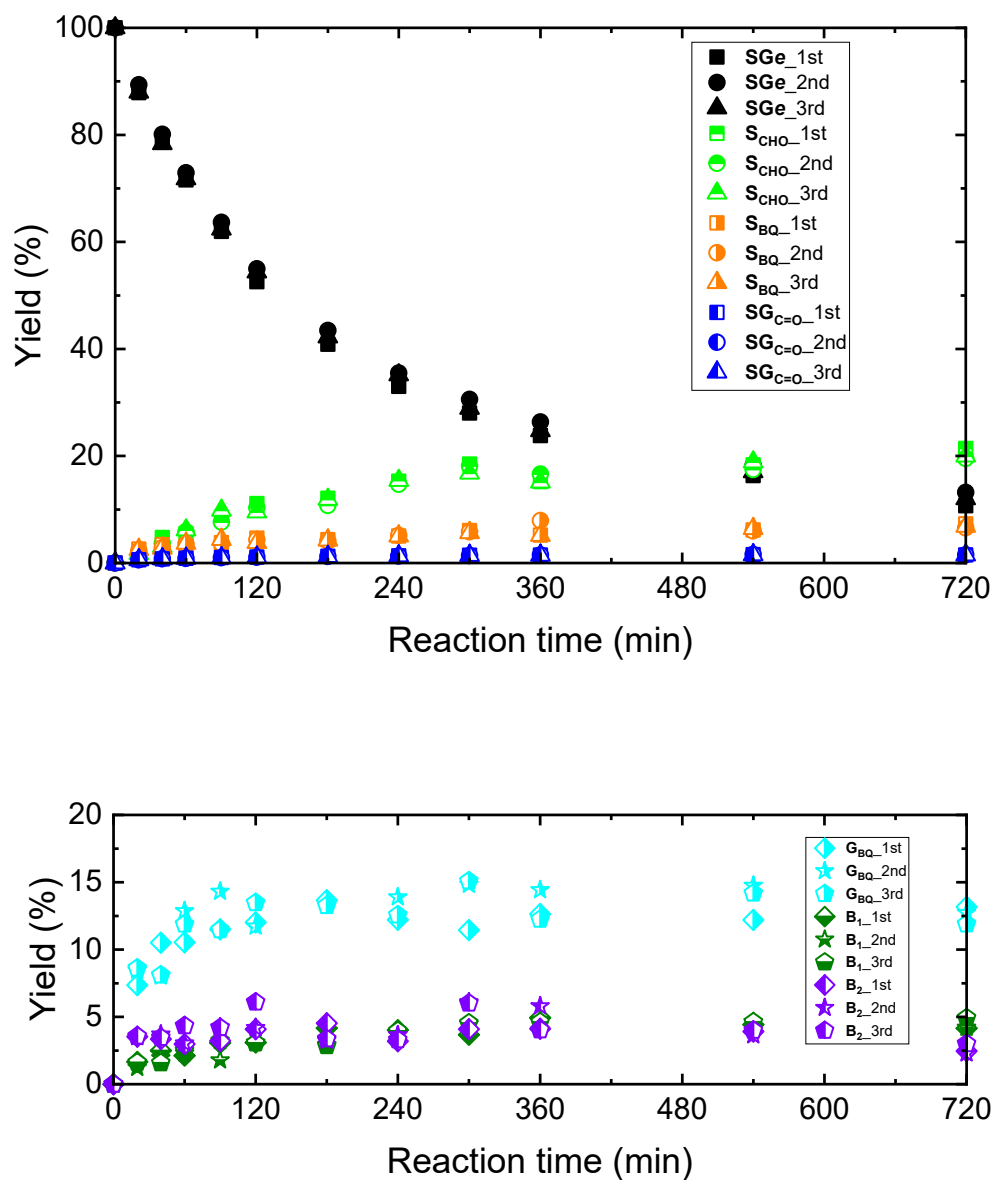


**Figure 5-15** Time course of the changes in the recovery yield of **SGe** and yields of products from A-ring (top) and B-ring (bottom) in the MnO<sub>2</sub> oxidation of **SGe**.

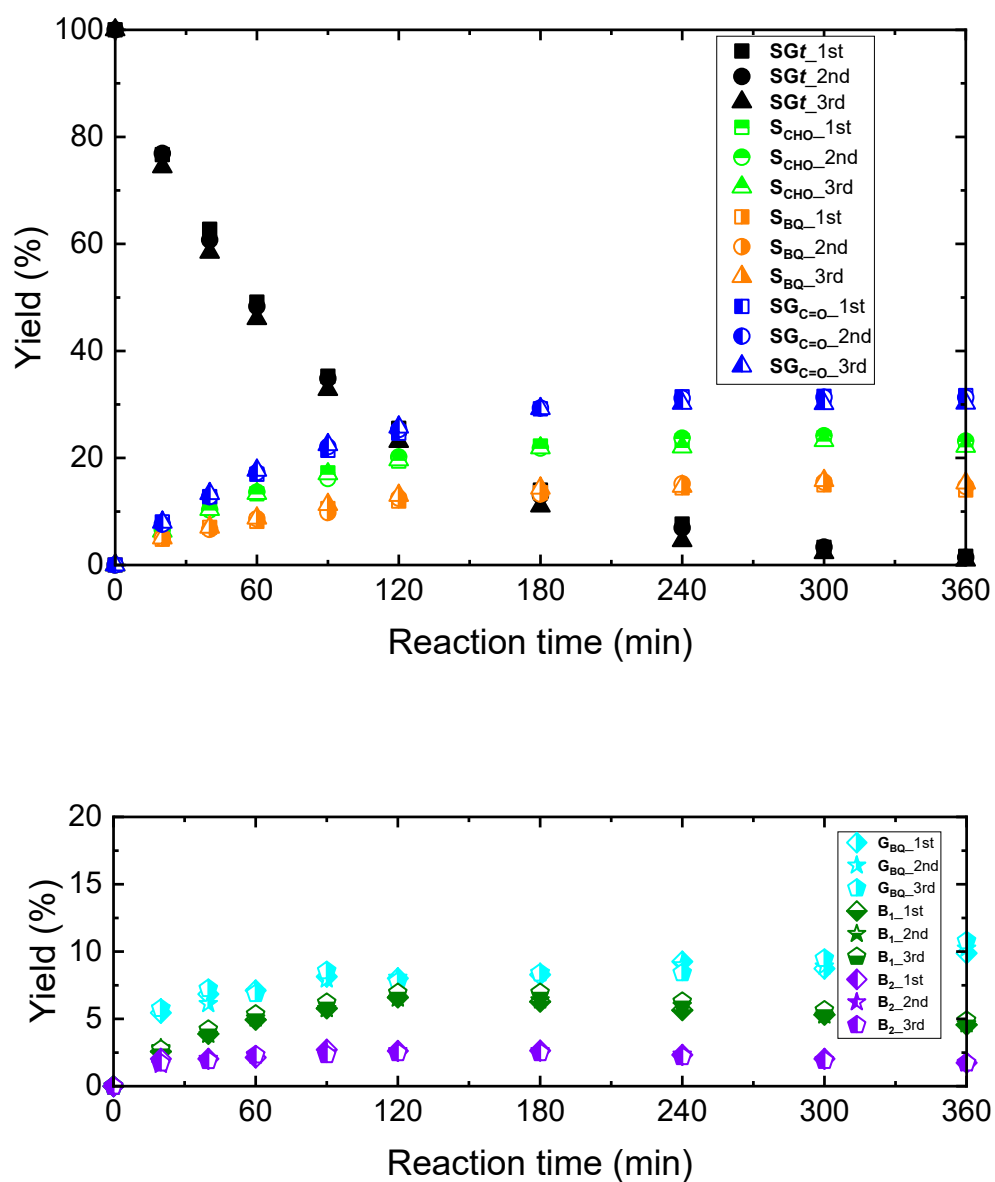


**Figure 5-16** Time course of the changes in the recovery yield of **SGt** and yields of products from A-ring (top) and B-ring (bottom) in the MnO<sub>2</sub> oxidation of **SGt**.

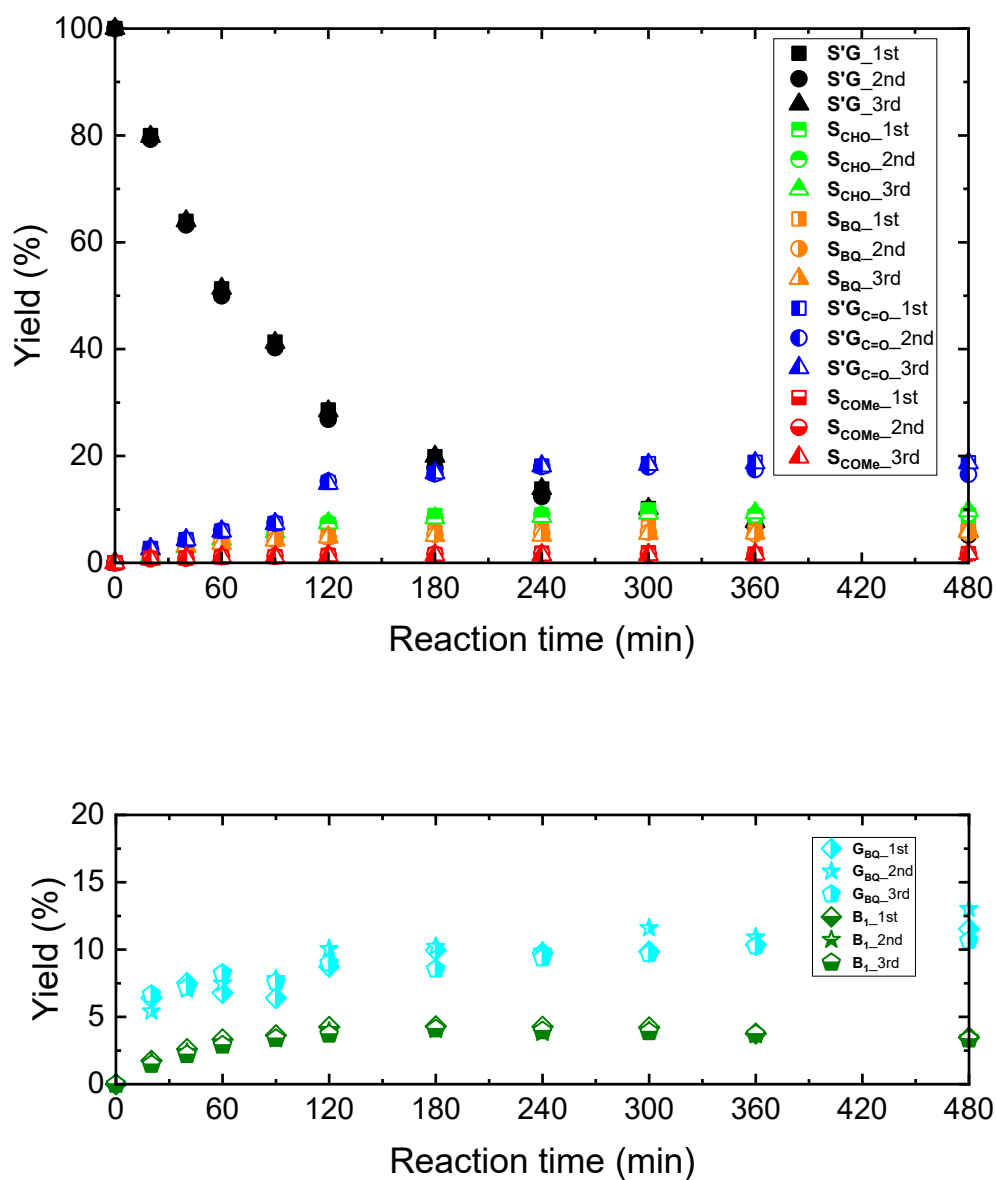


**Figure 5-17** Time course of the changes in the recovery yield of S'G and yields of products from A-ring (top) and B-ring (bottom) in the MnO<sub>2</sub> oxidation of S'G.

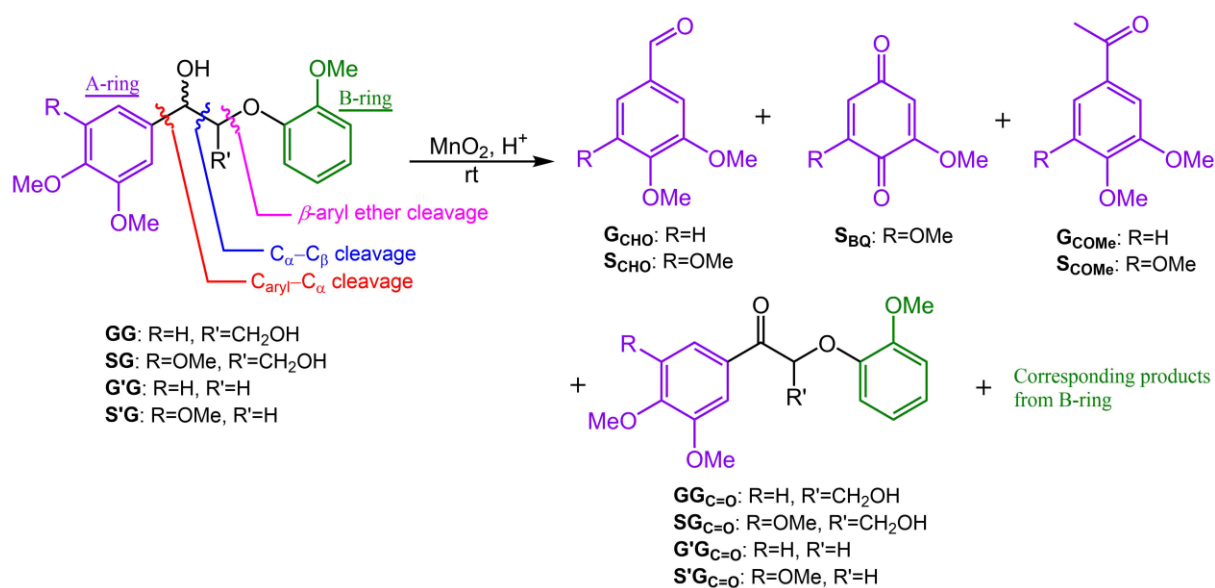


**Figure 5-18** Exclusive major reaction products derived from the A-rings and side-chains of the lignin model compounds.

**Table 5-2** Reaction products of  $\beta$ -O-4-type lignin model compounds in MnO<sub>2</sub> oxidation.

Compound	t <sup>a</sup> (min)	Conversion <sup>b</sup> (%)	Main products distribution (%)						
			G <sub>CHO</sub> /S <sub>CHO</sub> <sup>c</sup>	G <sub>BQ</sub>	S <sub>BQ</sub>	G <sub>COMe</sub> /S <sub>COMe</sub> <sup>c</sup>	GG <sub>c=O</sub> /G'G <sub>c=O</sub> /SG <sub>c=O</sub> /S'G <sub>c=O</sub> <sup>c</sup>	B <sub>1</sub>	B <sub>2</sub>
<b>GGe</b>	50	95.9±0.4	31.7±1.6	3.9±0.4	—	—	1.4±0.0	1.5±0.1	—
<b>GGt</b>	40	93.7±0.4	26.8±1.3	3.5±0.3	—	—	38.4±0.4	1.6±0.1	—
<b>G'G</b>	180	90.7±0.3	18.9±0.4	4.7±0.5	—	3.7±0.4	32.7±0.2	—	—
<b>SGe</b>	720	88.1±1.3	20.3±1.0	12.6±0.7	6.9±0.4	—	1.5±0.0	4.4±0.4	2.6±0.4
<b>SGt</b>	360	98.7±0.4	22.6±0.5	10.3±0.5	14.7±0.7	—	31.1±0.7	4.7±0.2	1.7±0.0
<b>S'G</b>	480	94.4±0.4	9.3±0.4	11.8±1.2	5.8±0.2	1.7±0.0	18.0±1.3	3.4±0.1	—

<sup>a</sup>A specific reaction time. <sup>b</sup>The conversion yield of each compound at the specific reaction time. <sup>c</sup>The yield of each product from each corresponding compound at the specific reaction time.

### 5.3.2 Effects of whether the A-ring is syringyl or guaiacyl, whether the side-chain is the *erythro* or *threo*, and whether the $\gamma$ -hydroxymethyl group is present or absent on the reaction rates of the MnO<sub>2</sub> oxidation

The disappearance of each compound was approximated well to a pseudo-first-order reaction. The pseudo-first-order reaction rate constants for the disappearances of these compounds are listed in **Table 5-3**.

When considering the effect of the type of aromatic A-ring, the reaction rates were in the order of: **GGe** > **SGe**, **GGt** > **SGt**, and **G'G** > **S'G**. These results indicate that the type of A-ring determines the reaction rates and the reactions of the **G**-type compounds are faster than those of the **S**-types. This is the same tendency in the oxidations of the C<sub>6</sub>-C<sub>1</sub>- and C<sub>6</sub>-C<sub>2</sub>-type monomeric lignin model compounds in Chapters 3 and 4, and can be explained by the descriptions in Chapter 3.

In the oxidations of **GG** and **SG**, the *threo* isomers were oxidized faster than the corresponding *erythro* isomers (**GGt** > **GGe** and **SGt** > **SGe**). It is presumed that MnO<sub>2</sub> aggregates can approach the *threo* isomers more readily than the *erythro* isomers due to the stereostructures of the side-chains. Previous studies presented evidences for the involvement of the manganese ester of a hydroxy group as intermediate during MnO<sub>2</sub> oxidation.<sup>[13-14]</sup> This type of large intermediates may be generated by the reactions between MnO<sub>2</sub> and the  $\alpha$ -hydroxy groups of **GG** and **SG**, and form more readily in the *threo* than *erythro* isomers. On the basis of the results as shown in **Table 5-2**, the difference in the distributions of the major reaction products between the *erythro* and *threo* isomers is mostly only the yields of the  $\alpha$ -ketone-type products. The yields were much higher in the oxidations of the *threo* isomers than in those of the *erythro* isomers. Instead, unidentified minor reaction products formed more greatly in the oxidations of the *erythro* isomers.

When considering the effect of the presence or absence of the  $\gamma$ -hydroxymethyl group, the reaction rates were in the order of: **GGt** > **GGe** > **G'G** and **SGt** > **S'G** > **SGe**. It was thus clarified that the presence of the  $\gamma$ -hydroxymethyl group surprisingly enhances the oxidations

except for **SGe** and hence does not originate simply from the steric factor. It is dependent on the type of the A-ring how the presence affects the oxidation. It is currently unclear why the oxidation rates are the above order.

**Table 5-3** Observed pseudo-first-order reaction rate constants ( $k_{\text{obs}}$ ), squares of the correlation coefficients ( $R^2$ ) in the approximations of lignin model compounds.

$C.e^a$	$k_{\text{obs}}^b$	$R^{2c}$	$C.t^d$	$k_{\text{obs}}^b$	$R^{2c}$	$C.C_6-C_2^e$	$k_{\text{obs}}^b$	$R^{2c}$
<b>GGe</b>	663±19	0.989	<b>GGt</b>	749±15	0.953	<b>G'G</b>	133±1	0.999
		0.986			0.979			0.999
		0.988			0.956			1.00
<b>SGe</b>	34.1±1.4	0.911	<b>SGt</b>	119±8	0.998	<b>S'G</b>	63.8±1.9	0.986
		0.900			0.998			0.985
		0.905			0.998			0.986

<sup>a</sup>The *erythro* isomer of compounds. <sup>b</sup>Unit:  $\times 10^{-4} \text{ min}^{-1}$ . The values after the '±' marks are the standard deviations of three duplicated runs. <sup>c</sup>The value obtained from each of three duplicated runs. <sup>d</sup>The *threo* isomer of compounds. <sup>e</sup>The C<sub>6</sub>-C<sub>2</sub> type of compounds.

### 5.3.3 Possible mechanisms for the reaction of GG and SG

**GG** and **SG** should basically react in the MnO<sub>2</sub> oxidation, following modes **1**, **2**, and **3** similarly to the model compounds treated in the previous chapters, as shown in **Figure 5-19**. However, the formation of **B<sub>1</sub>** suggests that the  $\gamma$ -hydroxy group is oxidized to the aldehyde and the consecutive retro-aldol condensation affords **B<sub>1</sub>** and the corresponding benzaldehyde derivatives (**GCHO** and **SCHO**). This can be a mode other than modes **1**, **2**, and **3**, although the oxidation of the  $\gamma$ -hydroxy group is not a common mode of MnO<sub>2</sub>. Because **GCHO** and **SCHO** were also produced in the oxidation of the C<sub>6</sub>-C<sub>2</sub>-type compounds (**G'G** and **S'G**), it seems that not only the oxidation of the  $\gamma$ -hydroxy group but also that of the  $\alpha$ -hydroxy group results in the formations of **GCHO** and **SCHO** in the oxidations of **GG** and **SG** despite proposing no possible mechanism for the formations. The oxidations of the  $\alpha$ -hydroxy groups to afford **GCHO** and **SCHO** must be *via* mode **2**, because mode **1** should be a route to the formation of only the  $\alpha$ -ketone-type compounds (**GGC=O** and **SGC=O**), which were confirmed to be stable in the MnO<sub>2</sub> oxidation when **GGC=O** and **SGC=O** were used as starting compounds in separate

experiments.

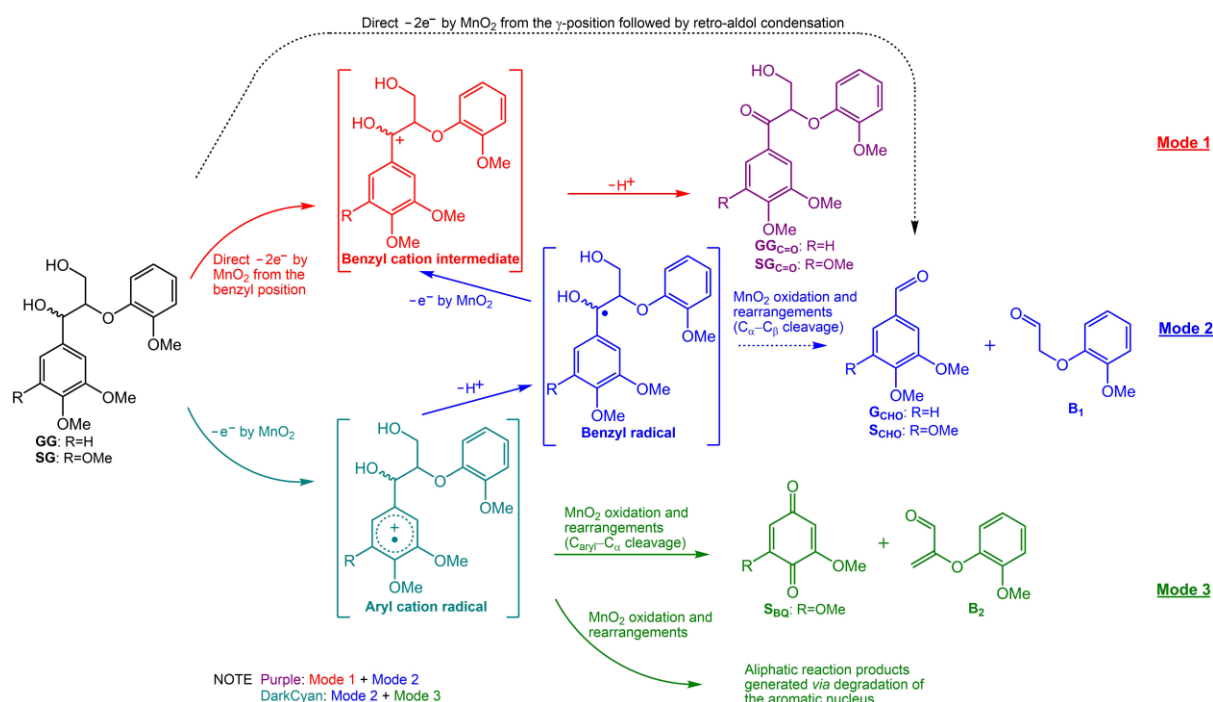


**Figure 5-19** Possible formation mechanisms for identified products *via* benzyl cation intermediates and aryl cation radicals in  $\text{MnO}_2$  oxidation reactions of compounds **GG** and **SG**.

The formation of **B<sub>2</sub>** in the oxidation of **SG** and its absence in the major products in the oxidation of **GG** show that **SG** undergoes mode 3 to afford **S<sub>BQ</sub>**, **B<sub>2</sub>**, and many unidentified aliphatic minor reaction products *via* the degradation of the **S**-nucleus while mode 2 is the only mode for **GG** when the **G**-nucleus is oxidized. **B<sub>2</sub>** is the dehydration product of 3-hydroxy-2-(2-methoxyphenoxy)propanal, which is the primary product from **SG** *via* mode 3. The formation of **G<sub>BQ</sub>** was described in section 5.3.1.

As shown in the previous section, the *threo* isomers were oxidized much faster than the *erythro* isomers, probably because  $\text{MnO}_2$  can approach to the *threo* isomers more readily than to the *erythro* isomers. **GG<sub>C=O</sub>** and **SG<sub>C=O</sub>** were produced with the amounts much larger in the oxidations of the *threo* isomers than in those of the *erythro* isomers, which was the only clear difference in the distributions of the major reaction products between the oxidations of these isomers, as recognized from **Table 5-2**. These facts suggest that the oxidations of the *threo*

isomers follow mode 1 more preferentially than those of the *erythro* isomers.

### 5.3.4 Possible mechanisms for the reaction of G'G and S'G

The mechanisms of the MnO<sub>2</sub> oxidation of G'G and S'G are similar to those of GG and SG, as shown in **Figure 5-20**. First of all, GG<sub>C=O</sub> and SG<sub>C=O</sub> were produced *via* mode 1. As mentioned in the previous section, GCHO and SCHO formed, probably *via* mode 2, although the mechanism is currently unclear. The oxidation of G'G and S'G afforded a small amount of acetylbenzene-type products (GCOMe and SCOMe, respectively). The reaction route is currently unclear, either, but should be *via* mode 2, as shown in the previous section.

B<sub>1</sub> was afforded together with SBQ *via* mode 3 in the oxidation of S'G despite its absence in that of G'G. This result shows that mode 3 is absent in the oxidation of G'G. The formation of GBQ was described in section 5.3.1.

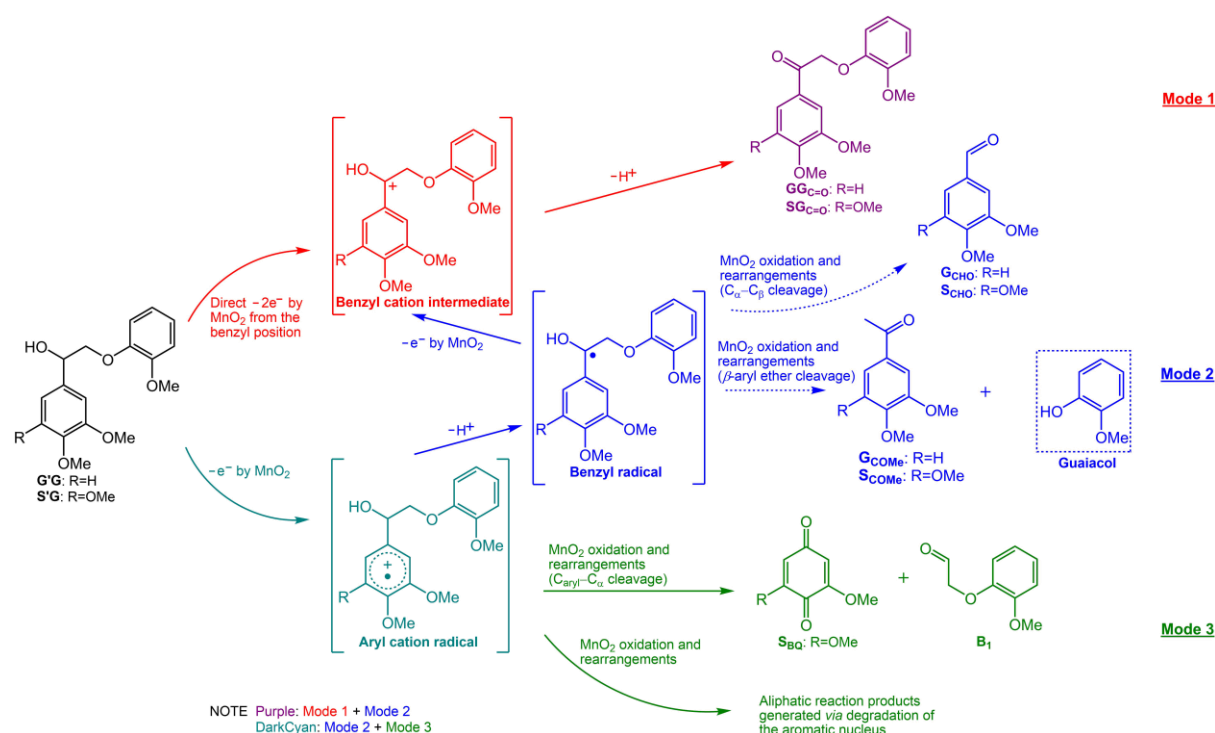


**Figure 5-20** Possible formation mechanisms for identified products *via* benzyl cation intermediates and aryl cation radicals in MnO<sub>2</sub> oxidation reactions of compounds G'G and S'G.

## 5.4 Conclusions

MnO<sub>2</sub> oxidized **GG**, **SG**, **G'G**, and **S'G** to afford not only the  $\alpha$ -ketone-type compounds, which are derived from the oxidation of the  $\alpha$ -hydroxy groups and the common products in the MnO<sub>2</sub> oxidations, but also the benzaldehyde-type compounds derived from the cleavages of the C $_{\alpha}$ -C $_{\beta}$  bonds. In addition, the products derived from the oxidation of the **S**-nuclei of **SG** and **S'G**, **SBQ** were also detected as the major together with **B<sub>2</sub>** and **B<sub>1</sub>**, respectively. The acetylbenzene-type compounds were also detected as the major products in the MnO<sub>2</sub> oxidation of **G'G** and **S'G**, which are derived from the cleavage of the  $\beta$ -O-4 bond. Although Chapters 3 and 4 suggested that the MnO<sub>2</sub> oxidation is at least suitable for bleaching of hardwood pulp due to the presence of the **S**-nuclei in the lignin, the formation of all these compounds except for the  $\alpha$ -ketone-type compounds shows that lignin macromolecule can be depolymerized by the MnO<sub>2</sub> oxidation. Therefore, the MnO<sub>2</sub> oxidation has a potential to contribute to delignification of actual bleaching of both hardwood and softwood pulps.

## 5.5 References

- [1] Boerjan, W.; Ralph, J.; Baucher, M. Lignin biosynthesis. In *Annual Review of Plant Biology*, **2003**; Vol. 54, pp 519-546.
- [2] Vanholme, R.; Demedts, B.; Morreel, K.; Ralph, J.; Boerjan, W. Lignin biosynthesis and structure. *Plant Physiology* **2010**, *153* (3), 895-905.
- [3] Lou, R.; Wu, S.; Lyu, G. Quantified monophenols in the bio-oil derived from lignin fast pyrolysis. *Journal of Analytical and Applied Pyrolysis* **2015**, *111*, 27-32.
- [4] Faix, O. Classification of lignins from different botanical origins by FT-IR spectroscopy. *Holzforschung* **1991**, *45* (s1), 21-28.
- [5] Kang, S.; Li, X.; Fan, J.; Chang, J. Hydrothermal conversion of lignin: A review. *Renewable and Sustainable Energy Reviews* **2013**, *27*, 546-558.
- [6] Li, C.; Zhao, X.; Wang, A.; Huber, G. W.; Zhang, T. Catalytic transformation of lignin for the production of chemicals and fuels. *Chemical Reviews* **2015**, *115* (21), 11559-11624.
- [7] Akiyama, T.; Goto, H.; Nawawi, D. S.; Syafii, W.; Matsumoto, Y.; Meshitsuka, G. *Erythro/threo* ratio of  $\beta$ -O-4 structures as an important structural characteristic of lignin. Part 4: Variation in the *erythro/threo* ratio in softwood and hardwood lignins and its relation to syringyl/guaiacyl ratio. *Holzforschung* **2005**, *59* (3), 276-281.
- [8] Posoknistakul, P.; Akiho, S.; Akiyama, T.; Yokoyama, T.; Matsumoto, Y. Stereo-preference in the degradation of the *erythro* and *threo* isomers of  $\beta$ -O-4-type lignin model compounds in oxidation processes III: In the reaction with chlorine- and manganese-based oxidants. *Journal of Wood Science* **2018**, *64* (4), 451-457.
- [9] Shimizu, S.; Yokoyama, T.; Akiyama, T.; Matsumoto, Y. Reactivity of lignin with different composition of aromatic syringyl/guaiacyl structures and *erythro/threo* side chain structures in  $\beta$ -O-4 type during alkaline delignification: As a basis for the different degradability of hardwood and softwood lignin. *Journal of Agricultural and Food Chemistry* **2012**, *60* (26), 6471-6476.

- [10] Adler, E.; Lindgren, B. O.; Saeden, U. The  $\beta$ -guaiacyl ether of  $\alpha$ -veratrylglycerol as a lignin model. *Svensk Papperstidning* **1952**, 55 (7), 245-254.
- [11] Ibrahim, W.; Lundquist, K. Synthesis of *erythro* and *threo* forms of lignin models of the arylglycerol  $\beta$ -guaiacyl ether type. *Acta Chemica Scandinavica* **1994**, 48, 149-151.
- [12] Li, S.; Lundquist, K.; Soubbotin, N. Separation of diastereomers of lignin model compounds of the 1, 3-diol type as borate complexes by ion-exchange chromatography. *Holzforschung* **1994**, 48 (6), 509-509.
- [13] Hall, T. K.; Story, P. R. Novel oxidative rearrangement with manganese dioxide. *Journal of the American Chemical Society* **1967**, 89 (25), 6759-6761.
- [14] Kwart, H.; George, T. J. Primary deuterium isotope effects in the oxidation of benzyl-a-d alcohol by transition elements and related reagents: Mechanisms of electron transfer. *Journal of Organic Chemistry* **1979**, 44 (1), 162-164.

## **6 Summary**

## Objectives

MnO<sub>2</sub>, proposed to have the possibility of being a pulp bleaching agent and lignin oxidant, is an environmentally friendly and recyclable chemical. However, few information was mentioned about its use in pulp bleaching or lignin oxidation processes.

The objectives of this work are to examine the role of MnO<sub>2</sub> as a catalyst in oxygen-alkali bleaching and as an oxidant to oxidatively degrade lignin. This work establishes a theoretical basis for the use of MnO<sub>2</sub> in the actual pulp bleaching and lignin oxidation processes. The main research targets in this work are as follows: (1) To investigate the utilization of MnO<sub>2</sub> as a pulp bleaching agent during oxygen-alkali bleaching, and as an oxidant to oxidize residual lignin in pulp. (2) To investigate the differences in the mechanisms of MnO<sub>2</sub> oxidation between C<sub>6</sub>-C<sub>1</sub>-type monomeric lignin model compounds with the *p*-hydroxyphenyl, guaiacyl, and syringyl nuclei. (3) To further investigate the oxidation mechanisms of MnO<sub>2</sub> by using C<sub>6</sub>-C<sub>2</sub>-type monomeric lignin model compounds with *p*-hydroxyphenyl, guaiacyl and syringyl nuclei. (4) To investigate the mechanisms of MnO<sub>2</sub> oxidative degradation of lignin by using dimeric non-phenolic  $\beta$ -O-4-type lignin model compounds.

In this work, the effect of adding manganese on the selectivity of the reaction was investigated by using model compounds of phenolic units of lignin and carbohydrates in the process of oxygen-alkali bleaching. Hardwood unbleached pulp was used to confirm the oxygen-alkali bleaching effect of MnO<sub>2</sub> addition. The delignification effect of MnO<sub>2</sub> as an oxidant under acidic conditions was also examined with hardwood unbleached pulp. The mechanism of MnO<sub>2</sub> oxidation of lignin was furthermore examined by employing monomeric lignin model compounds with the *p*-hydroxyphenyl, guaiacyl, and syringyl nuclei, as well as several dimeric non-phenolic  $\beta$ -O-4-type lignin model compounds under acidic condition.

## Utilization of Recyclable MnO<sub>2</sub> in Prebleaching Stage as a Catalyst for Oxygen Delignification or as a Delignifying Agent

In Chapter 2, the reaction of a phenolic compound (Valc) as an active oxygen species generator and a carbohydrate model compound (MGP) was conducted under oxygen-alkali bleaching conduction. MnO<sub>2</sub> is expected to catalyze decomposition of peroxides without formation of any AOS when it is added to an oxygen delignification process. In this system, Valc reacts with O<sub>2</sub> to consequently generate AOS which attack MGP. Because MGP was hardly degraded in this system, it was suggested that MnO<sub>2</sub> is a potential protector of carbohydrates.

MnO<sub>2</sub> was added to an oxygen delignification process of hardwood unbleached kraft pulp to examine whether or not the addition of MnO<sub>2</sub> protects carbohydrates from degradation. The addition of MnO<sub>2</sub> did not suppress the degradation of carbohydrates in the comparison with the reference oxygen delignification without the addition of MnO<sub>2</sub>. Because MnO<sub>2</sub> must have existed at outside of pulp fibers in this case, hardwood pulp was then oxygen-delignified after MnO<sub>2</sub> was *in-situ* generated in pulp fibers. The pulp was immersed in an acidic MnSO<sub>4</sub> solution to penetrate Mn<sup>2+</sup> into fibers, and then the Mn<sup>2+</sup> was oxidized to MnO<sub>2</sub> by O<sub>2</sub> bubbling after alkalification. The addition of the *in-situ* generated MnO<sub>2</sub> had a deleterious effect on the degradation of carbohydrates. The O<sub>2</sub> bubbling could not probably oxidize Mn<sup>2+</sup> to MnO<sub>2</sub> completely to remain some active Mn<sup>3+</sup>-related species *etc.* Comprehensively, it was not successful to utilize MnO<sub>2</sub> as a protector of carbohydrates in the oxygen delignification process.

Because MnO<sub>2</sub> is a potential oxidant of lignin under acidic conditions, it is significant to introduce a MnO<sub>2</sub> oxidation process into prebleaching stage. A MnO<sub>2</sub> oxidation stage was thus introduced subsequently to an oxygen delignification process which was terminated at the middle stage (the same conditions as the above), and the total bleachability was compared with that of the reference oxygen delignification. The MnO<sub>2</sub> oxidation stage was conducted at

a pH of 2.0 (sulfate buffer solution) and 70°C. Switching the oxygen delignification to the MnO<sub>2</sub> oxidation in the middle stage had a beneficial effect after the whole process relatively to the reference oxygen delignification process. It did not contrarily have any beneficial effect when the unbleached pulp was directly subjected to the MnO<sub>2</sub> oxidation without the first half oxygen delignification. Thus, the substitution of the MnO<sub>2</sub> oxidation stage with the latter half of the oxygen delignification can be a good bleaching sequence.

### **Differences in the Mechanisms of MnO<sub>2</sub> Oxidation between C<sub>6</sub>-C<sub>1</sub>-type Monomeric Lignin Model Compounds with the *p*-Hydroxyphenyl, Guaiacyl, and Syringyl Nuclei**

As discussed in Chapter 3, C<sub>6</sub>-C<sub>1</sub>-type monomeric lignin model compounds were oxidized by MnO<sub>2</sub> at a pH of 1.5 and room temperature to examine the difference in the oxidation reactions between *p*-hydroxyphenyl (**H**), guaiacyl (**G**), and syringyl (**S**) types. The **E**-type compounds were employed in this chapter, because the total Hammett's substituent constants ( $\sigma$  values) of two methoxy groups of the **G**-type compounds is  $-0.153 (= -0.268$  (*para*)  $+ 0.115$  (*meta*)), which is close to that of the ethyl group of the **E**-type compounds,  $-0.151$ . Reactivity at the benzyl position of an aromatic compound with functional groups on the aromatic nucleus in a chemical reaction commonly correlates well with their  $\sigma$  values.

Although MnO<sub>2</sub> commonly oxidizes alcohol groups present at the benzyl position, it certainly oxidized the **G**- and **S**-nuclei of compounds **I<sub>G</sub>** and **I<sub>S</sub>**, respectively, which do not have the benzyl position and substructures corresponding to the side-chain portion of lignin, under the employed conditions. Based on the observation in this chapter, three possible reaction modes can be proposed for the MnO<sub>2</sub> oxidation of compounds **II** and **III**. Mode **1** is direct oxidation of the benzyl position to afford the corresponding benzaldehyde-type products which is the general mode of MnO<sub>2</sub> oxidation. Mode **2** begins with the oxidation of the aromatic nucleus, but finally results in the oxidation of the benzyl position to afford benzaldehyde-type products. In this mode, the aromatic cation radical must be the primary intermediate, which is generated by the one-electron oxidation of the aromatic nucleus by

MnO<sub>2</sub>. Mode **3** also begins with the oxidation of the aromatic nucleus, and finally results in the oxidative degradation of the aromatic nucleus to 1,4-benzoquinone-type products as well as other unidentified aliphatic reaction products.

The oxidation rates of the benzyl alcohol derivatives were in the order of **G- > S- >> H- > E-type**, which suggests that the rates are determined by the electronic effects of their methoxy and ethyl functional groups on not only their benzyl positions but also their aromatic  $\pi$ -electron systems. The kinetic isotope effect was observed in the MnO<sub>2</sub> oxidations of the same derivatives deuterated at their benzyl hydroxymethyl groups. The observed magnitudes, which are estimated from the ratio of the rate constant of each compound **II** to the corresponding deuterated compound **III**, were in the order of **E- >> H- > G- >> S-type**. These magnitudes suggest that the contribution of oxidation of their aromatic nuclei (modes **2** and **3**), in which the kinetic isotope effect must not be observed, increases in the reverse order with increasing the electron density of the aromatic nuclei.

#### **Further Investigation of the Mechanisms of MnO<sub>2</sub> Oxidation using C<sub>6</sub>-C<sub>2</sub>-type Monomeric Lignin Model Compounds with the *p*-Hydroxyphenyl, Guaiacyl, and Syringyl Nuclei**

The hydroxy groups at the benzyl position in lignin commonly exist as secondary alcohols rather than primary alcohols like the C<sub>6</sub>-C<sub>1</sub>-type monomeric lignin model compounds used in Chapter 3. In Chapter 4, representative C<sub>6</sub>-C<sub>2</sub>-type monomeric lignin model compounds, in which the hydroxy groups exist as secondary alcohols, were reacted under the same conditions as those in Chapter 3 to compare differences in the MnO<sub>2</sub> oxidation between C<sub>6</sub>-C<sub>2</sub>-type monomeric lignin model compounds with the *p*-hydroxyphenyl, guaiacyl, and syringyl nuclei.

MnO<sub>2</sub> oxidized compounds **IV** with the rates in the order **G- > S- >> H- > E-type**. This order is the same as that of the C<sub>6</sub>-C<sub>1</sub>-type compounds **II**. The magnitudes of the observed kinetic isotope effects in the MnO<sub>2</sub> oxidations (ratio of the rate constant of compound **IV** to

the corresponding deuterated compound **V**) were in the order of **E**- >> **H**- > **G**- >> **S**-type. The order is also the same as that observed in the reactions of the C<sub>6</sub>-C<sub>1</sub>-type compounds. However, the magnitude of each compound was smaller than that observed in the reactions between compounds **II** and **III**. These smaller magnitudes indicate that the MnO<sub>2</sub> oxidation of the aromatic nuclei as the initial step (modes **2** and **3**) is more contributable among the three reaction modes **1**, **2**, and **3** in the MnO<sub>2</sub> oxidations of the C<sub>6</sub>-C<sub>2</sub>-type compounds **IV** and **V** than in those of the C<sub>6</sub>-C<sub>1</sub>-type compounds **II** and **III**. This must be owing to their larger steric factors at the benzyl carbon, interfering with the attack of MnO<sub>2</sub> on the carbons.

### **MnO<sub>2</sub> Oxidation of $\beta$ -O-4-type Lignin Model Compounds with Syringyl or Guaiacyl Nucleus Focusing on the Difference in the Reactivities between the *erythro* and *threo* Diastereomers**

It is well known that lignin is not simple monomeric structures, but a highly complex aromatic polymer. Among all the linkage-types between lignin monomeric units,  $\beta$ -O-4 bonds occupy with the highest content. In Chapter 5, six dimeric non-phenolic  $\beta$ -O-4-type lignin model compounds consisting of guaiacyl (**G**) and/or syringyl (**S**) nuclei with or without the *erythro* or *threo* side-chains (**GGe**, **GGt**, **G'G**, **SGe**, **SGt**, and **S'G**) were oxidized by MnO<sub>2</sub> to examine the dependence of the reactivity on these differences.

Interestingly, major reaction products were not only the corresponding  $\alpha$ -ketone derivatives, which are derived from the oxidation of the  $\alpha$ -hydroxy groups and common as products of the MnO<sub>2</sub> oxidation, but also benzaldehyde-type products derived from the cleavage of the C <sub>$\alpha$</sub> -C <sub>$\beta$</sub>  bond of each compound. In the reaction of **SG** or **S'G** carrying the **S**-nucleus as A-ring, 2,6-dimethoxybenzoquinone formed as a major reaction product derived from the oxidation of the **S**-nucleus followed by the cleavage of the C<sub>aryl</sub>-C <sub>$\alpha$</sub>  bond. In the reaction of **GG** or **G'G**, 2-methoxybenzoquinone was obtained. Because the MnO<sub>2</sub> oxidation of compound **II<sub>G</sub>**, **III<sub>G</sub>**, **IV<sub>G</sub>**, or **V<sub>G</sub>** afforded the corresponding benzaldehyde or acetylbenzene derivatives as the exclusive only major reaction product, 2-

methoxybenzoquinone obtained in the reaction of **GG** or **G'G** must have originated from the oxidation of the B-ring of **GG** or **G'G**. Acetylbenzene-type compounds were obtained from the reaction of C<sub>6</sub>-C<sub>2</sub>-type of **G'G** or **S'G**, which is different from C<sub>6</sub>-C<sub>3</sub>-type of **GG** or **SG**.

The reaction rates of these model compounds depended on their structures. When the effect of the different aromatic A-rings, **G**- and **S**-nuclei, is focused, the reaction rates were in the order of: **GGe** > **SGe**, **GGt** > **SGt**, and **G'G** > **S'G**, respectively. These results indicate that the presence of the additional methoxy group on the **S**-nucleus of the A-ring relative to the **G**-nucleus decelerates the reaction. For the C<sub>6</sub>-C<sub>3</sub>-type of **GG** or **SG**, the MnO<sub>2</sub> oxidation of the *threo* isomers was faster than the corresponding *erythro* isomers, namely, the order of these rates was **GGt** > **GGe**, or **SGt** > **SGe**, respectively. It is presumed that MnO<sub>2</sub> aggregates can approach the *threo* compounds more readily than the *erythro* compounds due to the stereostructures of the side-chains. When the side-chain structure is focused, the reaction rates were in the order of: **GGt** > **GGe** > **G'G**, and **SGt** > **S'G** > **SGe**. These results indicate that the presence of the  $\gamma$ -hydroxymethyl group accelerates the reactions of the compounds carrying the **G**-nucleus as the A-ring while it accelerates or decelerates those carrying the **S**-nucleus as the A-ring depending on the side-chain structure. Therefore, the effect of the presence of the  $\gamma$ -hydroxymethyl group originates not only simply from the steric factor but also from some interactions with the type of the aromatic A-ring.



## Acknowledgement

This research work was carried out in the Laboratory of Wood Chemistry, Department of Biomaterial Sciences, Graduate School of Agricultural and Life Sciences, The University of Tokyo (April 2018-March 2021). This great platform provided enough conditions for me to complete my doctoral research work. Thanks to many people for their support and encouragement during my study.

Thanks, Professor Yuji Matsumoto, for accepting me as a member of this big family. I can never forget how excited I was when I received the letter of acceptance.

Besides, I would like to express my deep gratitude to Associate Professor Tomoya Yokoyama, my supervisor, for his continuous support. Thanks for his immense knowledge, patience, and motivation. Without his support, guidance, and discussion, I could not complete my thesis.

I am very grateful to Dr. Takuya Akiyama for his valuable comments and suggestions throughout my research.

I also want to thank all the members of the Laboratory of Wood Chemistry, who supported and helped me through these years.

I would like to thank my thesis committee: Associate Professor Tsuguyuki Saito, and Associate Professor Kiyohiko Igarashi, for their helpful guidance and valuable comments on this thesis.

Thank my family for their heartwarming support and encouragement. Your encouragement gave me the courage to persevere.

Finally, I am grateful for the financial support by the Japanese Government (Monbukagakusho: MEXT) Scholarship for my life and study in Japan.



## List of Publications

### Journal articles

- [1] **Sun, S.**; Akiyama, T.; Yokoyama, T.; Matsumoto, Y. Utilization of recyclable MnO<sub>2</sub> in prebleaching stage as a catalyst for oxygen delignification or as a delignifying agent. *Lignin* **2020**, *1*, 1-10.
- [2] **Sun, S.**; Akiyama, T.; Yokoyama, T.; Matsumoto, Y. Differences in the mechanisms of MnO<sub>2</sub> oxidation between lignin model compounds with the *p*-hydroxyphenyl, guaiacyl, and syringyl nuclei. *Journal of Agricultural and Food Chemistry* **2020**, *68* (25), 6819-6825.
- [3] **Sun, S.**; Yokoyama, T. Effect of side-chain length in lignin model compound on MnO<sub>2</sub> oxidation: comparison of the oxidations between C<sub>6</sub>-C<sub>2</sub>- and C<sub>6</sub>-C<sub>1</sub>-type compounds *Journal of Wood Science* **2021**, submitted.

### Conference papers

- [1] **Sun, S.**; Akiyama, T.; Yokoyama, T.; Matsumoto, Y. Utilization of MnO<sub>2</sub> in prebleaching stage together with or subsequent to oxygen delignification. *Proceeding of The 20th International Symposium on Wood, Fiber, and Pulp Chemistry*, The University of Tokyo, Tokyo, Japan, **2019**; pp A-06. (Oral presentation)
- [2] **Sun, S.**; Akiyama, T.; Yokoyama, T.; Matsumoto, Y. Difference in the MnO<sub>2</sub> oxidations between *p*-hydroxyphenyl, guaiacyl, and syringyl type lignin model compounds. *Proceeding of 1st International Lignin Symposium*, Hokkaido University, Sapporo, Japan **2019**; pp 32. (Oral presentation)